Development of Electron Based Dissociation Techniques in Mass Spectrometry for the Structural Characterisation of Small Organic Ions and Modified Proteins

ARUNA SUNITHI PRAKASH

Durham University
Department of Chemistry

Development of Electron Based Dissociation Techniques in Mass Spectrometry for the Structural Characterisation of Small Organic Ions and Modified Proteins

A thesis submitted in partial fulfilment of the requirements for the degree of Doctor of Philosophy

Aruna Sunithi Prakash

2012

Abstract

The work detailed herein describes the developments made using electrons to initiate bond dissociation via electronic excitation. Electron Capture Dissociation (ECD) uses low energy electrons to analyse multiply charged cations, providing a complementary series of product ions to vibrational excitation techniques Collision-Induced Dissociation (CID) and Infrared Multiphoton Dissociation (IRMPD). ECD has been adapted to analyse small singly charged ions by increasing the electron energy, known as Electron-Induced Dissociation (EID). The effect of electron energy has been studied, indicating optimal results occurring at 18 - 20 eV. EID has been carried out on a range of small organic molecules, resulting in a high degree of fragmentation. EID results suggest that bond dissociation can occur via multiple dissociation mechanisms, forming a combination of odd-electron and even-electron species, resulting in a unique set of product ions. Developments have been made to combine Liquid Chromatography (LC) with EID in order to analyse complex mixtures of small organic molecules with a wide dynamic concentration range. In-depth analysis has been carried out by LC-EID and LC-CID on the pharmaceutical reaction mixture of cediranib, allowing structural inferences to be made for the ten unknown low abundance components observed in the sample, proving each compound to be analogous to cediranib.

Investigations of protein modifications have focussed on two proteins; the Multiple transferrable resistance Regulator (MtrR) protein and the Matrix (M) protein. ECD and CID successfully identified and located an insertion on the flexible N-terminus of the M protein that could not be resolved by X-ray crystallography. Mass spectrometry analysis has been used to identify the chemical alterations of both proteins resulting from reactions with small molecules, and ECD has been used to confirm the location of the reaction site for one modified peptide.

Contents

Abbreviations

AC	Alternating Current
AGC	Automatic Gain Control
AI ECD	Activated Ion Electron Capture Dissociation
APCI	Atmospheric Pressure Chemical Ionisation
ASAP	Atmospheric pressure Solids Analysis Probe
CAD	Collision-Activated Dissociation
CID	Collision-Induced Dissociation
DBE	Double Bond Equivalents (otherwise known as RDB)
DC	Direct Current
DI	Direct Infusion
DTT	Dithiothreitol
ECD	Electron Capture Dissociation
EDD	Electron Detachment Dissociation
EI	Electron Ionisation
EID	Electron-Induced Dissociation
EIEIO	Electron-Impact Excitation of Ions from Inorganics
EE	Electronic Excitation
EED	Electronic Excitation Dissociation
ETD	Electron Transfer Dissociation
ESI	Electrospray Ionisation
FT	Fourier-Transform
FT-ICR	Fourier Transform-Ion Cyclotron Resonance
FWHM	Full-Width-at-Half-Maximum
GC	Gas Chromatography
hECD	Hot Electron-Capture Dissociation
HPLC	High Performance Liquid Chromatography
hRSV	Human Respiratory Syncytial Virus
IRMPD	Infrared Multiphoton Dissociation
IR	Infrared
IT	Ion Trap
LC	Liquid Chromatography
LOD	Limit of Detection
M	Matrix [protein]
MALDI	Matrix-Assisted Laser Desorption/Ionisation
MS	Mass Spectrometry

MS/MS	Tandem Mass Spectrometry
MtrR	Multiple transferrable resistance Regulator [protein]
NBD-Cl	4-Chloro-7-nitrobenzofurazan
niECD	Negative Ion Electron Capture Dissociation
PDS	Photodissociation Spectroscopy
PTM	Post-Translational Modification
QET	Quasi-Equilibrium Theory
QToF	Quadrupole Time-of-Flight
RDB	Ring-plus-Double Bonds (otherwise known as DBE)
R.I.	Relative Intensity
S/N	Signal-to-Noise
TFA	Trifluoroacetic acid
Tris	Tris(hydroxymethyl)aminomethane
ToF	Time-of-Flight
UV	Ultra-Violet
VE	Vibrational Excitation

Amino Acid Abbreviations

Name	3-letter abv	1-letter abv	Molecular Formula
Alanine	Ala	A	C_3H_5NO
Arginine	Arg	R	$C_6H_{12}N_4O$
Asparagine	Asn	N	$C_4H_6N_2O_2$
Aspartic Acid	Asp	D	$C_4H_5NO_3$
Cysteine	Cys	C	C_3H_5NOS
Glutamic Acid	Glu	E	$C_5H_7NO_3$
Glutamine	Gln	Q	$C_5H_8N_2O_2$
Glycine	Gly	G	C_2H_3NO
Histidine	His	H	$C_6H_7N_3O$
Isoleucine	Ile	I	$C_6H_{11}NO$
Leucine	Leu	L	$C_6H_{11}NO$
Lysine	Lys	K	$C_6H_{12}N_2O$
Methionine	Met	M	C_5H_9NOS
Phenylalanine	Phe	F	C_9H_9NO
Proline	Pro	P	C_5H_7NO
Serine	Ser	S	$C_3H_5NO_2$

Threonine	Thr	T	$C_4H_7NO_2$
Tryptophan	Trp	W	$C_{11}H_{10}N_2O$
Tyrosine	Tyr	Y	$C_9H_9NO_2$
Valine	Val	V	C_5H_9NO

Units

°C	Degrees Celsius
A	Ampere
Å	Ångström
Da	Dalton
eV	Electron Volt
hr	Hour
keV	Kilo Electron Volt
kV	Kilovolt
L	Litres
M	Molarity in Moles per Litre
min	Minute
mg	Milligram
mL	Millilitre
mM	Millimole
mm	Millimetre
mmu	Milli Mass Units
ms	Millisecond
m/z	Mass-to-Charge
nm	Nanometre
pg	Picogram
pM	Picomole
ppm	Parts-Per-Million
psi	Pounds-per-Square-Inch
s	Second
T	Tesla
µg	Microgram
µL	Microlitre
µM	Micromole
µm	Micrometre
V	Volt

Declaration

The work presented herein was carried out in the Department of Chemistry at Durham University between October 2008 and March 2012. In April 2011 work was conducted at AstraZeneca, Alderley Edge over two days. Unless otherwise stated all work is my own and has not been submitted previously for a qualification at this or any other university.

Statement of Copyright

Acknowledgements

There are many people who I would like to thank for being instrumental in helping me ~~survive~~ complete my doctorate…

First and foremost I am incredibly grateful to Dr. Jackie Mosely, for all the guidance and support she has given me throughout my project and for providing me with every opportunity to learn and progress under her supervision. Special thanks to members of the Durham University Mass Spectrometry Group, past and present; in particular Dr. Mike Jones, Lara Turner, Dr. Dave Parker, Pete Stokes and Mike Smith, who have always been willing to give advice, bake cakes and proof-read the countless document drafts that have been sent their way.

My co-supervisor Dr. Paul Yeo has been invaluable, always taking the time to thoroughly explain the biological background to my experiments so as to minimise my confusion. My thanks to Dr. Matt Burton and James Freeth for working tirelessly to provide me with the many different protein samples I required to complete my project, and to all the members (past, present and honorary) of Lab 229 for supplying cakes, entertainment and procrastination on a regular basis.

Many thanks to our collaborators at AstraZeneca; Dr. Tony Bristow, Martin Sims, Paul Davey and Madeleine Vickers, for providing me with their time, instruments and compounds, all of which have proved to be indispensible to my project.

Last, but by no means least, I am incredibly grateful to my family and friends who have constantly been on hand to offer words of support and encouragement. Special mention should go to Laura, Louise and Rachael for putting up with the madness and to Marie-Hélène for reminding us that there is life after a PhD.

1. Introduction

1.1. Mass Spectrometry

Over the last century the use of mass spectrometry has grown in popularity, performance and functionality, resulting in it becoming an indispensible and informative analytical technique. Mass spectrometry separates and detects sample ions according to their mass-to-charge (*m/z*) ratios, allowing the molecular weight of the observed ions to be calculated and thereby confirming or refuting the identity of expected samples, or helping to identify unknown samples. The first mass spectra were recorded by J. J. Thomson in 1912, detecting atomic and diatomic ions hitting a photographic plate to generate a spectrum of charge-to-mass.[1] Since then, mass spectrometric analysis has advanced exponentially, generating MS data for > 100 kDa biological molecules and generating data that is accurate enough to suggest or confirm elemental composition. Major developments over the last forty years have included the advent of Electrospray Ionisation (ESI) and Matrix-Assisted Laser Desorption/Ionisation (MALDI), two methods of sample ionisation that have revolutionised the MS analysis of macromolecules. Both discoveries resulted in the presentation of the 2002 Nobel Prize for Chemistry to the pioneers John Fenn[2-6] and Koichi Tanaka[7-8] for ground-breaking developments in ESI and MALDI respectively. Other notable accomplishments include the development of high mass accuracy and resolving power MS instruments, such as Fourier Transform-Ion Cyclotron Resonance (FT-ICR)[9] and the Orbitrap mass spectrometer[10], both of which measure the frequency of ion precession within an ion-trapping cell, as opposed to directly measuring the mass-to-charge ratio, allowing ions to be detected with much higher mass accuracy. [11] The high mass accuracy and resolving power capabilities become particularly useful when analysing unknown compounds, complex mixtures or performing tandem mass spectrometry.[12]

The resolving power of an instrument, defined in **Equation 1.1**, is a key performance factor used to describe the ability to separate two ions with a very small mass difference at a defined peak height; where ***R*** is the resolution or resolving power, ***m*** is the mass of the peaks and ***Δm*** is the difference between the maxima of two resolved peaks, shown in **Figure 1.1(a)** to be separated at 10% peak height. Using this definition, an instrument with a resolving power of 100,000 FWHM would be able to fully resolve two peaks with a mass difference of 0.004 Da at *m/z* 400.

$$R = \frac{m}{\Delta m} \qquad \textbf{Equation 1.1}$$

The mass resolution of an isolated peak can also be described by **Equation 1.1**, where ***Δm*** is the peak width at 50% of the peak height, as shown in **Figure 1.1(b)**, known as the full width at half-maximum (FWHM). Using the FWHM definition, a peak at *m/z* 400 detected using an instrument with a resolving power of 100,000 FWHM would have a peak width of *m/z* 0.004 at 50% peak height.[13]

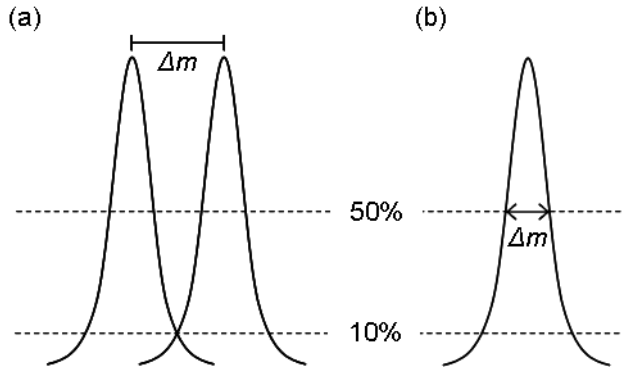

Figure 1.1: Diagram illustrating (a) the resolving power defined as the ability to distinguish between two peaks at a defined peak height and (b) the resolution of an isolated peak.

The mass accuracy of an instrument can have a significant effect on the ability to interpret the resulting mass spectra. Instruments with high resolving power, mass accuracy and precision can be used to predict or confirm the elemental composition of ions from their measured *m/z* ratios, and could distinguish between ions with the same nominal *m/z*, such as CO_2 (*m/z* 43.98928) and CH_3CHO (*m/z* 44.02567). The accuracy of the proposed molecular formula of an ion is quoted in parts-per-million (ppm), and can be determined by calculating the difference between the theoretical *m/z* of the molecular formula and the observed *m/z* using **Equation 1.2** and **Equation 1.3**.[14]

$$\Delta\ m/z = (\text{Observed } m/z) - (\text{Theoretical } m/z) \qquad \textbf{Equation 1.2}$$

$$\text{Accuracy (in ppm)} = \frac{\Delta\ m/z}{\text{Theoretical } m/z} \times 1000000 \qquad \textbf{Equation 1.3}$$

Tandem mass spectrometry, often known as MS/MS or MS^n, increases the amount of elemental and structural information that can be gleaned from a compound of interest by isolating specific ions in the mass spectrometer and increasing the internal energy of the ion in order to induce bond dissociation. The resulting product ions can provide important information regarding the structure of the precursor ion and can be performed on a similar timescale to that of full MS analysis.[15] The vast amount of structural and elemental information that it can provide has resulted in it becoming a well established technique with a wide range of applications in industries including pharmaceutical, agricultural, petroleum, plastics, biochemical, and many more. The hyphenation of chromatography, such as Liquid Chromatography (LC) or Gas Chromatography (GC), with MS/MS furthers the analysis of complex mixtures, including those with components spanning a wide dynamic concentration range, by utilising the benefits gained from chromatographic

separation of compounds prior to ionisation so as to minimise any interference or suppression between compounds. LC-MS/MS analyses are often carried out by alternating MS and MS/MS scans, allowing data to be generated regarding the intact sample ions and the product ions so as to maximise the amount of information that can be acquired during one experiment, reducing the turn-around time for analyses. Typically, the duration of LC peaks is measured over the range of a few seconds, thereby requiring MS/MS techniques capable of operating over a millisecond range.[16-22]

1.2. Collision-Induced Dissociation (CID)

Collision-Induced Dissociation, sometimes referred to as Collision Activated Dissociation (CAD), involves the excitation of sample ions through inelastic collisions with a neutral gas molecule such as helium or argon. Each collisions causes the transfer of energy from the gas to the ion, increasing the internal energy of the ion and creating a vibrationally excited intermediate state.[23-24] The vibrational energy is rapidly redistributed throughout the ion resulting in bond dissociation *via* the lowest energy pathways, breaking the weakest bonds in the molecule. The centre-of-mass collision energy is the maximum amount of energy that can be transferred between the collision gas and the ion, as dictated by the masses and velocities of each. The greater the mass of the collision gas, the greater the amount of energy that can be transferred to the ion, and therefore the centre-of-mass collision energy is increased.[15, 25] Quasi-Equilibrium Theory (QET) explains unimolecular bond dissociation in a high vacuum, stating that energy can be redistributed throughout all available degrees of freedom, such as rotational, electronic, vibrational and translational motion, making each microscopic state for the molecular ion equally possible. Additionally, QET states that the energy barrier between the precursor ion and product ions is unidirectional, therefore the bond dissociation is irreversible.[23, 26] The tendency for CID to follow the lowest energy

fragmentation pathways in the molecule often impedes structural characterisation, by preferentially cleaving certain weak bonds in the precursor ion and providing limited information.[27] Altering certain instrumental factors such as the collision gas or type of mass analyser can have a significant effect on the resultant product ion spectra. By using argon instead of helium, the size and mass of the neutral gas molecule is increased, resulting in greater centre-of-mass collision energy and therefore more energy transferred to the precursor ions upon collision, potentially increasing the allowed fragmentation pathways by permitting dissociation *via* higher energy routes.[15] Collision cells allow ions to travel the length of the cell through the collision gas prior to detection, allowing the possibility of multiple collisions, multiple bond cleavages and secondary product ion fragmentation (akin to MS^n). Conversely, ion/neutral collisions in ion traps result in less stable product ions that are ejected from the trap, reducing the probability of multiple collisions.[28] Although not as common, CID can be performed in the FT-ICR cell, a technique known as Sustained Off-Resonance Irradiation Collision-Induced Dissociation (SORI-CID), which requires the introduction of a collision gas into the FT-ICR cell. SORI-CID involves the excitation of the precursor ion at an RF voltage marginally above or below the ion cyclotron frequency. This off-resonance excitation causes the kinetic energy and the radius of ion motion to oscillate, and results in collisions between the precursor ion and the collision gas. The product ions generated by the collisions relax towards the centre of the FT-ICR cell until they can be detected. SORI-CID is not commonly used due to the disruption caused to the high vacuum system as the collision gas is introduced into the cell, requiring additional time to remove the collision gas and re-equilibrate the vacuum prior to ion detection, typically 2 - 3 seconds, which drastically increases the scan time.[25]

1.3. Infrared Multiphoton Dissociation (IRMPD)

Infrared Multiphoton Dissociation is a method of photodissociation that uses an infrared laser, for the purpose of this project a CO_2 laser of wavelength 10.6 μm, to increase the internal energy of trapped ions to create a vibrationally excited state that releases energy *via* bond dissociation. The laser introduces photons that are absorbed by the ion(s) of interest, each of which corresponds to 0.117 eV of energy, as calculated using Planck's equation detailed in **Equation 1.4**; where **h** represents Planck's constant (4.136×10^{-15} eV s^{-1})†, **c** is the speed of light (3×10^{-8} m s^{-1}) and **λ** correspond to the wavelength of the laser (10.6×10^{-6} m).

$$E = \frac{hc}{\lambda} \qquad \textbf{Equation 1.4}$$

Each absorbed photon contributes towards the stepwise activation of the ion gradually increasing the vibrational energy of the ion until it reaches its excited state. In order for bond dissociation to occur, the rate of energy absorption must be faster than the redistribution of energy throughout the ion. Once the internal energy increases beyond the lowest energy bond dissociation threshold, the rapid internal vibrational energy redistribution results in the cleavage of the weakest bonds. IRMPD does not require the presence of a collision gas in order to induce fragmentation, and therefore can be carried out in an FT-ICR cell without the loss of resolution caused by introducing a collision gas and disrupting the vacuum in the cell.[15, 29-31]

† Planck's constant is often expressed as 6.626×10^{-34} J s^{-1}; 1 J is equal to 6.241×10^{18} eV.

1.4. Electron Capture Dissociation (ECD)

Electron Capture Dissociation is a recent development in the field of MS/MS, pioneered by Zubarev*, et al.*,[32] that utilises low energy electrons for the fragmentation of multiply charged biological molecules such as peptides or proteins. It involves the interaction of electrons, 1-5 eV, with the multiply charged cations $[M+nH]^{n+}$, resulting in the capture of an electron and creating an unstable hypervalent $[M+nH]^{(n-1)+\bullet}$ species. The generation of this electronically excited odd-electron intermediate differentiates this technique from CID and IRMPD, and alters the internal bond energies that affect the subsequent bond dissociation.[33-34] Unlike CID and IRMPD, ECD product ions are no longer necessarily formed from the dissociation of the weakest bonds in the precursor ion, and therefore can provide complementary information to CID and IRMPD. Although the capture of an electron is a rapid process, longer irradiation times are required for ECD in order to promote the interaction between the narrow electron beam and the ion cloud.[15, 34] The poor overlap between the electron beam and the ion cloud results in comparatively low fragmentation efficiency, however ECD has often been found to generate a higher degree of sequence coverage than the vibrational techniques.[35] Studies have shown that weak or covalently bound modifications, which would typically be lost by vibrational excitation techniques, tend to be retained by ECD allowing for their identification and location.[32, 36-43] ECD is almost exclusively used with FT-ICR instruments due to their ability to trap electrons in the cell.[44] This combination provides the added advantage of allowing product ions to be measured to a high degree of accuracy, allowing potential molecular formulae to be generated for the observed peaks. ECD experiments are predominantly used with large biomolecules, such as protein and peptides, due to their tendency to form multiply charged molecular ions.

1.5. Proteins and Peptides Analysis

In the field of proteomics, MS and MS/MS analysis have become necessary and valuable tools for polypeptide sequencing, due to the high sensitivity and speed of analysis and the ability to generate a series of product ions following predictable fragmentation patterns. **Figure 1.2** details the existing nomenclature for peptide backbone cleavages, with N-terminal product ions labelled *a*, *b* and *c*, and C-terminal containing product ions labelled *x*, *y* and *z*.[45-48]

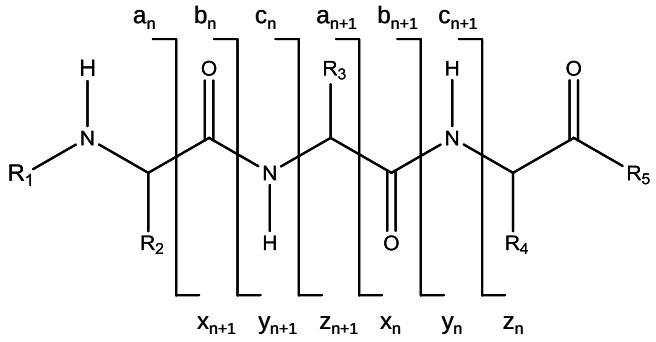

Figure 1.2: Common peptide backbone cleavages and their corresponding assignments.

MS/MS sequencing of peptides and proteins can be carried out by one of two approaches; the 'bottom-up' method or the 'top-down' method. The bottom-up approach involves proteolytic digestion of the protein of interest in order to form smaller peptides. The resultant peptide spectrum is known as a peptide mass-fingerprint, which can be used to identify or confirm the initial protein by database searching or comparison with an *in silico* digest. Performing MS/MS on tryptic peptides can identify or confirm a high degree of the amino acid sequence and pinpoint sequence modifications to the polypeptide. Bottom-up proteomics reduces any solubility issues involved with hydrophobic proteins, as smaller proteolytic peptides may be more soluble than the intact protein, and prevents any conformational hindrances.[49-51] Top-down proteomics involves performing MS/MS

on the intact polypeptide, eliminating the need for time-consuming protein purification and digestion experiments. The energy transferred during MS/MS can dissipate through more degrees of freedom, reducing the efficiency of fragmentation and resulting in poorer sequence coverage. Fragmentation of the intact protein is also affected by the secondary and tertiary protein conformations, the amino acid backbone folding and the three-dimensional structure of an intact protein molecule respectively, which may prevent bond dissociation in areas of the protein due to steric hindrance.[42, 51-54] Modifications to the polypeptide sequence, such as phosphorylation, may alter the tertiary structure of the ion in the gas phase, subsequently affecting intramolecular bonding. As a result, when conducting top-down proteomics the product ion spectrum from the modified species may differ to the product ions generated from the unmodified polypeptide.[39]

MS/MS analysis of polypeptides by CID or IRMPD, results in cleavage of the weakest bonds in the amino acid sequence, the CO-NH peptide bond, creating a series of *b* and *y* ions (see **Figure** 1.2).[55] Additionally, CID and IRMPD have the tendency to cleave labile covalently-bound modifications on proteins and peptides, hindering the identification and location of such modifications. The predictable fragmentation patterns generated by the CID of peptides and proteins allows for the identification or confirmation of the polypeptide amino acid sequence. As the molecular weight of the targeted polypeptide increases, the efficiency of CID analysis decreases due to the redistribution of energy through more degrees of freedom, therefore more energy is required to generate the same degree of fragmentation.[56] The number of charges on the precursor ion has been shown to significantly effect the resulting CID spectrum, with increased energy and greater instability associated with higher charge states of the precursor ion resulting in a higher degree of fragmentation and sequence coverage.[57-58]

Analysis of polypeptides by ECD has been found to generate a high degree of amino acid sequence coverage, while also retaining any labile modifications.[32] Using high mass accuracy MS instruments to calculate the empirical formulae of the product ions can confirm or suggest chemical formulae and structural assignments for each product ion, facilitating the identification of unknown modifications or mutations on the polypeptide. Whereas CID and IRMPD predominantly result in the dissociation of the peptide bond to form *b*/*y* ions, the major fragmentation pathway observed from ECD involves the homolytic cleavage of the N-C_α bond, resulting in radical site migration and creating an even-electron ***c'*** ion and an odd-electron $z^{\cdot}$ ion.[32] Hydrogen migration prior to bond dissociation is a common occurrence in ECD, producing odd-electron $c^{\cdot}$ ions and even-electron ***z'*** ions.[59-60] In addition to the backbone cleavages, ECD has been shown to preferentially dissociate disulphide bridges within the polypeptide.[33, 46, 61] The data generated by ECD has been shown to be complementary to data produced by vibrational excitation techniques such as CID and IRMPD due to the differences in preferred bond cleavages.[62-63] The cyclical nature of the proline amino acid inhibits the formation of the expected product ion formed *via* the N-C_α bond cleavage, as shown in **Figure 1.3**, therefore the number of proline components in a polypeptide sequence will limit the achievable sequence coverage by ECD. The effect of proline residues on CID and IRMPD spectra is very different from ECD. Firstly, since CID and IRMPD cleave the peptide bonds, sequence coverage is unaffected by the cyclical proline residues. Secondly, the high proton affinity associated with proline promotes protonation at these residues and results in increased probability of cleavage at the proline N-terminus.[36, 46, 64-66]

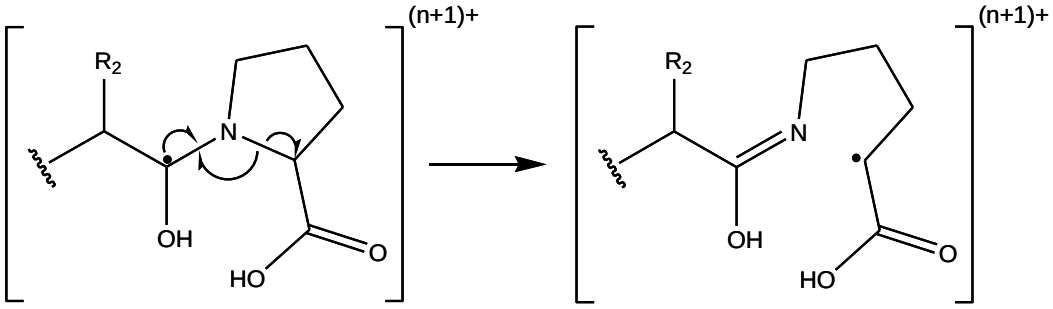

Figure 1.3: Mechanism of bond cleavage resulting from the ECD of proline.

There are two mechanisms which have been postulated to account for ECD bond dissociation; The Cornell method, or the 'Hot Hydrogen' method, posits that the electrons target one of the positively charged sites on the peptide, neutralising the charge and creating a hypervalent radical. This results in the ejection of a mobile hydrogen radical which is expected to traverse the peptide backbone and attack an oxygen of the peptide bond. This in turn causes the dissociation of the neighbouring N-C_α bond, as shown in **Figure 1.4**.[36-37]

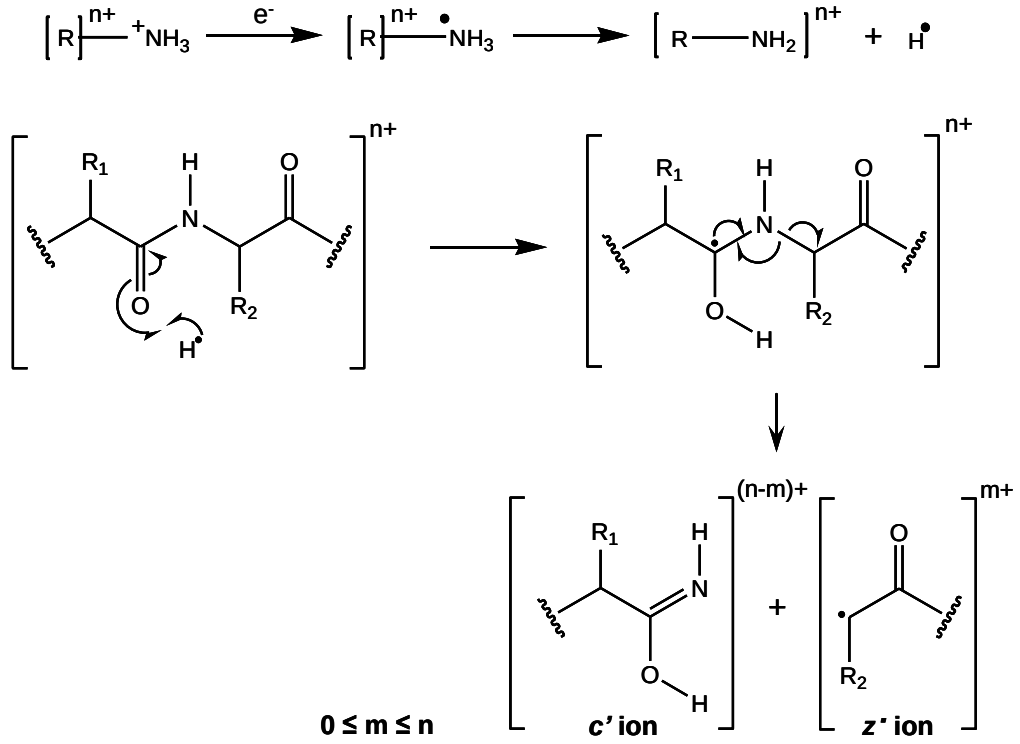

Figure 1.4: Fragmentation mechanism postulating electron capture at the protonated nitrogen atom.[36]

A mechanism for the dissociation of disulphide bonds has also been suggested by this method, proposing that the hydrogen radical can also attack the S-S bond and resulting in homolytic cleavage to form an S$^{\bullet}$ containing product and an SH containing fragment, as shown in **Figure 1.5**.

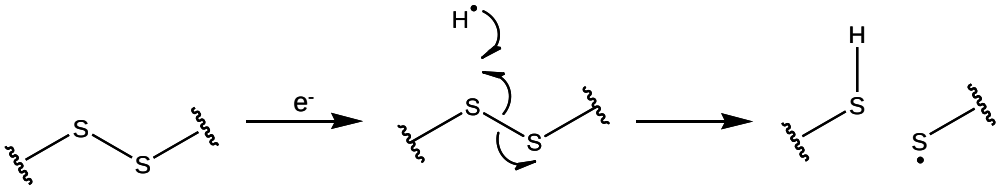

Figure 1.5: Proposed mechanism for the dissociation of disulphide bridges *via* the capture of a hydrogen radical.[36]

The Cornell method sufficiently explains the cleavage of the stronger N-C_{α} bond instead of the weaker peptide bond, however more recent experiments have cast doubts on the mobile hydrogen mechanism due to the large distances the hydrogen atom would be required to travel between protonation sites and the sites of bond cleavage. The second proposed fragmentation mechanism, called the Utah-Washington method or 'Superbase' method, alternatively suggests that the hypervalent radical centre induces intramolecular electron transfer to the site of bond cleavage or that the electron is captured directly at the cleavage site. **Figure 1.6** depicts the capture of the electron at the carbonyl group to form a radical anionic centre that subsequently reacts to dissociate the neighbouring N-C_{α} bond and neutralise the negative charge *via* a proximal H^{+}.[67-70]

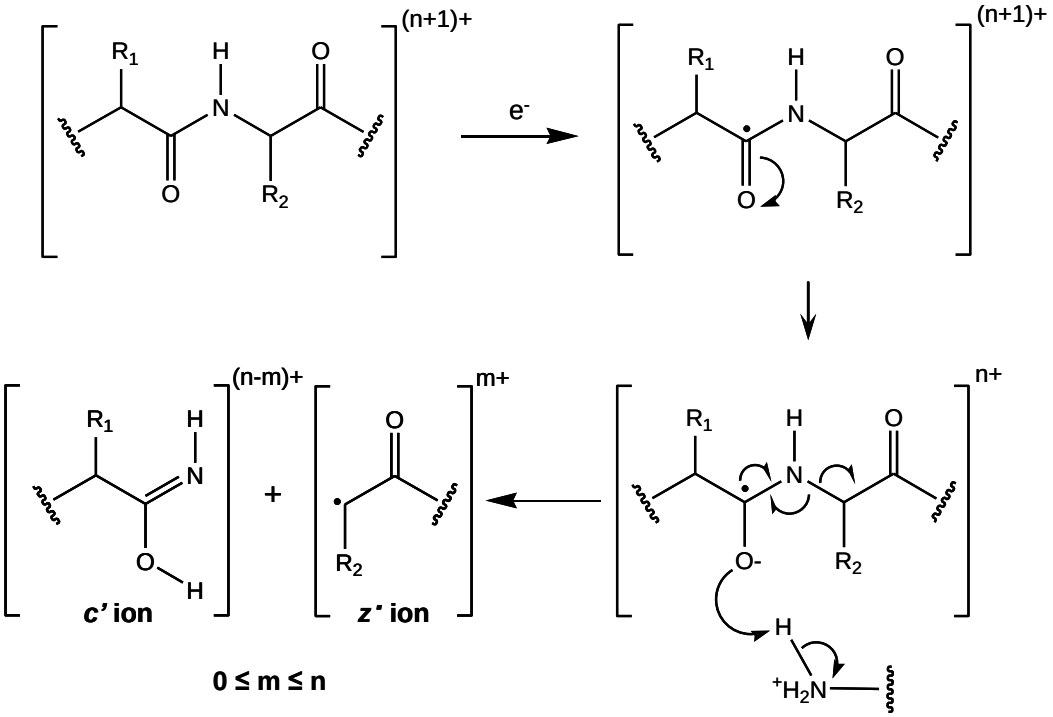

Figure 1.6: Fragmentation mechanism postulating capture of an electron at the carbonyl group, leading to dissociation of the N-C_α bond.[67, 71]

A similar mechanism is postulated for the dissociation of disulphide bridges by ECD, whereby the electron is captured by the S-S bond, breaking the bond to form a $S^{\bullet}$ containing fragment as well as an S^- containing fragment that subsequently reacts with a proximal H^+, as shown in **Figure 1.7**.

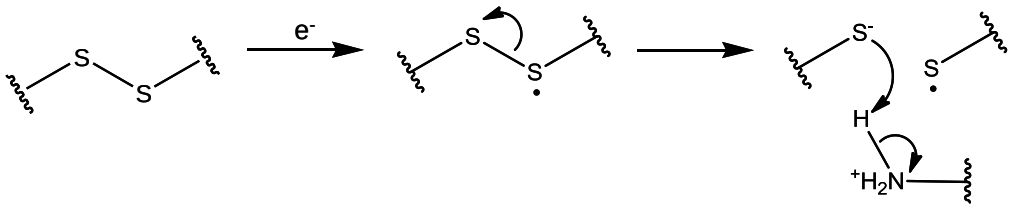

Figure 1.7: Proposed mechanism for the dissociation of disulphide bridges following the Utah-Washington method.[67, 71]

While the *c*/*z* product ions are the most commonly observed fragments in ECD spectra, they are not the only observed cleavage. Investigations into the use of ECD have noted that cleavage of the peptide bond to form *b*/*y* ions or the cleavage

of the C_α-CO and CO-NH bonds to form $a^{\bullet}/y$ ions (involving the neutral loss of CO) may also be observed. The observation of product ions usually generated by vibrational excitation techniques would suggest that ECD results in both the electronic excitation and vibrational excitation of the precursor ion.[36, 38, 46, 72-73]

At higher electron energies, beyond 5 eV, the technique becomes known as hot ECD (or hECD). This increase in energy has been found to be sufficient to induce secondary fragmentation, creating product ions from amino acid side chain losses in addition to the typical *a*, *b*, *c*, *y*, *z*, ions.[38, 46, 72, 74-76] This secondary fragmentation has been shown to provide valuable information regarding the polypeptide backbone, including being able to distinguish between the isobaric amino acids, leucine and isoleucine. The mechanisms suggested by Kjeldsen *et al.* propose the formation of *w* ions from the subsequent side-chain cleavages from $z^{\bullet}$ ions with terminal leucine or isoleucine residues, as shown in **Figure 1.8**, and suggest the possibility of *d* ions produced from $a^{\bullet}$ ions in a similar manner.[34, 72] This theory does not take into account the possibility of rearrangement within the intermediate fragment ion, initiated from the radical centre and resulting in side-chain fragmentation independent of the primary dissociation site.[76-78] The increase in electron energy has been shown to have an adverse effect on the S/N of the product ion spectra, a pattern which is thought to be due to the higher kinetic energies of the product ions and the diffusion of the ion cloud from higher energy collisions.[72]

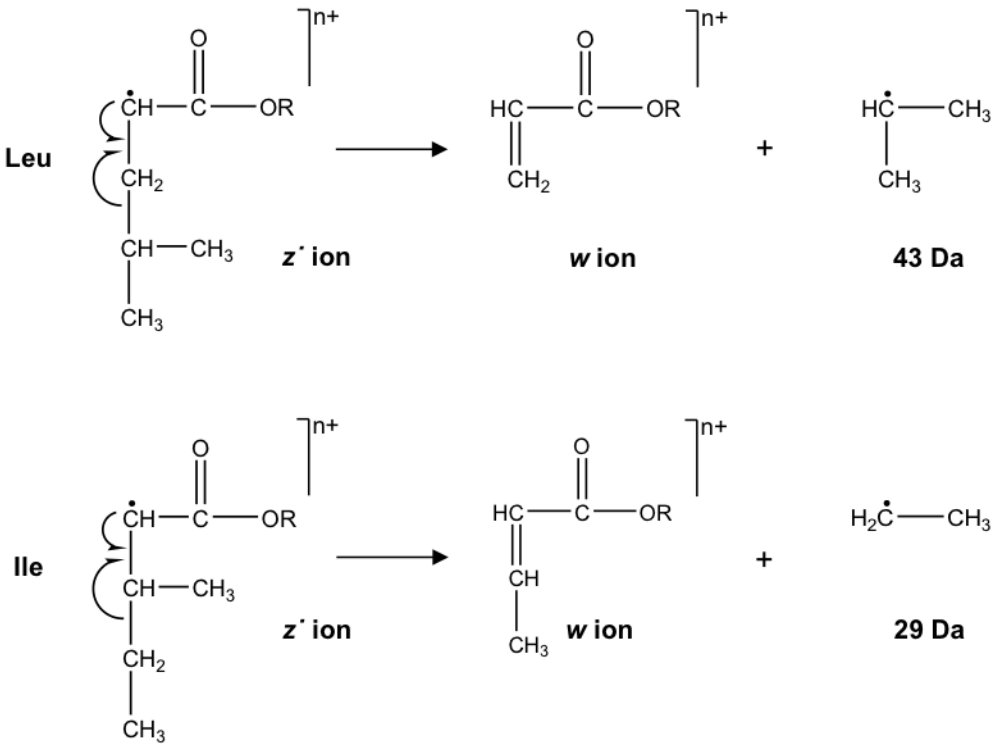

Figure 1.8: Proposed mechanism for the formation of *w* ions from the intermediate *z˙* ions of leucine (top) and isoleucine (bottom).

As with CID, increasing the molecular weight of the targeted polypeptide has been found to decrease the ECD efficiency. The structural conformation of proteins is thought to play a part in the decreased efficiency as intramolecular non-covalent bonds are formed to stabilise the secondary and tertiary structure of the protein, thus hampering the effect of ECD in the field of top-down proteomics. To overcome these barriers, activated ion ECD (AI ECD) was developed, using CID or IRMPD to help break the non-covalent bonds and vibrationally excite the protein before using ECD to dissociate the protein backbone. Results have shown that the combination of two MS/MS techniques can generate extensive terminal sequencing without the need for proteolytic digestion, however the central portion of the protein remains largely intact.[46, 52-54, 79-80]

The charge state of the precursor ion has been found to play an important role in the resulting product ion. Higher charge states are affected by increased coulombic repulsion within the molecule making them less stable and therefore fragment more readily, however the product ion spectrum generated tends to be more complicated due to the multiple charge states that each product ion may form. In addition, the increased number of charges on the molecule reduces the probability of a neutral fragment being formed. Conversely, a lower charge state precursor ion may not fragment as effectively as a higher charge state, however the number of charge states available to the product ions are reduced and therefore the product ion spectrum is simplified.[60, 72]

Further developments into using electrons to induce bond dissociation resulted in the technique Electron Transfer Dissociation (ETD) that, unlike ECD, does not require an expensive FT-ICR mass analyser and can be carried out on other, less expensive mass analysers, such as quadrupoles or ion traps. ETD utilises anionic molecules with low electron affinities, typically aromatic compounds such as fluoranthene or benzoic acid that can form odd-electron species capable of donating an electron to the multiply charged precursor ions to form an odd-electron species, initiating bond dissociation similar to ECD.[81-82] As with ECD, ETD predominantly forms *c* and *z* ions from the MS/MS of multiply charged polypeptides while retaining labile modifications on the protein backbone.[83] The energy transfer between the ion/ion interactions is lower than the ion/electron energy transfer undergone by ECD, due to collisonal cooling or energy redistribution throughout the anionic species prior to electron transfer, therefore the resulting fragmentation tends to be less efficient.[78, 84] Despite the reduced energy transfer, ETD has been shown to generate significant amino acid sequence coverage, providing significant polypeptide information.[85]

Thus far, electron capture-induced bond dissociation has primarily focused on positively charged ions, however Håkansson *et al.* have been developing ECD for the analysis of negatively charged precursor ions, termed negative ion ECD (niECD), which has been shown to generate the charge-increased $[M\text{-}nH]^{(n+1)-\bullet}$ species from electron capture by the $[M\text{-}nH]^{n-}$ precursor. Electron energies required for niECD were found to be slightly higher than ECD, at around 3.5 – 6.5 eV, and resulted in backbone cleavages analogous to ECD.[86] Increasing the electron energy even further, beyond 10 eV, has been found to generate fragmentation *via* the ejection of an electron from the precursor ion, forming the charge-reduced $[M\text{-}nH]^{(n-1)-\bullet}$ species. This technique, known as Electron Detachment Dissociation (EDD), generates a radical anionic centre that can initiate bond dissociation. The radical 'hole' created from electron detachment is proposed to move along the polypeptide backbone *via* neutralisation with an electron. The electron-hole recombination process results in electronic excitation of the precursor ion, which induces bond cleavage. The major product ions observed by EDD occur from the homolytic cleavage of the N-C_α bond to create *c*, *z* and $a^\bullet$ ions, the latter formed *via* loss of a neutral CO_2 in a method akin to ECD. Cleavage of the C_α-C bond has also been observed, generating the complementary $a^\bullet$ and *x* product ion series. Further similarities between EDD and ECD include secondary fragmentation resulting from radical-initiated side-chain cleavages.[34, 87-89]

1.6. Small Molecule Analysis

The MS and MS/MS analysis of biological molecules is a widely researched field that contributes towards a high proportion of published material, however it is not the only useful application. The analysis of small organic molecules is an important aspect of drug development in the pharmaceutical industry and has become a key area for the use of mass spectrometry. Mass spectrometry is commonly used to provide rapid elemental and structural confirmation, reaction monitoring and

identification of unknown compounds. MS/MS of small organic molecules tends not to follow systematic fragmentation patterns or rules due to the lack of a regular or predictable chemical structure that governs polypeptides. Functional groups present in the molecule can severely influence dissociation behaviour due to factors such as their electron-donating or electron-withdrawing properties, their influence on bond lengths and energies, and their ability to stabilise the charge or an unpaired electron.[90-91] As a result, the MS and MS/MS analysis of small molecules often involves unpredictable decomposition reactions, however certain observations and proposals have been made regarding commonly detected bond cleavages and proposed fragmentation mechanisms. MS/MS is typically carried out on even-electron molecular ions, such as $[M+H]^+$ or $[M-H]^-$, formed by electrospray or other atmospheric pressure ionisation techniques. A proposed guideline regarding fragmentation patterns of even-electron species, known as the parity rule or the even-electron rule, states that it is more favourable for an even-electron precursor ion to fragment *via* the loss of a neutral molecule to form an even-electron product ion than it is to lose an odd-electron radical to form an odd-electron product ion. This preference is suggested due to the inherent stability of even-electron species compared with odd-electron species, and the high energy required to split an electron pair.[92-93] More recent studies into the MS/MS of small organic molecules have suggested that while the formation of even-electron product ions by CID-MS/MS is extensive, odd-electron species are often observed due to the formation of stable radical species or low-energy intermediates. Aromatic compounds have been found to stabilise an unpaired electron, often creating a more stable species than the even-electron equivalent, resulting in a higher probability of forming odd-electron product ions.[94-95] Levsen *et al.* carried out an in-depth study into the analyses of protonated and deprotonated aromatic compounds containing functional groups such as carboxylic acids, alcohol groups, nitro-containing groups and halogens. CID MS/MS of the range of compounds noted a high probability for the

elimination of key functional groups to form stable neutral species; such as CO_2, NO_2, H_2O, SO_2, HX (X = halide) radical species; such as $H^{\bullet}$, $CO^{\bullet}$, $NO^{\bullet}$, $OH^{\bullet}$, $NH_2^{\bullet}$, $X^{\bullet}$, or charged species; such as SO_3^{-}, PO_3^{-}, $H_2PO_4^{-}$.[90-91] Other common cleavages include cleavages at carbon-heteroatom bonds, so that the heteroatom can stabilise the charge and/or radical.[94]

Small molecule analysis can also be carried out using Electron Ionisation (EI), an ionisation technique typically used on small (< 1 kDa) volatile molecules that interacts high energy (70 eV) electrons with the neutral molecules to be analysed. The energy of the electrons is much higher than the ionisation potential of the molecule being analysed, resulting in the ejection of an electron from the neutral species to form an odd-electron radical cation, as shown in **Scheme 1.1**.

$$\mathbf{M + e^-_{high} \rightarrow M^{+\bullet} + 2e^-} \qquad \textbf{Scheme 1.1}$$

The high energy transferred from the electrons to the ionised molecules increases the internal energy of the subsequent molecular ion, which combined with the increased instability of the odd-electron species often results in bond dissociation to form more stable fragment ions. Bond dissociation can occur *via* two methods; Firstly, homolytic cleavage, or radical-site initiated cleavage, which involves the migration of unpaired electrons to form an odd-electron radical cation and a neutral molecule, as shown in **Figure 1.9(a)**. The presence of heteroatoms or double bonds in the molecular ion promotes the homolytic cleavage, resulting cleavage at the α-β bond position. Secondly, heterolytic cleavage, otherwise known as charge-site initiation or inductive cleavage, which involves charge migration to form an even-electron cation and a neutral radical, as shown in **Figure 1.9(b)**.

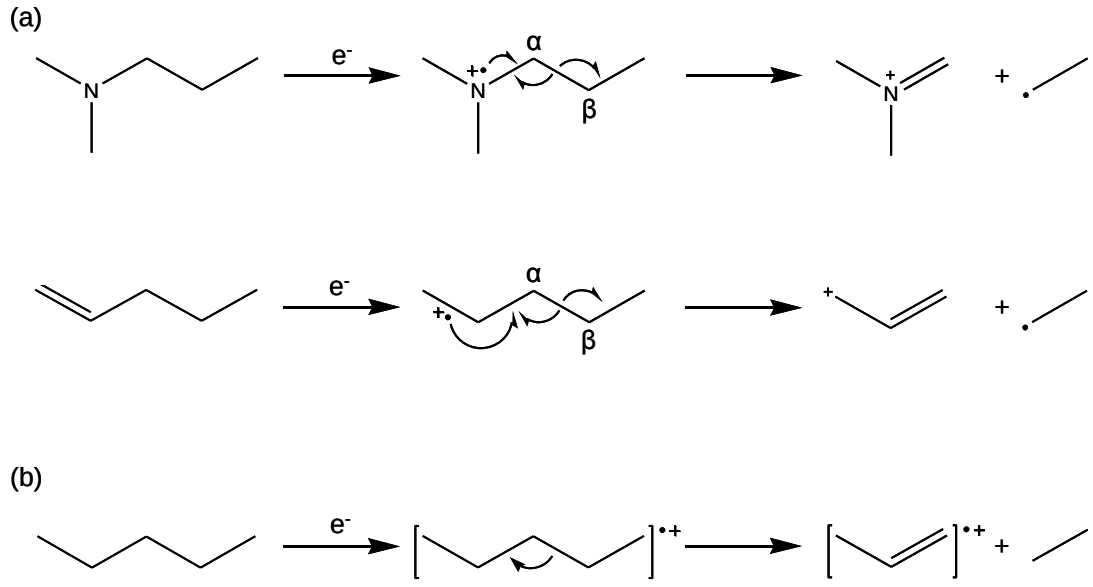

Figure 1.9: Examples of (a) homolytic α-β bond cleavages and (b) heterolytic bond cleavages.

The charge-site on the molecular ion can have a significant effect on the major fragmentation pathways, due to the influence of the charge on the length of neighbouring bonds.[96] The charge-site can act as an electron-withdrawing group, generating a slight negative charge on the neighbouring atoms, which in turn causes the α-β bond to lengthen thus making it more susceptible to bond cleavage. Conversely, the presence of an electron-donating group would contract the α-β bond and therefore alter the preferred bond cleavage. Other factors proposed to affect the fragmentation pathways of small molecules include the size of the molecular ion, steric hindrance effecting intramolecular rearrangement, bond angles or the stability of the intermediate and/or product ions.[97]

Similarities have been noted between EI MS and MS/MS, most notably the frequent neutral losses of specific functional groups, and the ability for each molecular ion to form odd-electron and even-electron fragment ions, therefore it is possible to generate the same fragment ion from each technique. Bond dissociation *via*

rearrangement reactions are common occurrences, both by EI MS and MS/MS, proceeding *via* the formation of more stable intermediates and therefore requiring less energy to overcome the transition-state energy barrier between the molecular ion and the fragment ion.[91] The McLafferty rearrangement, shown in **Figure 1.10**, is a common rearrangement for compounds capable of forming cyclical intermediates, resulting in migration of the γ-hydrogen and α-β bond cleavage.[98-99]

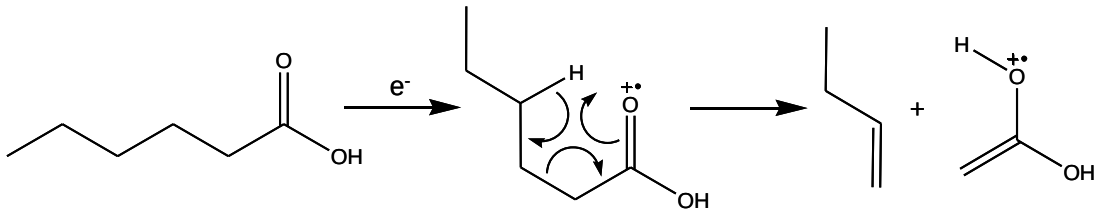

Figure 1.10: McLafferty rearrangement of a long chain carboxylic acid.

The high stability of cyclic structures, in particular aromatic rings, makes cross-ring cleavages less likely, although still possible, using CID MS/MS due to the tendency for CID to follow the lowest energy fragmentation pathways and therefore breaking the weakest bonds in the molecule. This may result in difficulties determining structural differences in analogous molecules, where the major fragmentation pathways provide limited information about the minor structural differences, such as the location of substituents around a ring. An in-depth study carried out by Niessen, investigated CID MS/MS of a range of protonated drug compounds, noted product ions resulting from cleavages across saturated cyclic groups, however no fragmentation was observed across aromatic groups.[94] Bond cleavages within unsaturated cyclical groups are far more likely by EI, due to the stabilisation of the unpaired electron by the ring and the high energy imparted on the molecule upon ionisation. The presence of an unpaired electron in an aromatic ring results in the disruption of the aromaticity, thereby increasing the probability of radical-site

initiated fragmentation within the ring or rearrangement in order to form a more stable ion.[90, 100]

1.7. Electron-Induced Dissociation (EID)

Electron-Induced Dissociation (EID) is recent development in the field of MS/MS that has roots originating in Electron Impact Excitation of Ions from Organics (EIEIO) and ECD. EIEIO was first introduced in the 1970s as an alternative to photodissociation spectroscopy (PDS) and CID, utilising the trapping ability of ICR instruments to interact compounds with a continuous electron beam. Neutral molecules were ionised by electrons of greater energy than their ionisation potential, essentially Electron Ionisation (EI) as shown in **Scheme 1.1**, to generate a singly charged radical cationic species ($M^{+\bullet}$) before subsequently reducing the energy of the electron beam to electronically excite the molecular ion and induce bond dissociation, as shown in **Scheme 1.2**. Comparisons with CID noted that while some product ions were common to both techniques, EIEIO and CID could each generate product ions not observed by the other, thought to result from differences in energy excitation; whether vibrational, rotational or electronic.[101-106]

$$\mathbf{M^{+\bullet} + e^-_{low} \rightarrow M^{+}*} \qquad \textbf{Scheme 1.2}$$

Subsequent developments in using electrons to induce bond dissociation include the increasingly prevalent MS/MS technique ECD, involving the interaction between low energy electrons (~5 eV) with multiply protonated species leading to electron capture followed by bond dissociation.[36, 71] Further progress in this field introduced the technique known as Electron Excitation Dissociation (EED), a two-step process that combines the experimental concepts from EIEIO and ECD to create an MS/MS method capable of fragmenting singly charged even-electron cations, such as $[M+H]^+$, generated by atmospheric ionisation techniques. High energy electrons,

between 10 eV and 70 eV, were required to induce secondary ionisation of the $[M+H]^+$ precursor by ejecting an electron from the precursor ion to generate the $[M+H]^{2+\bullet}$ species, as shown by **Scheme 1.3**.

$$[M+H]^+ + e^-_{high} \rightarrow [M+H]^{2+\bullet} + e^-_{low} + e^-_{high} \qquad \textbf{Scheme 1.3}$$

The low energy electrons that were ejected from the precursor ion were then reflected back into the FT-ICR cell where they recombined with the doubly charged radical cation to generate the singly charged electronically excited $[M+H]^{+}*$ species, as shown by **Scheme 1.4**.

$$[M+H]^{2+\bullet} + e^-_{low} \rightarrow [M+H]^{+}* \qquad \textbf{Scheme 1.4}$$

EED of singly protonated peptides noted the presence of *b*, *c*, *y* and *z* ions in the resulting MS/MS spectrum, indicating a correlation between EED and ECD. When the reflection of the low energy electrons was removed, only *b* and *y* ions were evident in the product ion spectrum, thought to result from the vibrational excitation of the $[M+H]^+$ species initiated from the high energy electrons. However, when the low energy electrons were recombined with the $[M+H]^{2+\bullet}$ species to create the electronically excited state, *c* and *z* ions were observed in addition to the *b* and *y* ions, thus suggesting that the mechanism of fragmentation is dependent on the type of excitation occurring and that vibrational excitation and electronic excitation fragmentation pathways are both capable from electron irradiation.[107-108] Minor adaptations to the EED method have resulted in the evolution of EID, a single-step technique that uses electrons of approximately 10 – 20 eV in order to directly induce fragmentation in singly charged species.[109] EID can be performed on an FT-ICR instrument using a pre-existing ECD setup, simply increasing the energy applied to the electron dispenser cathode beyond what is typical for ECD. The EID product ion

spectra have shown striking similarities to both ECD and EED, such as the observation of odd-electron and even-electron species, and the observation of product ions resulting from both vibrational excitation and electronic excitation. Investigations involving the EID of singly charged peptides noted that the product ions generated by EID closely resembled those that would be expected from the ECD of the corresponding multiply charged species, namely *a*, *b*, *y*, *c*, and *z* ions.[110-113] The similarities between the product ions generated by EID and ECD would suggest a similarity in the mechanism of bond dissociation, however the capture of an electron by a singly charge species would result in charge neutralisation. Following the proposed EED mechanisms, high energy electrons would cause secondary ionisation of the precursor; however this alone would not necessarily result in bond dissociation without further energy input. Should the formation of EID product ions follow this route, it would imply that further interaction between the $[M+H]^{2+\bullet}$ species and the electrons occurs prior to fragmentation. Ly *et al.* noted the presence of doubly charged product ions from a singly charged precursor, suggesting the loss of a neutral moiety from the $[M+H]^{2+\bullet}$ species.[111] The observation of product ions expected from vibrational excitation techniques suggests that either the electrons are able to impart vibrational energy on the trapped ions in addition to electronic energy or rapid energy conversion from electronic to vibrational occurs within the precursor ion prior to fragmentation.[112] The evidence thus far indicates that EID of singly charged cations follows competing fragmentation pathways, resulting in varied and informative product ion spectra. A notable feature of EID fragmentation is the presence of product ion multiplets; peaks differing by 1 Da that correspond to species with the same elemental composition save for the number of hydrogen atoms. This mixture of odd-electron and even-electron species suggest that rapid migration or rearrangement of hydrogen radicals occurs prior to fragmentation.[59, 113]

Recent advances have involved the application of EID to non-peptidic compounds, such as cationic clusters,[114-115] metal-ligand complexes,[116-117] amino acids,[113, 118] metal-bound fatty acids[119] and inorganic metallo-porphyrins.[120] With the structural uniformity present in polypeptides no longer a factor, the method and effectiveness of the technique would be expected to change, however several common features have become evident. EID is still shown to generate both odd-electron and even-electron species upon fragmentation of a singly charged cation, and often results in product ion multiplets resulting from $H^{\bullet}$ migration. Furthermore, doubly charged product ions are generated from the EID of the singly charged precursor, further indicating that bond dissociation occurs *via* electron ionisation. EID product ions also observed by CID confirm the competing vibrational and electronic excitation pathways; however a variation in product ion abundances between techniques has been observed, suggesting that the preferred fragmentation pathways vary for each MS/MS technique. Data gathered from EID has been shown to be complementary to CID and IRMPD, with the effectiveness of each technique varying depending on the targeted compound its charge state, thereby indicating that employing EID in conjunction with other MS/MS techniques would vastly increase the amount of structural information available.

Negative ion EID has thus far been carried out on singly deprotonated peptides,[121-122] metabolites[123] and carbohydrates[124] demonstrating the validity of this technique for a wide range of compounds. As with positive ion analysis, anionic MS/MS has noted significant similarities between EID and the multiply charged equivalent EDD. The EID of the $[M-H]^-$ species of acidic peptides generated *a*, *b*, *c*, *x*, *y* and *z* ions, including both odd-electron and even- electron species, while retaining covalently bound modifications such as phosphorylation or sulphonation.[121] The extensive side chain fragmentation also observed parallels the cross-ring fragmentation generated from the EID analysis of metabolites and carbohydrates, and increases the amount

of structural information available. Håkansson *et al.* noted significant variations in product ion spectra when the applied electron energy was altered; at lower energies the degree of fragmentation declined whereas at higher energies the spectrum quality deteriorated as both the precursor ion and product ion intensities dropped. An optimal energy range was established between 15 – 20 eV, however for energies outside this range the electron irradiation times could be altered to improve the resulting product ion spectra.[123]

1.8. References

1. McLafferty, F.W.: A Century of Progress in Molecular Mass Spectrometry *Annu. Rev. Anal. Chem.* **2011,** *4*, 1-22

2. Fenn, J.B.: Ion Formation from Charged Droplets - Roles of Geometry, Energy, and Time *J. Am. Soc. Mass Spectrom.* **1993,** *4*, 524-535

3. Fenn, J.B., Mann, M., Meng, C.K., Wong, S.F., Whitehouse, C.M.: Electrospray Ionization for Mass-Spectrometry of Large Biomolecules *Science* **1989,** *246*, 64-71

4. Whitehouse, C.M., Dreyer, R.N., Yamashita, M., Fenn, J.B.: Electrospray Interface for Liquid Chromatographs and Mass Spectrometers *Anal. Chem.* **1985,** *57*, 675-679

5. Yamashita, M., Fenn, J. B.: Negative Ion Production with the Electrospray Ion Source *J. Phys. Chem.* **1984,** *88*, 4671-4675

6. Yamashita, M., Fenn, J.B.: Electrospray Ion Source - Another Variation on the Free-Jet Theme *J. Phys. Chem.* **1984,** *88*, 4451-4459

7. Abate, R., Ballistreri, A., Montaudo, G., Garozzo, D., Impallomeni, G., Critchley, G., Tanaka, K.: Quantitative Applications of Matrix-Assisted Laser-Desorption Ionization with Time-of-Flight Mass-Spectrometry - Determination of Copolymer Composition in Bacterial Copolyesters *Rapid Commun. Mass Spectrom.* **1993,** *7*, 1033-1036

8. Tanaka, K., Waki, H., Ido, Y., Akita, S., Yoshida, Y., Yoshida, T., Matsuo, T.: Protein and Polymer Analyses Up to *m/z* 100 000 by Laser Ionization Time-of-Flight Mass Spectrometry *Rapid Commun. Mass Spectrom.* **1988,** *2*, 151-153

9. Marshall, A.G., Roe, D.C.: Theory of Fourier-Transform Ion Cyclotron Resonance Mass Spectroscopy: Response to Frequency-Sweep Excitation *J. Chem. Phys* **1980,** *73*, 1581-1590

10. Hu, Q., Noll, R.J., Li, H., Makarov, A., Hardman, M., Graham Cooks, R.: The Orbitrap: A New Mass Spectrometer *J. Mass Spectrom.* **2005,** *40*, 430-443

11. Marshall, A.G., Grosshans, P.B.: Fourier Transform Ion Cyclotron Resonance Mass Spectrometry: The Teenage Years *Anal. Chem.* **1991,** *63*, 215A-229A

12. Marshall, A.G.: Milestones in Fourier Transform Ion Cyclotron Resonance Mass Spectrometry Technique Development *Int. J. Mass Spectrom.* **2000,** *200*, 331-356

13. Bristow, A.W.T.: Accurate Mass Measurement for the Determination of Elemental Formula - A Tutorial *Mass Spectrom. Rev.* **2006,** *25*, 99-111

14. de Hoffmann, E., Stroobant, V.; Mass Spectrometry: Principles and Applications, 2nd ed.; John Wiley & Sons: 2002;

15. Sleno, L., Volmer, D.A.: Ion Activation Methods for Tandem Mass Spectrometry *J. Mass Spectrom.* **2004,** *39*, 1091-1112

16. Cooper, H.J., Akbarzadeh, S., Heath, J.K., Zeller, M.: Data-Dependent Electron Capture Dissociation FT-ICR Mass Spectrometry for Proteomic Analyses *J. Proteome Res.* **2005,** *4*, 1538-1544

17. Creese, A.J., Cooper, H.J.: Liquid Chromatography Electron Capture Dissociation Tandem Mass Spectrometry (LC-ECD-MS/MS) versus Liquid Chromatography Collision-Induced Dissociation Tandem Mass Spectrometry (LC-CID-MS/MS) for the Identification of Proteins *J. Am. Soc. Mass Spectrom.* **2007,** *18*, 891-897

18. Palmblad, M., Tsybin, Y.O., Ramström, M., Bergquist, J., Håkansson, P.: Liquid Chromatography and Electron-Capture Dissociation in Fourier Transform Ion Cyclotron Resonance Mass Spectrometry *Rapid Commun. Mass Spectrom.* **2002,** *16*, 988-992

19. Li, W., Hendrickson, C.L., Emmett, M.R., Marshall, A.G.: Identification of Intact Proteins in Mixtures by Alternated Capillary Liquid Chromatography Electrospray Ionization and LC ESI Infrared Multiphoton Dissociation Fourier Transform Ion Cyclotron Resonance Mass Spectrometry *Anal. Chem.* **1999,** *71*, 4397-4402

20. Davidson, W., Frego, L.: Micro-High-Performance Liquid Chromatography/Fourier Transform Mass Spectrometry with Electron-Capture Dissociation for the Analysis of Protein Enzymatic Digests *Rapid Commun. Mass Spectrom.* **2002,** *16*, 993-998

21. Huang, E., Henion, J.: LC/MS and LC/MS/MS Determination of Protein Tryptic Digests *J. Am. Soc. Mass Spectrom.* **1990,** *1*, 158-165

22. Huddleston, M.J., Bean, M.F., Carr, S.A.: Collisional Fragmentation of Glycopeptides by Electrospray Ionization LC/MS and LC/MS/MS: Methods for Selective Detection of Glycopeptides in Protein Digests *Anal. Chem.* **1993,** *65*, 877-884

23. Shukla, A.K., Futrell, J.H.: Tandem Mass Spectrometry: Dissociation of Ions by Collisional Activation *J. Mass Spectrom.* **2000,** *35*, 1069-1090

24. McLafferty, F.W.: Tandem Mass Spectrometry *Science* **1981,** *214*, 280-287

25. Laskin, J., Futrell, J.H.: Activation of Large Ions in FT-ICR Mass Spectrometry *Mass Spectrom. Rev.* **2005,** *24*, 135-167

26. McLafferty, F.W., Wachs, T., Lifshitz, C., Innorta, G., Irving, P.: Substituent Effects in Unimolecular Ion Decompositions. XV. Mechanistic Interpretations and the Quasi-Equilibrium Theory *J. Am. Chem. Soc.* **1970,** *92*, 6867-6880

27. McLafferty, F.W., Fridriksson, E.K., Horn, D.M., Lewis, M.A., Zubarev, R.A.: Biochemistry - Biomolecule Mass Spectrometry *Science* **1999,** *284*, 1289-1290

28. March, R.E.: Quadrupole Ion Traps *Mass Spectrom. Rev.* **2009,** *28*, 961-989

29. Little, D.P., Speir, J.P., Senko, M.W., O'Connor, P.B., McLafferty, F.W.: Infrared Multiphoton Dissociation of Large Multiply-Charged Ions for Biomolecule Sequencing *Anal. Chem.* **1994,** *66*, 2809-2815

30. Eyler, J.R.: Infrared Multiple Photon Dissociation Spectroscopy of Ions in Penning Traps *Mass Spectrom. Rev.* **2009,** *28*, 448-467

31. Håkansson, K., Cooper, H.J., Emmett, M.R., Costello, C.E., Marshall, A.G., Nilsson, C.L.: Electron Capture Dissociation and Infrared Multiphoton Dissociation MS/MS of an N-glycosylated Tryptic Peptide to Yield Complementary Sequence Information *Anal. Chem.* **2001,** *73*, 4530-4536

32. Zubarev, R.A., Kelleher, N.L., McLafferty, F.W.: Electron Capture Dissociation of Multiply Charged Protein Cations. A Nonergodic Process *J. Am. Chem. Soc.* **1998,** *120*, 3265-3266

33. McLafferty, F.W., Horn, D.M., Breuker, K., Ge, Y., Lewis, M.A., Cerda, B., Zubarev, R.A., Carpenter, B.K.: Electron Capture Dissociation of Gaseous Multiply Charged Ions by Fourier-Transform Ion Cyclotron Resonance *J. Am. Soc. Mass Spectrom.* **2001,** *12*, 245-249

34. Zubarev, R.A.: Reactions of Polypeptide Ions with Electrons in the Gas Phase *Mass Spectrom. Rev.* **2003,** *22*, 57-77

35. Kruger, N.A., Zubarev, R.A., Horn, D.M., McLafferty, F.W.: Electron Capture Dissociation of Multiply Charged Peptide Cations *Int. J. Mass Spectrom.* **1999,** *187*, 787-793

36. Zubarev, R.A., Haselmann, K.F., Budnik, B., Kjeldsen, F., Jensen, F.: Towards an Understanding of the Mechanism of Electron-Capture Dissociation: A Historical Perspective and Modern Ideas *Eur. J. Mass Spectrom.* **2002,** *8*, 337-349

37. Zubarev, R.A., Horn, D.M., Fridriksson, E.K., Kelleher, N.L., Kruger, N.A., Lewis, M.A., Carpenter, B.K., McLafferty, F.W.: Electron Capture Dissociation for Structural Characterization of Multiply Charged Protein Cations *Anal. Chem.* **2000,** *72*, 563-573

38. Polfer, N.C., Haselmann, K.F., Zubarev, R.A., Langridge-Smith, P.R.R.: Electron Capture Dissociation of Polypeptides Using a 3 Tesla Fourier Transform Ion Cyclotron Resonance Mass Spectrometer *Rapid Commun. Mass Spectrom.* **2002,** *16*, 936-943

39. Creese, A.J., Cooper, H.J.: The Effect of Phosphorylation on the Electron Capture Dissociation of Peptide Ions *J. Am. Soc. Mass Spectrom.* **2008,** *19*, 1263-1274

40. Bakhtiar, R., Guan, Z.Q.: Electron Capture Dissociation Mass Spectrometry in Characterization of Peptides and Proteins *Biotechnol. Lett.* **2006,** *28*, 1047-1059

41. Mosely, J.A., Murray, B.S., Parker, D.: Electron-Capture Dissociation and Collision-Induced Dissociation of Lanthanide Metal-Ligand Complexes and Lanthanide Metal-Ligand Complexes Bound to Phosphopeptides *Eur. J. Mass Spectrom.* **2009,** *15*, 145-155

42. McLafferty, F.W.: Tandem Mass Spectrometric Analysis of Complex Biological Mixtures *Int. J. Mass Spectrom.* **2001,** *212*, 81-87

43. Stensballe, A., Jensen, O.N., Olsen, J.V., Haselmann, K.F., Zubarev, R.A.: Electron Capture Dissociation of Singly and Multiply Phosphorylated Peptides *Rapid Commun. Mass Spectrom.* **2000,** *14*, 1793-1800

44. Voinov, V., Deinzer, M., Beckman, J., Barofsky, D.: Electron Capture, Collision-Induced, and Electron Capture-Collision Induced Dissociation in Q-TOF *J. Am. Soc. Mass Spectrom.* **2011,** *22*, 607-611

45. Roepstorff, P., Fohlman, J.: Proposal for a Common Nomenclature for Sequence Ions in Mass Spectra of Peptides *Biomedical Mass Spectrometry* **1984,** *11*, 601-601

46. Cooper, H.J., Håkansson, K., Marshall, A.G.: The Role of Electron Capture Dissociation in Biomolecular Analysis *Mass Spectrom. Rev.* **2005,** *24*, 201-222

47. Biemann, K.: Contributions of Mass Spectrometry to Peptide and Protein Structure *Biomed. Environ. Mass Spectrom.* **1988,** *16*, 99-111

48. Biemann, K.: Mass Spectrometry of Peptides and Proteins *Annu. Rev. Biochem.* **1992,** *61*, 977-1010

49. Domon, B., Aebersold, R.: Review - Mass Spectrometry and Protein Analysis *Science* **2006,** *312*, 212-217

50. Yates, J.R.: Mass Spectral Analysis in Proteomics *Annu. Rev. Biophys. Biomol. Struct.* **2004,** *33*, 297-316

51. Bogdanov, B., Smith, R.D.: Proteomics by FTICR Mass Spectrometry: Top Down and Bottom Up *Mass Spectrom. Rev.* **2005,** *24*, 168-200

52. Horn, D.M., Ge, Y., McLafferty, F.W.: Activated Ion Electron Capture Dissociation for Mass Spectral Sequencing of Larger (42 kDa) Proteins *Anal. Chem.* **2000,** *72*, 4778-4784

53. Breuker, K., Jin, M., Han, X.M., Jiang, H.H., McLafferty, F.W.: Top-Down Identification and Characterization of Biomolecules by Mass Spectrometry *J. Am. Soc. Mass Spectrom.* **2008,** *19*, 1045-1053

54. Ge, Y., Lawhorn, B.G., ElNaggar, M., Strauss, E., Park, J.H., Begley, T.P., McLafferty, F.W.: Top Down Characterization of Larger Proteins (45 kDa) by Electron Capture Dissociation Mass Spectrometry *J. Am. Chem. Soc.* **2002,** *124*, 672-678

55. Smith, R.D., Loo, J.A., Barinaga, C.J., Edmonds, C.G., Udseth, H.R.: Collisional Activation and Collision-Activated Dissociation of Large Multiply Charged Polypeptides and Proteins Produced by Electrospray Ionization *J. Am. Soc. Mass Spectrom.* **1990,** *1*, 53-65

56. Memboeuf, A., Nasioudis, A., Indelicato, S., Pollreisz, F., Kuki, A., Keki, S., van den Brink, O.F., Vekey, K., Drahos, L.: Size Effect on Fragmentation in Tandem Mass Spectrometry *Anal. Chem.* **2010,** *82*, 2294-2302

57. Loo, J.A., Edmonds, C.G., Smith, R.D.: Tandem Mass Spectrometry of Very Large Molecules: Serum Albumin Sequence Information from Multiply Charged Ions Formed by Electrospray Ionization *Anal. Chem.* **1991,** *63*, 2488-2499

58. Downard, K.M., Biemann, K.: The Effect of Charge State and the Localization of Charge on the Collision-Induced Dissociation of Peptide Ions *J. Am. Soc. Mass Spectrom.* **1994,** *5*, 966-975

59. O'Connor, P.B., Lin, C., Cournoyer, J.J., Pittman, J.L., Belyayev, M., Budnik, B.A.: Long-Lived Electron Capture Dissociation Product Ions Experience Radical Migration via Hydrogen Abstraction *J. Am. Soc. Mass Spectrom.* **2006,** *17*, 576-585

60. Kalli, A., Håkansson, K.: Comparison of the Electron Capture Dissociation Fragmentation Behavior of Doubly and Triply Protonated Peptides from Trypsin, Glu-C, and Chymotrypsin Digestion *J. Proteome Res.* **2008,** *7*, 2834-2844

61. Zubarev, R.A., Kruger, N.A., Fridriksson, E.K., Lewis, M.A., Horn, D.M., Carpenter, B.K., McLafferty, F.W.: Electron Capture Dissociation of Gaseous Multiply-Charged Proteins is Favored at Disulfide Bonds and Other Sites of High Hydrogen Atom Affinity *J. Am. Chem. Soc.* **1999,** *121*, 2857-2862

62. Zubarev, R.A., Zubarev, A.R., Savitski, M.M.: Electron Capture/Transfer versus Collisionally Activated/Induced Dissociations: Solo or Duet? *J. Am. Soc. Mass Spectrom.* **2008,** *19*, 753-761

63. Savitski, M.M., Kjeldsen, F., Nielsen, M.L., Zubarev, R.A.: Complementary Sequence Preferences of Electron-Capture Dissociation and Vibrational Excitation in Fragmentation of Polypeptide Polycations *Angew. Chem. Int. Edit.* **2006,** *45*, 5301-5303

64. Axelsson, J., Palmblad, M., Håkansson, K., Håkansson, P.: Electron Capture Dissociation of Substance P Using a Commercially Available Fourier Transform Ion Cyclotron Resonance Mass Spectrometer *Rapid Commun. Mass Spectrom.* **1999,** *13*, 474-477

65. Bleiholder, C., Suhai, S., Harrison, A.G., Paizs, B.: Towards Understanding the Tandem Mass Spectra of Protonated Oligopeptides. 2: The Proline Effect in Collision-Induced Dissociation of Protonated Ala-Ala-Xxx-Pro-Ala (Xxx = Ala, Ser, Leu, Val, Phe, and Trp) *J. Am. Soc. Mass Spectrom.* **2011,** *22*, 1032-1039

66. Schwartz, B.L., Bursey, M.M.: Some Proline Substituent Effects in the Tandem Mass Spectrum of Protonated Pentaalanine *Biol. Mass Spectrom.* **1992,** *21*, 92-96

67. Simons, J.: Mechanisms for S–S and N–C_α Bond Cleavage in Peptide ECD and ETD Mass Spectrometry *Chem. Phys. Lett.* **2010,** *484*, 81-95

68. Neff, D., Simons, J.: Analytical and Computational Studies of Intramolecular Electron Transfer Pertinent to Electron Transfer and Electron Capture Dissociation Mass Spectrometry *J. Phys. Chem. A* **2010,** *114*, 1309-1323

69. Swierszcz, I., Skurski, P., Simons, J.: Dipole and Coulomb Forces in Electron Capture Dissociation and Electron Transfer Dissociation Mass Spectroscopy *J. Phys. Chem. A* **2012,** *116*, 1828-1837

70. Turecek, F., Chen, X.H., Hao, C.T.: Where Does the Electron Go? Electron Distribution and Reactivity of Peptide Cation Radicals Formed by Electron Transfer in the Gas Phase *J. Am. Chem. Soc.* **2008,** *130*, 8818-8833

71. Syrstad, E.A., Turecek, F.: Toward a General Mechanism of Electron Capture Dissociation *J. Am. Soc. Mass Spectrom.* **2005,** *16*, 208-224

72. Kjeldsen, F., Haselmann, K.F., Sorensen, E.S., Zubarev, R.A.: Distinguishing of Ile/Leu Amino Acid Residues in the PP3 Protein by (Hot) Electron Capture Dissociation in Fourier Transform Ion Cyclotron Resonance Mass Spectrometry *Anal. Chem.* **2003,** *75*, 1267-1274

73. Liu, H.C., Håkansson, K.: Abundant b-type Ions Produced in Electron Capture Dissociation of Peptides without Basic Amino Acid Residues *J. Am. Soc. Mass Spectrom.* **2007,** *18*, 2007-2013

74. Kjeldsen, F., Haselmann, K.F., Budnik, B.A., Jensen, F., Zubarev, R.A.: Dissociative Capture of Hot (3-13 eV) Electrons by Polypeptide Polycations: An Efficient Process Accompanied by Secondary Fragmentation *Chem. Phys. Lett.* **2002,** *356*, 201-206

75. Williams, J.P., Creese, A.J., Roper, D.R., Green, B.N., Cooper, H.J.: Hot Electron Capture Dissociation Distinguishes Leucine from Isoleucine in a Novel Hemoglobin Variant, Hb Askew, beta54(D5)Val-->Ile *J. Am. Soc. Mass Spectrom.* **2009,** *20*, 1707-13

76. Chalkley, R.J., Brinkworth, C.S., Burlingame, A.L.: Side-Chain Fragmentation of Alkylated Cysteine Residues in Electron Capture Dissociation Mass Spectrometry *J. Am. Soc. Mass Spectrom.* **2006,** *17*, 1271-1274

77. Moore, B.N., Ly, T., Julian, R.R.: Radical Conversion and Migration in Electron Capture Dissociation *J. Am. Chem. Soc.* **2011,** *133*, 6997-7006

78. Li, X.J., Lin, C., Han, L., Costello, C.E., O'Connor, P.B.: Charge Remote Fragmentation in Electron Capture and Electron Transfer Dissociation *J. Am. Soc. Mass Spectrom.* **2010,** *21*, 646-656

79. Sze, S.K., Ge, Y., Oh, H., McLafferty, F.W.: Top-Down Mass Spectrometry of a 29-kDa Protein for Characterization of any Posttranslational Modification to within One Residue *P. Natl. Acad. Sci. USA* **2002,** *99*, 1774-1779

80. Tsybin, Y.O., Witt, M., Baykut, G., Kjeldsen, F., Håkansson, P.: Combined Infrared Multiphoton Dissociation and Electron Capture Dissociation with a Hollow Electron Beam in Fourier Transform Ion Cyclotron Resonance Mass Spectrometry *Rapid Commun. Mass Spectrom.* **2003,** *17*, 1759-1768

81. Syka, J.E.P., Coon, J.J., Schroeder, M.J., Shabanowitz, J., Hunt, D.F.: Peptide and Protein Sequence Analysis by Electron Transfer Dissociation Mass Spectrometry *P. Natl. Acad. Sci. USA* **2004,** *101*, 9528-9533

82. McLuckey, S.A., Stephenson, J.L.: Ion/Ion Chemistry of High-Mass Multiply Charged Ions *Mass Spectrom. Rev.* **1998,** *17*, 369-407

83. Mikesh, L.M., Ueberheide, B., Chi, A., Coon, J.J., Syka, J.E.P., Shabanowitz, J., Hunt, D.F.: The Utility of ETD Mass Spectrometry in Proteomic Analysis *Biochim. Biophys. Acta - Prot. Proteom.* **2006,** *1764*, 1811-1822

84. Coon, J.J., Ueberheide, B., Syka, J.E.P., Dryhurst, D.D., Ausio, J., Shabanowitz, J., Hunt, D.F.: Protein Identification Using Sequential Ion/Ion Reactions and Tandem Mass Spectrometry *P. Natl. Acad. Sci. USA* **2005,** *102*, 9463-9468

85. Molina, H., Matthiesen, R., Kandasamy, K., Pandey, A.: Comprehensive Comparison of Collision Induced Dissociation and Electron Transfer Dissociation *Anal. Chem.* **2008,** *80*, 4825-4835

86. Yoo, H.J., Wang, N., Zhuang, S.Y., Song, H.T., Hakansson, K.: Negative-Ion Electron Capture Dissociation: Radical-Driven Fragmentation of Charge-Increased Gaseous Peptide Anions *J. Am. Chem. Soc.* **2011,** *133*, 16790-16793

87. Budnik, B.A., Haselmann, K.F., Zubarev, R.A.: Electron Detachment Dissociation of Peptide Di-Anions: An Electron-Hole Recombination Phenomenon *Chem. Phys. Lett.* **2001,** *342*, 299-302

88. Kalli, A., Hakansson, K.: Preferential Cleavage of S-S and C-S Bonds in Electron Detachment Dissociation and Infrared Multiphoton Dissociation of Disulfide-linked Peptide Anions *Int. J. Mass Spectrom.* **2007,** *263*, 71-81

89. Anusiewicz, I., Jasionowski, M., Skurski, P., Simons, J.: Backbone and Side-Chain Cleavages in Electron Detachment Dissociation (EDD) *J. Phys. Chem. A* **2005,** *109*, 11332-11337

90. Holcapek, M., Jirasko, R., Lisa, M.: Basic Rules for the Interpretation of Atmospheric Pressure Ionization Mass Spectra of Small Molecules *J. Chromatogr. A* **2010,** *1217*, 3908-3921

91. Levsen, K., Schiebel, H.M., Terlouw, J.K., Jobst, K.J., Elend, M., Preib, A., Thiele, H., Ingendoh, A.: Even-Electron Ions: A Systematic Study of the Neutral Species Lost in the Dissociation of Quasi-Molecular Ions *J. Mass Spectrom.* **2007,** *42*, 1024-1044

92. McLafferty, F.W.: Unimolecular Decompositions of Even-Electron Ions *Org. Mass Spectrom.* **1980,** *15*, 114-121

93. Karni, M., Mandelbaum, A.: The 'Even-Electron Rule' *Org. Mass Spectrom.* **1980,** *15*, 53-64

94. Niessen, W.M.A.: Fragmentation of Toxicologically Relevant Drugs in Positive-Ion Liquid Chromatography-Tandem Mass Spectrometry *Mass Spectrom. Rev.* **2011,** *30*, 626-663

95. Thurman, E.M., Ferrer, I., Pozo, O.J., Sancho, J.V., Hernandez, F.: The Even-Electron Rule in Electrospray Mass Spectra of Pesticides *Rapid Commun. Mass Spectrom.* **2007,** *21*, 3855-3868

96. Holman, S.W., Wright, P., Langley, G.J.: The Low-Energy Collision-Induced Dissociation Product Ion Spectra of Protonated Beta-Blockers Reveal an Analogy to Fragmentation Behaviour Under Electron Ionisation Conditions *J. Mass Spectrom.* **2011,** *46*, 1182-1185

97. Kingston, D.G.I., Bursey, J.T., Bursey, M.M.: Intramolecular Hydrogen Transfer in Mass Spectra. II. McLafferty Rearrangement and Related Reactions *Chem. Rev.* **1974,** *74*, 215-242

98. Nibbering, N.: The McLafferty Rearrangement: A Personal Recollection *J. Am. Soc. Mass Spectrom.* **2004,** *15*, 956-958

99. McLafferty, F.W.: Mass Spectrometric Analysis. Molecular Rearrangements *Anal. Chem.* **1959,** *31*, 82-87

100. McLafferty, F.W., Turecek, F.; Interpretation of Mass Spectra, 4th ed.; University Science Books: 1993;

101. Cody, R.B., Freiser, B.S.: Electron-Impact Excitation of Ions from Organics - Alternative to Collision-Induced Dissociation *Anal. Chem.* **1979,** *51*, 547-551

102. Cody, R.B., Freiser, B.S.: Electron Impact Excitation of Ions in Fourier Transform Mass Spectrometry *Anal. Chem.* **1987,** *59*, 1054-1056

103. Freiser, B.S.: Trapping of Positive-Ions in Electron-Beam of an Ion-Cyclotron Resonance Spectrometer *Int. J. Mass Spectrom.* **1978,** *26*, 39-47

104. Freiser, B.S.: Electron-Impact Ionization of Argon Ions by Trapped Ion-Cyclotron Resonance Spectroscopy *Int. J. Mass Spectrom.* **1980,** *33*, 263-267

105. Freiser, B.S., Beauchamp, J.L.: Electron-Impact Dissociation of Cyanobenzene Radical Cations by Ion-Cyclotron Resonance Spectroscopy *Chem. Phys. Lett.* **1976,** *42*, 380-382

106. Gord, J.R., Horning, S.R., Wood, J.M., Cooks, R.G., Freiser, B.S.: Energy Deposition During Electron Induced Dissociation *J. Am. Soc. Mass Spectrom.* **1993,** *4*, 145-151

107. Nielsen, M.L., Budnik, B.A., Haselmann, K.F., Olsen, J.V., Zubarev, R.A.: Intramolecular Hydrogen Atom Transfer in Hydrogen-Deficient Polypeptide Radical Cations *Chem. Phys. Lett.* **2000,** *330*, 558-562

108. Budnik, B.A., Zubarev, R.A.: $MH^{2+\bullet}$ Ion Production from Protonated Polypeptides by Electron Impact: Observation and Determination of Ionization Energies and a Cross-Section *Chem. Phys. Lett.* **2000,** *316*, 19-23

109. Budnik, B.A., Haselmann, K.F., Elkin, Y.N., Gorbach, V.I., Zubarev, R.A.: Applications of Electron-Ion Dissociation Reactions for Analysis of Polycationic Chitooligosaccharides in Fourier Transform Mass Spectrometry *Anal. Chem.* **2003,** *75*, 5994-6001

110. Sargaeva, N.P., Lin, C., O'Connor, P.B.: Identification of Aspartic and Isoaspartic Acid Residues in Amyloid β Peptides, Including Aβ1−42, Using Electron−Ion Reactions *Anal. Chem.* **2009,** *81*, 9778-9786

111. Ly, T., Yin, S., Loo, J.A., Julian, R.R.: Electron-Induced Dissociation of Protonated Peptides Yields Backbone Fragmentation Consistent with a Hydrogen-Deficient Radical *Rapid Commun. Mass Spectrom.* **2009,** *23*, 2099-2101

112. Fung, Y.M.E., Adams, C.M., Zubarev, R.A.: Electron Ionization Dissociation of Singly and Multiply Charged Peptides *J. Am. Chem. Soc.* **2009,** *131*, 9977-9985

113. Lioe, H., O'Hair, R.A.J.: Comparison of Collision-Induced Dissociation and Electron-Induced Dissociation of Singly Protonated Aromatic Amino Acids, Cystine and Related Simple Peptides using a Hybrid Linear Ion Trap-FT-ICR Mass Spectrometer *Anal. Bioanal. Chem.* **2007,** *389*, 1429-1437

114. Feketeova, L., O'Hair, R.A.J.: Comparison of Collision- versus Electron-Induced Dissociation of Sodium Chloride Cluster Cations *Rapid Commun. Mass Spectrom.* **2009,** *23*, 60-64

115. Feketeová, L., O'Hair, R.A.J.: Electron-Induced Dissociation of Doubly Protonated Betaine Clusters: Controlling Fragmentation Chemistry Through Electron Energy *Rapid Commun. Mass Spectrom.* **2009,** *23*, 3259-3263

116. Feketeová, L., Ryzhov, V., O'Hair, R.A.J.: Comparison of Collision- versus Electron-Induced Dissociation of Pt(II) Ternary Complexes of Histidine- and Methionine-Containing Peptides *Rapid Commun. Mass Spectrom.* **2009,** *23*, 3133-3143

117. Kaczorowska, M.A., Cooper, H.J.: Electron Induced Dissociation: A Mass Spectrometry Technique for the Structural Analysis of Trinuclear Oxo-Centred Carboxylate-Bridged Iron Complexes *J. Am. Soc. Mass Spectrom.* **2010,** *21*, 1398-1403

118. Feketeová, L., Wong, M.W., O'Hair, R.A.J.: The Role of Metal Cation in Electron-Induced Dissociation of Tryptophan *Eur. Phys. J. D* **2010,** *60*, 11-20

119. Yoo, H.J., Håkansson, K.: Determination of Double Bond Location in Fatty Acids by Manganese Adduction and Electron Induced Dissociation *Anal. Chem.* **2010,** *82*, 6940-6946

120. Kaczorowska, M.A., Cooper, H.J.: Electron Induced Dissociation (EID) Tandem Mass Spectrometry of Octaethylporphyrin and its Iron(III) Complex *Chem. Commun.* **2011,** *47*, 418-20

121. Kalli, A., Hess, S.: Fragmentation of Singly, Doubly, and Triply Charged Hydrogen Deficient Peptide Radical Cations in Infrared Multiphoton Dissociation and Electron Induced Dissociation *J. Am. Soc. Mass Spectrom.* **2012,** *23*, 244-263

122. Kalli, A., Grigorean, G., Håkansson, K.: Electron Induced Dissociation of Singly Deprotonated Peptides *J. Am. Soc. Mass Spectrom.* **2011,** *22*, 2209-2221

123. Yoo, H.J., Liu, H.C., Håkansson, K.: Infrared Multiphoton Dissociation and Electron-Induced Dissociation as Alternative MS/MS Strategies for Metabolite Identification *Anal. Chem.* **2007,** *79*, 7858-7866

124. Wolff, J.J., Laremore, T.N., Aslam, H., Linhardt, R.J., Amster, I.J.: Electron-Induced Dissociation of Glycosaminoglycan Tetrasaccharides *J. Am. Soc. Mass Spectrom.* **2008,** *19*, 1449-1458

2. Instrumentation

There is a wide range of mass spectrometers available, each with specific purposes and capabilities. Every MS instrument separates and detects ions according to their mass-to-charge ratios (*m/z*), resulting in a spectrum of *m/z* against abundance. Varying the type of mass analyser, and therefore the detectable mass range, resolving power and mass accuracy capabilities, can have a dramatic effect on the resulting MS or MS/MS spectra.

There are three stages to mass spectrometric analysis;

- Ionisation of the sample, converting the neutral sample molecules into gaseous ions.
- Separation of sample ions according to their mass-to-charge ratios.
- Detection of the ions, creating an electronic signal to generate a spectrum of intensity against mass-to-charge.

There are a large number of ionisation techniques and mass analysers that have been developed over the years, therefore the instrumentation detailed in this chapter has been focussed solely on the four mass spectrometers that have been utilised to carry out the work discussed in **Chapters 3**, **4** and **5**;

- Trace GCMS (ThermoFinnigan Corp.), a quadrupole mass analyser fitted with an Electron Ionisation (EI) source.
- LTQ-FT (ThermoFinnigan Corp.), a linear ion trap and an FT-ICR mass analyser connected in series, and fitted with an Electrospray (ESI) source.

- QToF Premier XE (Waters Ltd.), a quadrupole mass analyser, quadrupole collision cell and a Time-of-Flight mass analyser connected in series; fitted with an ESI source.
- Xevo QToF (Waters Ltd.) a quadrupole mass analyser, quadrupole collision cell and a Time-of-Flight mass analyser connected in series; fitted with interchangeable ESI and Atmospheric pressure Solids Analysis Probe (ASAP) sources.

2.1. Ion Sources

The method of ionising samples prior to mass analysis can affect the type and stability of the generated molecular ions, which in turn can have a significant affect on subsequent MS analysis. Soft ionisation techniques (such as ESI) have the tendency to keep the molecular ion intact, facilitating the confirmation of the expected compound(s). Hard ionisation techniques (such as Electron Ionisation) tend to exert more energy on the sample, which often leads to unstable molecular ions that dissociate to form more stable product ion species. ESI, ASAP and EI have been discussed further, each of which provides an alternative approach to compound characterisation.

2.1.1. Electrospray Ionisation

ESI is a soft atmospheric pressure ionisation technique that primarily forms intact sample molecular ions and can be controlled to minimise in-source dissociation. ESI is suitable for continuous sample/solvent introduction, allowing it to be combined with Liquid Chromatography (LC), flow injection analysis or direct infusion. **Figure 2.1** shows a schematic of a typical ESI source operating in positive ionisation mode. The voltage applied to the ESI capillary needle coupled with the nitrogen nebulisation gas surrounding the needle creates an aerosol of charged droplets.

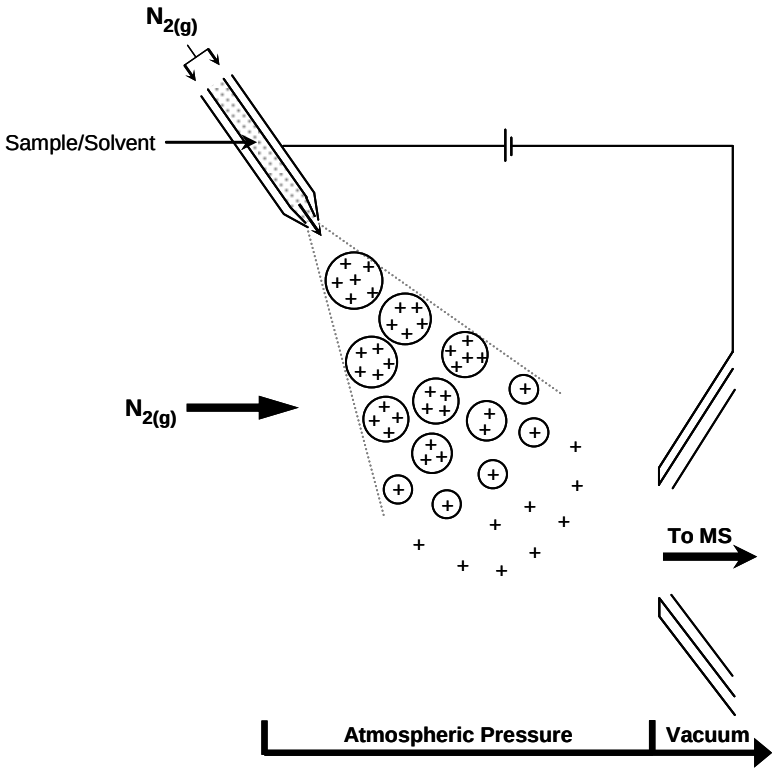

Figure 2.1: Schematic of an ESI source, illustrating positive ionisation mode.

Two possible mechanisms for electrospray have been proposed. The charge-reduced model postulates that as the solvent evaporates, the charge density of the droplets increases until the coulombic repulsion between the ions exceeds the surface tension of the solvent droplets (the Rayleigh limit) causing the droplets to split into smaller and smaller droplets. The solvent evaporation process is facilitated by a flow of nitrogen desolvation gas, resulting in gaseous analyte ions. The second mechanism, the ion evaporation model, suggests that the coulombic repulsion in a small highly charged solvent droplet forces ions to be ejected from the surface of the droplet to form the gaseous analyte ions. A voltage and vacuum gradient between the capillary needle and the source cone draws the analyte ions through the source cone and into the mass spectrometer. An off-axis ESI probe prevents neutral molecules and negatively charged ions[‡] from passing through the source cone. In

[‡] In the case of negative ionisation, positive ions would be repelled from the source.

positive ionisation mode, the molecular ions are primarily formed through ion/molecule interactions, the sample molecules interact with positively charged species such as protons (H^+), sodium (Na^+) or ammonium (NH_4^+) from the solute to create the positively charged molecular ions such as $[M+nH]^{n+}$, $[M+nNa]^{n+}$ or $[M+nNH_4]^{n+}$. In negative ionisation mode, the deprotonated molecular ion is commonly observed at $[M-nH^+]^{n-}$, although adducts may still be observed such as $[M+Cl]^-$ or $[M+HCOO]^-$.[1-5] High molecular weight compounds such as proteins and polymers contain multiple solvation sites, encouraging the formation of multiply charged species upon ESI that are observed at lower *m/z* values, thereby allowing mass analysers with a limited mass-range to be used. This is particularly important when using quadrupole or FT-ICR mass spectrometers that operate inefficiently at extended *m/z* ranges.

2.1.2. Atmospheric pressure Solids Analysis Probe

ASAP ionisation is a recent development in the field of direct analysis, creating a versatile ionisation technique used for the rapid analysis of volatile and semi-volatile compounds by thermally vaporising samples. ASAP removes the need for time-consuming sample preparation and allows the analysis of insoluble compounds by directly applying solid or solution phase samples to a disposable glass melting point capillary in the ASAP probe.[6] **Figure 2.2** shows a schematic of an ASAP source, illustrating an off-axis sample probe operating in positive ionisation mode.

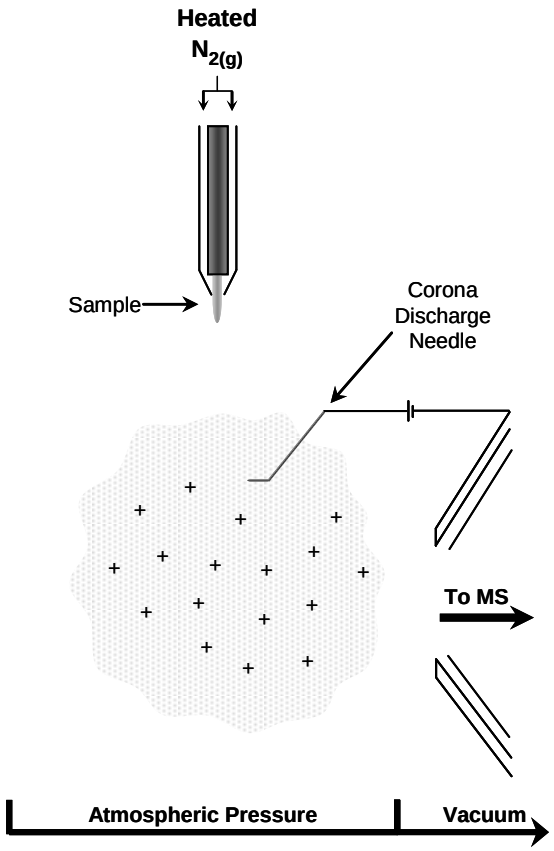

Figure 2.2: Schematic of an ASAP source, illustrating positive ionisation mode.

A stream of heated nitrogen desolvation gas is used to volatilise the sample on the glass capillary. A charged corona discharge needle is then used to ionise the gaseous sample molecules, which are then drawn into the mass spectrometer due to the potential gradient between the corona needle and the source cone. Ionisation of the sample molecules is proposed to result from charge transfer from the nitrogen desolvation gas, as shown in **Schemes 2.1 – 2.4**.[7]

$$N_2 + e^- \rightarrow N_2^{+\bullet} + 2e^- \qquad \textbf{Scheme 2.1}$$

$$N_2^{+\bullet} + 2N_2 \rightarrow N_4^{+\bullet} + N_2 \qquad \textbf{Scheme 2.2}$$

$$N_4^{+\bullet} + H_2O \rightarrow H_2O^{+\bullet} + 2N_2 \qquad \textbf{Scheme 2.3}$$

$$H_2O^{+\bullet} + H_2O \rightarrow H_3O^+ + OH^\bullet$$ **Scheme 2.4**

Rearrangement of the proposed reaction schemes can be used to suggest mechanisms for the ionisation of sample molecules **[M]** to form the protonated molecular ion, radical cation and hydride abstracted molecular ion respectively, as shown in **Schemes 2.5 – 2.7**.

$$H_3O^+ + [M] \rightarrow [M+H]^+ + H_2O$$ **Scheme 2.5**

$$N_2^{+\bullet} + [M] \rightarrow [M]^{+\bullet} + N_2$$ **Scheme 2.6**

$$H_3O^+ + [M] \rightarrow [M\text{-}H^-]^+ + H_2O + H_2$$ **Scheme 2.7**

ASAP is capable of analysing a wide range of compounds, with varying polarities, molecular weights and volatilities.[6, 8] The temperature of desolvation gas can be altered as necessary; higher gas temperatures benefit the analysis of less volatile samples but may promote degradation of thermally labile compounds, while lower temperatures are more suited for highly volatile samples that may readily dissociate at high temperature. An auxiliary ESI probe is often present to introduce a calibrant solution for improved mass accuracy.

The type of molecular ions generated through ASAP ionisation is primarily dependent on the sample being analysed, however altering the ASAP source conditions can be used to manipulate the molecular ion as required.[7] In positive ionisation mode the presence of water or other protic solvents, whether from the sample preparation or remnants in the source, may promote the generation of the $[M+H]^+$ species due to the proton-rich environment as long as the sample has a

sufficient proton affinity. The auxiliary ESI probe can be used as a means of introducing the liquids into the source during ASAP analysis. Conversely, introducing a proton-scavenger into the source enclosure or removing any residual moisture by using high temperatures and N_2 gas would encourage the production of the radical cation $M^{+\bullet}$ or the hydride abstracted $[M\text{-}H^-]^+$ species.[6-7]

2.1.3. Electron Ionisation

The technique known as Electron Ionisation, historically referred to as Electron Impact, is a well-established ionisation technique that is carried out under vacuum, and therefore is commonly combined with Gas Chromatography (GC). High energy electrons are emitted from a heated wire filament and accelerated to 70 eV prior to interaction with the gaseous sample molecules.[9-10] The interaction between the electron and the sample molecule creates a positively charged radical cationic species ($M^{+\bullet}$), as shown in **Scheme 2.8**.

$$\mathbf{M + e^- \rightarrow M^{+\bullet} + 2e^-}$$ **Scheme 2.8**

The odd-electron molecular ions are typically less stable than the even-electron species generated by ESI due to higher internal energy, and therefore often results in bond dissociation and/or molecular rearrangement to form more stable products. The level of instability is largely dependant on the structure of the analysed compounds; however a high degree of in-source fragmentation is a common occurrence in EI spectra resulting in a low abundance or even non-existent molecular ion. EI is typically suited for volatile, low molecular weight (< 1 kDa) compounds with < 70 eV ionisation potentials. EI generates highly reproducible MS spectra, allowing mass spectral libraries to be created so as to aid sample identification by spectral comparison. EI has been carried out in order to compare

the effect of electron/molecule interactions with the proposed electron/ion interactions of EID.[11]

2.2. Mass Analysers

2.2.1. Quadrupole Mass Analyser

The GC Trace mass spectrometer comprises of an EI ion source connected to a single quadrupole mass analyser. Quadrupole mass analysers consist of four identical parallel rods arranged, as shown in **Figure 2.3**, with opposite rods acting as a pair. Each pair has a DC voltage and an RF voltage applied to them. The RF voltages applied to each pair of rods are identical in amplitude but different in polarity. When an ion enters the quadrupole it will be attracted to the rods of opposite charge (i.e. a positive ion will be drawn towards the negatively charged rods), which if allowed to collide will effectively neutralise the ion. The RF voltages rapidly alternate the polarity of the rods, thereby forcing ions to oscillate along the length of the quadrupole.[12]

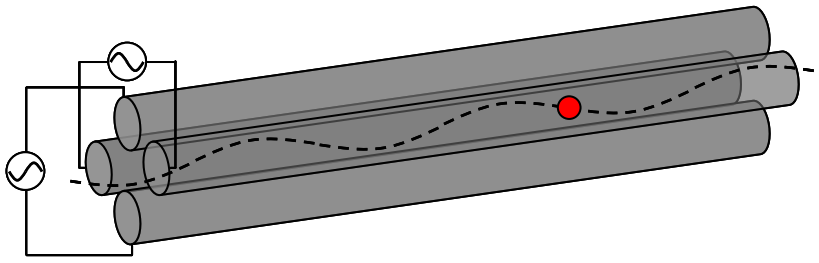

Figure 2.3: Diagram illustrating the motion of ions through a quadrupole.

The Mathieu equations shown in **Equation 2.1** and **Equation 2.2** indicate the motion of ions along the quadrupoles.

$$a_u = \frac{8zeU}{m\omega^2 r_0^2}$$ **Equation 2.1**

$$q_u = \frac{4zeV}{m\omega^2 r_0^2}$$ **Equation 2.2**

Where a_u and q_u are related to the x- and y-coordinates of an ion travelling through the quadrupole, r_0 is the radius of the quadrupole, ***U*** corresponds to the DC voltage applied to the rods, ***V*** is the amplitude of the RF voltage, ω is a constant corresponding to the angular frequency, ***m*** is the mass of the ion, ***z*** is the number of charges on the ion, e is the charge of an electron. For each ion, ***U*** and ***V*** are variable, and the ion is stable as long as the values of a_u and q_u remain less than r_0. **Figure 2.4** indicates the stability curves associated with ions travelling through a quadrupole, with each curve representing ions of a specific *m/z*. The optimum variation in ***U*** and ***V*** occurs when only ions of one *m/z* are transmitted at any given time, as shown in **Figure 2.4**, allowing ions to be separated according to their *m/z* values.[13]

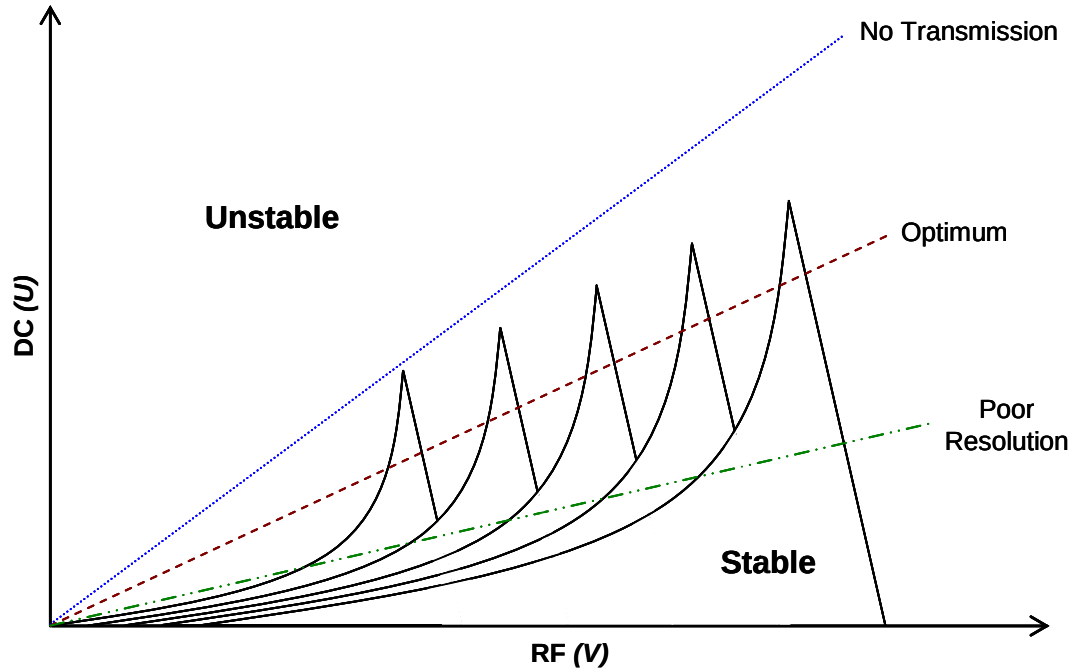

Figure 2.4: Stability diagram for ions in a quadrupole mass analyser.

Quadrupoles have incredible versatility allowing them to not only separate ions according to their *m/z*, but can be used as a collision cell for performing CID MS/MS or function as RF-only ion guides or focussing lenses between components of the mass spectrometer. Quadrupoles can also function as ion trap mass analysers, an example of which is incorporated into the LTQ-FT.

2.2.2. FT-ICR Mass Analyser

Figure 2.5 shows the schematic of an LTQ-FT (ThermoFinnigan) mass spectrometer, comprising of an ESI ion source and two mass analysers; a Linear Ion Trap (IT or LIT) and an FT-ICR cell connected sequentially. Quadrupolar ion guides are used to transmit ions between the source and the mass analysers.

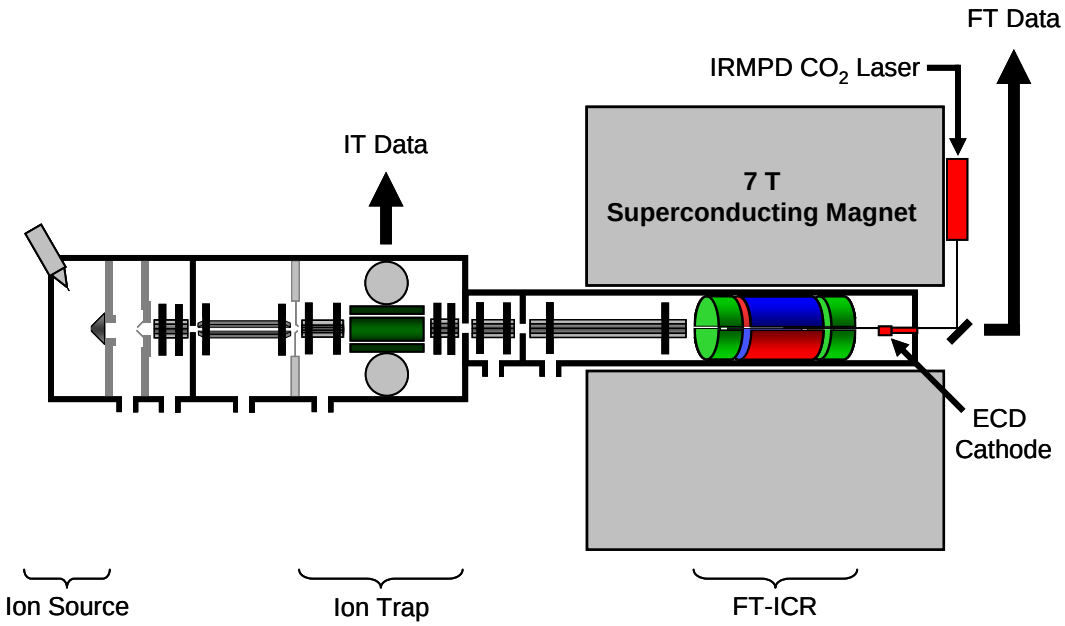

Figure 2.5: Schematic of the Thermo LTQ-FT.

Linear Ion Trap

The Linear Ion Trap (a subset of Quadrupole Ion Traps) is made up of four parallel hyperbolic rods, each of which is made up of three sections as shown in **Figure 2.6**. During ion accumulation or transmission, the front and back electrodes act as lenses allowing the ions to pass through into the centre of the trap or ejecting ions through the back lens to clear the trap. When a Direct Current (DC) voltage is applied to the front and back electrodes, they become trapping plates keeping ions confined within the central section of the trap. A helium buffer gas (or damping gas) is contained within the ion trap at 10^{-3} Torr, and is used to collisionally cool ions that enter the trap in order to reduce the kinetic energy of the ions and hold ions in the centre of the trap. The rods that make up the main body of the trap are subjected to an Alternating Current (AC) voltage, sometimes known as the main RF voltage or the storage voltage, with a different polarity applied to each opposing pair, as shown in **Figure 2.6(a)**.[14]

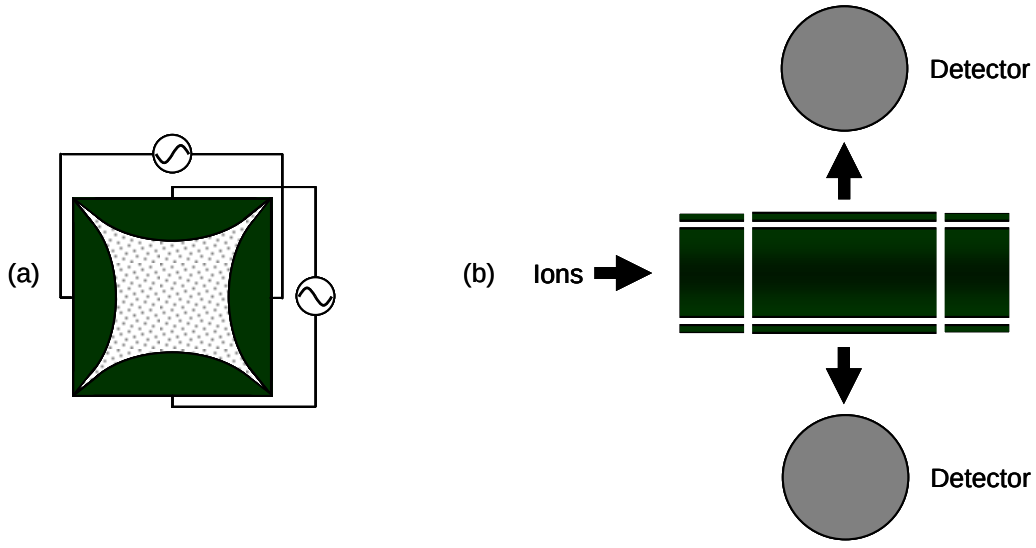

Figure 2.6: Schematic of (a) the front view of a linear ion trap and (b) the side view.

The Mathieu equations shown in **Equation 2.1** and **Equation 2.2** apply to ions in the Ion Trap. The resonance frequency of each ion is dependent on the *m/z* ratio, thereby allowing ions of different *m/*z to be separated. Trapped ions oscillate within the confines of the trap until the main RF voltage is gradually increased, increasing the kinetic energy of ions with the same resonance frequency and resulting in an increase in the magnitude of the ion motion. **Figure 2.7** shows the stability curve associated with ions in a linear ion trap. The DC voltage remains constant, therefore ions travel along the q_u axis as the RF voltage is varied. As the RF voltage is ramped, ions reach their limit of stability and are ejected from the trap in order of increasing *m/z*. One pair of opposing rods, known as the exit rods, has a cut out section through which the ejected ions travel towards a conversion dynode detector.

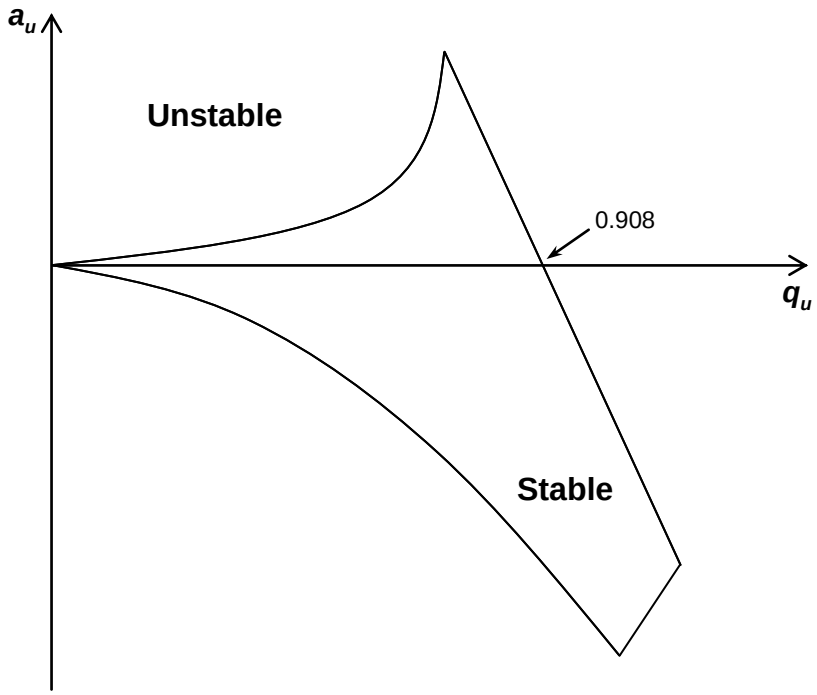

Figure 2.7: Stability diagram an ion in the linear ion trap.

Isolation of an ion of interest is carried out by increasing the DC and RF voltages to eject ions from the trap, with the exception of the ion of interest, resulting in an isolated precursor ion that can be subjected to MS^n experiments. CID MS/MS is performed in the ion trap by applying a resonance excitation RF voltage to the exit rods, which increases the kinetic energy of the stored ions and causes multiple collisions between the helium buffer gas and the precursor ions. **Figure 2.8** shows the stability curve associated with the precursor ion and the placement of the product ions along the curve. Ions with q_z values less than 0.908, typically corresponding to ions of *m/z* less than one-third of the precursor ion, are not stable enough to remain in the trap and are therefore not observed in the resulting MS/MS spectrum. This rule, known as the one-third cut-off or low-mass cut-off, results in a restricted mass range for CID analysis carried out in an ion trap, and reducing the amount of structural information that may be gleaned from the resulting MS/MS spectrum.[15]

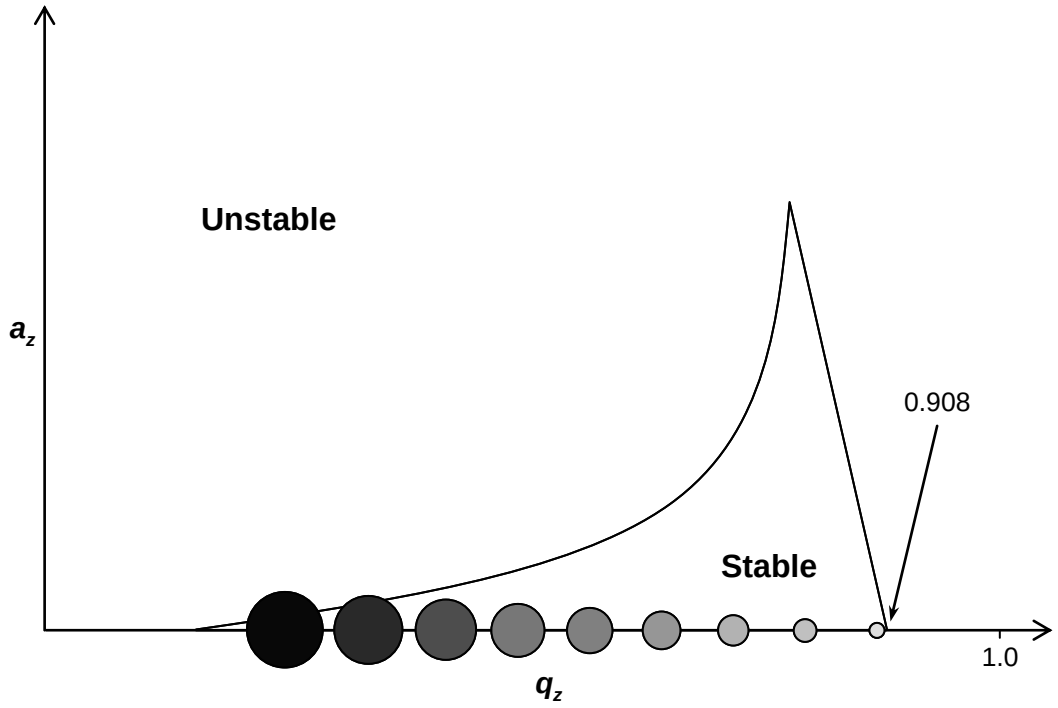

Figure 2.8: Diagram of ion ejection in the linear ion trap.

Product ions generated by CID in the ion trap can be detected *in situ* or transmitted into the FT-ICR cell to utilise the high resolution and mass accuracy.

Fourier Transform-Ion Cyclotron Resonance

The Fourier Transform-Ion Cyclotron Resonance (FT-ICR) mass analyser is the highest resolution MS instrument available, comparable with the Orbitrap mass analyser,[16-17] with high sensitivity and mass accuracy capabilities. In the LTQ-FT, the FT-ICR cell, sometimes known as a Penning trap, is cylindrical and situated within a static magnetic field inside the bore of a 7 Tesla superconducting magnet. FT-ICR mass analysers measure ions according to their frequency of precession, rather than measuring ion velocity, and therefore is not affected by the kinetic energy distribution among ions of the same *m/z*. The FT-ICR cell is held at high vacuum so as to prevent collisions between the trapped ions and gas molecules, which would affect the ion cyclotron frequencies and the resulting mass accuracy. At higher magnetic fields, the ICR frequency increases and the time required

decreases, resulting in increased resolving power and accuracy.[18-19] **Figure 2.9** shows the schematic of a Penning Trap, with ions entering the trap in the same direction as the magnetic field, **B**, defined as the z-axis.[19-25]

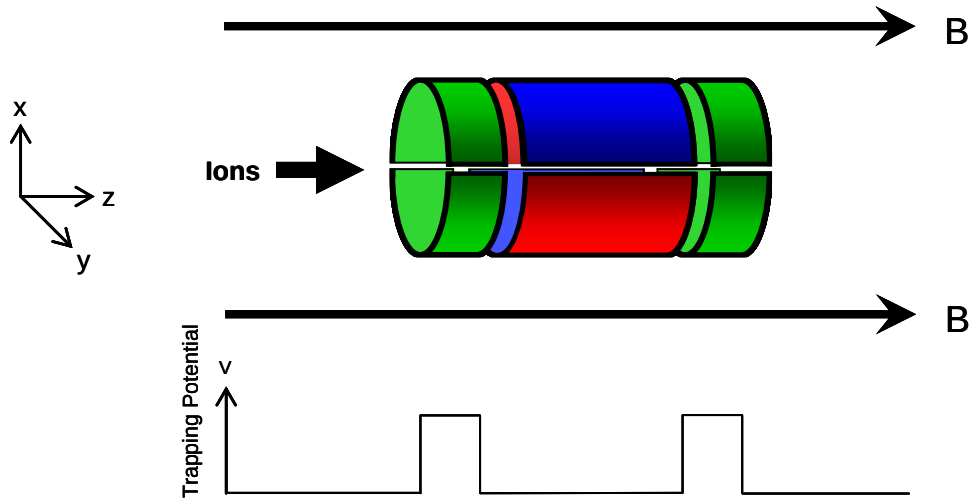

Figure 2.9: Schematic of a Penning Trap.

As with the ion trap, the Penning Trap includes two trapping electrodes at either end of the cell, which confine ions within the cell when an electric potential, known as the trapping potential, is applied. The main body of the Penning Trap consists of four electrodes; a pair of excitation electrodes and a pair of detection electrodes. Ions trapped within the FT-ICR cell adopt three types of motion;[18]

- Cyclotron Motion: High frequency (5 kHz – 5 MHz) ion precessions along the x/y plane. The ion cyclotron frequency is dependant on the *m/z* of the ion, and can therefore be used to determine the *m/z* of an ion.
- Trapping Motion: A slight motion along the z-axis between the trapping electrodes.
- Magnetron Motion: Low frequency (1 - 100 Hz) ion precessions along the x/y plane, independent of the *m/z* of the ion, resulting from the effect of the

electric and magnetic fields. Injecting ions into the FT-ICR cell parallel to the magnetic field ensures the radius of magnetron motion is minimised, making the effect on the resulting mass spectrum negligible.[18]

When a particular RF voltage is applied to the excitation electrodes, ions with the same ion cyclotron frequency experience an increase in the radius of ion cyclotron motion, causing the ions to move towards the edge of the cell as shown in **Figure 2.10**.[26-28]

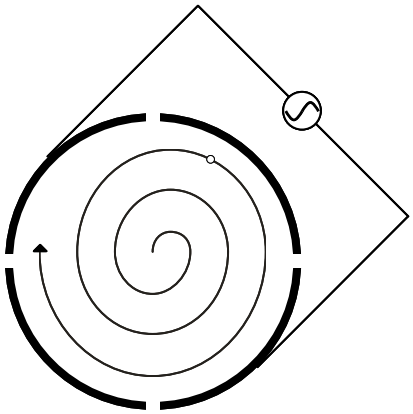

Figure 2.10: An RF voltage applied to the excitation electrodes causes the radius of the ion cyclotron motion to increase.

As the ions travel near the electrodes, as shown in **Figure 2.11**, the detection electrodes record the signal generated by all the ions, by attracting or repelling electrons from the detection plate depending on the polarity of the ions and resulting in an image current. The image current of a single ion would be sinusoidal, however FT-ICR records the image current of all trapped ions simultaneously by scanning the RF frequencies, exciting all the ions and generating a more complex image current resulting from a combination of the ion cyclotron frequencies. A mathematical operator known as the Fourier Transform can then be used to extract the individual ion cyclotron frequencies.[24]

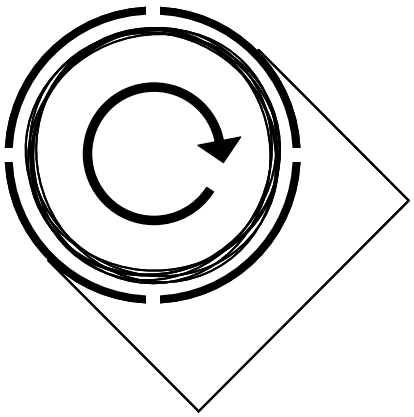

Figure 2.11: Pathway of excited ions in Penning trap exhibiting cyclotron motion.

The Fourier transformation results in a spectrum of cyclotron frequency against signal intensity, which can then be converted into a spectrum of mass-to-charge against intensity using **Equation 2.3**, where ***B*** is the applied magnetic field strength, v_c is the ion cyclotron frequency, ***m*** is the mass of the ion and ***q*** is the charge on the ion.[18, 23]

$$v_c = \frac{qB}{2\pi m} \qquad \textbf{Equation 2.3}$$

Equation 2.3 can be rearranged to show that the mass-to-charge ratio is inversely proportional to the cyclotron frequency, as shown in **Equation 2.4**.

$$m/q = \frac{B}{2\pi} \bullet \frac{1}{v_c} \qquad \textbf{Equation 2.4}$$

The ion cyclotron motion can be described in terms of the angular frequency, ω_c, which is directly related to the ion cyclotron frequency, as shown in **Equation 2.5**.

$$\omega_c = 2\pi\nu_c$$ **Equation 2.5**

The voltages applied to the trapping electrodes in order to confine ions within the Penning trap create a non-uniform electric field along the FT-ICR cell that causes ions to oscillate slightly along the z-axis. The variation in the electric field has a small reductive effect on the forces contributing to the ion cyclotron motion, as described in **Equation 2.6**, where ω is the reduced ion cyclotron frequency and ω_z is the angular trapping frequency.

$$\omega = \frac{\omega_c}{2} + \sqrt{\left(\frac{\omega_c}{2}\right)^2 - \frac{\omega_z^2}{2}}$$ **Equation 2.6**

In order to compensate for the effect of the trapping voltages, frequency-to-mass conversion and mass calibration must be carried out using the reduced ion cyclotron frequencies so as to achieve high mass accuracy.[23, 29] The detection of ions in the Penning Trap is non-destructive, allowing ions to be contained and detected for a considerable length of time. A longer image current results in better resolution of the resulting MS spectrum, however the duty cycle will also increase.[20, 30]

The schematic in **Figure 2.5** indicates the placement of the indirectly heated cathode required for performing ECD MS/MS and the 20 W CO_2 laser for performing IRMPD MS/MS, both of which are situated behind the FT-ICR cell.

2.2.3. Quadrupole Time-of-Flight Mass Analyser

The Xevo QTof includes two interchangeable ion sources, an ESI source and ASAP source, attached to a quadrupole mass analyser, a T-wave collision cell and a ToF mass analyser connected in series, as shown in the schematic in **Figure 2.12**.

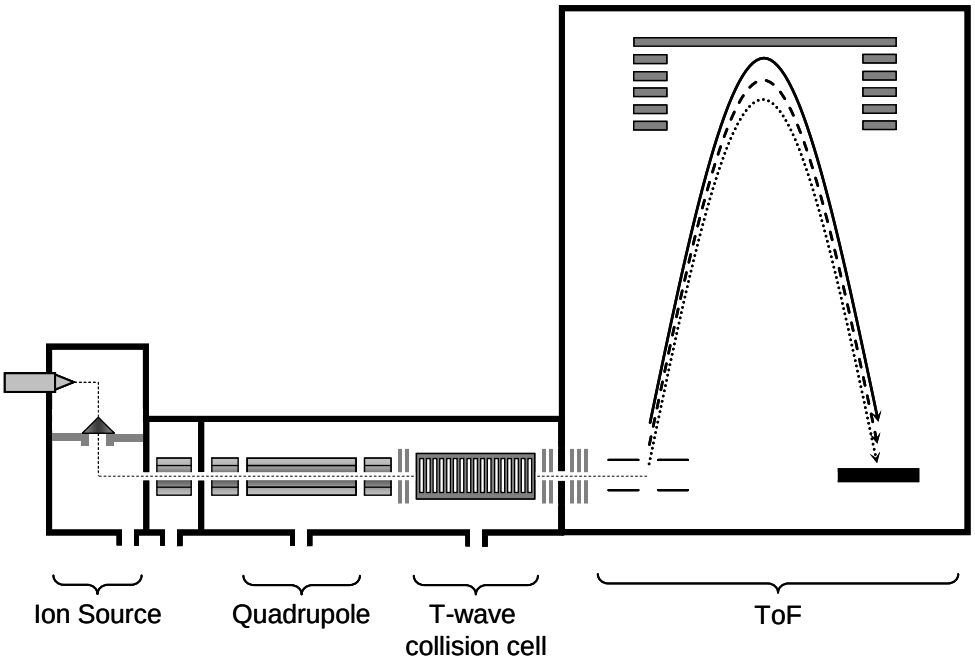

Figure 2.12: Schematic of the Xevo QToF.

The QToF Premier XE mass spectrometer consists of an ESI ion source connected to a quadrupole mass analyser, a T-wave collision cell and a Time-of-Flight mass analyser connected in series, as shown in the schematic in **Figure 2.13**.

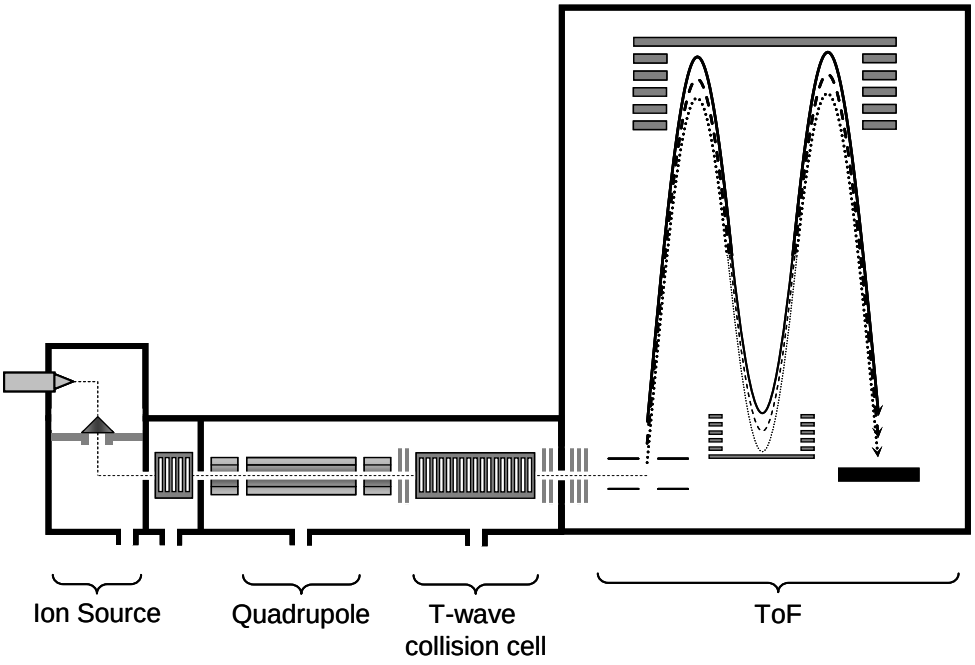

Figure 2.13: Schematic of the QToF Premier XE.

The quadrupole mass analyser has two purposes; firstly as an ion guide, scanning through the RF voltages in order to transmit all sample ions towards the Time-of-Flight mass analyser for detection. Secondly, the quadrupole can be used to isolate a specific ion, by applying only one RF voltage to eliminate all ions except for the precursor ion of interest. The T-wave collision cell consists of a stack of ring electrodes with opposing RF voltages applied to adjacent electrodes. A DC voltage is applied to each electrode in turn, creating a 'travelling wave' propelling ions towards the exit to the cell. The collision cell contains an argon buffer gas, held at a pressure of 7 psi, which is used for CID MS/MS of the ions travelling through the cell. Increasing the velocity of the ions through the collision cell, by altering the speed of the travelling wave and the DC voltage, induces collisions between the precursor ions and the argon gas molecules, resulting in product ion formation *via* CID.[31]

Time-of-Flight (ToF) mass analysers measure the time taken for ions to travel a fixed distance in a vacuum, as shown in the schematic in **Figure 2.14** and using **Equation 2.7**, where $\boldsymbol{E_k}$ is the kinetic energy of each ion, $\boldsymbol{m}$ is the mass of the ion and $\boldsymbol{v}$ is the velocity of the ion. Following this equation, two ions with the same charge but different masses that are given the same kinetic energy will travel at different velocities, with the ion of lesser mass travelling faster than the ion with greater mass. Using **Equation 2.8**, the lower mass (and therefore faster) ions will take a shorter time, $\boldsymbol{t}$, to travel along the fixed distance, $\boldsymbol{d}$. Increasing the length of the field-free region subsequently increases the time taken for ions to reach the detector, but also increases the time difference between the ions, increasing the resolving power of the detector.[32-33]

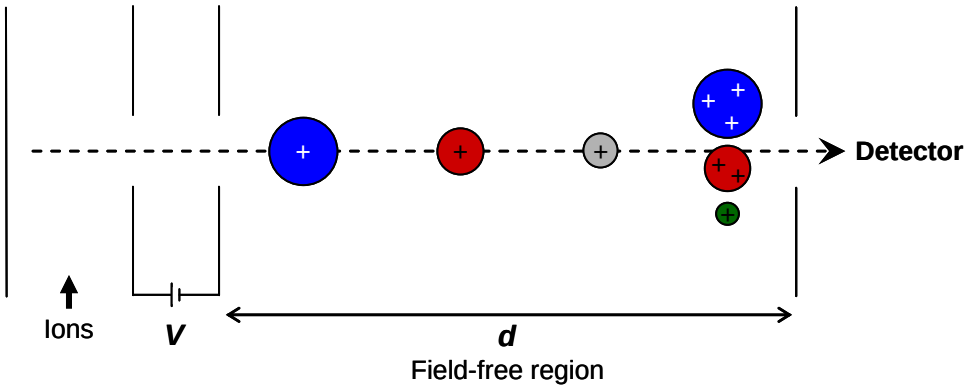

Figure 2.14: Schematic of a ToF mass analyser.

$$E_k = \frac{1}{2}mv^2$$ **Equation 2.7**

$$v = \frac{d}{t}$$ **Equation 2.8**

$$E_k = qV$$ **Equation 2.9**

Equation 2.9 expresses the kinetic energy applied to the ions with respect to the charge of an electron, q, and the accelerating voltage, V. Rearranging **Equation 2.7**, **Equation 2.8** and **Equation 2.9** to express the mass-to-charge ratio, results in **Equation 2.10**, where the mass-to-charge ratio is proportional to t^2 when $\frac{2V}{d^2}$ is constant. Following this equation, as the mass-to-charge of a particular ion decreases (i.e. the mass decreases or the charge increases), the time taken to travel the length of the flight tube decreases.

$$m/q = \frac{2V}{v^2} = \frac{2Vt^2}{d^2}$$ **Equation 2.10**

A ToF mass analyser requires a discrete packet of ions in order to distinguish between ions of varying mass, therefore in order to combine a ToF analyser with ion sources that allow continuous sample introduction (such as ESI), orthogonal acceleration is required, whereby the ions enter the analyser perpendicular to the flight tube and are 'kicked' in a 90° angle by a pulsed voltage to create the required packet of ions.[34] **Figure 2.15** displays a schematic of a ToF mass analyser fitted with orthogonal acceleration and an ion reflectron. A reflectron is a series of electrodes of increasing voltage that act as an ion mirror, reflecting the path of the ions. The reflectron effectively increases the length of the flight path for the ions and therefore increasing the mass resolution, without increasing the physical length of the analyser. The reflectron also corrects minor variations in the kinetic energy of ions with the same *m/z*, further improving the mass resolution.[35-37] In the case of the QTof Premier XE, two reflectrons can be employed that lengthen the ion path by approximately four times the length of the field-free region.

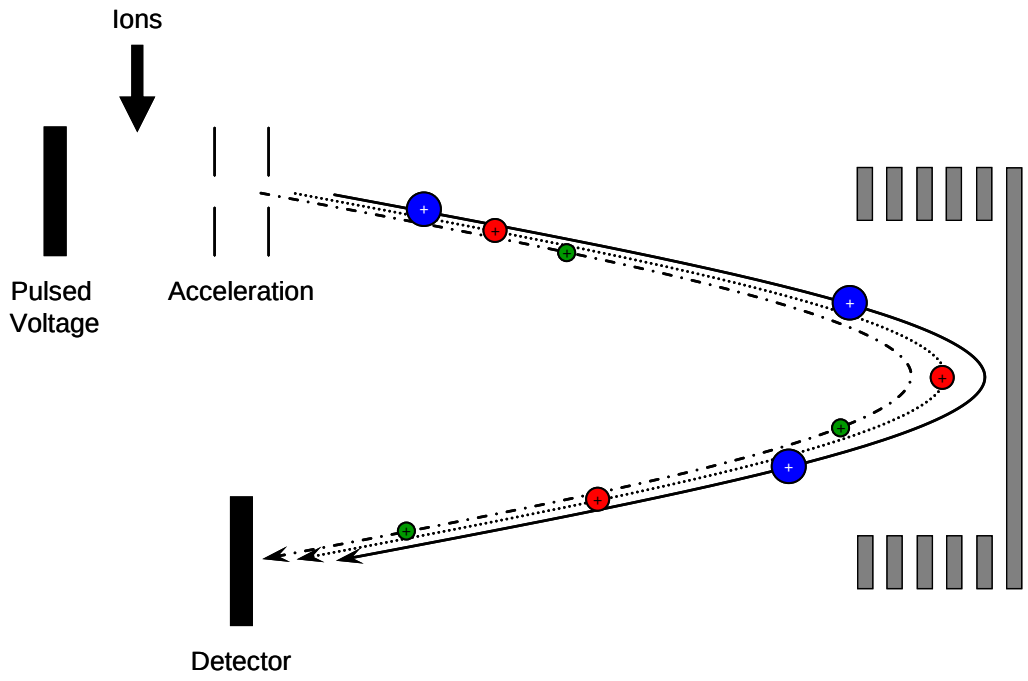

Figure 2.15: Schematic of an ToF mass spectrometer fitted with a reflectron and orthogonal acceleration.

2.2.4. Summary of mass analyser performance

Performance criteria such as resolving power, mass accuracy, speed, sensitivity and mass range should be considered for each mass analyser, prioritising factors according to the focus of MS analysis. Instruments with higher resolving powers are essential for the analysis of isobaric compounds or complex mixtures, due to the ability to separate ions with a small *m/z* difference. Mass accuracy becomes a key factor when analysing unknown compounds or when using MS/MS to generate structural information. Speed of analysis is significant when carrying out LCMS and LCMS/MS or when rapid sample turnaround is required for high-throughput analyses. Sensitivity of the mass analyser affects the dynamic concentration range that can be analysed, with lower sensitivity mass analysers requiring higher sample concentrations. Mass range is arguably the least important performance factor due to the advent of soft ionisation techniques that allow larger molecules to form multiply charged species that appear at in the lower *m/z* region, however ionisation techniques that typically form singly charged ions, such as Matrix-assisted Laser Desorption/Ionisation (MALDI) often require mass analysers with a higher mass range, such as ToF analysers.

Due to the focus on MS/MS, in particular EID, the work carried out herein has predominantly been carried out on an FT-ICR, making use of the high mass accuracy and resolving power to characterise MS/MS product ions and identify unknown compounds. Comparisons have been made between data generated on an FT-ICR and Linear Ion Trap, Quadrupole and Time-of-Flight mass analysers.

2.3. References

1. Straub, R.F., Voyksner, R.D.: Negative Ion Formation in Electrospray Mass Spectrometry *J. Am. Soc. Mass Spectrom.* **1993,** *4*, 578-587

2. Gaskell, S.J.: Electrospray: Principles and practice *J. Mass Spectrom.* **1997,** *32*, 677-688

3. Fenn, J.B.: Ion Formation from Charged Droplets - Roles of Geometry, Energy, and Time *J. Am. Soc. Mass Spectrom.* **1993,** *4*, 524-535

4. Yamashita, M., Fenn, J.B.: Electrospray Ion Source - Another Variation on the Free-Jet Theme *J. Phys. Chem.* **1984,** *88*, 4451-4459

5. Kebarle, P., Tang, L.: From Ions in Solution to Ions in the Gas Phase - The Mechanism of Electrospray Mass Spectrometry *Anal. Chem.* **1993,** *65*, A972-A986

6. McEwen, C.N., McKay, R.G., Larsen, B.S.: Analysis of Solids, Liquids, and Biological Tissues Using Solids Probe Introduction at Atmospheric Pressure on Commercial LC/MS Instruments *Anal. Chem.* **2005,** *77*, 7826-7831

7. Petucci, C., Diffendal, J.: Atmospheric Solids Analysis Probe: A Rapid Ionization Technique for Small Molecule Drugs *J. Mass Spectrom.* **2008,** *43*, 1565-1568

8. Lloyd, J.A., Harron, A.F., McEwen, C.N.: Combination Atmospheric Pressure Solids Analysis Probe and Desorption Electrospray Ionization Mass Spectrometry Ion Source *Anal. Chem.* **2009,** *81*, 9158-9162

9. Nier, A.O.: A Mass Spectrometer for Isotope and Gas Analysis *Rev. Sci. Instrum.* **1947,** *18*, 398-411

10. Chait, E.M.: Ionization Sources in Mass Spectrometry *Anal. Chem.* **1972,** *44*, 77a-91a

11. Sleno, L., Volmer, D.A.: Ion Activation Methods for Tandem Mass Spectrometry *J. Mass Spectrom.* **2004,** *39*, 1091-1112

12. Paul, W., Steinwedel, H.: Ein Neues Massenspektrometer Ohne Magnetfeld *Z Naturforsch A* **1953,** *8*, 448-450

13. Mathieso, E., Harris, T.J.: Quadrupole Mass Spectrometer *Am. J. Phys.* **1969,** *37*, 1054-1059

14. March, R.E.: An Introduction to Quadrupole Ion Trap Mass Spectrometry *J. Mass Spectrom.* **1997,** *32*, 351-369

15. March, R.E.: Quadrupole Ion Traps *Mass Spectrom. Rev.* **2009,** *28*, 961-989

16. Hu, Q., Noll, R.J., Li, H., Makarov, A., Hardman, M., Graham Cooks, R.: The Orbitrap: A New Mass Spectrometer *J. Mass Spectrom.* **2005,** *40*, 430-443

17. Perry, R.H., Cooks, R.G., Noll, R.J.: Orbitrap Mass Spectrometry: Instrumentation, Ion Motion and Applications *Mass Spectrom. Rev.* **2008,** *27*, 661-699

18. Amster, I.J.: Fourier Transform Mass Spectrometry *J. Mass Spectrom.* **1996,** *31*, 1325-1337

19. Marshall, A.G., Hendrickson, C.L.: Fourier Transform Ion Cyclotron Resonance Detection: Principles and Experimental Configurations *Int. J. Mass Spectrom.* **2002,** *215*, 59-75

20. Marshall, A.G., Hendrickson, C.L., Jackson, G.S.: Fourier Transform Ion Cyclotron Resonance Mass Spectrometry: A Primer *Mass Spectrom. Rev.* **1998,** *17*, 1-35

21. Marshall, A.G.: Fourier Transform Ion Cyclotron Resonance Mass Spectrometry *Accounts Chem. Res.* **1985,** *18*, 316-322

22. Marshall, A.G.: Milestones in Fourier Transform Ion Cyclotron Resonance Mass Spectrometry Technique Development *Int. J. Mass Spectrom.* **2000,** *200*, 331-356

23. Marshall, A.G., Grosshans, P.B.: Fourier Transform Ion Cyclotron Resonance Mass Spectrometry: The Teenage Years *Anal. Chem.* **1991,** *63*, 215A-229A

24. Grosshans, P.B., Shields, P.J., Marshall, A.G.: Comprehensive Theory of the Fourier Transform Ion Cyclotron Resonance Signal for all Ion Trap Geometries *J. Chem. Phys.* **1991,** *94*, 5341-5352

25. Guan, S., Marshall, A.G.: Ion Traps for Fourier Transform Ion Cyclotron Resonance Mass Spectrometry: Principles and Design of Geometric and Electric Configurations *Int. J. Mass Spectrom.* **1995,** *146–147*, 261-296

26. Hipple, J.A., Sommer, H., Thomas, H.A.: A Precise Method of Determining the Faraday by Magnetic Resonance *Phys. Rev.* **1949,** *76*, 1877-1878

27. Grosshans, P.B., Marshall, A.G.: General Theory of Excitation in Ion Cyclotron Resonance Mass Spectrometry *Anal. Chem.* **1991,** *63*, 2057-2061

28. Grosshans, P.B., Marshall, A.G.: Cyclotron Orbital Radius Determination in Fourier Transform Ion Cyclotron Resonance Mass Spectrometry *Int. J. Mass Spectrom.* **1992,** *115*, 1-19

29. Shi, S.D.H., Drader, J.J., Freitas, M.A., Hendrickson, C.L., Marshall, A.G.: Comparison and Interconversion of the Two Most Common Frequency-to-Mass Calibration Functions for Fourier Transform Ion Cyclotron Resonance Mass Spectrometry *Int. J. Mass Spectrom.* **2000,** *195*, 591-598

30. Guan, S., Marshall, A.G.: Stored Waveform Inverse Fourier Transform (SWIFT) Ion Excitation in Trapped-Ion Mass Spectometry: Theory and Applications *Int. J. Mass Spectrom.* **1996,** *157–158*, 5-37

31. Giles, K., Pringle, S.D., Worthington, K.R., Little, D., Wildgoose, J.L., Bateman, R.H.: Applications of a Travelling Wave-Based Radio-Frequency Only Stacked Ring Ion Guide *Rapid Commun. Mass Spectrom.* **2004,** *18*, 2401-2414

32. Mamyrin, B.A.: Time-of-Flight Mass Spectrometry (Concepts, Achievements, and Prospects) *Int. J. Mass Spectrom.* **2001,** *206*, 251-266

33. Guilhaus, M.: Principles and Instrumentation in Time-Of-Flight Mass-Spectrometry - Physical and Instrumental Concepts *J. Mass Spectrom.* **1995,** *30*, 1519-1532

34. Guilhaus, M., Selby, D., Mlynski, V.: Orthogonal Acceleration Time-of-Flight Mass Spectrometry *Mass Spectrom. Rev.* **2000,** *19*, 65-107

35. Cotter, R.J.: Peer Reviewed: The New Time-of-Flight Mass Spectrometry *Anal. Chem.* **1999,** *71*, 445A-451A

36. Cotter, R.J.: Time-of-Flight Mass Spectrometry for the Structural Analysis of Biological Molecules *Anal. Chem.* **1992,** *64*, A1027-A1039

37. Wiley, W.C., McLaren, I.H.: Time-of-Flight Mass Spectrometer with Improved Resolution *Rev. Sci. Instrum.* **1955,** *26*, 1150-1157

3. Electron-Induced Dissociation of Small Singly Charged Molecules.

3.1. Introduction

EID is a fledgling technique and has thus far been carried out on limited compound classes. In order to further investigate the applications and limitations of EID, the work detailed herein has focussed on the use of EID to structurally characterise small organic molecules, an area not yet investigated. An in-depth study has concentrated on the factors affecting the degree of fragmentation, such as the precursor ion abundances, the charge-carrying species, the electron energy and the electron irradiation time. Comparisons have been carried out between EID and more traditional MS and MS/MS techniques such as EI, CID and IRMPD, in order to determine whether EID can be viewed as a replacement to the more conventional techniques or, as previously suggested, as an additional and beneficial tool to increase the available structural information. A range of small (<1 kDa) organic molecules, including pharmaceutical compounds, food dyes and oligosaccharides, have been analysed by EID, CID and IRMPD in order to discern any patterns that may arise. All of the molecules analysed contain at least one aromatic ring and one heteroatom, as well as a variety of functional groups. MS/MS analysis was carried out on each observed molecular ion, not just the protonated species.

3.2. Results and Discussion

3.2.1. Analysis of haloperidol

MS/MS analysis was carried out on haloperidol, structure shown in **Figure 3.1**, an antipsychotic drug compound chosen to represent a model pharmaceutical compound. A 5 μg mL^{-1} solution of haloperidol in methanol was directly infused into the FT-ICR mass spectrometer using an electrospray source, preferentially forming

the singly protonated molecular ion at *m/z* 376.1. The electron energies have been calculated according to the voltage offset applied to the cathode, as detailed in **Chapter 8: Materials and Methods**.

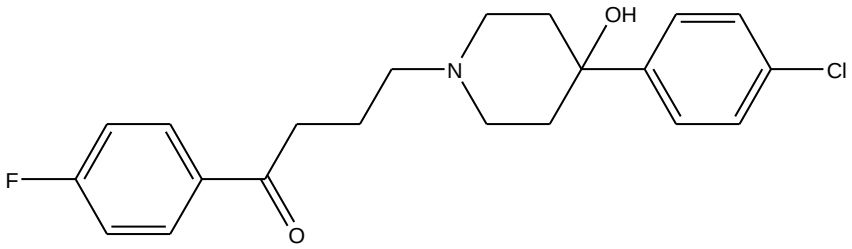

Figure 3.1: Structure of haloperidol with empirical formula $C_{21}H_{23}NO_2FCl$

Preliminary MS/MS experiments were carried out by irradiating the $[M+H]^+$ precursor with low energy electrons of 3.79 eV at an electron irradiation time of 70 ms, the typical parameters used for ECD analysis. The resulting spectrum, shown in **Figure 3.2**, revealed 4 product ions all of which were lower than 0.2% the relative abundance of the precursor ion. The molecular formulae assignments for each observed ion and the calculated relative abundance of each ion, with respect to the total ion abundances, have been summarised in **Table 3.1**. The Ring-plus-Double-Bond (RDB) values have been calculated for each assigned molecular formula from the number and valences of each element using **Equation 3.1**, where **x** is the number of elements with valence 4 (such as C, Si), **y** is the number of elements with valence 1 (H, F, Cl, Br, I) and **z** is the number of elements with valence 3 (N, P).

$$\mathbf{RDB = x - \tfrac{1}{2}\, y + \tfrac{1}{2}\, z + 1} \qquad \textbf{Equation 3.1}$$

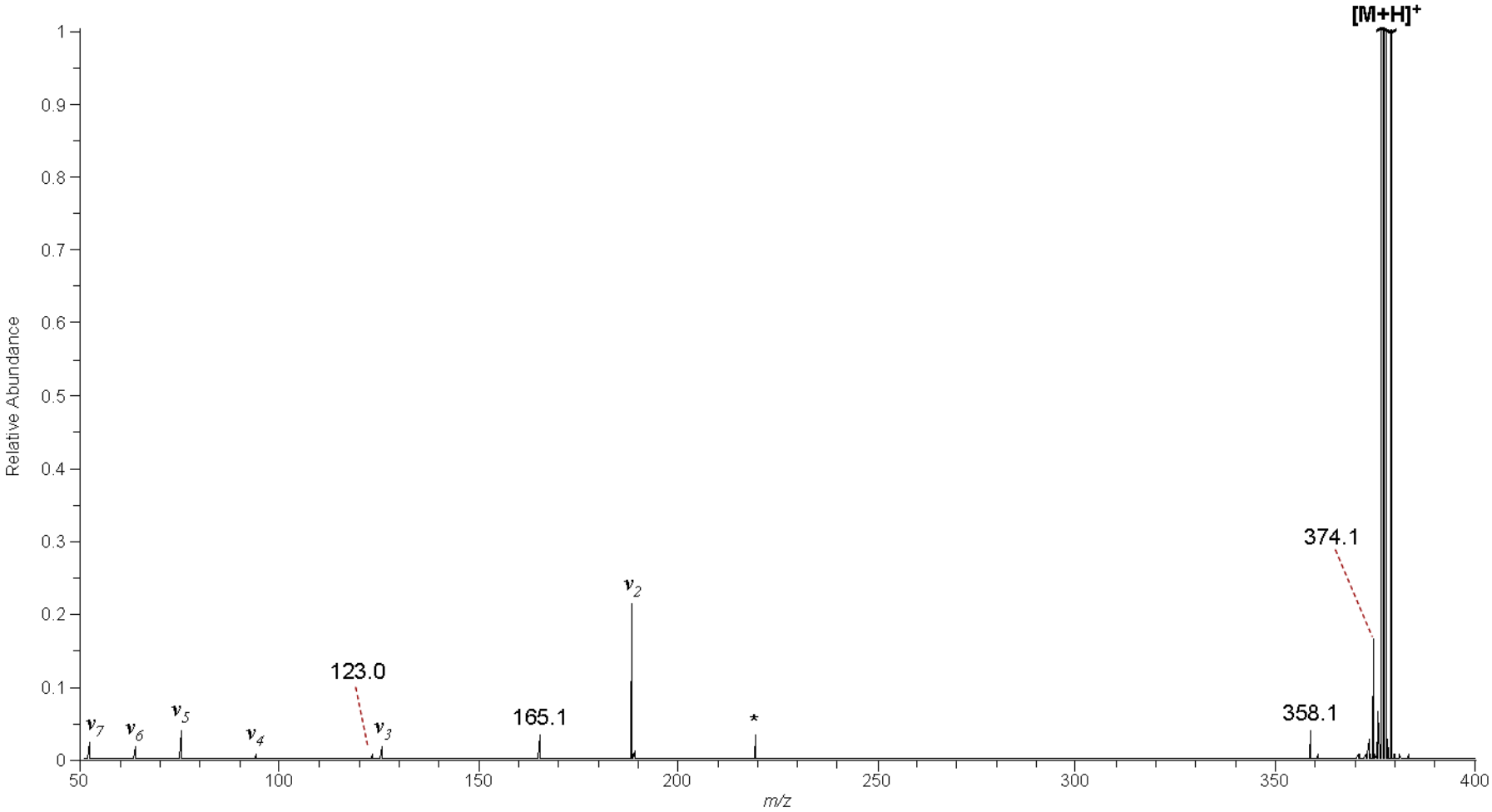

Figure 3.2: Spectrum generated from the irradiation of haloperidol $[M+H]^+$ with 3.79 eV electrons. Peaks labelled * or ν denote electronic noise and harmonic peaks respectively, and can be disregarded.

Observed Ion *m/z*	Molecular Formula	RDB	ECD / ppm	Relative Intensity / %
376.14741	**$C_{21}H_{24}NO_2FCl$**	**9.5**	**0.0**	**99.752**
374.13176	$C_{21}H_{22}NO_2FCl$	10.5	1.1	0.165
358.13685	$C_{21}H_{22}NOFCl$	10.5	1.5	0.042
165.07102	$C_{10}H_{10}OF$	5.5	-0.4	0.033
123.02407	C_7H_4OF	5.5	-1.3	0.008

Table 3.1: Summary of the ions observed in the low energy EID spectrum of the protonated haloperidol shown in Figure 3.2. The spectrum has been calibrated using the known precursor ion molecular formula.

RDB values ending in ½ are consistent with even-electron product ions, resulting from the loss of a neutral fragment(s) from the even-electron precursor ion. Conversely product ions assigned integer RDB values are consistent with an odd-electron product ion corresponding to a radical cation/anion formed from the loss of a radical species from the even-electron precursor ion. The product ions detailed in **Table 3.1** are all shown to be even-electron species. The most abundant product ion, observed at *m/z* 374.1, is proposed to result from the neutral loss of H_2 from the precursor ion. The product ion at *m/z* 358.1 is expected to result from the loss of H_2O from the piperidine ring. The remaining 2 product ions, at *m/z* 165.1 and *m/z* 123.0 are purported to be formed *via* the dissociation of bonds on the butanone chain, resulting in fragments containing the fluorine-substituted benzene ring. By comparison, CID of haloperidol generated 11 product ions, including 3 of the product ions observed by EID at *m/z* 358.1, *m/z* 165.1 and *m/z* 123.0. EID of haloperidol thus far indicates that although it can generate product ions from singly charged precursor ions, further development and improvement is required in order to make it a suitable and informative method for structural characterisation.

Effect of altering electron energy

In order to determine the optimal energy level for EID analysis, the electron energy applied to the haloperidol $[M+H]^+$ precursor was gradually increased from -0.21 eV to 23.79 eV (as calculated from the offset applied to the ECD cathode) in stepwise increments of 1 eV. At each energy level the relative abundance of the precursor ion and each product ion has been calculated with respect to the total ion abundances. A graph following the effect of increasing the electron energy on the total relative intensity of the ions observed in the haloperidol MS/MS spectrum is shown in **Figure 3.3**. The experiment was repeated twice and the resulting relative abundances for each product ion were averaged. The standard deviation for each data point has been calculated from the ion abundances measured from each experiment and are displayed as error bars. A maximum of 49 product ions were generated at 23.79 eV. All product ions that remain below 0.5% of the total ion abundance have been removed from the graph for clarity.

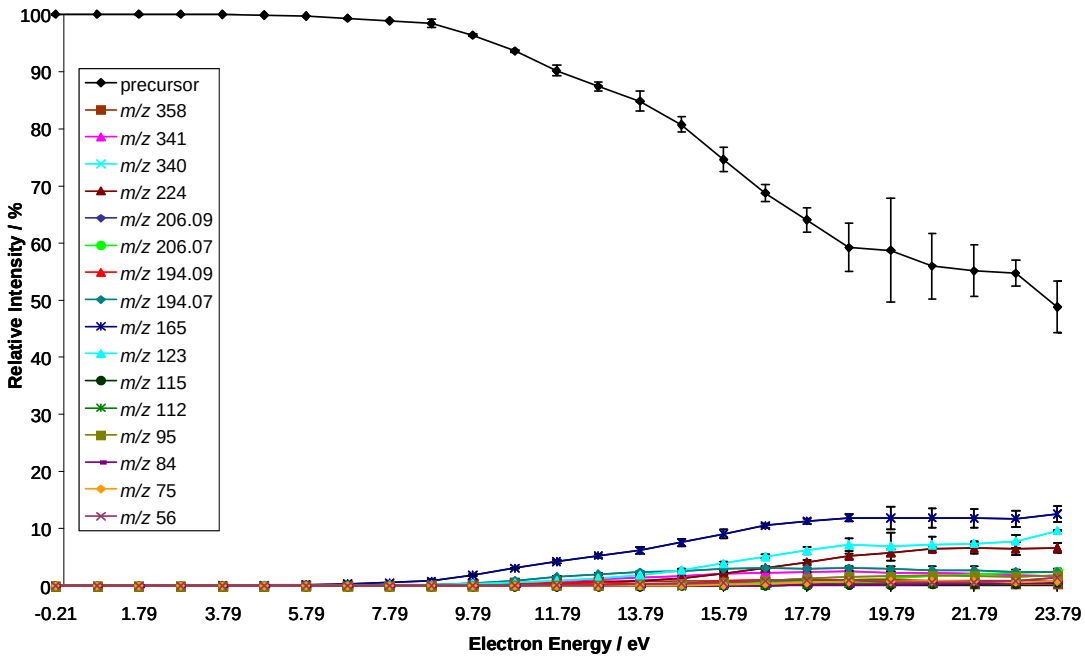

Figure 3.3: The effect of electron energy on the ion abundance of haloperidol $[M+H]^+$ precursor and the product ions.

Below 7.79 eV the effect of altering the electron energy was minimal, with neither the precursor ion nor the product ion abundances showing a significant deviation. As the electron energy was increased beyond 7.79 eV, the relative abundance of the precursor ion follows a steady decline until 19.79 eV, where it appears to plateau, indicating that an equilibrium has been reached between ion activation and the formation of product ions. At the highest electron energy, 23.79 eV, the precursor ion abundance appears to drop, suggesting that the increase in energy overcomes the bond dissociation equilibrium or neutralisation of the precursor ion starts to occur. The graph shown in **Figure 3.4** does not include the precursor ion curve in order to observe the trends followed by the product ion abundances. The product ions are shown to follow the reciprocal trend to that of the precursor ion, following a gradual upwards trajectory with a small plateau or decline after 19.79 eV observed for some product ions. The ion abundances vary according to the each product ion, indicating that the effect of the electron energy is different for each product ion and is not simply a linear progression. The formation of product ions is observed from an electron energy as low as 3.79 eV, however the key turning point appears to occur after 7.79 eV. This differs from investigations carried out by Lioe *et al.*,[1] who investigated the effect of electron energy on tryptophan $[M+H]^+$, noting an emergence of EID product ions above 13 eV.

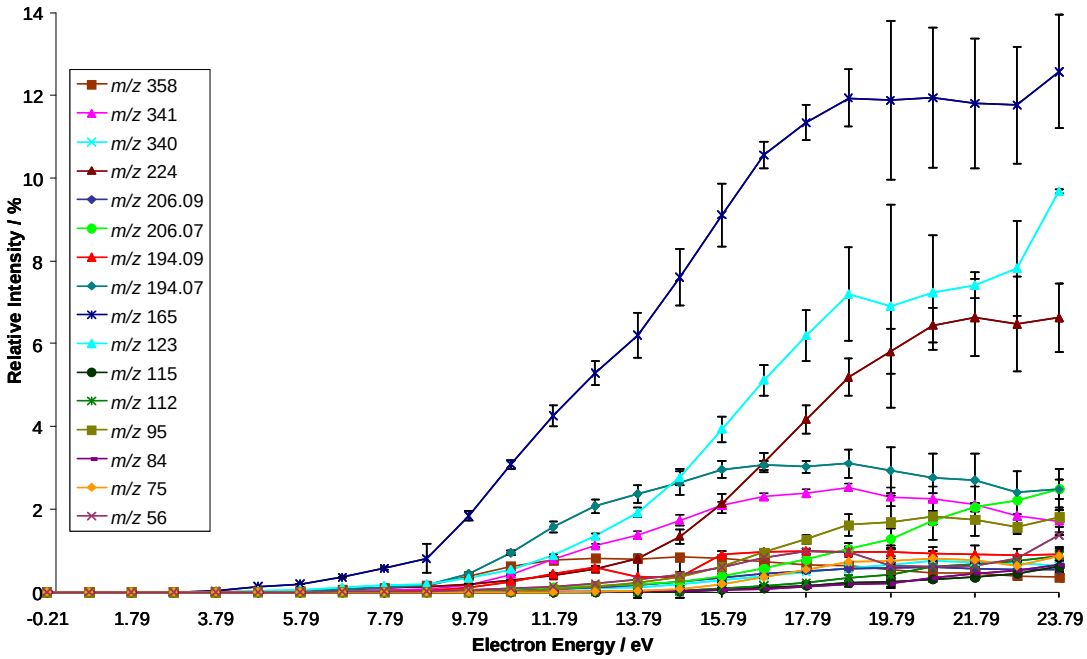

Figure 3.4: The effect of increasing the electron energy on the relative intensity of the haloperidol product ions.

The electron energy where product ion abundances reach a maximum appears to vary slightly between ions, averaging around 18.79 eV – 20.79 eV. The magnitude of the error bars increases significantly above electron energy 18.79 eV, suggesting that the high electron energy affects the reproducibility of the product ion spectra. This effect is thought to be a consequence of the higher kinetic energies of the product ions and higher energy collisions resulting in ion cloud diffusion.[2]

As the electron energy was increased, the mass accuracies of the precursor ion and the product ions were seen to deteriorate, noting a sharp increase in the mass deviation of the precursor ion as the energy is increased beyond 7.79 eV. This pattern is thought to result from the deterioration of the vacuum inside the FT-ICR cell as the increasing energy of the electrons heats the inside of the FT-ICR cell. The loss in accuracy coincides with a change in vacuum pressure of the FT-ICR Penning Gauge, increasing from 1.25 $x10^{-10}$ Torr during MS analysis to a maximum of 1.90 $x10^{-10}$ Torr at high electron energies, thereby supporting a link between

mass accuracy and vacuum. In order to counter the decline in mass accuracy, post-acquisition calibration has been carried out using the precursor ion molecular formula. At high electron energies a number of peaks were seen to appear in the low *m/z* region (< *m/z* 120) that could not be assigned as fragments of the haloperidol precursor ion, and were therefore purported to correspond to contaminants being emitted from the cathode at high energies. Validation steps have been carried out, detailed in **Chapter 9: Appendix A**, in order to determine which peaks can be assigned as artefacts or chemical noise. Peaks determined to correspond to chemical noise, silicones, plasticisers, or harmonics have been disregarded in all further spectra. Having studied the effect of electron energy on the resulting MS/MS spectra, further experiments have been carried out at 18.79 eV in order to minimise the detrimental effects of the increased electron energy on mass accuracy, peak intensity variation and the increase in artefacts, while maintaining a high degree of fragmentation.

EID MS/MS of haloperidol $[M+H]^+$

Figure 3.5(a) shows the MS/MS spectrum obtained from the EID of haloperidol with an expansion of the lower 2% of the y-axis scale shown in **Figure 3.6(a)** to highlight the low intensity product ions. A comparison between the EID spectrum of haloperidol, carried out at 18.79 eV, and the lower energy EID spectrum, at 3.79 eV, shown in **Figure 3.2** indicates that the number and intensity of the products ions have been greatly improved, with an additional 40 product ions observed by EID bringing the total number of product ions to 44. The major product ion in the lower energy EID spectrum corresponding to the loss of H_2 at *m/z* 374.1, has become one of the lower intensity product ions at 0.083% relative to the precursor ion in the 18.79 eV EID spectrum, reduced from 0.165% in the 3.79 eV EID spectrum. This decrease in relative intensity at the higher electron energy implies that either the dissociation pathways have changed at increased energy, preferentially forming

different product ions, or that the product ion at *m/z* 374.1 undergoes secondary fragmentation to form lower *m/z* product ions. Due to the high number of product ions formed from the EID of haloperidol, evidence of secondary activation and bond dissociation, the relative intensity of one product ion decreasing as another increases, is not clear from the graph in **Figure 3.4**.

CID analysis was also performed on the haloperidol $[M+H]^+$ species, with MS detection carried out in both the FT-ICR cell (hereafter labelled CID-FT), see **Figure 3.5(b)** and **Figure 3.6(b)**, and in the ion trap (hereafter labelled CID-IT), see **Figure 3.5(c)** and **Figure 3.6(c)**. The normalised collision energy employed for CID-FT and CID-IT analyses was 25 arbitrary units, as per manufacturer's software. CID-IT generated 11 product ions, however only 4 were also detected in the FT spectrum, indicating that 7 product ions were lost during transmission between mass analysers. The relative intensities of the ions has been shown to vary considerably between the CID spectra, most notably the precursor ion that can be seen at < 0.1% in the CID-IT spectrum is the second most intense peak in the CID-FT spectrum. The shift in relative peak intensities and loss of ions is thought to occur due to differences in energy between the precursor ion and product ions, specifically the lower product ion internal energies resulting from collisional cooling or the release of energy through bond dissociation, reducing the efficiency of axial ejection from the ion trap and transmission to the FT-ICR cell.[3-4]

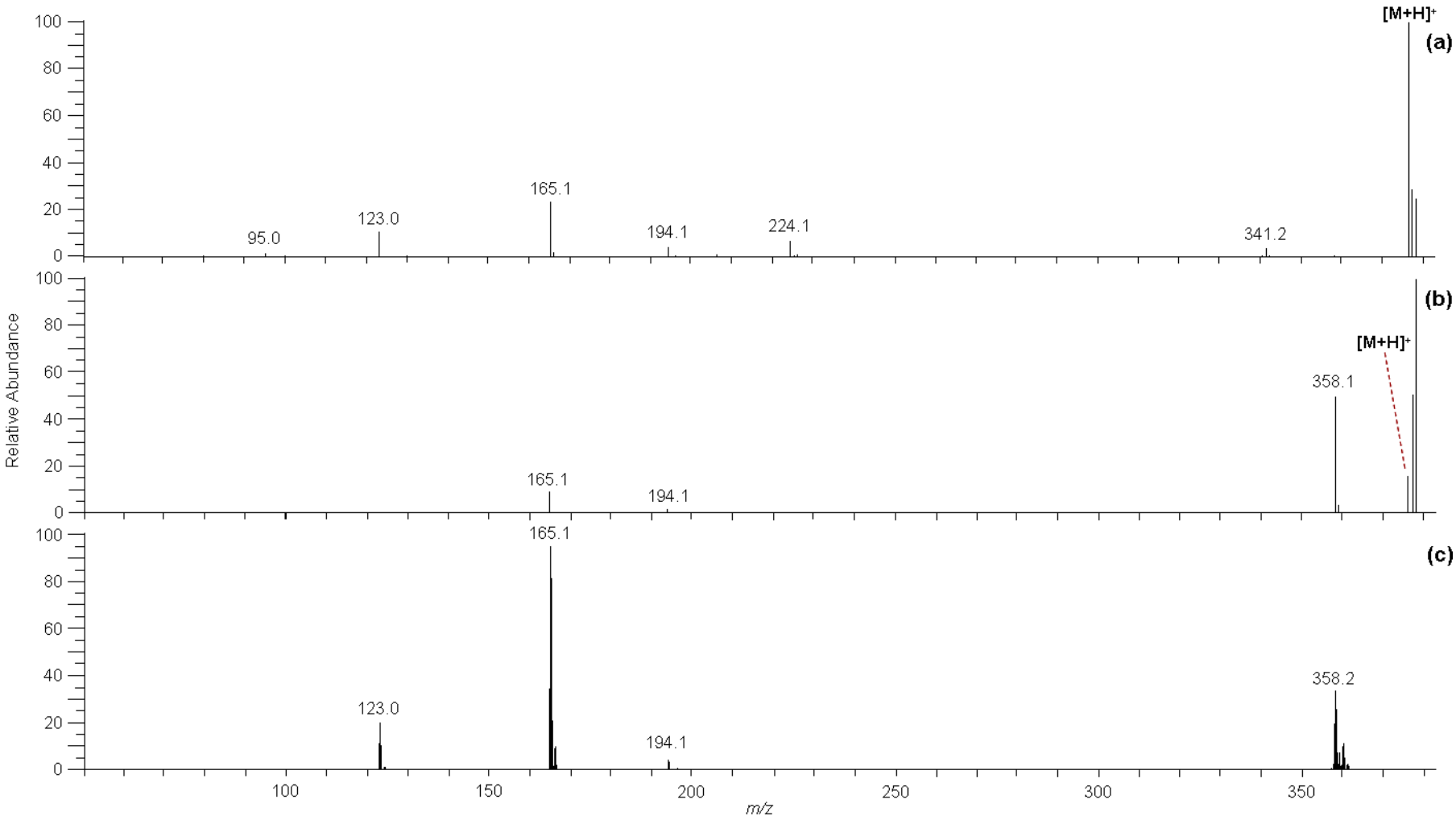

Figure 3.5(a) EID (b) CID-FT and (c) CID-IT spectra generated from the MS/MS of the haloperidol $[M+H]^+$.

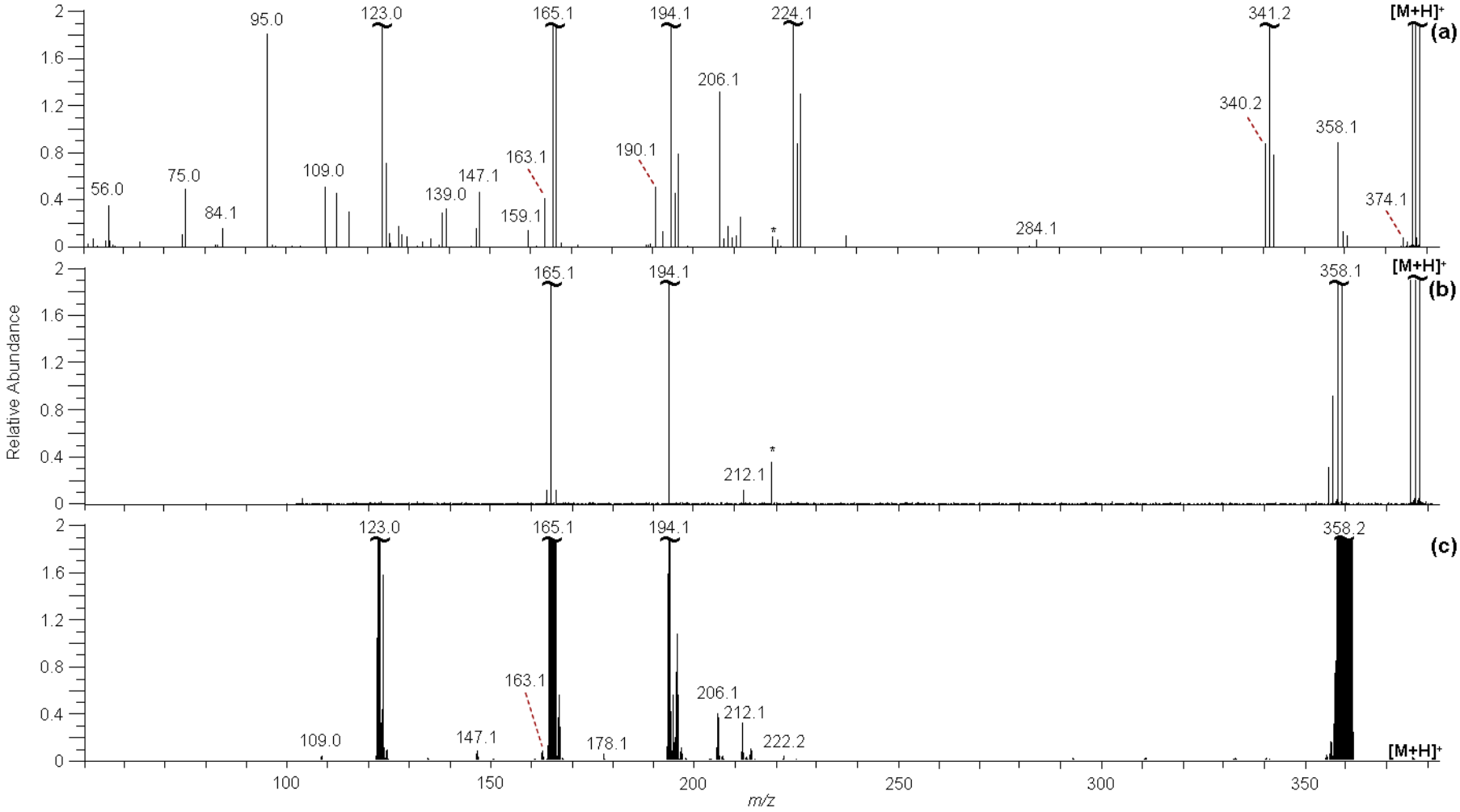

Figure 3.6: Expansion of 2% of the y-axis of the (a) EID (b) CID-FT and (c) CID-IT spectra of haloperidol from Figure 3.5.

Of the 44 product ions observed in the EID spectrum, 8 are also observed in one or both of the CID spectra. Accurate mass measurements from the FT data have suggested molecular formulae for each of the observed product ions, of which the 8 common product ions are shown in **Table 3.2** along with proposed structural assignments. The RDB values for the assigned molecular formulae in **Table 3.2** indicate that each common product ion is an even-electron species.

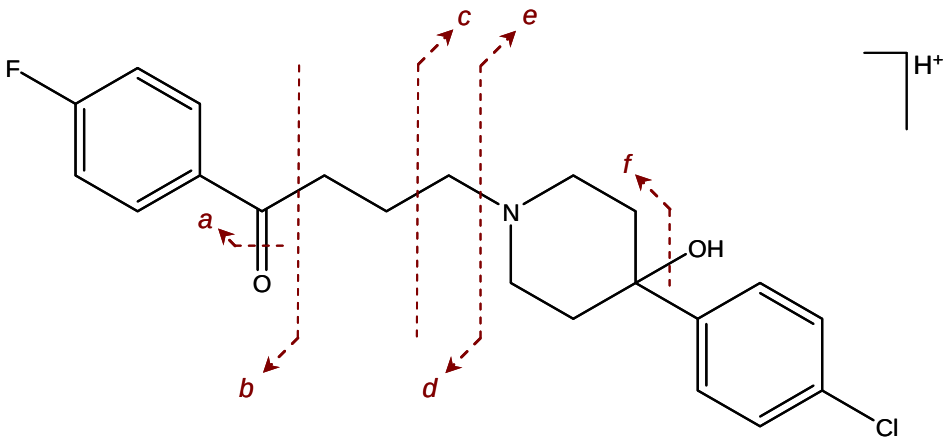

Product Ion *m/z*	Chemical Formula	RDB	*Proposed Bond Cleavage(s)*
358.1	$C_{21}H_{22}NOFCl$	10.5	*f*
206.1	$C_{12}H_{13}NCl$	6.5	*c f*
194.1	$C_{11}H_{13}NCl$	5.5	*e f*
165.1	$C_{10}H_{10}OF$	5.5	*d*
163.1	$C_{10}H_{8}OF$	6.5	*d*
147.1	$C_{10}H_{8}F$	6.5	*a d*
123.0	$C_{7}H_{4}OF$	5.5	*b*
109.0	$C_{7}H_{6}F$	4.5	*a b*

Table 3.2: Summary of product ions generated by both EID and CID of the haloperidol $[M+H]^+$. The proposed bond cleavages do not illustrate hydrogen loss/migration.

The major product ion in the EID spectrum, seen at *m/z* 165.1 at a relative ion abundance of 23.7%, is also observed in the CID spectrum and is proposed to correspond to the cleavage of the C-N bond (labelled ***d*** in **Table 3.2**) to form a fragment containing the fluoro-substituted benzene ring. Two possible reaction

schemes have been postulated in **Figure 3.7**, both involving bond dissociation initiated from the nitrogen lone pair.

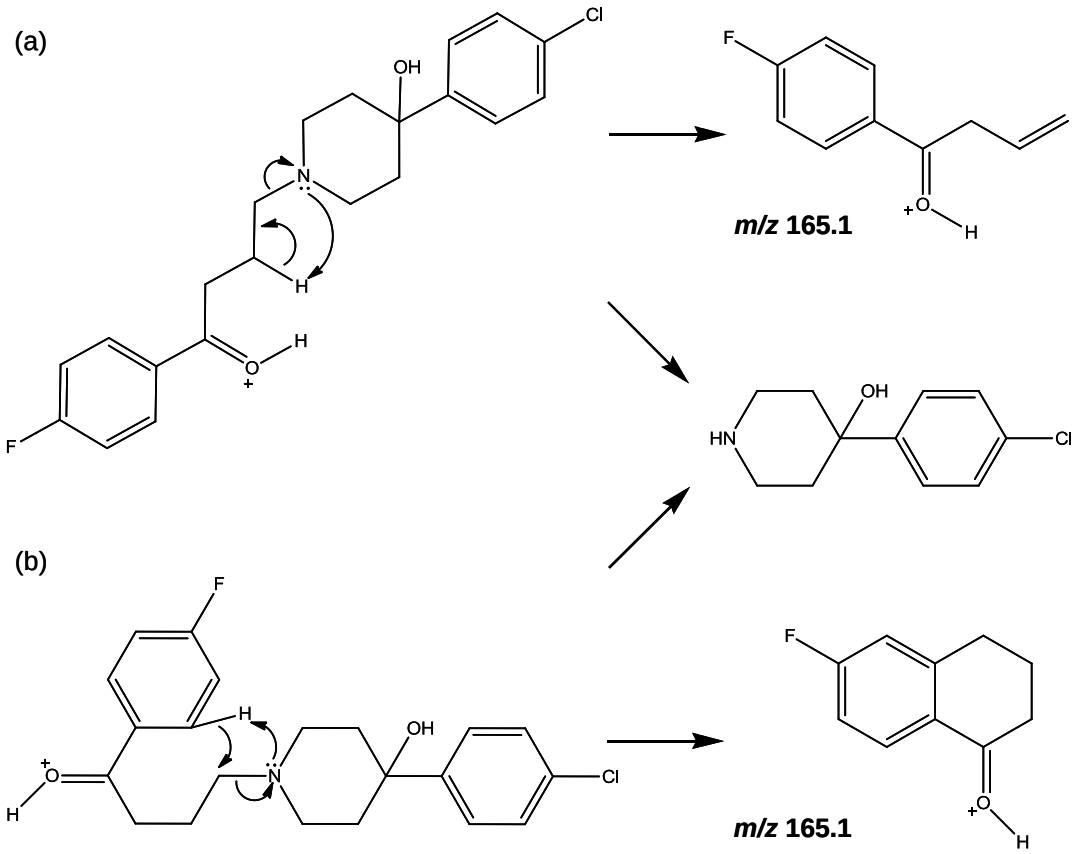

Figure 3.7: Proposed reaction mechanism for bond cleavage *d* (Table 3.2), forming the product ion at *m/z* 165.1 (a) the linear heterolytic cleavage of the N-C bond or (b) the cyclisation of the butanone chain to form a cyclical product ion.

Figure 3.7(a) shows the fragmentation pathway occurring *via* the linear heterolytic cleavage of the C-N bond, to form the even-electron product ion and a neutral species. An alternative fragmentation pathway has been proposed in **Figure 3.7(b)**, involving the rotation of the flexible butanone chain, which gives rise to the possibility of forming more stable rearrangements or cyclic product ions resulting in stable cyclic intermediates. **Table 3.3** summarises the product ions observed solely in the EID product ion spectrum and the corresponding bond cleavages associated with each ion.

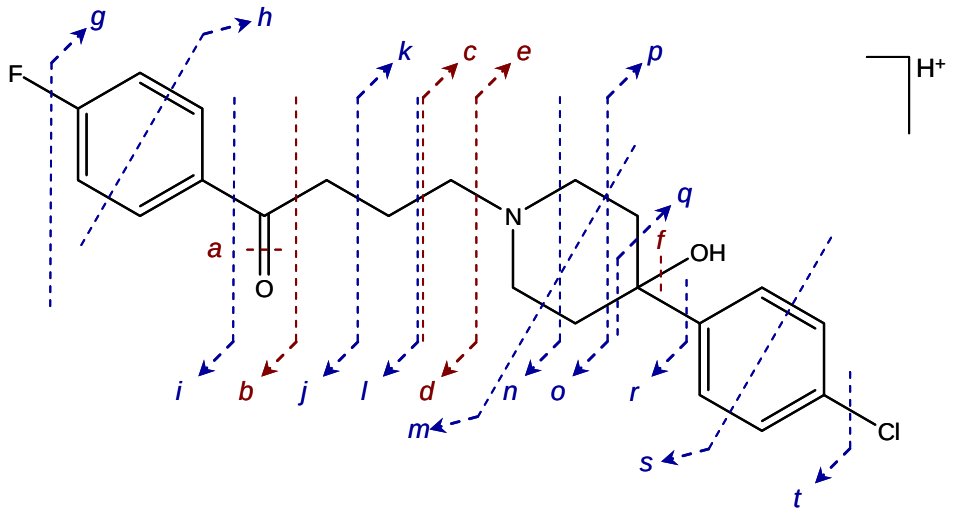

Product Ion *m/z*	Chemical Formula	RDB	Proposed Bond Cleavage(s)
374.1	$C_{21}H_{22}NO_2FCl$	10.5	loss of H_2
341.2	$C_{21}H_{24}NO_2F$	10	*t*
340.2	$C_{21}H_{23}NO_2F$	10.5	*t*
284.1	$C_{18}H_{19}NOF$	9.5	*s*
237.1	$C_{13}H_{16}NOCl$	6	*k*
224.1	$C_{12}H_{15}NOCl$	5.5	*c*
221.1	$C_{13}H_{16}NCl$	6	*k f*
220.1	$C_{13}H_{15}NCl$	6.5	*k f*
211.1	$C_{11}H_{14}NOCl$	5	*e*
210.1	$C_{11}H_{13}NOCl$	5.5	*e*
209.1	$C_{11}H_{12}NOCl$	6	*e*
206.1	$C_{12}H_{13}NOF$	6.5	*n*
194.1	$C_{11}H_{13}NOF$	5.5	*m*
192.1	$C_{11}H_{11}NCl$	6.5	*e f*
190.1	$C_{12}H_{16}NO$	5.5	*f h r*
159.1	$C_{11}H_{13}N$	6	*e f t*
146.1	$C_{10}H_7F$	7	*a d*

Product Ion *m/z*	Chemical Formula	RDB	Proposed Bond Cleavage(s)
139.0	C_7H_4OCl	5.5	*q*
138.0	C_8H_7OF	5	*b*
137.0	C_8H_6Cl	5.5	*f p*
135.1	C_9H_8F	5.5	*a j*
133.0	C_9H_6F	6.5	*a j*
129.1	$C_{10}H_9$	6.5	*a d g*
128.1	$C_{10}H_8$	7	*a d g*
127.1	$C_{10}H_7$	7.5	*a d g*
125.0	C_7H_6Cl	4.5	*f q*
115.1	C_9H_7	6.5	*a g l*
112.1	$C_6H_{10}NO$	2.5	*c r*
95.0	C_6H_4F	4.5	*i*
84.1	$C_5H_{10}N$	1.5	*e f r*
75.0	C_6H_3	5.5	*g i*
74.0	C_6H_2	6	*g i*
57.1	C_3H_7N	1	*e o*
56.0	C_3H_6N	1.5	*e o*

Table 3.3: Summary of product ions of haloperidol $[M+H]^+$ unique to EID. Proposed bond cleavages do not illustrate hydrogen loss/migration. Cleavages labelled in blue are not observed at 3.79 eV.

The product ions detailed in **Table 3.3** are shown to be a mixture of odd-electron and even-electron species, suggesting that EID occurs *via* multiple fragmentation pathways creating product ions formed *via* heterolytic cleavage, homolytic cleavage or intramolecular rearrangements. The proposed bond cleavages indicate that EID has the ability to cleave a greater number of bonds than CID, most importantly generating cross-ring fragmentation that was not observed by CID. Cleavage across aromatic rings, labelled ***h*** and ***s*** in **Table 3.3**, is proposed to follow electron interaction at the aromatic ring, disrupting the π-electron system and initiating bond dissociation.[5-6] Due to the high mass precision of the FT-ICR MS, the mass difference between the peaks can be measured accurately and precisely enough to differentiate between the mass of ^{1}H, 1.007825 Da, and the mass difference between the ^{12}C and ^{13}C isotopes, 1.003355 Da, as shown in **Figure 3.8**, lending confidence to molecular formulae assignments. The observation of product ion multiplets corresponding to species differing only in the number of hydrogen atoms confirms the tendency for EID to allow intramolecular hydrogen migration or abstraction, a pattern that is commonly observed by ECD. The process of electron capture and subsequent bond dissociation is rapid, typically in the picosecond time scale[7], suggesting that hydrogen scrambling occurs prior to electron capture[8] or after bond dissociation.[9] Evidence of hydrogen scrambling by CID is also widespread, however due to the slower vibrational energy redistribution, intramolecular hydrogen migration is thought to be possible before or after bond dissociation.[10] EID is proposed to follow any one of several fragmentation pathways, including electronic excitation, vibrational excitation or secondary ionisation leading to electron capture, therefore the mechanism of hydrogen migration is thought to be dependant on the preceding ion activation step.

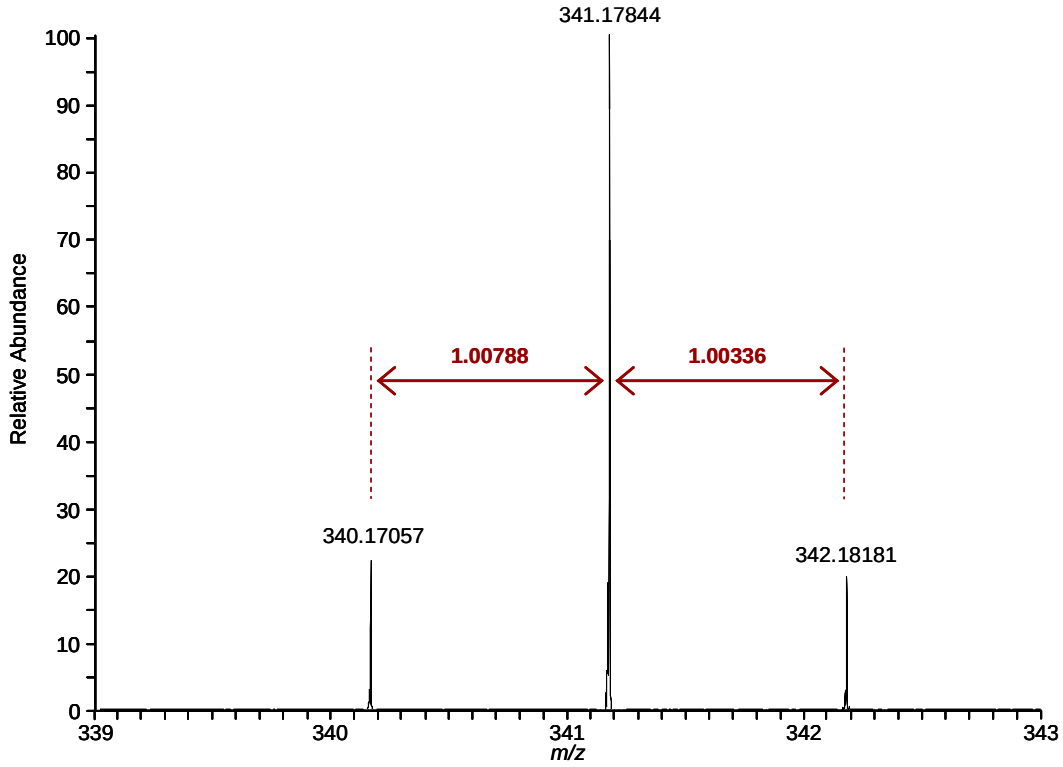

Figure 3.8: Peak grouping observed in the haloperidol EID spectrum, where the *m/z* 340.2 and *m/z* 341.2 peaks differ by an $H^{\bullet}$, corresponding to the loss of HCl and $Cl^{\bullet}$ respectively, and the *m/z* 342.2 corresponds to the ^{13}C species.

Limit of Detection for EID MS/MS

In order to determine the lower Limit of Detection (LOD) for EID, analysis of haloperidol was carried out at a range of concentrations between 50 pg mL^{-1} and 5 µg mL^{-1} *via* direct infusion and compared with CID-FT and CID-IT on the LTQ-FT. The automatic gain control (AGC) adjusts the ion injection time according to the number of ions entering the FT cell, so as to avoid space charge effects caused by too many ions trapped in the cell. At low sample concentrations, the injection time required to meet the AGC target may be greater than the specified injection time limit, thereby trapping and detecting an insufficient number of ions and affecting the mass accuracy and signal-to-noise of the resulting spectrum. As a result, the lower LOD may vary according to the preset AGC and injection time limits. For the purpose of these experiments, the maximum injection time and the AGC target settings were fixed for all sample concentrations, as detailed in **Chapter 8:**

Materials and Methods. The product ion spectra were generated by averaging 25 MS/MS scans for each technique so as to ensure a fair comparison. The experiments were carried out in triplicate and the average numbers of product ions generated for each sample have been charted in **Figure 3.9**. At a concentration of 1 ng mL^{-1} product ions start to appear by EID, gradually increasing in number until reaching a maximum at the concentration of 1 µg mL^{-1}. By comparison, CID-IT analysis generated 4 product ions from the 50 pg mL^{-1} sample, gradually increasing until 0.5 µg mL^{-1} where the number of product ions plateaus. Due to the loss of low energy ions during transmission between the ion trap and the FT, CID-FT generates fewer product ions at each concentration, the lower LOD increases to 0.5 ng mL^{-1} and the maximum number of product ions is observed at 10 ng mL^{-1}.

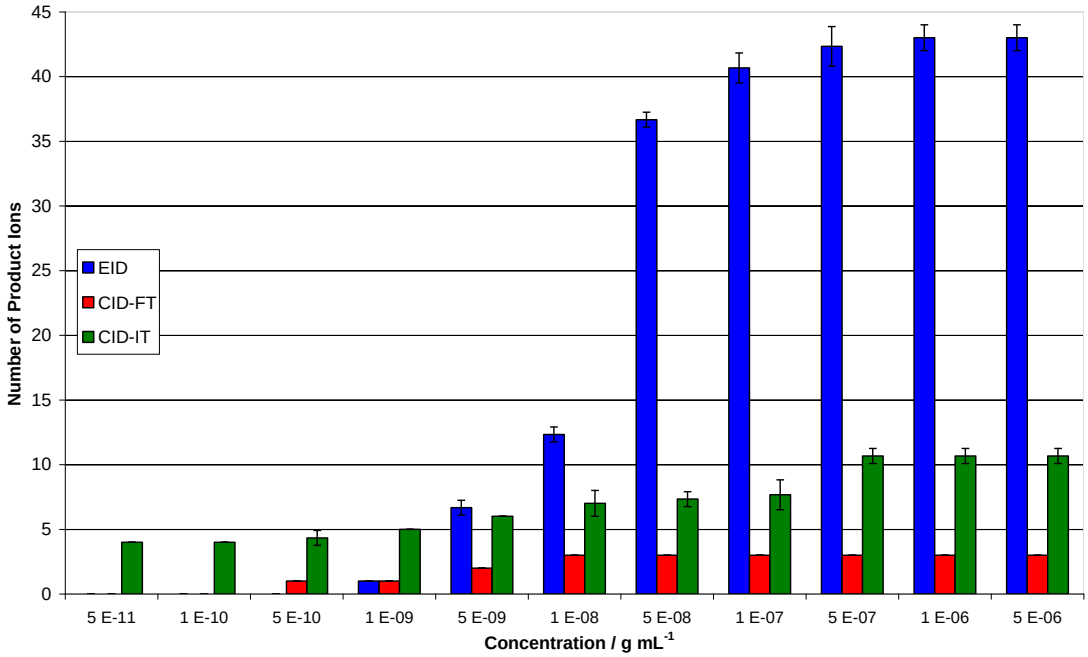

Figure 3.9: Graph indicating the number of product ions generated at each sample concentration from the MS/MS of haloperidol.

EID has been shown to be less sensitive than CID, requiring higher sample concentrations to produce MS/MS data, however EID was found to generate up to four times as many product ions for haloperidol, at concentrations higher than 5 ng

mL^{-1}, indicating the vast amount of structural information that can be gained by using EID. The detection limits are dependent on a number of instrumental and sample factors, including maximum injection time, AGC target, ionisation efficiency and MS/MS efficiency, and therefore the lower LOD may vary for different compounds and instrumental settings. Although not universal, the results determined for haloperidol provide an insight into the capabilities of EID.

EID MS/MS of haloperidol $[M+Na]^+$

Samples ionised by ESI are often observed as adducts corresponding to different charge-carrying species, such as $[M+Na]^+$, $[M+K]^+$ or $[M+NH_4]^+$. In certain cases these molecular ions may be preferentially formed over the protonated species, therefore it important to understand the effect different charge-carriers may have on the MS/MS product ions. The MS spectrum of haloperidol included the sodium-adducted species at *m/z* 398, which was targeted for further MS/MS analysis. The product ion spectrum generated from the EID of the haloperidol $[M+Na]^+$ is shown in **Figure 3.10(a)** and in the expansion of 0 - 2% of the y-axis scale in **Figure 3.11(a)**, and has been compared to the EID spectrum generated from the $[M+H]^+$ precursor as shown in **Figure 3.10(b)** and **Figure 3.11(b)**.

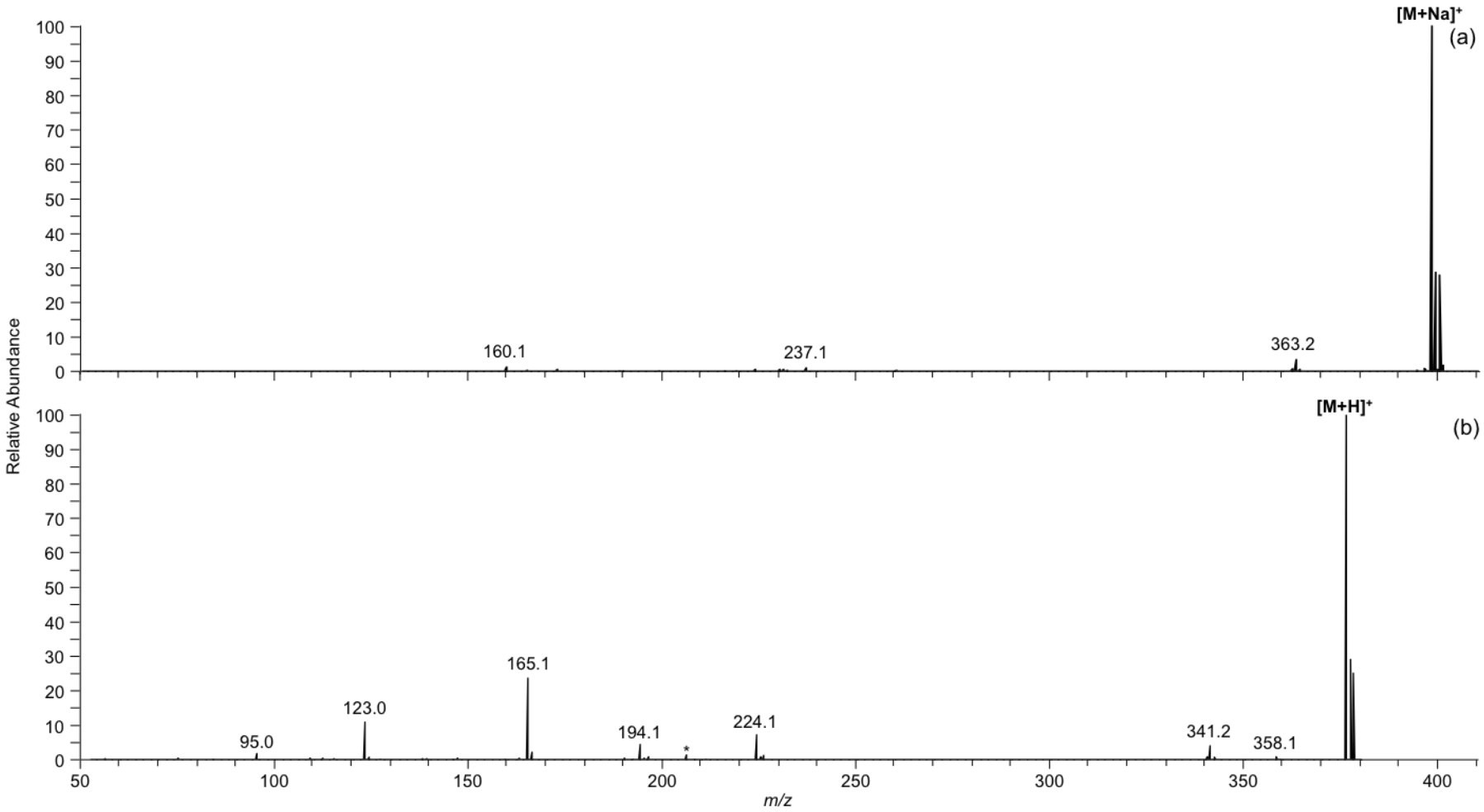

Figure 3.10: EID spectra of haloperidol (a) $[M+Na]^+$ and (b) $[M+H]^+$.

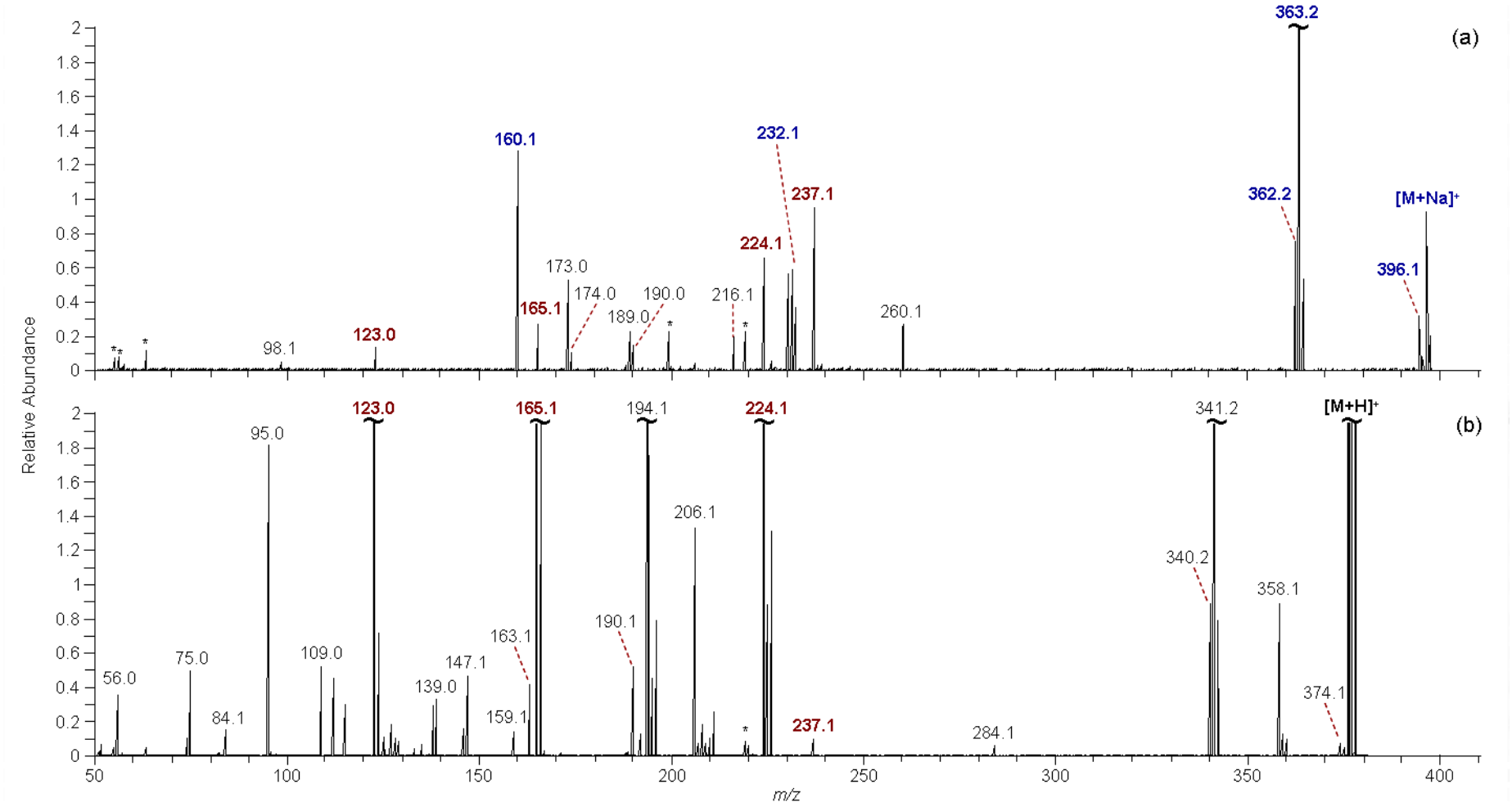

Figure 3.11: Expansion of the EID spectra of haloperidol (a) $[M+Na]^+$ and (b) $[M+H]^+$ shown in Figure 3.10. Product ions common to both precursors are highlighted in red. Product ions highlighted in blue represent sodium-adducted species that are observed in protonated form in $[M+H]^+$.

The EID of the sodium-adducted precursor ion generated 18 product ions, far less than the 37 generated by the protonated species, however only 4 of these product ions are seen to lose the sodium cation to form product ions common with the protonated EID spectrum, as highlighted in **Figure 3.11** and graphically represented in **Figure 3.12**. These common ions are thought to occur *via* charge transfer from the sodium cation, thereby resulting in the loss of a sodium atom and the formation of a protonated product ion. Of the remaining 14 product ions in the $[M+Na]^+$ spectrum, only 5 correspond to the sodium-adducted equivalents of product ions observed in the protonated spectrum, including the product ion formed by the loss of H_2 from the precursor ion, and consequently 9 product ions are exclusively formed by the $[M+Na]^+$ species. The product ions observed from the EID of the $[M+Na]^+$ species have been detailed in **Table 3.4**, indicating the proposed bond cleavages.

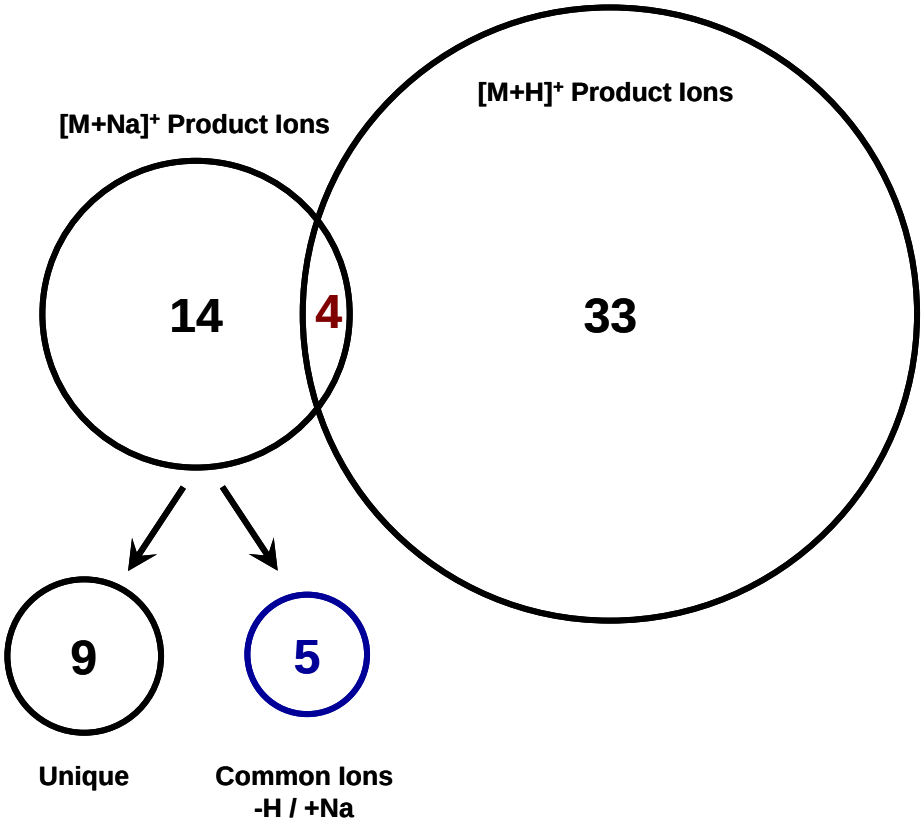

Figure 3.12: Venn diagram displaying the comparison between product ions generated by the EID of $[M+H]^+$ and $[M+Na]^+$ precursors.

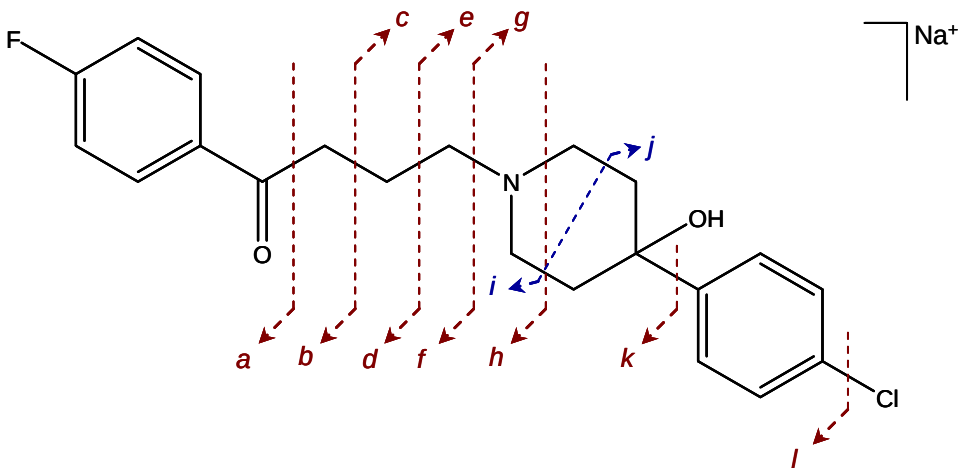

Product Ion *m/z*	Chemical Formula	RDB	Proposed Bond Cleavage(s)	Present in $[M+H]^+$ EID
396.1	$C_{21}H_{21}NO_2FClNa$	10.5	*loss of H_2*	*- Na / +H*
363.2	$C_{21}H_{23}NO_2FNa$	10	*l*	*- Na / +H*
362.2	$C_{21}H_{22}NO_2FNa$	10.5	*l*	*- Na / +H*
260.1	$C_{13}H_{16}NOClNa$	5.5	*c*	-
237.1	$C_{13}H_{16}NOCl$	6	*c*	*Y*
232.0	$C_{11}H_{12}NOClNa$	5.5	*g*	*- Na / +H*
231.1	$C_{12}H_{15}NOFNa$	5	*i*	-
230.1	$C_{12}H_{14}NOFNa$	5.5	*i*	-
224.1	$C_{12}H_{15}NOCl$	5.5	*e*	*Y*
216.1	$C_{11}H_{12}NOFNa$	5.5	*h*	-
190.0	C_9H_8OClNa	5	*j*	-
189.0	C_9H_7OClNa	5.5	*j*	-
174.0	C_9H_8OFNa	5	*d*	-
173.0	C_9H_7OFNa	5.5	*d*	-
165.1	$C_{10}H_{10}OF$	5.5	*f*	*Y*
160.0	C_8H_6OFNa	5	*b*	*- Na / +H*
123.0	C_7H_4OF	5.5	*a*	*Y*
98.1	$C_6H_{12}N$	1.5	*e k*	-

Table 3.4: Summary of product ions formed by EID of haloperidol $[M+Na]^+$. Proposed bond cleavages do not illustrate hydrogen loss/migration. Bond cleavages in blue are not observed in the protonated EID data. Y indicates product ions common to $[M+H]^+$ and $[M+Na]^+$.

The product ions and bond cleavages proposed in **Table 3.4** indicate a significant reduction in the number of bonds broken upon EID of the $[M+Na]^+$ species compared to the protonated EID data shown in **Table 3.2** and **Table 3.3**. Cross-ring cleavages within the aromatic rings are no longer observed, however a new bond

cleavage within the piperidine ring has emerged. This observation implies that the charge-carrying species can not only influence the number of product ions formed, but also the resulting fragmentation pathways and therefore analysing multiple molecular ions for any given compound can increase the amount of structural information that can be produced. The product ions shown in **Table 3.4**, in particular product ions at *m/z* 165.1 and *m/z* 98.1, suggest that the sodium cation can reside in at least 2 different positions on the haloperidol molecule, either on the piperidine ring or the fluoro-substituted benzaldehyde group whereas by comparison the product ions formed from the $[M+H]^+$ precursor suggest protonation could occur on the piperidine ring or either of the benzene groups. Knowledge of cation locations could allow for the manipulation of MS/MS product ions in order to focus structural information on specific areas of the precursor ion. Investigations into sodium affinities of small molecules and amino acids have determined that the interaction between Na^+ and aromatic, π-electron systems is particularly stable.[11-12] This suggests that, in the case of haloperidol, the metal cation can reside on the piperidine ring or either of the benzene groups, although confirmation of the sodium residing on the chloro-subsitituted benzene is not possible from MS/MS data alone.

3.2.2. EID of doubly charged cations

Multiply charged ions are observed less frequently during ESI MS analysis of small organic molecules due to the requirement of more than one charge site in such close proximity, however on occasion, when the cation affinity is sufficiently high, multiply charged species can be formed. Haloperidol was not observed as a doubly charged ion, therefore further study has been carried out on cediranib, structure shown in **Figure 3.13**, which was observed as a singly and doubly protonated molecular ion, at *m/z* 451.2 and *m/z* 226.1 respectively, postulated to reside on one of the heteroatoms.

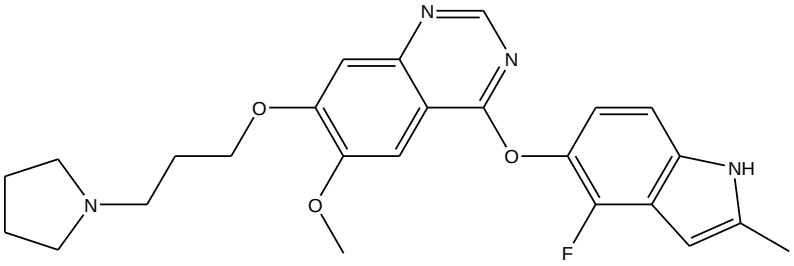

Figure 3.13: Structure of cediranib

Cediranib $[M+H]^+$ and $[M+2H]^{2+}$ were irradiated with 18.79 eV electrons, generating product ion spectra for EID and hECD respectively. A direct comparison between the EID of the $[M+H]^+$ precursor, see **Figure 3.15(a),** and the $[M+2H]^{2+}$ precursor, see **Figure 3.15(b)**, indicated a comparable degree of fragmentation generate by each species, with 43 and 40 product ions respectively. Despite the similarity in the number of product ions, each spectrum contains product ions that are unique to their respective precursor ion, with only 27 product ions common to both molecular ions. A distinct variation in the product ion abundances is also evident between the two spectra. The most abundant product ion in the EID spectrum of the $[M+H]^+$ species corresponds to the peak at *m/z* 112.1*,* which is proposed to result from the cleavage of the C-O bond to generate the propylpyrrolidine fragment. The propylpyrrolidine group is observed as the most abundant ion from CID, indicating that the C-O bond is the weakest bond in the molecule. Conversely, the most abundant product ion generated from the $[M+2H]^{2+}$ precursor is observed at *m/z* 338.1 corresponds to the cleavage of the same C-O bond to form the reciprocal fragment, as shown in **Figure 3.14.** The change in the major product ion between the $[M+H]^+$ and $[M+2H]^{2+}$ precursor ions suggests that electron capture, and subsequent charge neutralisation, occurs at the propylpyrrolidine arm of the doubly charged species, thereby creating a neutral propylpyrrolidine fragment and the singly charged indole-quinazoline.

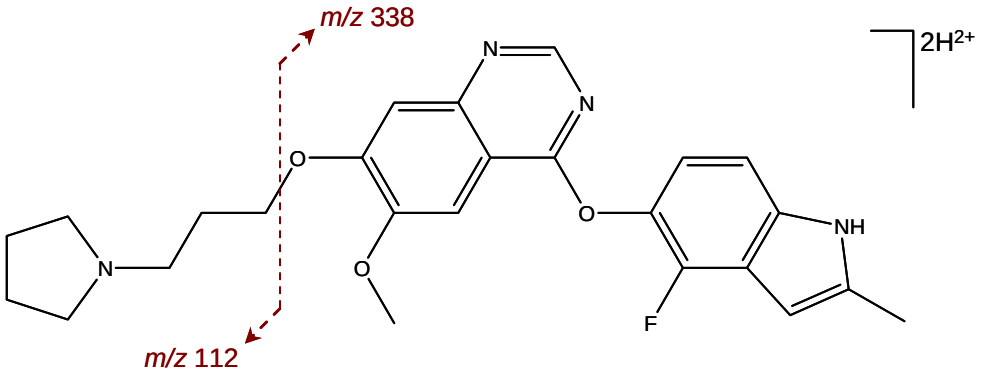

Figure 3.14: Major bond cleavage occurring *via* the MS/MS of cediranib.

A significant observation in the EID spectrum of the $[M+H]^+$ species was the presence of 2 doubly charged product ions, at *m/z* 216.1 and *m/z* 215.6, consistent with the loss of $F^{\bullet}$ and HF respectively. The formation of doubly charged product ions from a singly charged precursor is consistent with the proposed theory that bond dissociation by EID occurs through electron ionisation, forming the $[M+H]^{2+\bullet}$ intermediate that can lose neutral species to form doubly charged product ions, as shown in **Scheme 3.1** and **Scheme 3.2**.[13-14]

$$\mathbf{[M+H]^+ + e^- \rightarrow [M+H]^{2+\bullet} + 2e^-} \qquad \textbf{Scheme 3.1}$$

$$\mathbf{[M+H]^{2+\bullet} \rightarrow [product\ ion + H]^{2+} + neutral^{\bullet}} \qquad \textbf{Scheme 3.2}$$

Singly charged product ions are proposed to form *via* one of several dissociation pathways, detailed in **Schemes 3.3 – 3.6**; vibrational excitation of the $[M+H]^+$ precursor, electronic excitation of the $[M+H]^+$ precursor, electron capture by the $[M+H]^{2+\bullet}$ intermediate, or bond dissociation of the $[M+H]^{2+\bullet}$ intermediate to form 2 singly charged product ions.

$$\mathbf{[M+H]^+ \rightarrow [M+H]^{+*}} \qquad \textbf{Scheme 3.3}$$

$$[M+H]^+ + e^- \rightarrow [M+H]^{+*} + e^- \qquad \textbf{Scheme 3.4}$$

$$[M+H]^+ + e^- \rightarrow [M+H]^{2+\bullet} + 2e^- \rightarrow [M+H]^{+*} + e^- \qquad \textbf{Scheme 3.5}$$

$$[M+H]^{2+\bullet} \rightarrow [\text{product ion}]^+ + [\text{product ion}]^{+\bullet} \qquad \textbf{Scheme 3.6}$$

No evidence of doubly charged product ions was seen from EID of haloperidol, suggesting that the $[M+H]^{2+\bullet}$ intermediate is short-lived, more unstable than the cediranib $[M+H]^{2+\bullet}$, rapidly capturing an electron to form the $[M+H]^{+*}$ excited state ion prior to bond dissociation, as shown in **Scheme 3.5**.[13]

The EID spectrum of the cediranib $[M+2H]^{2+}$ contained 7 doubly charged product ions, including the 2 generated by the $[M+H]^+$ precursor, which were generated by neutral losses from the precursor. There is no evidence of triply charged species formed from the electron ionisation of the doubly charged precursor, suggesting that either the $[M+2H]^{3+\bullet}$ species is a short-lived intermediate or that the mechanism of fragmentation proceeds *via* an alternative route, such as electron capture, electronic excitation (without secondary ionisation) or vibrational excitation.[1, 14]

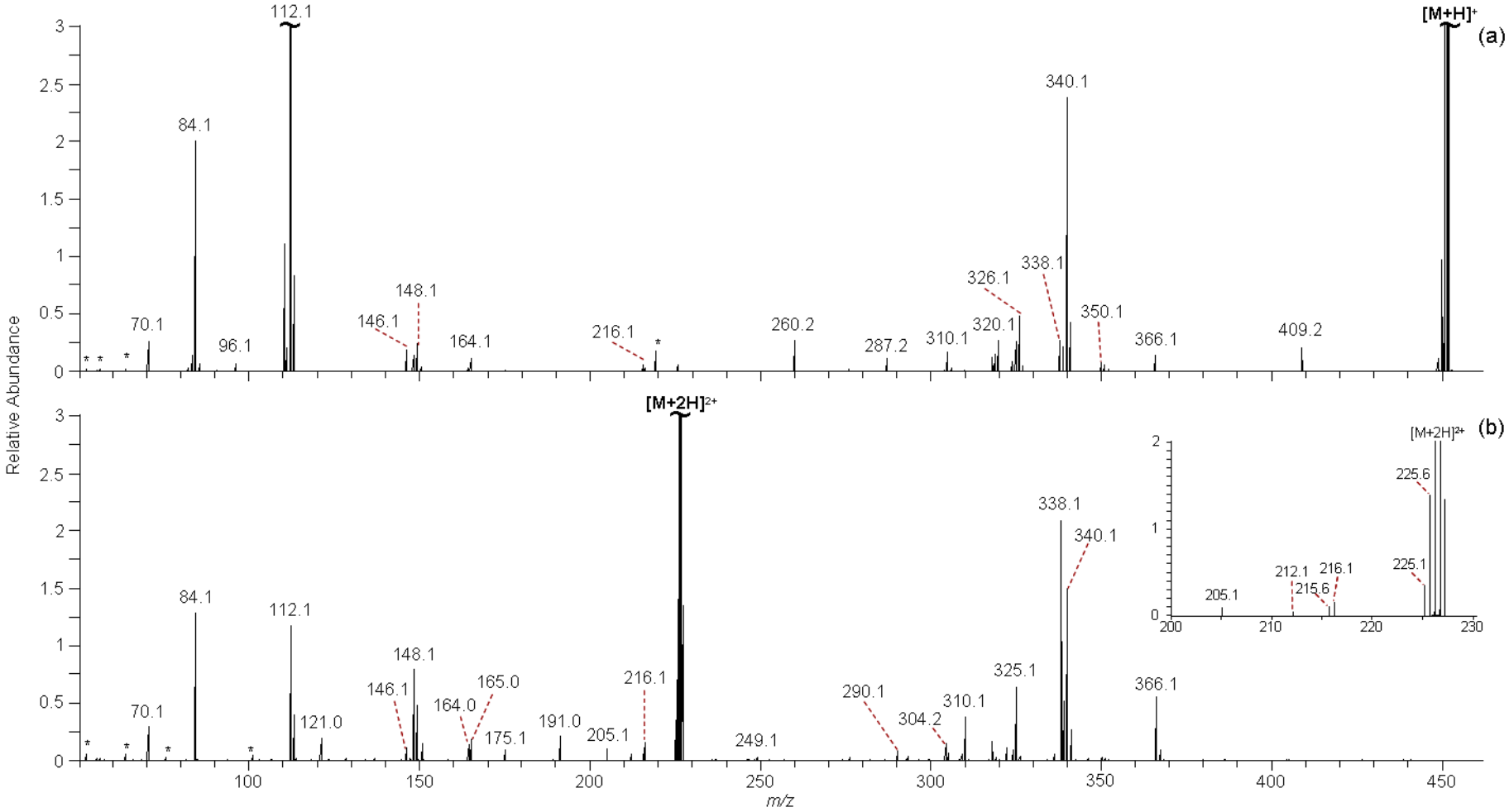

Figure 3.15: EID of (a) the $[M+H]^+$ precursor and (b) the $[M+2H]^{2+}$ precursor of cediranib. Inset: Expansion of (b) indicating doubly charged product ions formed from neutral losses from the $[M+2H]^{2+}$ species.

3.2.3. EID analysis of anions

EID analysis has also been carried out on negatively charged precursor ions, to determine whether the ionisation polarity has an effect on the ion activation and subsequent dissociation. Among the compounds analysed by negative ion EID was the food dye Allura Red, structure shown in **Figure 3.16**, which contains two SO_3Na functional groups, both of which have the ability to lose a sodium cation resulting in the negatively charged SO_3^- group. As a result, two molecular ions were observed; the $[M\text{-}Na]^-$ and the $[M\text{-}2Na]^{2-}$, which were targeted for MS/MS analysis.

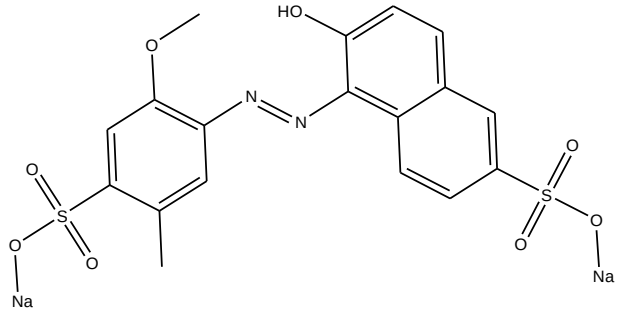

Figure 3.16: Structure of Allura Red (E129)

A direct comparison between EID of the Allura Red $[M\text{-}Na]^-$ and $[M\text{-}2Na]^{2-}$ precursors has been shown in **Figure 3.17**. Electron irradiation of the doubly charged species is expected to result in electron detachment, akin to the EDD of multiply charged polypeptides. The spectrum generated from the singly charged precursor resulted in only 1 product ion, at *m/z* 182.0, corresponding to the molecular formula $C_7H_4NO_3S$ and resulting from the cleavage of the N=N bond and the loss of the methoxy group from the benzene ring to form the 2-methylbenzenesulphonate fragment. The spectrum generated from the doubly charged precursor shows a significantly higher degree of fragmentation resulting in 19 product ions, including 3 doubly charged product ions following neutral losses from the precursor ion.

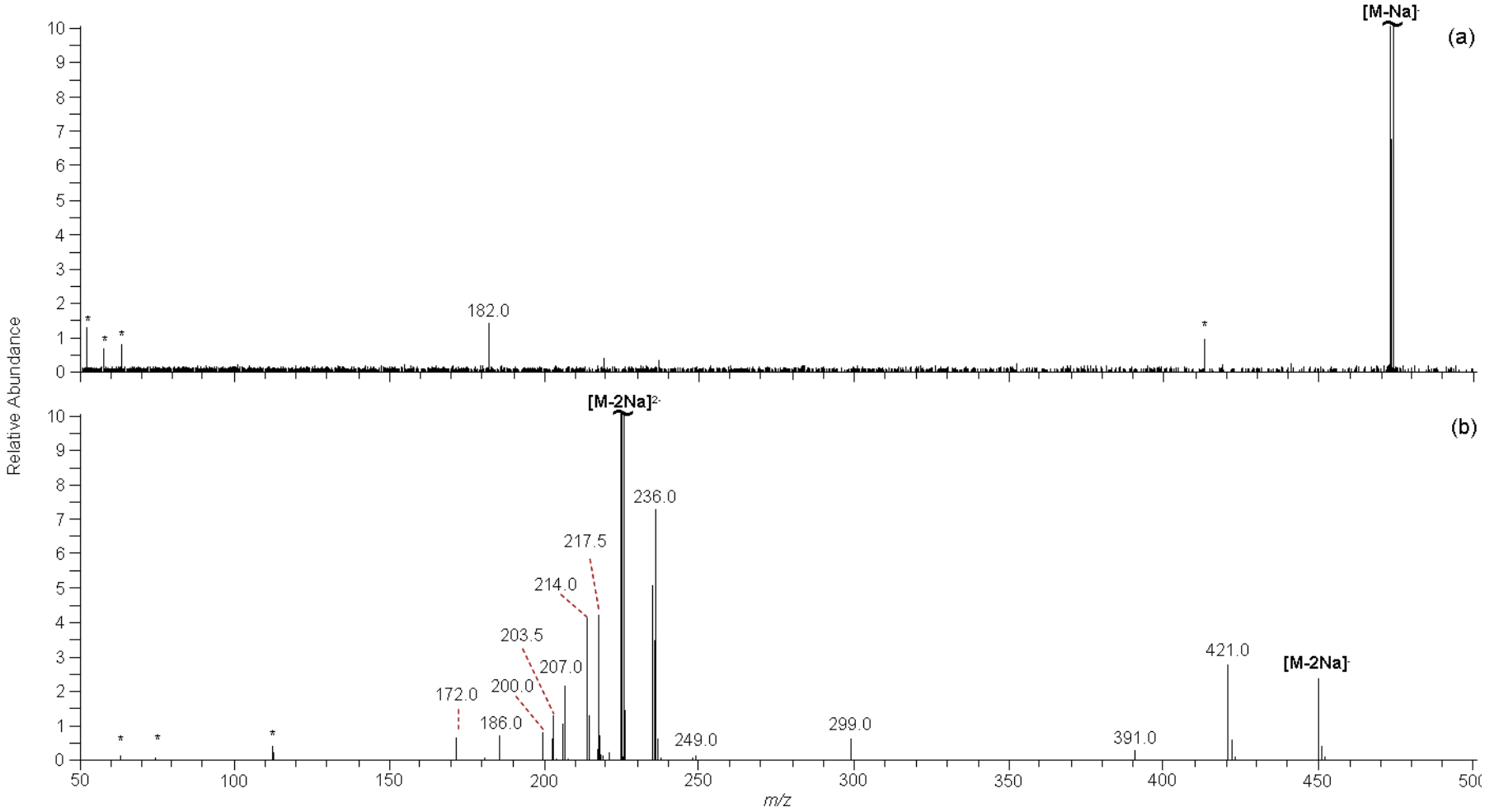

Figure 3.17: EID spectrum of (a) the $[M-Na]^-$ precursor and (b) the $[M-2Na]^{2-}$ precursor of Allura Red.

The peak at *m/z* 182.0 in the $[M\text{-}Na]^-$ spectrum is not observed in the $[M\text{-}2Na]^{2-}$ spectrum, however a peak at *m/z* 186.0 with the empirical formula $C_7H_8NO_3S$ is observed, corresponding to a fragment containing the same portion of the Allura Red structure, as indicated in **Figure 3.18**.

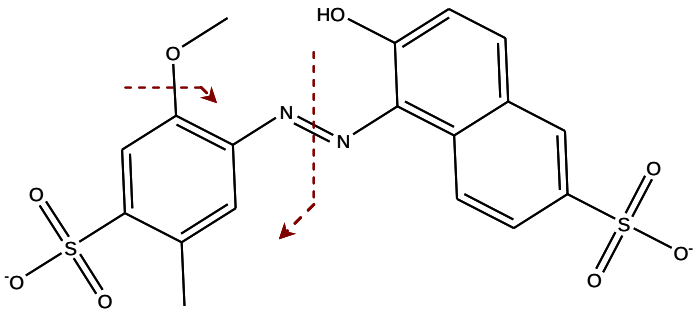

Figure 3.18: Proposed bond cleavages to form the product ion at *m/z* 186.0 in the $[M\text{-}2Na]^{2-}$ spectrum.

A peak at *m/z* 450.0 corresponds to the charge-reduced species $[M\text{-}2Na]^{-\bullet}$, suggesting that one possible dissociation mechanism involves electron ejection, effectively EDD[15], from the doubly charged precursor to create an unstable radical anion that results in bond dissociation to form more stable product ions, as shown in **Scheme 3.7**.

$$\mathbf{[M\text{-}2Na]^{2-} + e^- \rightarrow [M\text{-}2Na]^{-\bullet} + 2e^-} \qquad \textbf{Scheme 3.7}$$

Bond dissociation *via* electron detachment may account for the differences in product ion spectra between the singly and doubly charge precursor ions. The presence of doubly charged product ions suggests that dissociation of the $[M\text{-}2Na]^{2-}$ can also proceed *via* electronic or vibrational excitation of the precursor ion, resulting in the loss of neutral fragments, as shown in **Scheme 3.8** and **Scheme 3.9** respectively.

$$[M\text{-}2Na]^{2-} + e^- \rightarrow [M\text{-}2Na]^{2-*} + e^- \qquad \textbf{Scheme 3.8}$$

$$[M\text{-}2Na]^{2-} \rightarrow [M\text{-}2Na]^{2-*} \qquad \textbf{Scheme 3.9}$$

Doubly charged product ions may also be formed *via* electron capture by the charge-reduced intermediate to form the electronically-excited doubly charged species, shown in **Scheme 3.10**, followed by the loss of neutral fragments.

$$[M\text{-}2Na]^{2-} + e^- \rightarrow [M\text{-}2Na]^{-\bullet} + e^- \rightarrow [M\text{-}2Na]^{2-*} \qquad \textbf{Scheme 3.10}$$

Product ions resulting from the loss of the N_2 group, while retaining both the benzene and naphthalene groups, indicates the tendency for structural rearrangements before or during bond dissociation. Product ions resulting from structural rearrangements were also noted in the CID and IRMPD spectra suggesting that the rearrangements may be due, to some extent, to the vibrational excitation of the precursor ion. **Figure 3.19** indicates the bond cleavages occurring to form a product ion resulting from structural rearrangement, with the molecular formula $C_{16}H_{11}O_4S$, which is observed by EID, CID and IRMPD.

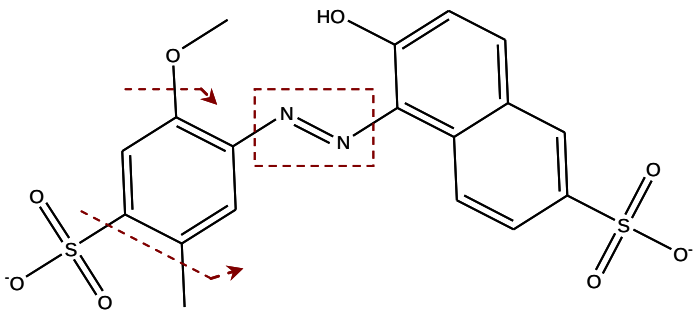

Figure 3.19: Structural rearrangement of Allura Red, forming the product ion $C_{16}H_{11}O_4S$ at *m/z* 299.0.

The 5 product ions proposed to result from structural rearrangement to lose the N_2 group all contain the hydroxy-napthalene group and the benzene ring, suggesting that a cyclisation reaction occurs between the oxygen and the benzene group, releasing the N_2 group.

3.2.4. MS/MS analysis of a range of small organic molecules

A wider range of small organic molecules, between 100 – 1000 Da and observed with different charge-carrying species, have been analysed by MS/MS. The product ions generated by CID-FT share a high commonality to the product ions observed by CID-IT, and therefore have been excluded from further interpretation unless accurate mass measurements are required. In order to comprehensively compare EID with the available MS/MS techniques and overcome the one-third cut-off rule governing CID carried out in the ion trap, MS/MS analysis has also been carried out using IRMPD performed in the FT-ICR cell, and CID performed on a QToF mass analyser. The resulting product ion data for each compound has been summarised in **Table 3.5**, detailing the number of product ions generated by EID, CID-IT, QToF-CID and IRMPD, as well as the number of unique product ions observed.

Compound	Precursor Ion	EID	CID-IT	QToF-CID	IRMPD
Haloperidol	$[M+H]^+$	**44 (28)**	11 (1)	24 (7)	4 (0)
	$[M+Na]^+$	**18 (15)**	11 (6)	4 (3)	0 (0)
	$[M-H]^-$	0 (0)	9 (3)	**14 (9)**	8 (1)
Allura Red	$[M-Na]^-$	1 (0)	21 (2)	**30 (17)**	16 (0)
	$[M-2Na]^{2-}$	19 (3)	22 (3)	31 **(12)**	**39** (8)
AZ_B1	$[M+H]^+$	**70 (30)**	31 (6)	44 (2)	30 (1)
	$[M+Na]^+$	**14 (12)**	8 (5)	3 (0)	3 (1)
	$[M-H]^-$	0 (0)	**21 (8)**	4 (1)	1 (0)
AZ_B2	$[M+H]^+$	**39 (26)**	16 (4)	12 (2)	10 (0)
	$[M+Na]^+$	**43 (37)**	11 (5)	5 (2)	2 (0)
	$[M-H]^-$	7 (4)	12 (0)	5 (0)	**47 (33)**
AZ_B3	$[M+H]^+$	7 (1)	18 (1)	**21 (4)**	18 (2)
	$[M+Na]^+$	**17 (14)**	2 (0)	8 (5)	0 (0)
AZ_B4	$[M+H]^+$	**25 (17)**	5 (1)	12 (3)	5 (0)
	$[M+Na]^+$	**1 (1)**	0 (0)	0 (0)	**1 (1)**
AZ_C1	$[M+H]^+$	**22 (10)**	13 (4)	9 (0)	4 (0)
	$[M+Na]^+$	3 (2)	**10 (7)**	**10** (6)	3 (1)
AZ_C2	$[M+Na]^+$	**23 (14)**	16 (1)	14 (3)	6 (0)
	$[M-H]^-$	16 **(4)**	20 (1)	**25** (2)	16 (2)
AZ_C3	$[M+Na]^+$	7 (1)	8 (1)	**9 (3)**	5 (0)
	$[M-H]^-$	5 (1)	5 (1)	**14 (5)**	12 (4)
AZ_C4	$[M+Na]^+$	**21 (11)**	6 (1)	9 (1)	7 (3)
	$[M-H]^-$	0 (0)	7 (0)	10 (2)	**15 (6)**
AZ_C5	$[M+Na]^+$	16 (6)	**19 (7)**	14 (1)	11 (1)
	$[M-H]^-$	0 (0)	1 (0)	**8 (6)**	4 (2)
Brilliant Blue	$[M-Na]^-$	6 (0)	42 (7)	32 (4)	**43 (10)**
	$[M-2Na]^{2-}$	21 (4)	**30** (7)	27 **(9)**	6 (0)
Caffeine	$[M+H]^+$	**10** (0)	9 (1)	**10 (2)**	1 (0)
Cediranib	$[M+H]^+$	**43 (36)**	8 (3)	5 (0)	2 (0)
	$[M+Na]^+$	**31 (27)**	3 (1)	3 (1)	3 (0)
	$[M-H]^-$	8 (0)	40 (0)	**45 (11)**	43 (6)
Diphenhydramine	$[M+H]^+$	**10 (4)**	2 (0)	8 (3)	3 (0)
	Fragment	14 (0)	9 (0)	**17 (6)**	4 (0)
Gefitinib	$[M+H]^+$	**42 (25)**	13 (5)	19 (2)	4 (0)
	$[M+Na]^+$	6 **(3)**	**7** (2)	3 (0)	1 (0)
	$[M-H]^-$	1 (0)	12 (1)	16 (4)	**23 (8)**
	$[M+Cl]^-$	0 (0)	1 (0)	7 (1)	**23 (17)**
Omeprazole	$[M+H]^+$	**49 (21)**	15 (1)	31 (5)	6 (0)
	$[M+Na]^+$	**27 (14)**	13 (0)	11 (2)	5 (1)
	$[M+K]^+$	9 (2)	**17 (6)**	4 (3)	9 (1)
	$[M-H]^-$	2 (0)	**10 (4)**	5 (1)	5 (0)
Raffinose	$[M+Na]^+$	**47 (37)**	15 (6)	7 (0)	7 (0)
	$[M-H]^-$	2 (0)	13 (0)	24 (0)	**35 (15)**
Reserpine	$[M+H]^+$	**132 (71)**	48 (1)	50 (9)	39 (3)
	$[M-H]^-$	1 (0)	18 (3)	14 (4)	**29 (15)**
Ritonavir	$[M+H]^+$	**16 (6)**	20 (3)	22 (1)	10 (0)
	$[M+Na]^+$	41 **(16)**	25 (1)	**48** (11)	7 (1)
Sulfamethazine	$[M+H]^+$	**20 (7)**	9 (0)	14 (3)	7 (0)
	$[M+Na]^+$	6 (3)	3 (1)	4 (2)	2 (0)
Sunset Yellow	$[M-Na]^-$	5 (0)	27 (0)	**45 (26)**	27 (4)
	$[M-2Na]^{2-}$	17 (5)	14 (4)	**22 (11)**	11 (2)
Terfenadine	$[M+H]^+$	**87 (45)**	3 (0)	24 (5)	15 (1)
	$[M+Na]^+$	**13 (12)**	4 (2)	3 (2)	0 (0)

Table 3.5: Summary of product ions generated from each MS/MS technique for each compound and observed molecular ions. Unique product ions have been shown in parentheses.

The technique(s) generating the greatest number of product ions and/or the highest number of unique product ions for each molecular ion have been highlighted in red in **Table 3.5**. Of the four MS/MS techniques, each is seen to excel for different molecular ions, suggesting that no one technique is infallible. In order to determine if any trends are beginning to form, the number of product ions generated by each technique and polarity have been summarised in **Table 3.6**.

		EID	CID-IT	QToF-CID	IRMPD
Cationic Precursors	**Total Product Ions**	965	408	481	234
	Average Number of Product Ions	28	12	14	7
Anionic Precursors	**Total Product Ions**	112	325	378	403
	Average Number of Product Ions	6	17	20	21

Table 3.6: Summary of the total number and the average number of product ions generated by each technique for each ion polarity.

EID was found to generate an average of 28 product ions for positively charged precursors compared to 6 product ions for negatively charged precursors, supporting the previous observation that EID favours cationic precursors. This trend is consistent with comparisons between ECD and EDD, where ECD of multiply charged cations has been seen to generate a higher degree of fragmentation than EDD.[16] Discounting the 3 doubly charged anionic precursors, the average number of product ions generated by EID of anions reduces by 50%, suggesting that electron detachment is the primary dissociation mechanism for negatively charged species.

The structures of the analysed compounds, shown in **Figure 3.20**, **Figure 3.21** and **Figure 3.22**, each contained at least one aromatic ring and one heteroatom. The

five most abundant ions in each EID spectrum were studied and the proposed bond cleavages have been indicated on each structure. Two compounds containing an N=N bond in the centre of the molecule (Allura Red and Sunset Yellow) generated product ions formed *via* the loss of N_2 from the molecular ion. Similar rearrangements were observed for compounds AZ_B2 and AZ_C4, both of which contained a CH_3SO_2 group and noted the loss of SO_2 whilst retaining the methyl end group, and Sulfamethazine, which lost SO_2 from the centre of the molecule. A high proportion of the EID bond cleavages occur on single bonds, such as the C-C alkyl bonds, however EID was also seen to generate cross-ring fragmentation and product ions formed *via* multiple bond cleavages, allowing a high degree of structural information to be gathered, including information regarding the location of ring substituents. By comparison, CID tends to cleave bonds adjacent to aromatic groups, keeping the stable ring systems intact, thereby giving EID the advantage for compounds containing aromatic rings. The ability to cleave multiple bonds is important for providing information about the central portion of the molecules and not solely the end groups. Common losses include stable species such as CO, CO_2, SO_2, SO_3, HCl, CH_3SO_2, N_2, CH_3O, CH_3, H_2O, *t*-butyl have been observed, supporting previous literature investigations into common fragmentation pathways of even-electron molecular ions.[5, 17-18] A direct comparison between the product ions generated by $[M+H]^+$ and $[M+Na]^+$ precursors showed that, barring three compounds, the protonated precursor ions generated more product ions and cleaved more bonds than the equivalent sodium-adducted precursor ion, suggesting that the sodium cation may restrict electron interaction sites or migration within the precursor ion. This trend is consistent with studies carried out by O'Hair *et al.*[19] into EID of tryptophan, which postulated that the presence of a metal cation has a significant effect on the product ions formed and severely limits the amounts of hydrogen scrambling observed.

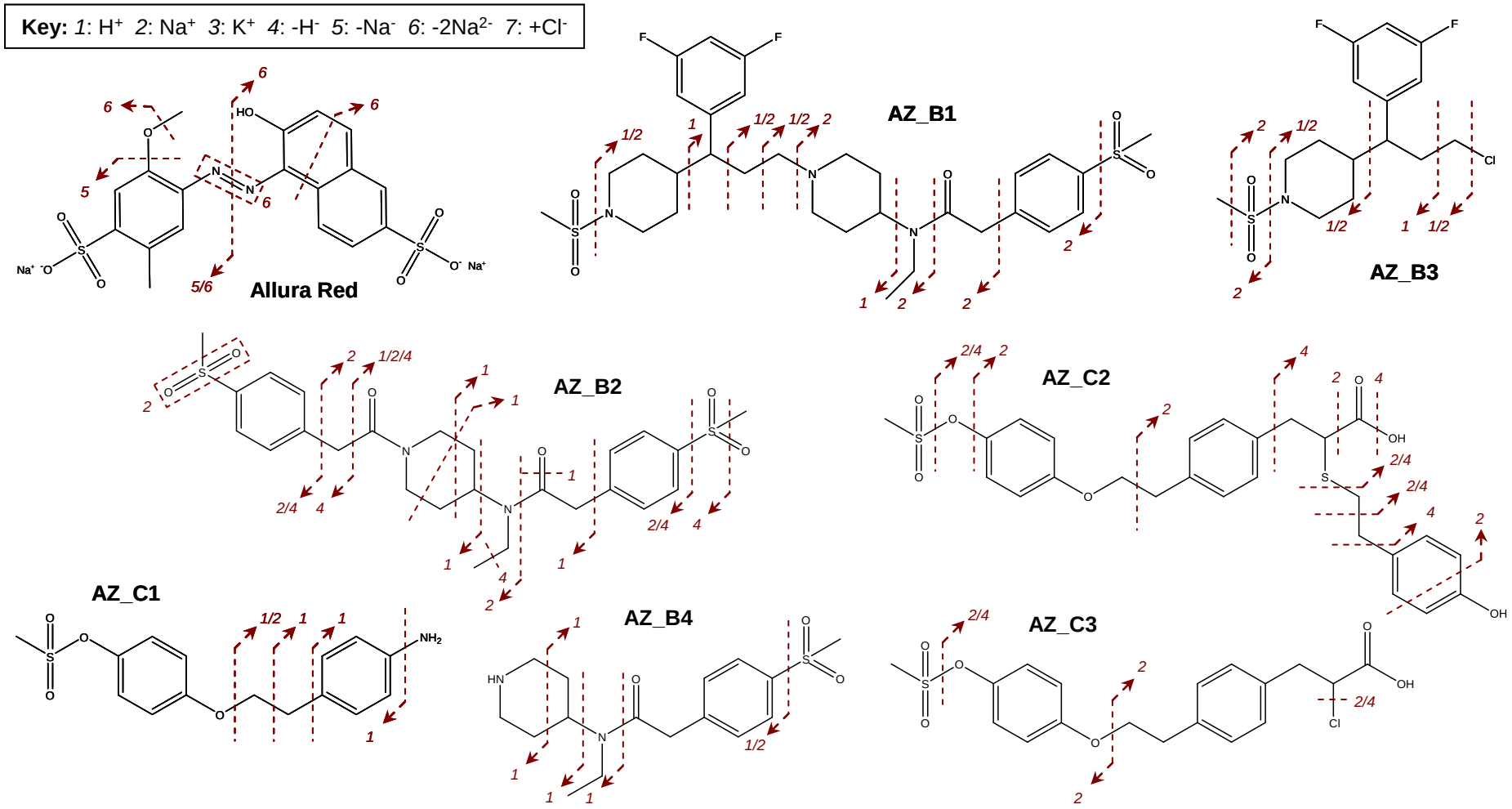

Figure 3.20: Proposed EID bond cleavages generating the most intense product ions for compounds discussed in Table 3.5 (Allura Red – AZ_C3).

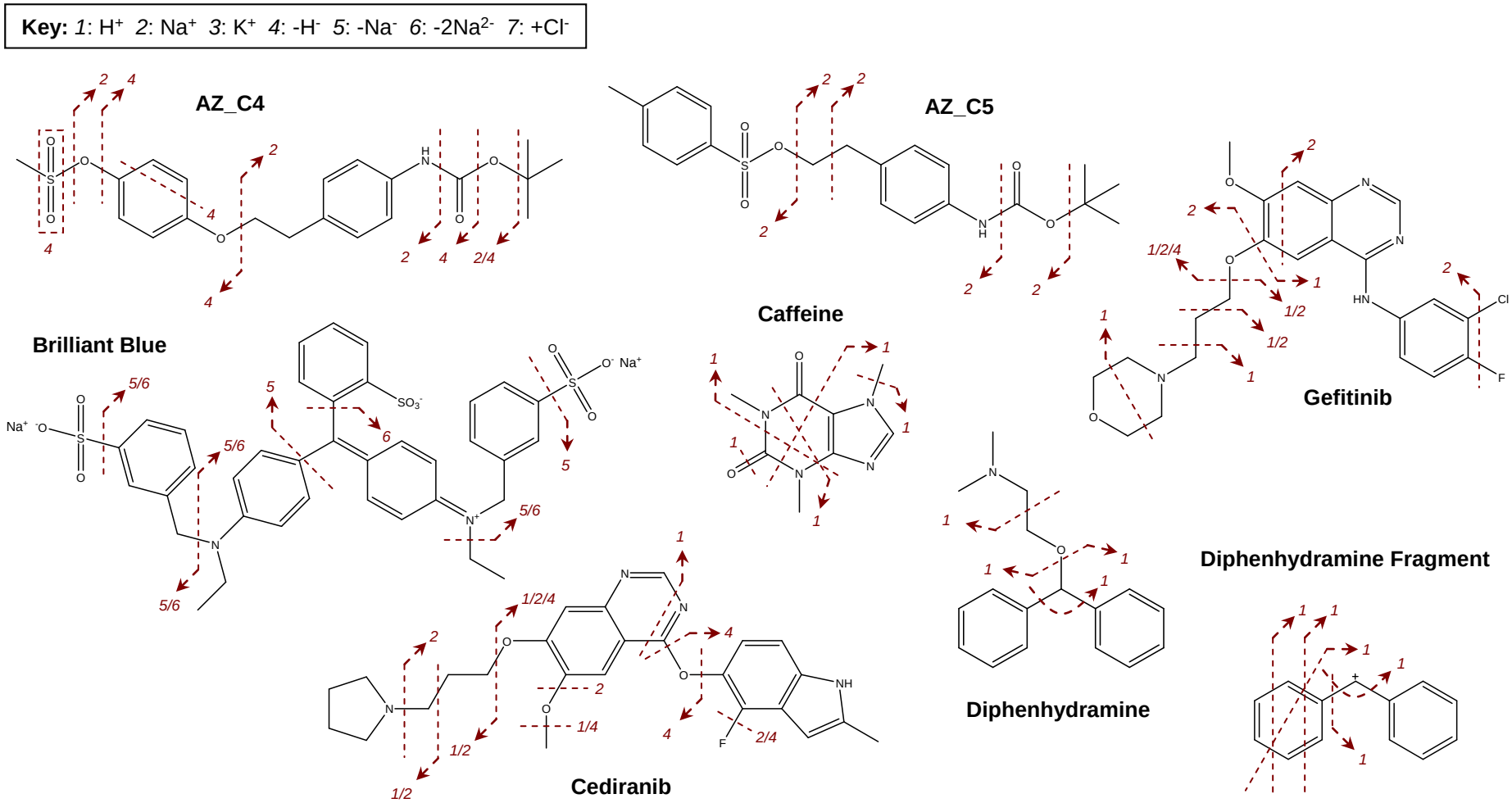

Figure 3.21: Proposed EID bond cleavages generating the most intense product ions for compounds discussed in Table 3.5 (AZ_C4 - Gefitinib).

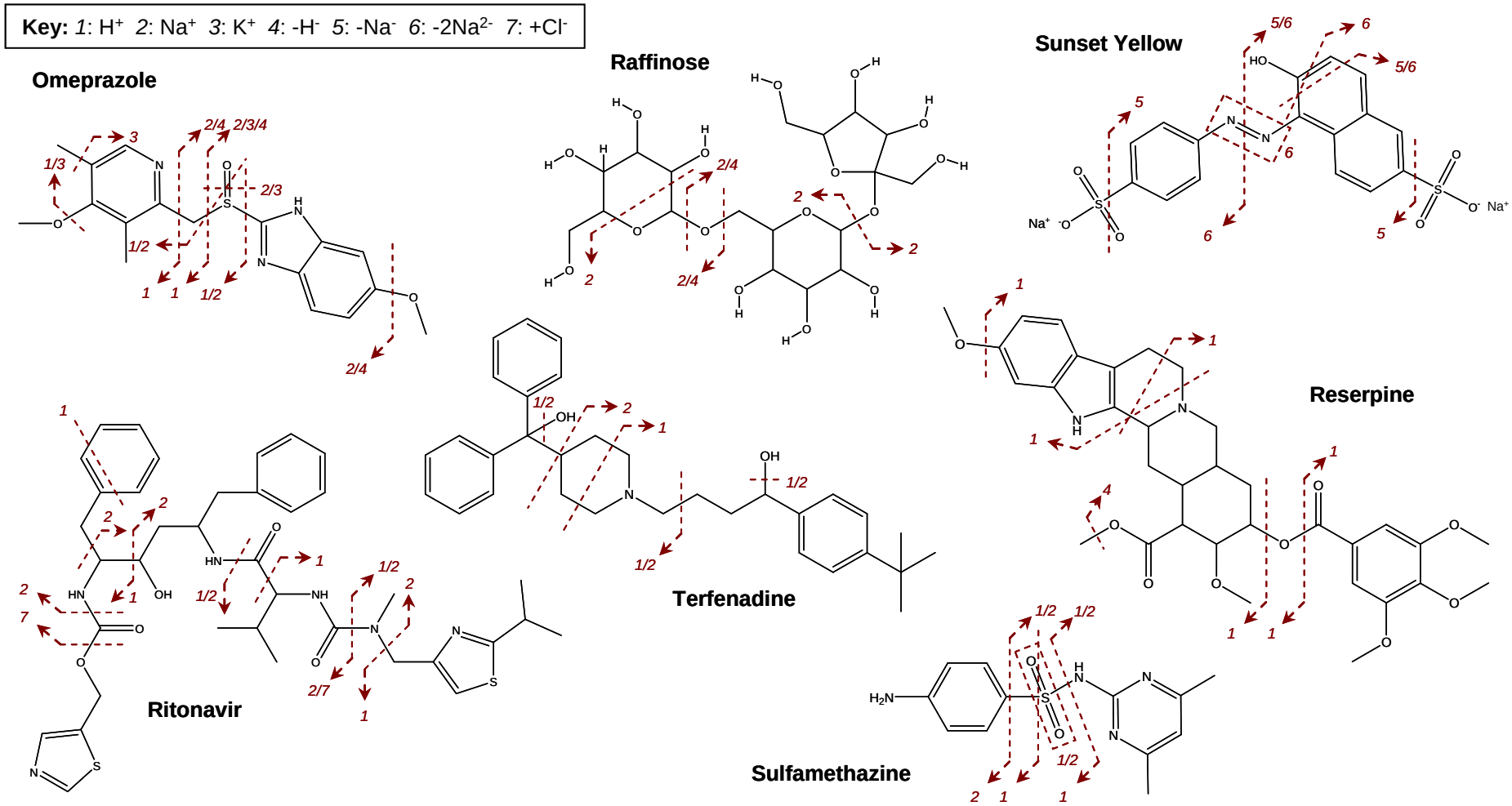

Figure 3.22: Proposed EID bond cleavages generating the most intense product ions for compounds discussed in Table 3.5 (Omeprazole - Terfenadine).

3.2.5. Effect of altering electron irradiation time

In order to improve the EID spectra generated from negatively charged precursor ions, experiments were carried out to observe whether changing the length of electron irradiation would have a beneficial effect on the resulting product ion spectra. EID analysis of the haloperidol $[M-H]^-$ species at the default electron irradiation time of 70 ms failed to generate any product ions. Further EID analysis was carried out at the fixed electron energy of 18.79 eV but altering the electron irradiation times between 10 ms to 150 ms, in 10 ms increments, in order to determine whether a change in the irradiation time could induce bond dissociation. As the irradiation time was increased, the absolute intensity of the precursor ion was seen to steadily decrease, however no product ions were observed suggesting that the EID of the haloperidol $[M-H]^-$ species results in the neutralisation of the precursor ion *via* electron ejection. The data generated by EID of haloperidol at varying electron energies has not been shown.

Further work was carried out on cediranib, which was found to generate 8 product ions by EID of the $[M-H]^-$ at the default irradiation time of 70 ms. The relative abundances of the observed product ions were calculated at each electron irradiation time, ranging from 10 ms to 150 ms. The experiment was repeated three times and the relative ion abundances at each irradiation time were averaged and have been graphically represented in **Figure 3.23**.

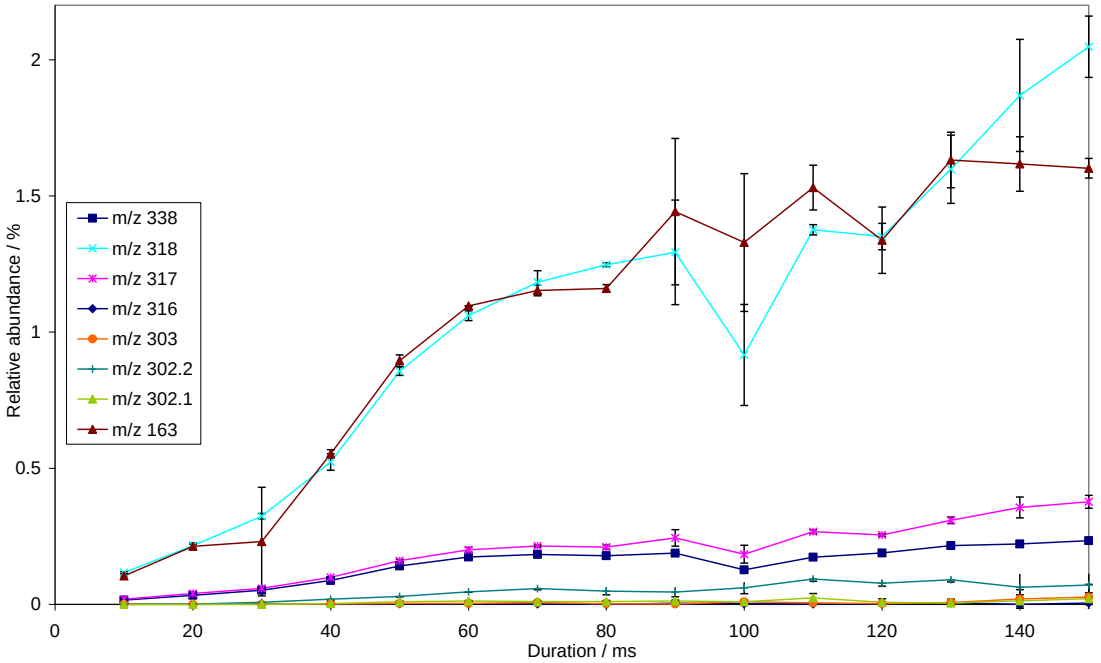

Figure 3.23: The effect of electron irradiation on the relative intensity of the observed product ions.

As the irradiation time increases, the relative abundances of the product ions were seen to increase, indicating that the efficiency of fragmentation varies with the electron irradiation time. The greatest effect of irradiation time is observed between 10 ms and 50 ms, where the relative ion abundances are seen to gradually increase. Irradiation times longer than 50 ms are shown to have little effect on the product ion abundances, displaying a relatively stable signal. Below 20 ms, the three lowest abundant product ions were not observed, suggesting that altering the irradiation times can not only affect the peak intensities but also the number of product ions.

3.2.6. Comparison between EID and alternative ionisation techniques

Following on from the observations made from altering the charge carrying species, further work has been carried out to determine what effect changing the ionisation technique, and thus changing the molecular ion, has on bond dissociation. The compound haloperidol has been analysed using Electron Ionisation (EI) and

Atmospheric pressure Solids Analysis Probe (ASAP), previously described in **Chapter 2**, comparing the resulting data with the previously observed spectra from EID, CID-FT, CID-IT, QToF-CID and IRMPD.

Electron Ionisation

Whereas electrospray ionisation readily results in proton transfer from solvent to sample generating the even-electron $[M+H]^+$ species at *m/z* 376.1 and minimal in-source dissociation, EI generates the unstable odd electron $M^{+\bullet}$ radical cation at *m/z* 375.1 that readily dissociates. One of the proposed fragmentation pathways followed by EID occurs *via* the secondary ionisation of the $[M+H]^+$ precursor to form an odd-electron species, and odd-electron product ions are commonly observed, therefore a comparison between EI and EID spectra has been carried out in order to determine any similarities, as shown in **Figure 3.24**.

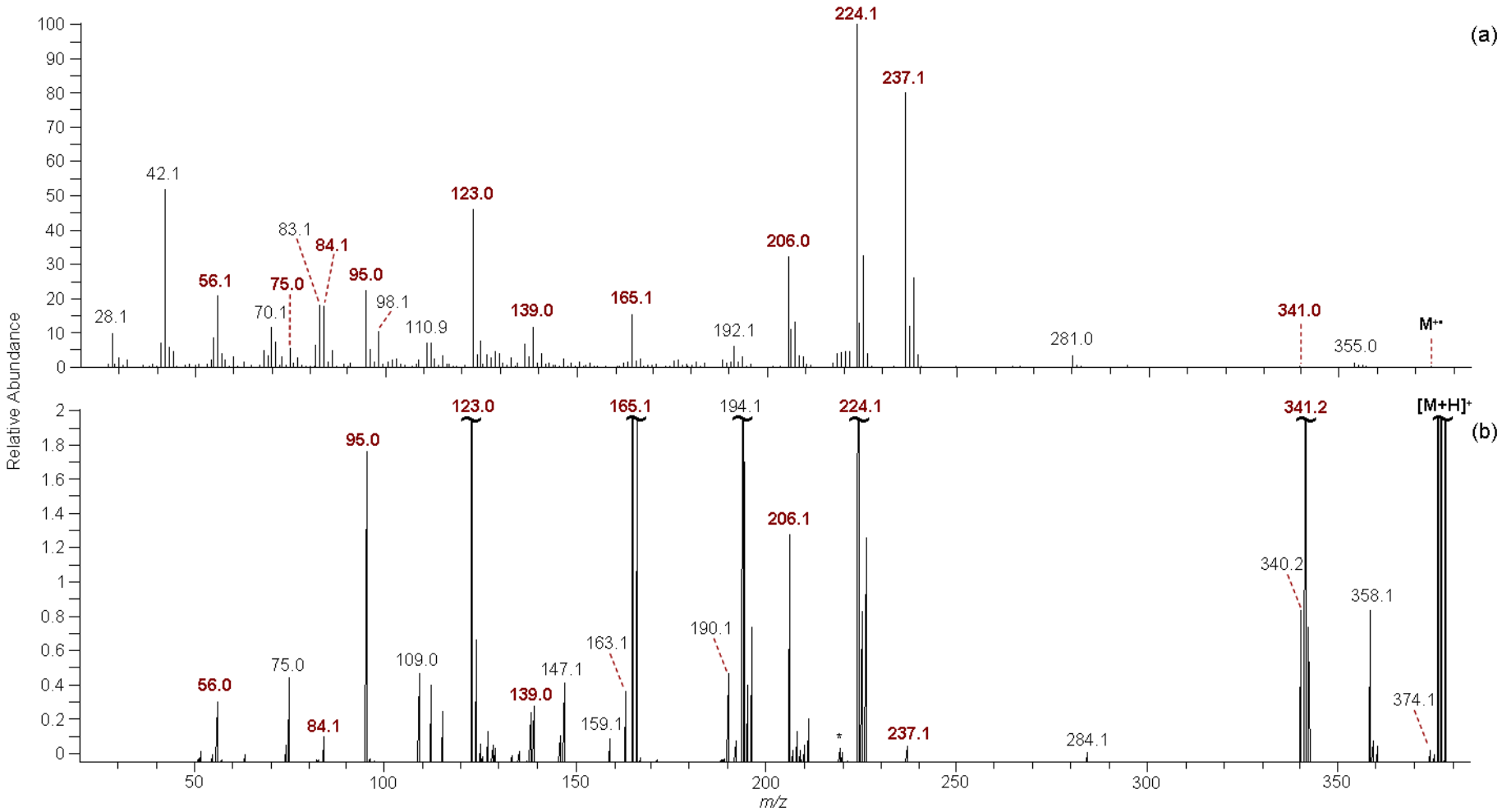

Figure 3.24: Analysis of haloperidol by (a) EI and (b) EID. Common ions are highlighted in red.

The EI spectrum of haloperidol contained 41 ions, compared with 37 generated by the EID of the $[M+H]^+$ species, however only 15 ions were common to both techniques. The commonalities between EI and EID suggest that the dissociation of the $M^{+\bullet}$ radical cation follows a similar fragmentation pathway to EID of the $[M+H]^+$ precursor, further suggesting that EID dissociation can occur *via* an odd-electron species. The product ions generated by EI MS and the product ions observed by the ESI MS/MS analysis of the $[M+H]^+$ species, and have been summarised in **Table 3.7**. IRMPD was the only technique that was not shown to generate any unique product ions, whereas each of the other methods generated at least one unique product ion. The low percentages of common product ions (< 41%) between the EID product ions and each of the other techniques further supports the complementary nature of EID and the benefits of using multiple dissociation techniques when attempting to structurally characterise unknown compounds.

	EID	**CID-IT**	**QToF-CID**	**IRMPD**	**EI**
Total Product Ions	37	11	24	4	41
Unique Product Ions	14	1	3	0	21
Product Ions Common with EID	N/A	8	15	3	15

Table 3.7: Summary of the number of product ions generated by each MS and MS/MS technique.

Atmospheric pressure Solids Analysis Probe

ASAP analysis was carried out in an attempt to generate the $M^{+\bullet}$ radical cation species, in order to determine whether CID of the odd-electron molecular ion would generate different product ion spectra compared with CID of the even-electron molecular ion. The ASAP analysis of a 1 mg mL^{-1} sample of haloperidol in methanol

was found to preferentially generate the $[M+H]^+$ species at *m/z* 376.1. By comparison, the MS spectrum generated from the solid haloperidol sample under dry source conditions produced both the $[M\text{-}H^-]^+$ and $[M+H]^+$ species, as shown in **Figure 3.25**.

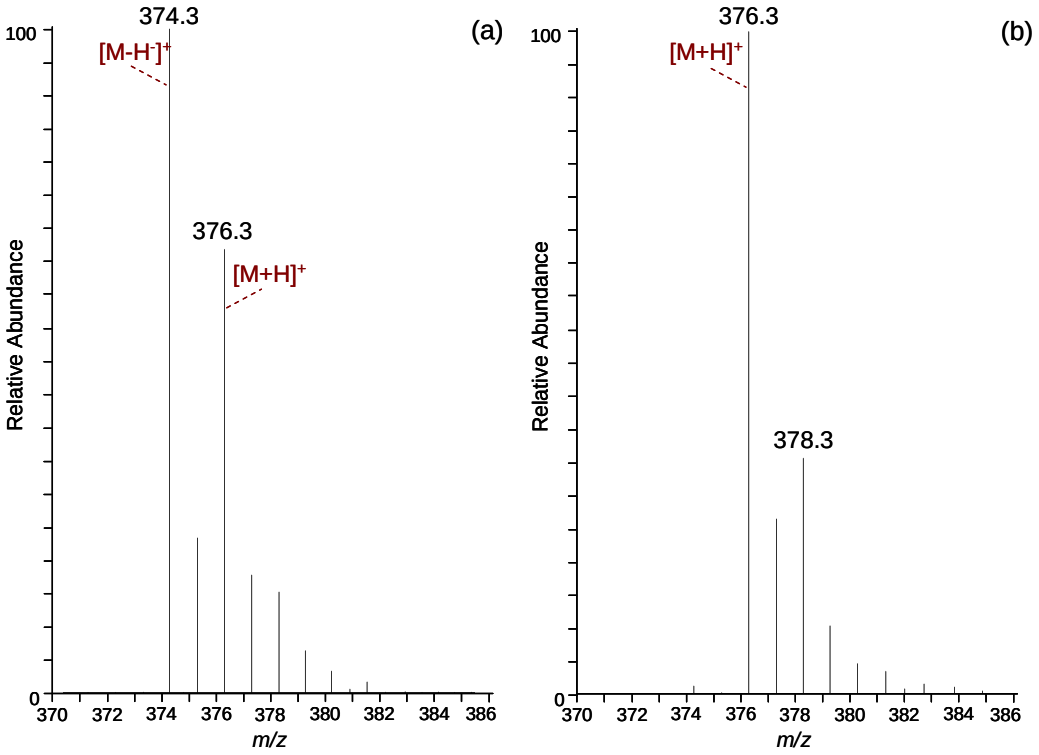

Figure 3.25: ASAP MS of (a) solid-state haloperidol generating a combination of the $[M+H]^+$ and $[M\text{-}H^-]^+$ species and (b) solution-state haloperidol generating only the protonated species.

The isotopic profile of the solution-state sample displays the typical isotope pattern associated with a chlorine-containing compound. The peak at *m/z* 376.3 in the solid-state sample is expected to correspond to an amalgamation of the $[M+H]^+$ species and the ^{37}Cl isotope of the $[M\text{-}H^-]^+$ species. The peak at *m/z* 375.3 in the solid-state sample is consistent with ^{13}C isotope of the hydride-abstracted species, not the $M^{+\bullet}$ species. ASAP-CID analysis was performed on both the protonated species formed from the solution-state sample and the hydride-abstracted species from the solid-state sample. The $M^{+\bullet}$ radical cation was not observed, therefore

comparisons between CID of odd-electron species with EID of even-electron species could not be carried out.

A direct comparison between the spectra generated by ASAP-CID of the $[M+H]^+$ and the $[M-H^-]^+$ precursors noted 3 significant product ions in each spectrum that could be used to locate the protonation site or hydride abstraction site. Each of the 3 product ions in the $[M-H^-]^+$ spectrum are observed at 2 Da less than the product ions in the $[M+H]^+$ spectrum, consistent with a difference of H_2. **Table 3.8** details the 3 product ion pairs and their corresponding bond cleavages. The 3 product ions generated from the protonated species are also observed by EID and CID-FT, allowing the molecular formulae and structural assignments to be proposed.

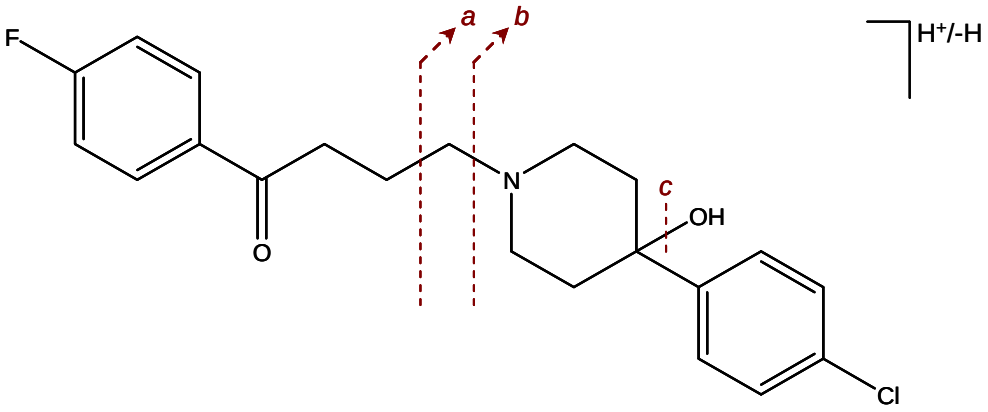

Product Ion *m/z*		Chemical Formula	RDB	*Proposed Bond Cleavage(s)*
$[M+H]^+$	$[M-H^-]^+$			
358.1	-	$C_{21}H_{22}NOFCl$	10.5	*c*
-	356.1	$C_{21}H_{20}NOFCl$	11.5	*c*
206.1	-	$C_{12}H_{13}NCl$	6.5	*a c*
-	204.1	$C_{12}H_{11}NCl$	7.5	*a c*
194.1	-	$C_{11}H_{13}NCl$	5.5	*b c*
-	192.1	$C_{11}H_{11}NCl$	6.5	*b c*

Table 3.8: Summary of the 3 product ion pairs generated by ASAP-CID of haloperidol.

The 3 product ion pairs are all proposed to contain the 4-(4-chlorophenyl)piperidine structure of the haloperidol molecule, suggesting that the likely location for hydride abstraction is on the piperidine ring, suspected to occur at a carbon atom adjacent to the nitrogen atom resulting in a positive charge on the nitrogen.

Further work detailed herein has focused on developing EID as a fast and efficient method for LC-MS/MS analysis of pharmaceutical molecules, therefore validation of ASAP-MS and the manipulation of source conditions to generate the $M^{+\bullet}$ molecular ion has not been carried out.

3.3. Conclusions

Studies thus far have confirmed the suitability for EID analysis of small singly charged molecules, producing a high degree of fragmentation and unique structural information that other techniques have failed to produce. Inspection of the resulting EID product ion spectra noted the presence of odd-electron and even-electron product ions, as well as commonalities between EID and other dissociation techniques, which suggests that competing fragmentation mechanisms occur following the interaction with electrons. The mechanistic theory of secondary ionisation preceding electron capture or dissociative stabilisation, as shown in **Schemes 3.1** – **3.2** and **Schemes 3.5 – 3.6**, is supported by the observation of doubly charged product ions resulting from singly charged cationic precursors.[8, 13, 20-21] Electron interaction with doubly charged anionic precursors was shown to undergo electron detachment to generate the charge-reduced species, akin to secondary ionisation of the singly charged cations. Electron irradiation of doubly charged cationic and anionic precursors resulted in a combination of singly and doubly charged product ions, proposed to occur *via* one of several fragmentation mechanisms, including electron capture/detachment, electronic excitation and

vibrational excitation. Similarities between product ions generated by EID and vibrational energy MS/MS techniques are thought to result from vibrational excitation caused by interactions with high energy electrons or internal energy conversion.[21] The data acquired thus far suggests that EID is more suitable for analysing positively charged species over negatively charged precursor ions.

Altering the charge-carrying species for each compound has been shown to have an effect on the resulting product ion spectra from each MS/MS technique, resulting in an increase in the amount of structural information achievable by considering data from molecular ions with different cations. Results have shown that EID can form product ions that retain the charge-carrying species, producing structural information regarding the location of the charge(s) on the precursor ion. The 23 compounds that have been analysed thus far do not form a stringent enough series of analogues that would allow any underlying trends to be determined, however further study would hope to build upon the results detailed herein and highlight any patterns that emerge from the manipulation of precursor ion functional groups or charge-carrying species. The vast majority of EID bond cleavages occur in close proximity to a heteroatom and/or aromatic ring, a feature commonly observed by EI, however due to the high proportion of heteroatoms and cyclical groups in each compound the observed trend is inconclusive. The complementary nature of EID proves that when used in conjunction with traditional MS/MS techniques, the amount of structural information that can be acquired from each compound can be maximised.

3.4. References

1. Lioe, H., O'Hair, R.A.J.: Comparison of Collision-Induced Dissociation and Electron-Induced Dissociation of Singly Protonated Aromatic Amino Acids, Cystine and Related Simple Peptides using a Hybrid Linear Ion Trap-FT-ICR Mass Spectrometer *Anal. Bioanal. Chem.* **2007,** *389*, 1429-1437

2. Kjeldsen, F., Haselmann, K.F., Sorensen, E.S., Zubarev, R.A.: Distinguishing of Ile/Leu Amino Acid Residues in the PP3 Protein by (Hot) Electron Capture Dissociation in Fourier Transform Ion Cyclotron Resonance Mass Spectrometry *Anal. Chem.* **2003,** *75*, 1267-1274

3. March, R.E.: Quadrupole Ion Traps *Mass Spectrom. Rev.* **2009,** *28*, 961-989

4. Sleno, L., Volmer, D.A.: Ion Activation Methods for Tandem Mass Spectrometry *J. Mass Spectrom.* **2004,** *39*, 1091-1112

5. Holcapek, M., Jirasko, R., Lisa, M.: Basic Rules for the Interpretation of Atmospheric Pressure Ionization Mass Spectra of Small Molecules *J. Chromatogr. A* **2010,** *1217*, 3908-3921

6. McLafferty, F.W., Turecek, F.; Interpretation of Mass Spectra, 4th ed.; University Science Books: 1993;

7. Zubarev, R.A., Kelleher, N.L., McLafferty, F.W.: Electron Capture Dissociation of Multiply Charged Protein Cations. A Nonergodic Process *J. Am. Chem. Soc.* **1998,** *120*, 3265-3266

8. Nielsen, M.L., Budnik, B.A., Haselmann, K.F., Olsen, J.V., Zubarev, R.A.: Intramolecular Hydrogen Atom Transfer in Hydrogen-Deficient Polypeptide Radical Cations *Chem. Phys. Lett.* **2000,** *330*, 558-562

9. O'Connor, P.B., Lin, C., Cournoyer, J.J., Pittman, J.L., Belyayev, M., Budnik, B.A.: Long-Lived Electron Capture Dissociation Product Ions Experience Radical Migration via Hydrogen Abstraction *J. Am. Soc. Mass Spectrom.* **2006,** *17*, 576-585

10. Demmers, J.A.A., Rijkers, D.T.S., Haverkamp, J., Killian, J.A., Heck, A.J.R.: Factors Affecting Gas-Phase Deuterium Scrambling in Peptide Ions and Their Implications for Protein Structure Determination *J. Am. Chem. Soc.* **2002,** *124*, 11191-11198

11. Armentrout, P.B., Rodgers, M.T.: An Absolute Sodium Cation Affinity Scale: Threshold Collision-Induced Dissociation Experiments and ab Initio Theory *J. Phys. Chem. A* **1999,** *104*, 2238-2247

12. Dunbar, R.C.: Complexation of Na^+ and K^+ to Aromatic Amino Acids: A Density Functional Computational Study of Cation-π Interactions *J. Phys. Chem. A* **2000,** *104*, 8067-8074

13. Budnik, B.A., Zubarev, R.A.: $MH^{2+\bullet}$ Ion Production from Protonated Polypeptides by Electron Impact: Observation and Determination of Ionization Energies and a Cross-Section *Chem. Phys. Lett.* **2000,** *316*, 19-23

14. Ly, T., Yin, S., Loo, J.A., Julian, R.R.: Electron-Induced Dissociation of Protonated Peptides Yields Backbone Fragmentation Consistent with a Hydrogen-Deficient Radical *Rapid Commun. Mass Spectrom.* **2009,** *23*, 2099-2101

15. Budnik, B.A., Haselmann, K.F., Zubarev, R.A.: Electron Detachment Dissociation of Peptide Di-Anions: An Electron-Hole Recombination Phenomenon *Chem. Phys. Lett.* **2001,** *342*, 299-302

16. Kaczorowska, M.A., Cooper, H.J.: Electron Capture Dissociation, Electron Detachment Dissociation, and Collision-Induced Dissociation of Polyamidoamine (PAMAM) Dendrimer Ions with Amino, Amidoethanol, and Sodium Carboxylate Surface Groups *J. Am. Soc. Mass Spectrom.* **2008,** *19*, 1312-1319

17. Levsen, K., Schiebel, H.M., Terlouw, J.K., Jobst, K.J., Elend, M., Preib, A., Thiele, H., Ingendoh, A.: Even-Electron Ions: A Systematic Study of the Neutral Species

Lost in the Dissociation of Quasi-Molecular Ions *J. Mass Spectrom.* **2007,** *42*, 1024-1044

18. Niessen, W.M.A.: Fragmentation of Toxicologically Relevant Drugs in Positive-Ion Liquid Chromatography-Tandem Mass Spectrometry *Mass Spectrom. Rev.* **2011,** *30*, 626-663

19. Feketeová, L., Wong, M.W., O'Hair, R.A.J.: The Role of Metal Cation in Electron-Induced Dissociation of Tryptophan *Eur. Phys. J. D* **2010,** *60*, 11-20

20. Kaczorowska, M.A., Cooper, H.J.: Electron Induced Dissociation: A Mass Spectrometry Technique for the Structural Analysis of Trinuclear Oxo-Centred Carboxylate-Bridged Iron Complexes *J. Am. Soc. Mass Spectrom.* **2010,** *21*, 1398-1403

21. Fung, Y.M.E., Adams, C.M., Zubarev, R.A.: Electron Ionization Dissociation of Singly and Multiply Charged Peptides *J. Am. Chem. Soc.* **2009,** *131*, 9977-9985

4. The Development of Electron-Induced Dissociation combined with LC-MS to Analyse Complex Mixtures.

4.1. Introduction

LC-MS and LC-MS/MS analysis has become an essential tool in the pharmaceutical industry for the identification of drug molecules due to the ability to perform rapid compound screening and provide in-depth structural characterisation and confirmation. Chromatography allows components from complex mixtures to be separated and analysed individually, which is particularly important for the MS detection of components with a dynamic range of concentrations. LC-MS/MS is often carried out by CID, however as shown in **Chapter 3**, this technique has limitations that may restrict structural identification and may not be the most suitable technique for analysing certain compounds, such as analogous molecules with minor structural differences.[1] EID has been shown to generate a high degree of fragmentation from the MS/MS analysis of small singly charged molecules, representative of pharmaceutical molecules, providing complementary data to CID, and hence the combination of LC-MS with EID is a natural, but as yet unaccomplished, progression. The direct infusion EID of Haloperidol $[M+H]^+$ discussed in **Chapter 3** was carried out over 1 minute, generating 23 MS/MS scans and resulting in the spectrum shown in **Figure 4.1(a),** averaging 1 scan every 2.6 s. The time taken for each scan includes ion accumulation, isolation of the precursor ion, transmission to the FT-ICR cell, electron irradiation of the precursor ion and detection of the ions. Typically, chromatographic peaks elute over few seconds, therefore in order to combine EID with LC-MS it is necessary to obtain meaningful MS/MS data from over a short time-frame, and therefore from a few MS/MS scans.

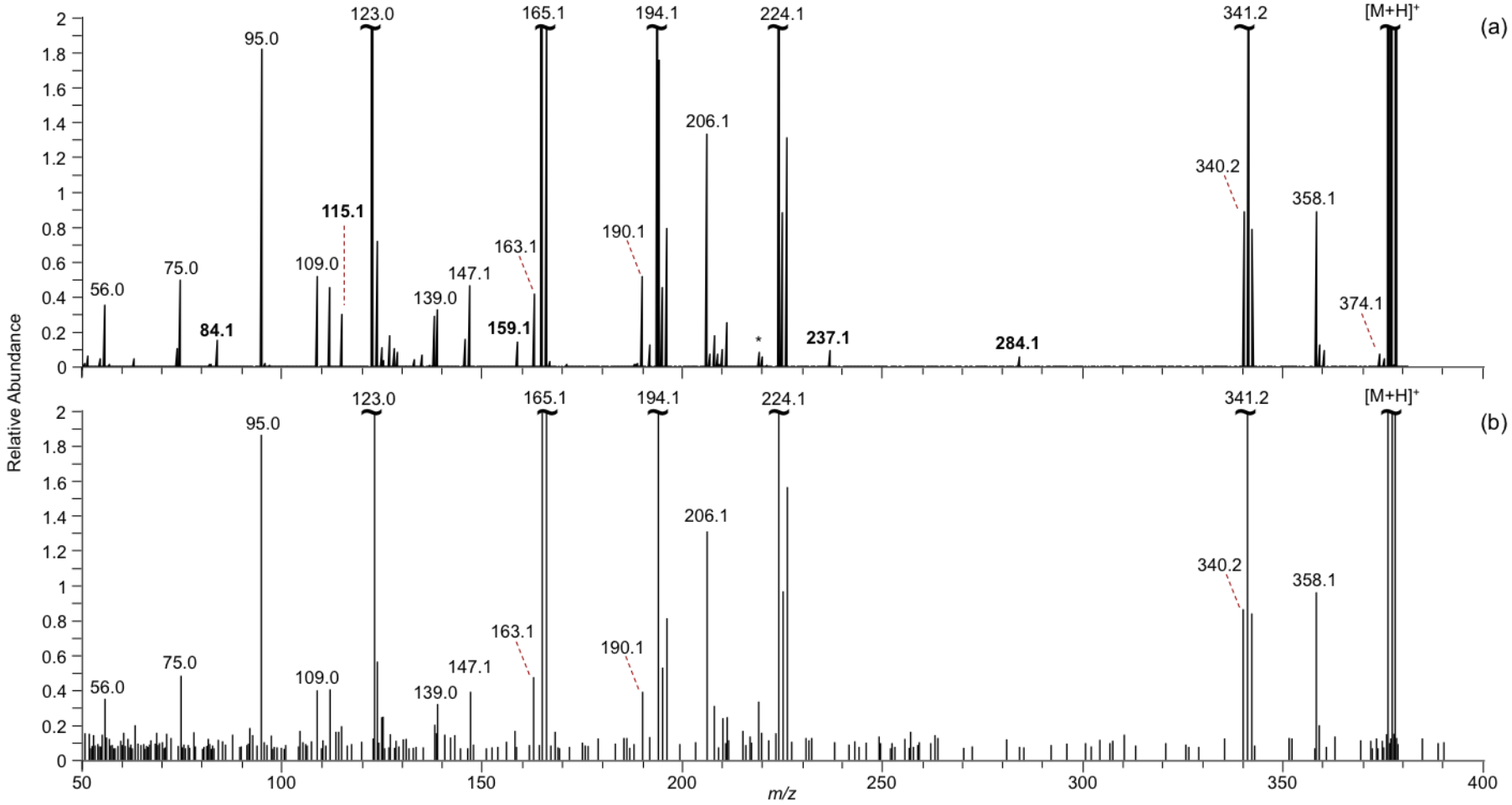

Figure 4.1: EID spectrum of Haloperidol from (a) 23 MS/MS scans and (b) 1 MS/MS scan. Product ions labelled in bold are not observed in the single-scan EID spectrum.

The spectrum generated by only 1 EID scan from Haloperidol $[M+H]^+$, shown in **Figure 4.1(b)**, shows a decrease in the signal-to-noise (S/N) compared with **Figure 4.1(a)**, thereby concealing the low abundance product ions that emerge in the spectrum averaged over multiple scans. Crucially, the single scan EID spectrum still contains important product ion data, demonstrating the feasibility of combining EID with LC-MS.

The work described herein has focused on the development of LC-EID as a viable tool for the structural characterisation of complex mixtures of small molecules. LC-EID was primarily developed for the purpose of analysing a pharmaceutical development sample of cediranib that contained several low abundance compounds. Preliminary analysis of cediranib by QToF-CID generated limited structural information from only 5 product ions, as shown in **Figure 4.2**, thereby prompting further analysis by EID.

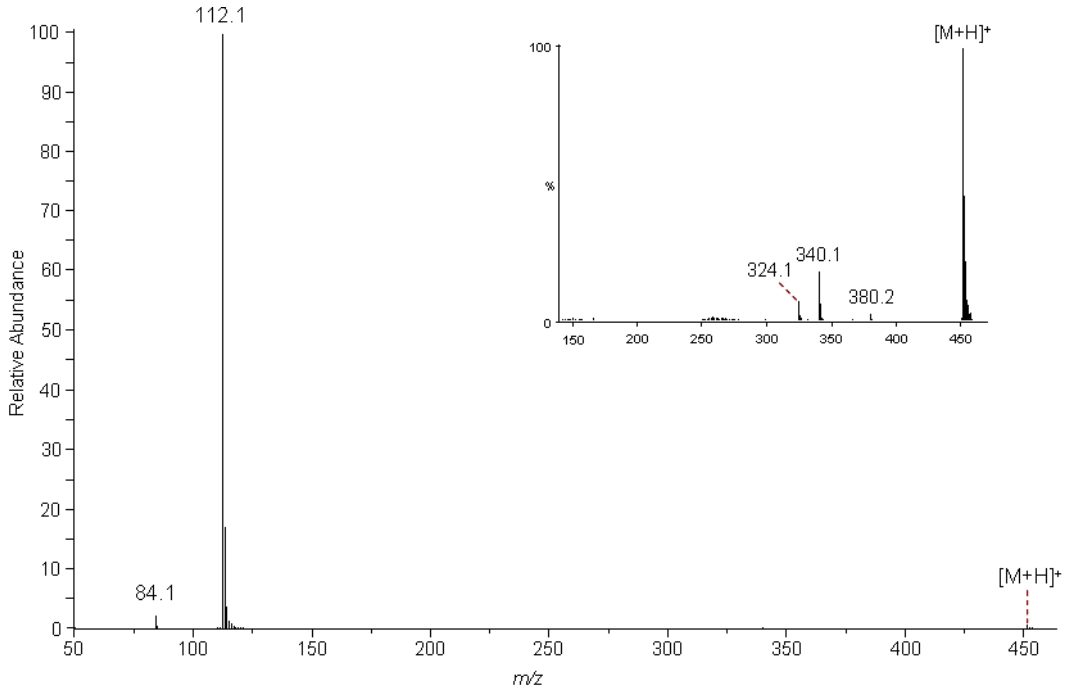

Figure 4.2: QToF-CID spectrum of cediranib [M+H]+. (inset) Expansion of higher *m/z* region to highlight low abundance product ions.

Direct infusion EID of cediranib generated 43 product ions, shown in **Figure 3.15(a)**, supporting the development of LC-EID as a method to analyse any unknown compounds in the sample. Validation of LC-EID has been carried out using Haloperidol as a progression from the direct infusion EID studies carried out in **Chapter 3**. The steps that contribute towards each FT duty cycle are shown in **Figure 4.3**. In order to sufficiently minimise the EID duty cycle, parameters such as ion injection time and detection time can be reduced, subsequently increasing the number of EID scans that can be acquired over a fixed LC peak width.

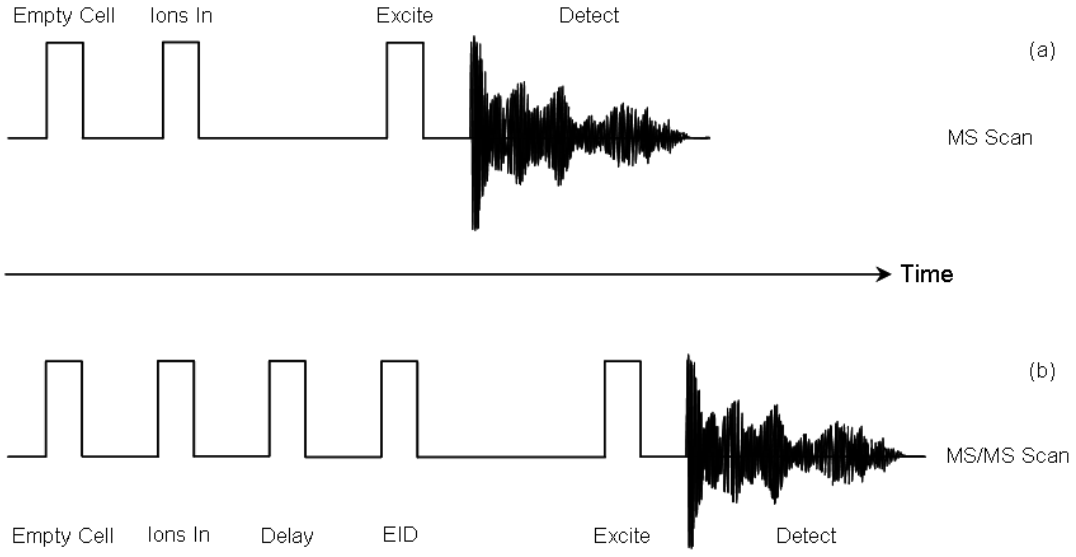

Figure 4.3: Diagram detailing the duty cycle for (a) an MS scan and (b) an EID MS/MS scan on an FT-ICR mass analyser.

4.2. Results and Discussion

4.2.1. Analysis of cediranib

The pharmaceutical compound cediranib (trade name Recentin™), 4-[(4-fluoro-2-methyl-1H-indol-5-yl)oxy]-6-methoxy-7-(3-pyrrolidin-1-ylpropoxy)quinazoline shown in **Figure 4.4**, was developed by AstraZeneca as a potential cancer treatment drug.[2-4] A process development sample of this compound contained several unknown components of low abundance, components that would be significantly

reduced during further stages of drug development but that require identification in order to determine their activity and any effects they may have if present in the final drug. Direct infusion EID of cediranib, detailed in **Chapter 3**, generated 43 product ions compared with 8 product ions by CID, suggesting that LC-EID would prove to be a beneficial tool. Cediranib and the unknown compounds have been subjected to LC-EID and LC-CID-IT analyses with the aim of generating significant structural information that could lead towards the identification of each unknown species. LC-CID-FT was also carried out, however due to the loss of ions with low internal energy during transmission between the ion trap and the FT-ICR cell, the results from LC-CID-FT have only been alluded to when accurate mass was required to postulate molecular formulae.

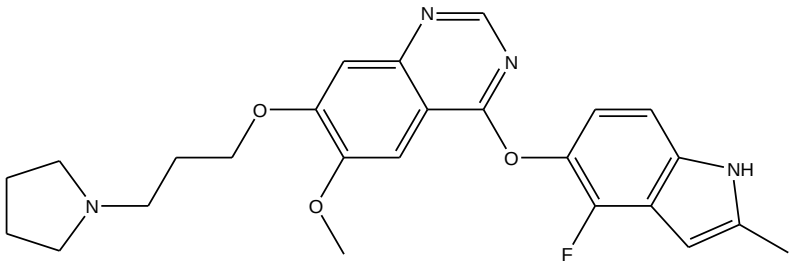

Figure 4.4: Structure of cediranib.

LC-MS of cediranib

A 2 mg mL^{-1} sample of cediranib was analysed by LC-MS in order to observe and identify any compounds present in the sample at concentrations far lower than the target molecule. The resulting Total Ion Chromatogram (TIC) contained 10 unknown low abundance species in addition to the cediranib molecule that were absent in preceding control experiments carried out on a solvent-only sample. The 11 compounds have been labelled in the chromatogram in **Figure 4.5**. The most intense peak **3** is consistent with the protonated cediranib, observed at *m/z* 451.1, with the empirical formula $C_{25}H_{28}N_4O_3F$ with a mass accuracy of 0.6 ppm. The 10

unknown species observed in the TIC are all less than 10% of the peak intensity of the cediranib peak and are assumed to be by-products of synthesis or impurities in the reaction mixture. The apparent low concentrations of these compounds demands the hyphenation of chromatography prior to further analysis in order to eliminate any detrimental effects caused by the high concentration of the major compound, such as ion suppression or incomplete precursor ion isolation due to ions close in *m/z*.

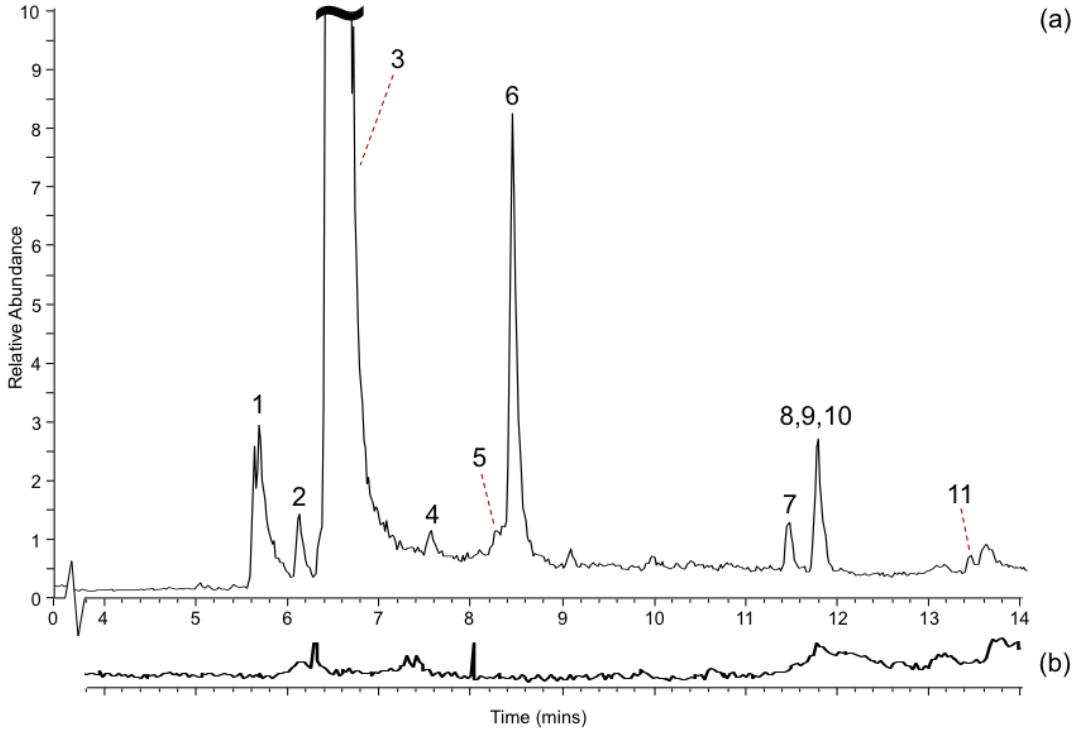

Figure 4.5(a): Total Ion Chromatogram (TIC) from LC-MS analysis of cediranib compared with (b) a blank LC-MS chromatogram. Peaks labelled 1 - 11 indicate components proven to be from the cediranib sample.

A list of the ten most likely molecular formulae for each unknown compound was calculated using the elemental limits $C_{0\text{-}50}H_{0\text{-}100}N_{0\text{-}10}O_{0\text{-}10}F_{0\text{-}5}$ and a mass tolerance of 2 ppm. The isotopic profile of LC peak **10** suggested the presence of chlorine, which was therefore included in the elemental limits. Criteria such as the nitrogen rule, which states that even-electron ions of an even *m/z* have an odd number of

nitrogen atoms and vice versa, the relative intensity of the ^{13}C isotope and the feasibility of the suggested molecular formulae were used to reduce the number of possible molecular formulae. The proposed molecular formulae are shown in **Table 4.1**.

LC Peak	Observed MS peak *m/z*	Proposed molecular formula $[M+H]^+$	Theoretical *m/z*	RDB	Accuracy /ppm
1	562.31863	$C_{32}H_{41}N_5O_3F$	562.31879	14.5	-0.3
2	899.40539	$C_{50}H_{53}N_8O_6F_2$	899.40506	27.5	0.4
3	451.21371	$C_{25}H_{28}N_4O_3F$	451.21400	13.5	-0.6
4	788.30043	$C_{43}H_{40}N_7O_6F_2$	788.30026	26.5	0.2
5	481.18808	$C_{25}H_{26}N_4O_5F$	481.18817	14.5	-0.2
6	340.10901	$C_{18}H_{15}N_3O_3F$	340.10920	12.5	-0.5
7	447.18258	$C_{25}H_{24}N_4O_3F$	447.18270	15.5	-0.3
8	430.15601	$C_{25}H_{21}N_3O_3F$	430.15615	16.5	-0.3
9	339.10133	$C_{18}H_{14}N_3O_3F$	339.10137	13	-0.1
10	921.22676	$C_{48}H_{33}N_{10}O_5F_3Cl$	921.22705	35.5	-0.3
11	691.21147	$C_{37}H_{29}N_6O_6F_2$	691.21112	25.5	0.5

Table 4.1: Summary of the base peaks observed in the MS chromatogram corresponding to LC peaks 1 – 11, labelled in Figure 4.5.

LC-MS/MS analysis of cediranib

The LC-MS/MS analysis of the protonated cediranib, LC Peak **3** in the TIC (see **Figure 4.5**), was carried out by adapting an existing 20 minute LC method to include alternating MS and MS/MS scans throughout the experiment, targeting the cediranib $[M+H]^+$ at *m/z* 451.2 with high energy electrons (~17.5 eV). The detection time was reduced by acquiring data at a resolving power of 50,000 FWHM, instead of 100,000 FWHM, in order to shorten the time taken for each scan whilst maintaining the high resolving power and mass accuracy capabilities of the FT-ICR instrument. The maximum ion injection time was set at 1500 ms in order to allow enough ions to accumulate prior to MS/MS dissociation. Two image currents were averaged for each MS/MS scan in order to improve the S/N of the detected ions, hereafter

defined as the number of microscans. The product ion spectrum was produced by averaging MS/MS scans across the chromatographic peak.

A comparison between the LC-CID and LC-EID spectra is shown in **Figure 4.6** with an expansion in **Figure 4.7**. Whereas the LC-CID spectrum is limited by the one-third cut-off that restricts the lower *m/z* limit in the linear ion trap, the LC-EID spectrum shows a wide range of fragmentation providing significant structural information. The major product ion observed in the LC-EID spectrum at *m/z* 112.1 is proposed to correspond to the propylpyrrolidine arm as shown in **Figure 4.8(a)**, formed *via* the heterolytic cleavage of the C-O bond. Conversely, the major product ion in the CID spectrum at *m/z* 340.2 corresponds to the reciprocal fragment, the indole-quinazoline structure of the cediranib molecule, shown in **Figure 4.8(b)**. The product ion corresponding to the propylpyrrolidine arm is not observed in the CID spectrum due to the one-third cut-off.

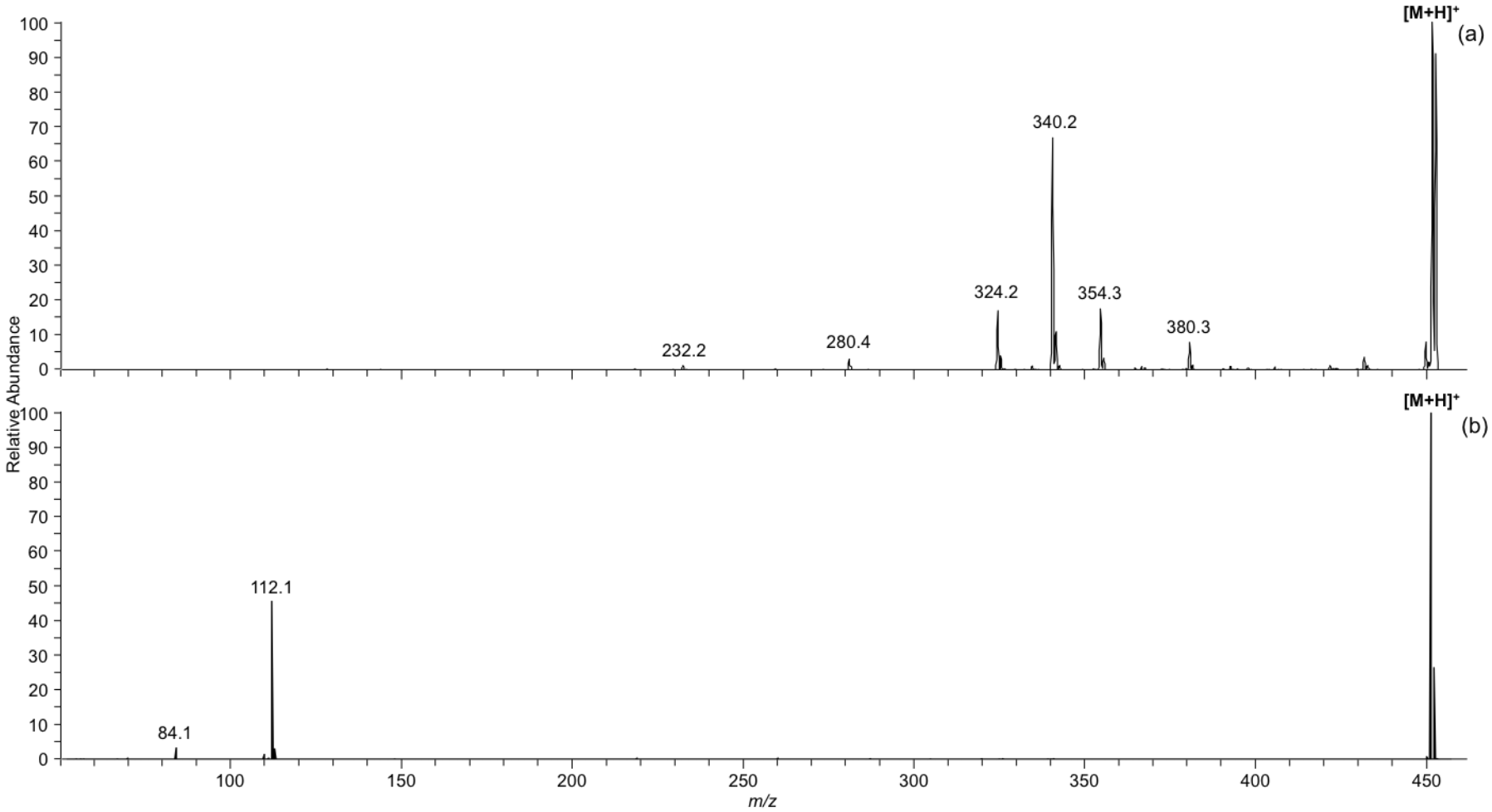

Figure 4.6: LC-MS/MS of the cediranib $[M+H]^+$ by (a) CID and (b) EID.

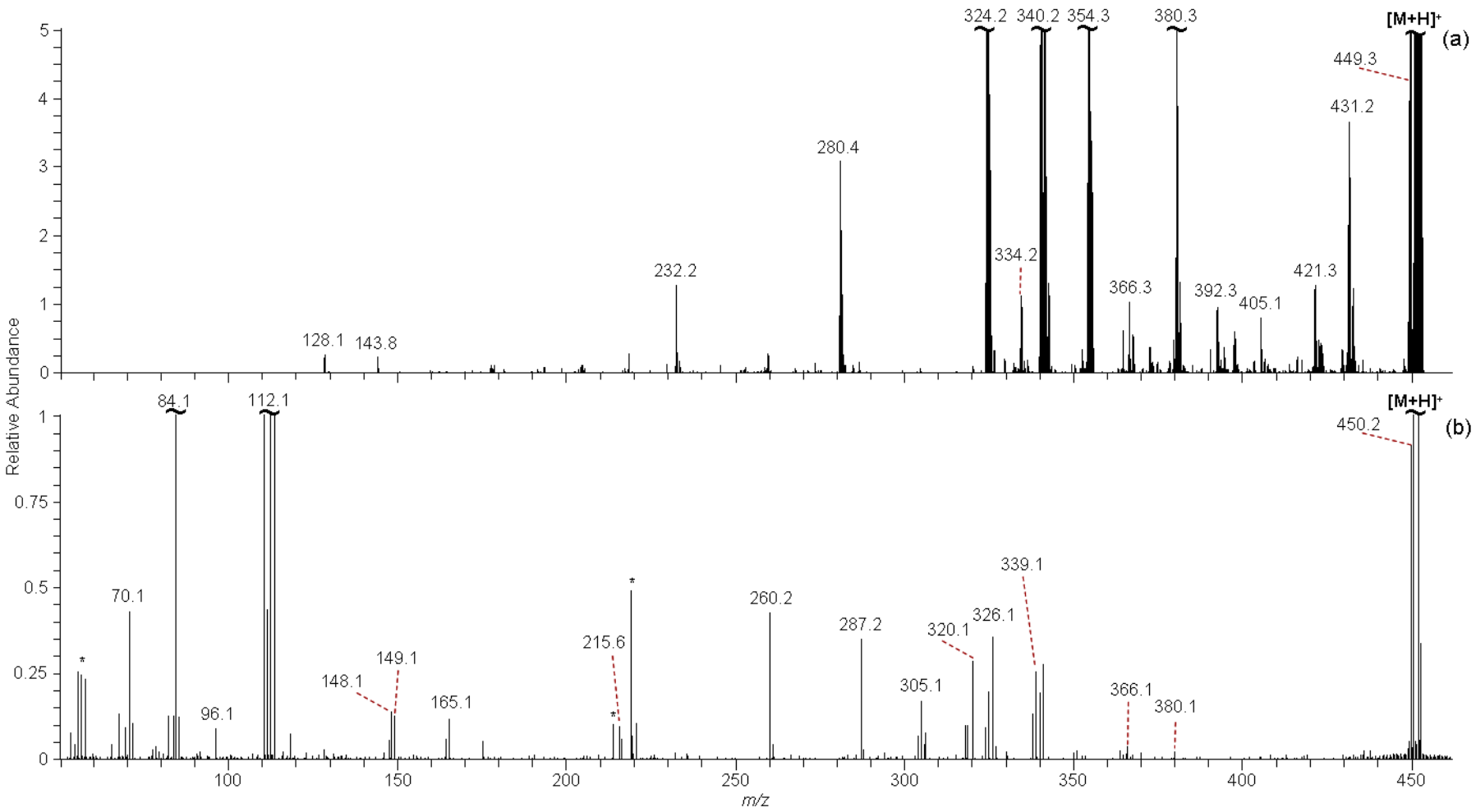

Figure 4.7: Expansion of Figure 4.6 allowing low abundance product ions generated by (a) LC-CID and (b) LC-EID of cediranib to be observed. Peaks labelled * denote artefacts or chemical noise peaks.

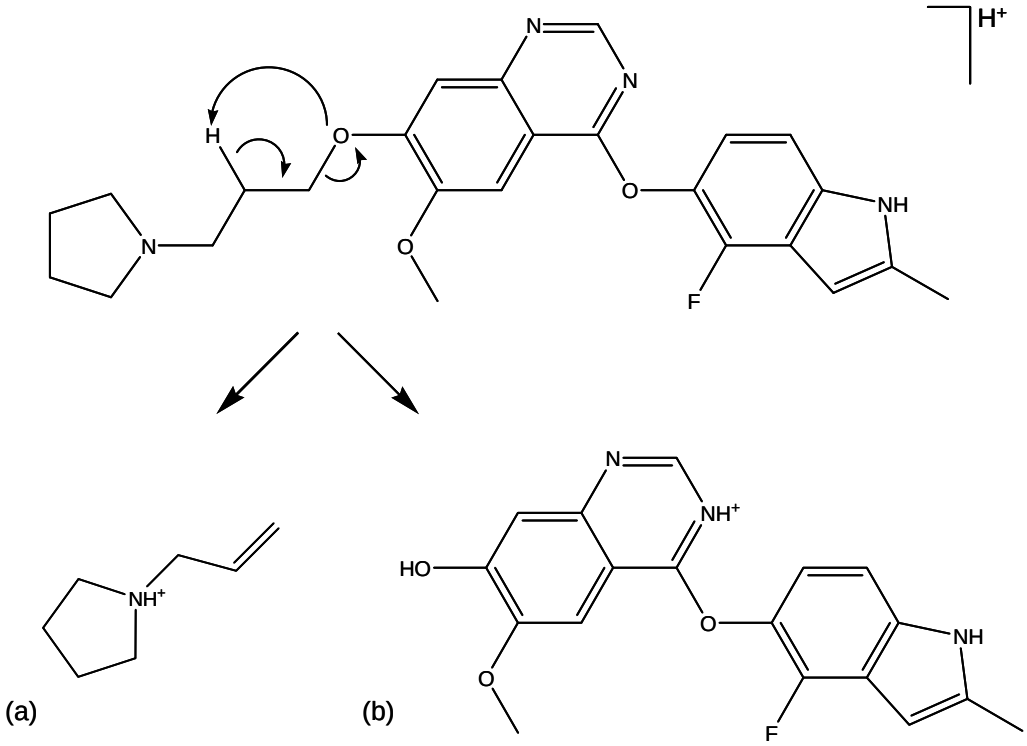

Figure 4.8: Formation of (a) the propylpyrroldine group and (b) the indole-quinazoline group *via* the cleavage of the C-O bond in cediranib.

As mentioned in **Chapter 3**, low *m/z* peaks from the cold cathode electron gun are evident at higher electron energy levels that may disguise low *m/*z product ions, however in this instance there is a clear separation between the product ion at *m/z* 70.06517, corresponding to the pyrrolidine ring of the propylpyrrolidine arm, and a chemical noise peak at *m/z* 70.07774, as shown in **Figure 4.9**. The chemical noise peak is thought to be a hydrocarbon with molecular formula C_5H_{10}, which is emitted from the ECD cathode or the FT-ICR cell at high electron energies, as discussed in **Chapter 3**.

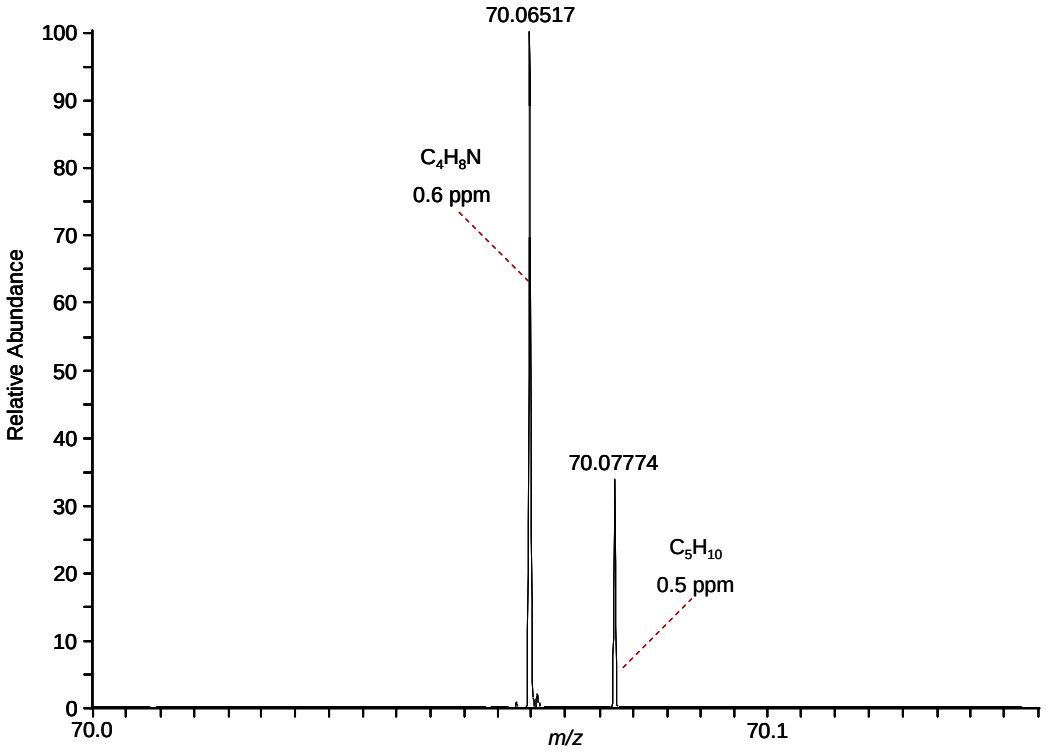

Figure 4.9: High resolution of the FT-ICR allows the distinction between two ions with the same nominal mass.

A direct comparison between the LC-CID and LC-EID spectra indicates 6 product ions that are common to both techniques, at *m/z* 449.2, *m/z* 380.1, *m/z* 366.1, *m/z* 340.1 and *m/z* 324.1. A peak at *m/z* 431.2 is unique to CID and corresponds to the neutral loss of HF from the cediranib molecular ion. The formation of this product ion is thought to proceed *via* a cyclisation reaction as shown in **Figure 4.10**, and is supported by the increase in the RDB from 13.5 to 14.5.

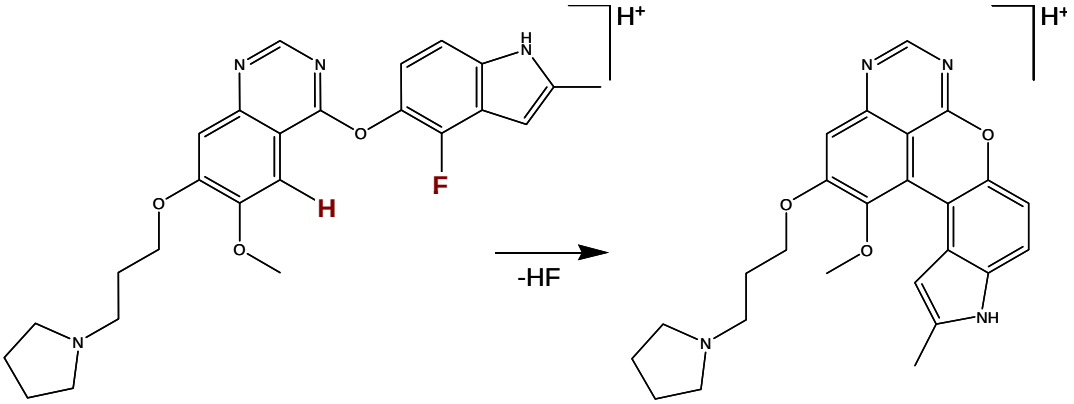

Figure 4.10: Proposed route of formation for the product ion at *m/z* 431.2, generated from the loss of HF.

Overall, LC-EID of cediranib was found to generate 31 product ions compared to 15 by LC-CID, however the minimal overlap between the product ions indicates that both techniques can provide unique information and can complement each other. The spectra shown in **Figure 4.6** and **Figure 4.7** demonstrate the feasibility of using LC-EID and the complementary data provided by LC-EID and LC-CID of cediranib, initiating the analysis of each unknown low abundance compounds in order to generate structural information. The LC-MS/MS method used to analyse cediranib $[M+H]^+$ was altered to target each unknown compound in turn. Two of the unknown species, LC peaks **1** and **6** have been studied in depth and are discussed below. Post acquisition calibration was carried out on the resulting LC-MS/MS spectra using the precursor ion molecular formulae detailed in **Table 4.1** and where possible, the product ion corresponding to propylpyrrolidine moiety. For detailed product ion information for cediranib and LC peaks **1** and **6**, see **Chapter 10: Appendix B**.

4.2.2. LC-MS/MS analysis of LC peak 1

The first of the unknown compounds at *m/z* 562.3, which is seen to elute at 5.69 minutes (LC peak **1**) in **Figure 4.5**, has been studied in depth by both LC-CID,

shown in **Figure 4.11(a)** (with an expansion in **Figure 4.12(a)**), and LC-EID, shown in **Figure 4.11(b)** and **Figure 4.12(b)**. CID generated 14 product ions compared with 23 product ions formed by EID. Significantly, a product ion observed in the LC-EID spectrum at *m/z* 451.2 is proposed to have the same empirical formula as the protonated cediranib molecule, suggesting that the unknown species is chemically related to cediranib. The relationship between the cediranib and the unknown compound can be confirmed by comparing the product ions generated from the MS/MS of *m/z* 562.3 in **Figure 4.11** with the spectra in **Figure 4.6**. There are 15 product ions, highlighted in red in **Figure 4.12**, which are common to both the species at *m/z* 562.3 and cediranib, 12 of which are unique to EID and the remaining 3 are unique to CID. The common ions include the peaks that are proposed to correspond to the indole-quinazoline group and the propylpyrrolidine arm. The high number of commonalities between the dissociation of the cediranib and that of the unknown species further implies a relationship between the two compounds. The observation of the peaks at *m/z* 449.2 and *m/z* 451.2 suggests that the unknown compound is equivalent to a cediranib molecule with an unknown addition. Structural assignments have been proposed for the common ions using the empirical formulae and the associated RDB values, and have been detailed in **Table 4.2**.

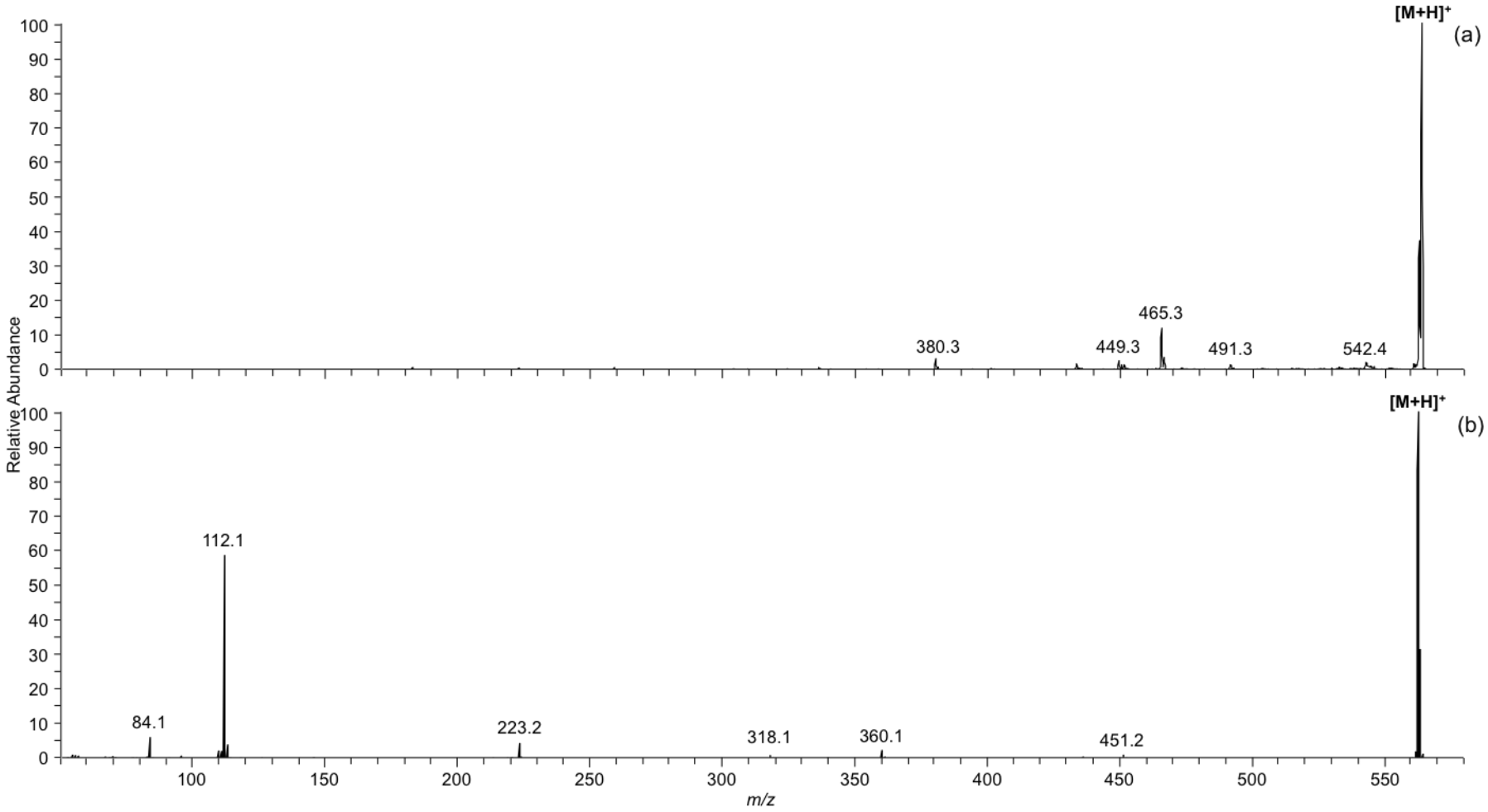

Figure 4.11: Comparison between (a) LC-CID and (b) LC EID of *m/z* 562.3, labelled LC peak 1 in Figure 4.5.

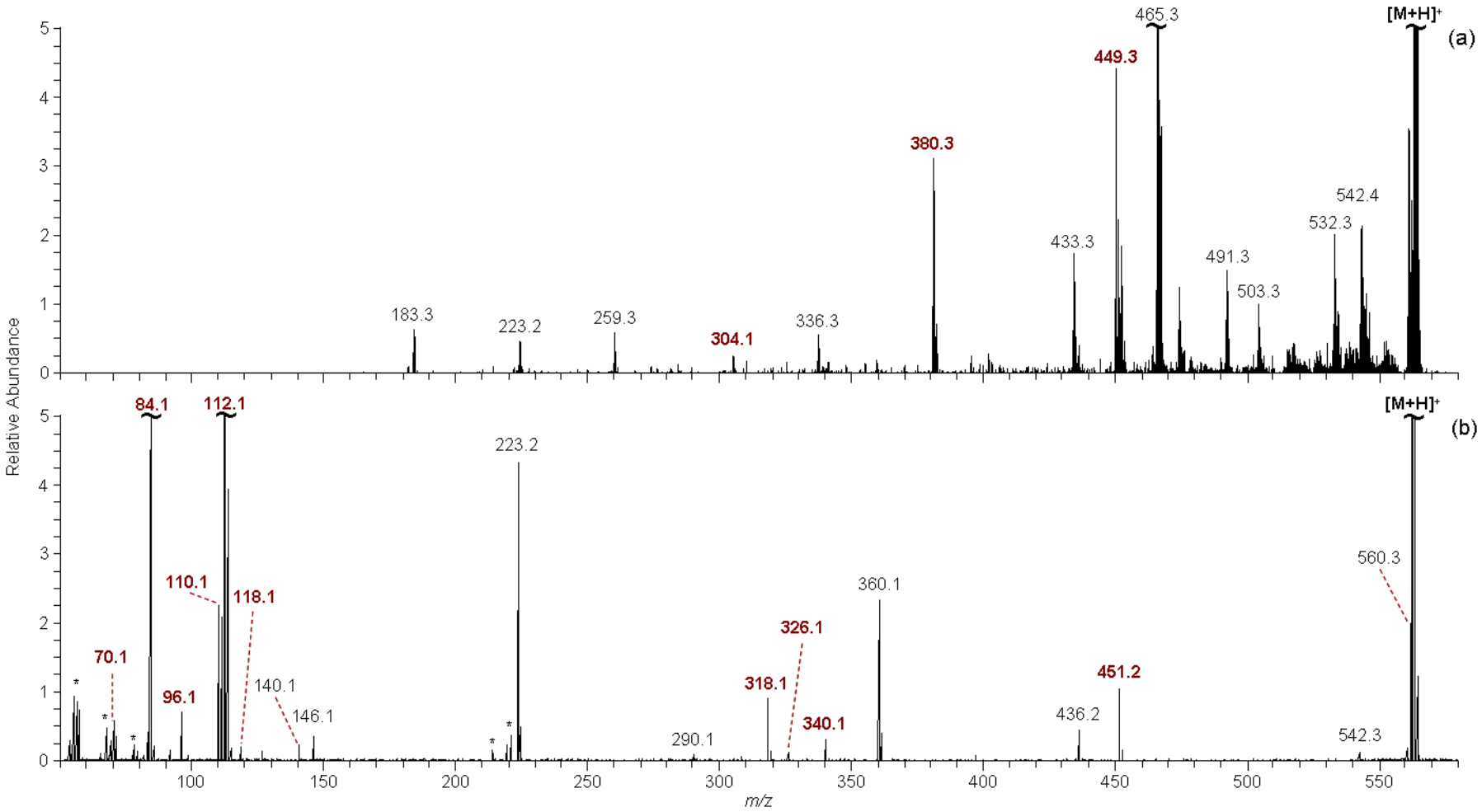

Figure 4.12: Expansion of Figure 4.11, showing (a) the LC-CID spectrum and (b) the LC-EID spectrum of the unknown species observed in LC peak 1 at *m/z* 562.3. Peaks labelled in red correspond to product ions also observed by the MS/MS of cediranib. Peaks labelled * denote artefacts or chemical noise peaks.

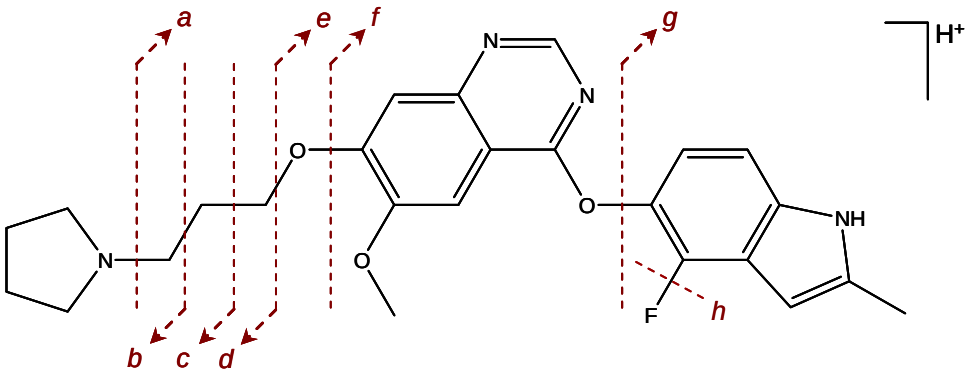

Product Ion m/z	Chemical Formula	RDB	Proposed Bond Cleavage(s)
451.2	$C_{25}H_{28}N_4O_3F$	13.5	cediranib $[M+H]^+$
449.2	$C_{25}H_{26}N_4O_3F$	14.5	loss of H_2 from cediranib
380.1	$C_{21}H_{19}N_3O_3F$	13.5	*a*
340.1	$C_{18}H_{15}N_3O_3F$	12.5	*e*
318.1	$C_{18}H_{12}N_3O_3$	14.5	*e h*
304.1	$C_{18}H_{14}N_3O_2$	13.5	*f h*
119.1	C_8H_9N	5	*g h*
118.1	C_8H_8N	5.5	*g h*
112.1	$C_7H_{14}N$	1.5	*d*
111.1	$C_7H_{13}N$	2	*d*
110.1	$C_7H_{12}N$	2.5	*d*
96.1	$C_6H_{10}N$	2.5	*b*
84.1	$C_5H_{10}N$	1.5	*b*

Table 4.2: Summary of ions common to LC peak 1 and cediranib $[M+H]^+$. The proposed bond cleavages do not illustrate hydrogen loss/migration.

The neutral loss of 111.1 Da from the precursor ion *m/z* 562.3 to form the product ion at *m/z* 451.2 is consistent with the loss of a fragment of $C_7H_{13}N$ that is thought to correspond to a second propylpyrrolidine arm that has attached to the target molecule during synthesis. The site of this addition was investigated by studying the product ion spectra from the unknown compound, focussing on the product ions not generated by the MS/MS of cediranib. In particular, there are two product ions that have been identified as significant, firstly a peak at *m/z* 223.2 that is observed by EID and CID of *m/z* 562.3, corresponding to the chemical formula $C_{14}H_{27}N_2$ with an error of 0.6 ppm error. This fragment is consistent with two propylpyrrolidine arms

joined together, suggesting that the additional arm has been substituted onto one of the seven carbon atoms, labelled C(1) to C(7) in **Figure 4.13**, or the nitrogen atom on the pyrrolidine ring, N(8).

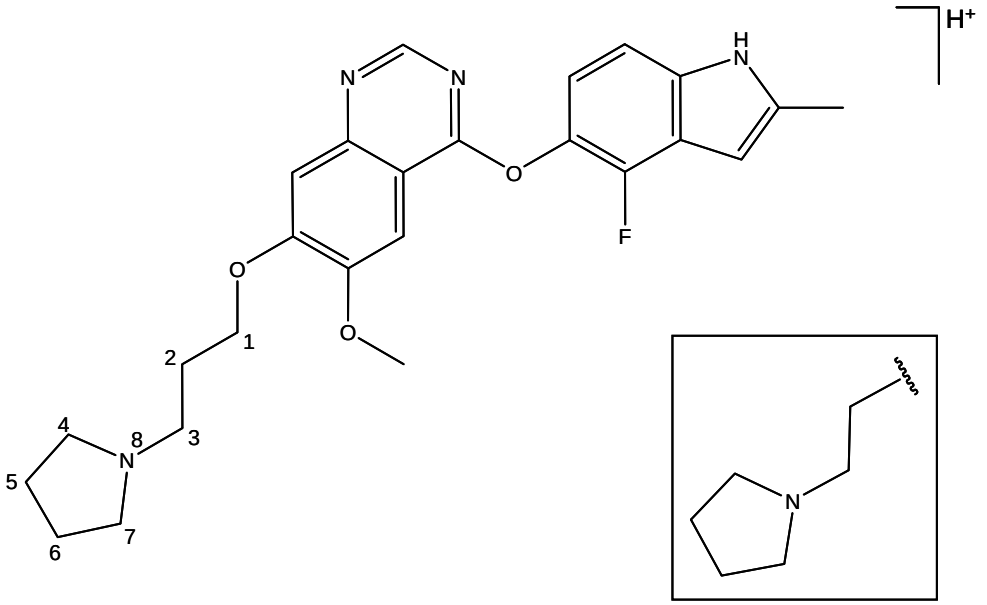

Figure 4.13: The cediranib molecular structure plus an additional propylpyrrolidine moiety (inset) that is expected to combine to form the unknown *m/z* 562.3 compound.

The second informative product ion is observed at *m/z* 360.1 and is only generated by EID. This fragment corresponds to the chemical formula $C_{21}H_{18}N_3O_3$, with an error of 1.4 ppm, and is due to the neutral loss of one intact propylpyrrolidine arm plus the pyrrolidine ring of the second arm and hydrogen fluoride ($C_7H_{14}N + C_4H_8N + HF$). The loss of HF is proposed to occur *via* the cyclisation reaction detailed in **Figure 4.10**. This further indicates that the addition of the second propylpyrrolidine arm has taken place on the pyrrolidine ring, C(4) - C(7) or N(8). Preparative separation and NMR analysis conducted at AstraZeneca has confirmed that this unknown compound is the result of a second propylpyrrolidine arm substituting onto the nitrogen atom of the cediranib pyrrolidine ring, resulting in the structure shown in

Figure 4.14(a). Proposed structures for the two notable product ions at *m/z* 223.2 and *m/z* 360.1 are shown in **Figure 4.14(b)** and **(c)**.

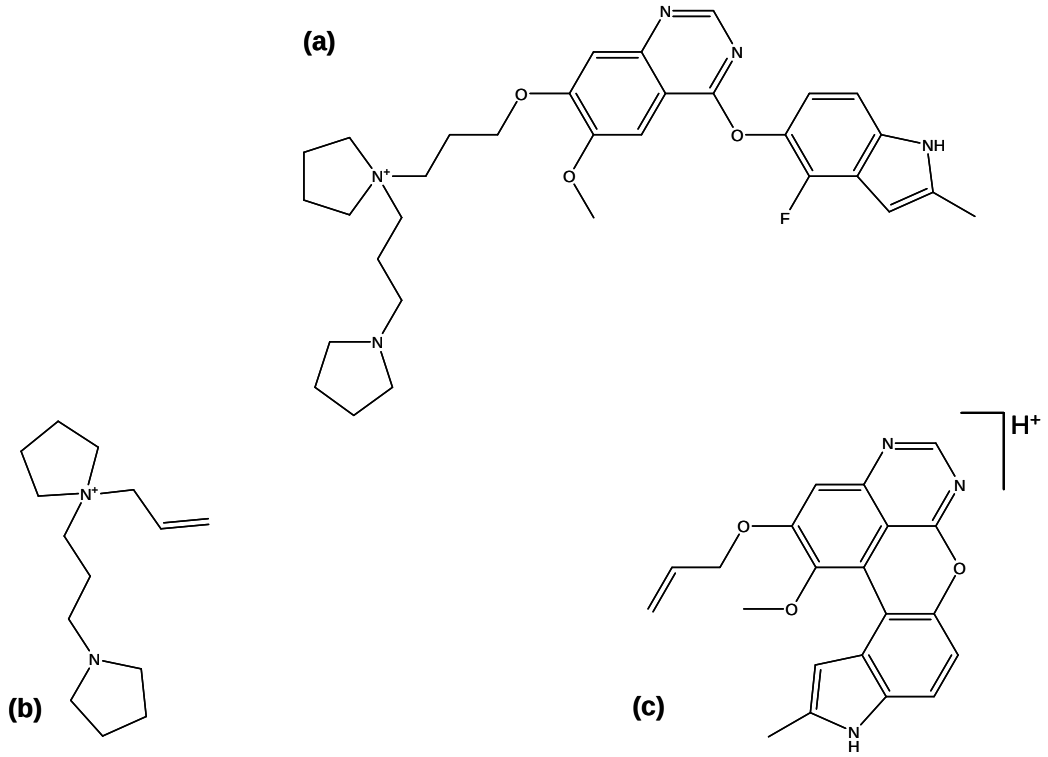

Figure 4.14: (a) Confirmed structure of the previously unknown compound at *m/z* 562 that is present at low concentrations in the cediranib sample, and proposed structures of product ions at (b) *m/z* 223 and (c) *m/z* 360.

4.2.3. LC-MS/MS analysis of LC peak 6

The peak labelled **6** in **Figure 4.5** is observed at *m/z* 340.1 and is consistent with the molecular formula of $C_{18}H_{15}N_3O_3F$. This precursor ion has the same empirical formula as the product ion observed from the EID and CID of cediranib, which was determined to be the indole-quinazoline structure as shown in **Figure 4.8**. Inspection of the LC-EID and LC-CID spectra generated for the *m/z* 340.1 species identifies 17 product ions which are also observed in the product ion spectra from the cediranib, highlighted in **Figure 4.15**, which supports the relationship between the two compounds. The common ions and their proposed structural characterisations have been summarised in **Table 4.3**.

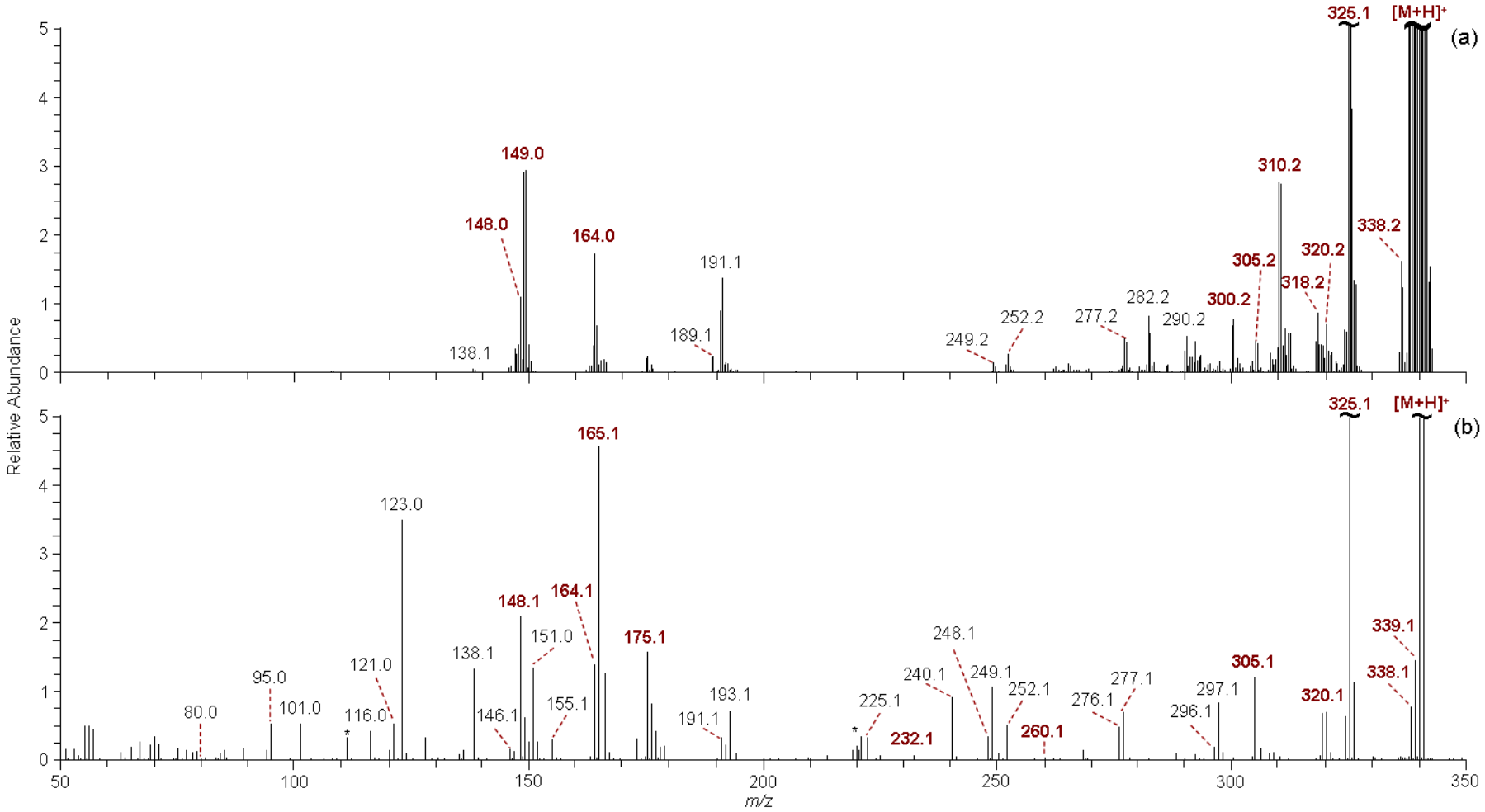

Figure 4.15: (a) LC-CID and (b) LC-EID spectra for LC peak 6 at *m/z* 340.1. Product ions also observed from the MS/MS of cediranib $[M+H]^+$ have been highlighted in red. Peaks labelled * denote artefacts or chemical noise peaks.

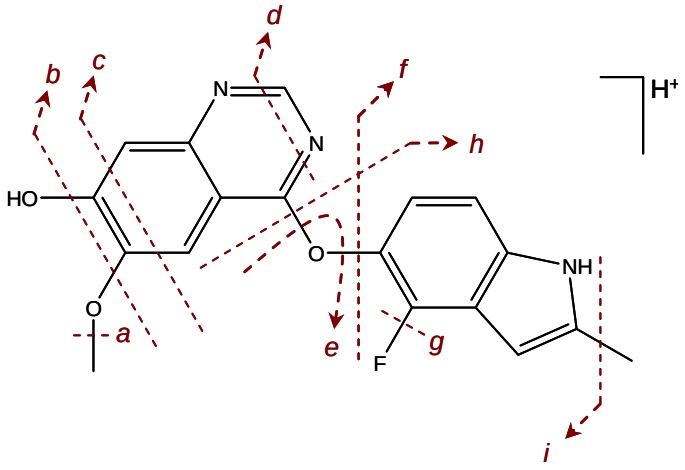

Observed Ion *m/z*	Molecular Formula	RDB	Proposed Bond Cleavage(s)
340.1	$C_{18}H_{15}N_3O_3F$	12.5	precursor
339.1	$C_{18}H_{14}N_3O_3F$	13	loss of H from precursor
338.1	$C_{18}H_{13}N_3O_3F$	13.5	loss of H_2 from precursor
325.1	$C_{17}H_{12}N_3O_3F$	13	*a / i*
324.1	$C_{17}H_{11}N_3O_3F$	13.5	*a / i*
320.1	$C_{18}H_{14}N_3O_3$	13.5	*g*
319.1	$C_{18}H_{13}N_3O_3$	14	*g*
318.1	$C_{18}H_{12}N_3O_3$	14.5	*g*
305.1	$C_{17}H_{11}N_3O_3$	14	*a g / g i*
304.1	$C_{17}H_{10}N_3O_3$	14.5	*a g / g i*
260.1	$C_{16}H_{10}N_3O$	13.5	*b g i*
232.1	$C_{15}H_{10}N_3$	12.5	*c g e*
175.1	$C_{10}H_8N_2F$	7.5	*d*
165.1	C_9H_8NOF	6	*h*
164.1	C_9H_7NOF	6.5	*h*
149.1	C_9H_8NF	6	*f*
148.1	C_9H_7NF	6.5	*f*

Table 4.3: Summary of ions observed from the MS/MS of *m/z* 340.1 and cediranib.

The bond cleavage labelled ***g*** is expected to proceed *via* the cyclisation reaction shown for cediranib in **Figure 4.10**, resulting in the loss of HF. The high number and nature of the product ions that are common to the cediranib suggests that this unknown species is in fact the same species as the product ion at *m/z* 340.1 seen in the MS/MS spectra in **Figure 4.6** and corresponds to the spontaneous loss of the propylpyrrolidine moiety from the target molecule during synthesis. This is further confirmed by the RDB assignment for the unknown species that is 12.5 and is consistent with the indole-quinazoline structure**.** The product ion observed at *m/z*

232.1, proposed to result from multiple bond cleavages, includes the loss of the oxygen connecting the indole and quinazoline rings, bond cleavage ***e***, which is thought to be facilitated by the distortion of the molecule upon cyclisation to lose HF.

The spectrum obtained from the LC-EID of this compound showed considerable fragmentation, generating 70 products ions compared to 21 and 35 by LC-CID-FT and LC-CID-IT respectively. Of the 70 EID product ions, more than 75% of are observed as part of peak groupings corresponding to the same bond cleavage but with a varying number of hydrogen atoms, with the remaining 20 of these product ions resulting from 'unique' bond cleavages. While the evidence of peak multiplets is more prevalent by EID, it is also widely noted in the CID spectrum for this compound, suggesting that the aromatic regions of the indole-quinazoline group can form highly stable odd-electron species.

4.2.4. LC-MS/MS data for LC peaks 1 - 11

The information obtained from the LC-MS/MS analysis of the cediranib sample has been compiled and detailed in **Table 4.4**, showing the total number of product ions obtained for each eluting compound from each fragmentation technique. A comparison between the CID-FT and EID shows that EID is the superior technique for 9 of the 11 compounds, producing a higher degree of fragmentation than CID-FT. This is expected to be partly due to the one-third cut-off that governs CID carried out in an ion trap, thereby inhibiting the detection of product ions in the low *m/z* regions in which EID was found to generate up to 10 product ions. The EID and CID-FT analysis of LC peak **4**, see **Figure 4.17,** results in both techniques generating the same two product ions, suggesting that vibrational excitation processes may be governing EID of LC peak **4**. LC peak **11**, shown in **Figure 4.23**, generates two more product ions by CID FT than EID, confirming the complementary nature of the two techniques and the benefits of using more than

one MS/MS technique. The inclusion of CID-IT data significantly increases the number of observed product ions and alters the trend slightly, with 4 compounds showing a greater effect from CID-IT than EID, however accurate mass measurements and molecular formulae assignments cannot be made from ion trap data alone.

LC Peak Number	*m/z*	Number of product ions observed			Common product ions between EID and CID-IT		Number of product ions common between cediranib and unknown	
		EID	CID					
			FT	IT				
1	562.3	23	0	14	3	9.7%	15	37.5%
2	899.4	5	2	8	2	18.2%	6	18.2%
3	451.2	31	3	15	6	12.2%	N/A	
4	788.3	2	2	11	2	20.0%	6	54.5%
5	481.2	19	4	5	3	14.3%	9	40.9%
6	340.1	70	21	35	32	41.0%	17*	19.5%
7	447.2	26	1	3	3	11.5%	11	42.3%
8	430.2	45	17	29	28	60.8%	9	19.6%
9	339.1	35	0	26	16	35.6%	12*	26.7%
10	921.2	6	3	7	5	62.5%	2	25.0%
11	691.2	1	3	13	1	7.7%	3	23.1%

Table 4.4: Summary of all product ions generated by EID and CID for each observed compound. Values marked * include the precursor ion. Percentages have been calculated from the total number of product ions.

The percentage of ions that are common to each technique is seen to vary between 7% and 63%, demonstrating that both CID and EID have the ability to provide unique information and reaffirming their complementary nature. Each unknown compound was found to generate product ions common with cediranib, suggesting a connection between the compounds, however the structures proposed for the cediranib product ions lend confidence to the assumption that all 10 compounds are structurally related to the target molecule. The indole-quinazoline structure was found to be a common feature in all of the 10 unknown compounds, with at least 3

compounds, including LC peak **1**, proposed to correspond to modified cediranib, due to the presence of a product ion consistent with the cediranib molecular formula. The similarities between each unknown compound and cediranib strongly suggest that each compound is an analogue of the target molecule created unintentionally during chemical synthesis or formed from the degradation of cediranib. EID has been shown to generate a wealth of information from singly protonated species that has aided in the identification of analogous compounds, and when used in conjunction with CID has allowed structural assignments to be made.

The LC-CID and LC-EID spectra for LC peaks **2**, **4**, **5**, **7** – **11** are shown in **Figures 4.16** – **4.23**. Peaks that are also observed in the MS/MS spectra for cediranib $[M+H]^+$ have been labelled in red, so as to highlight the common product ions that indicate a structural relationship to cediranib. The number of common peaks in each spectrum and the proposed molecular formulae suggest that the unknown compounds are all chemically related to cediranib; however the structures remain proprietary information of AstraZeneca and cannot be discussed further.

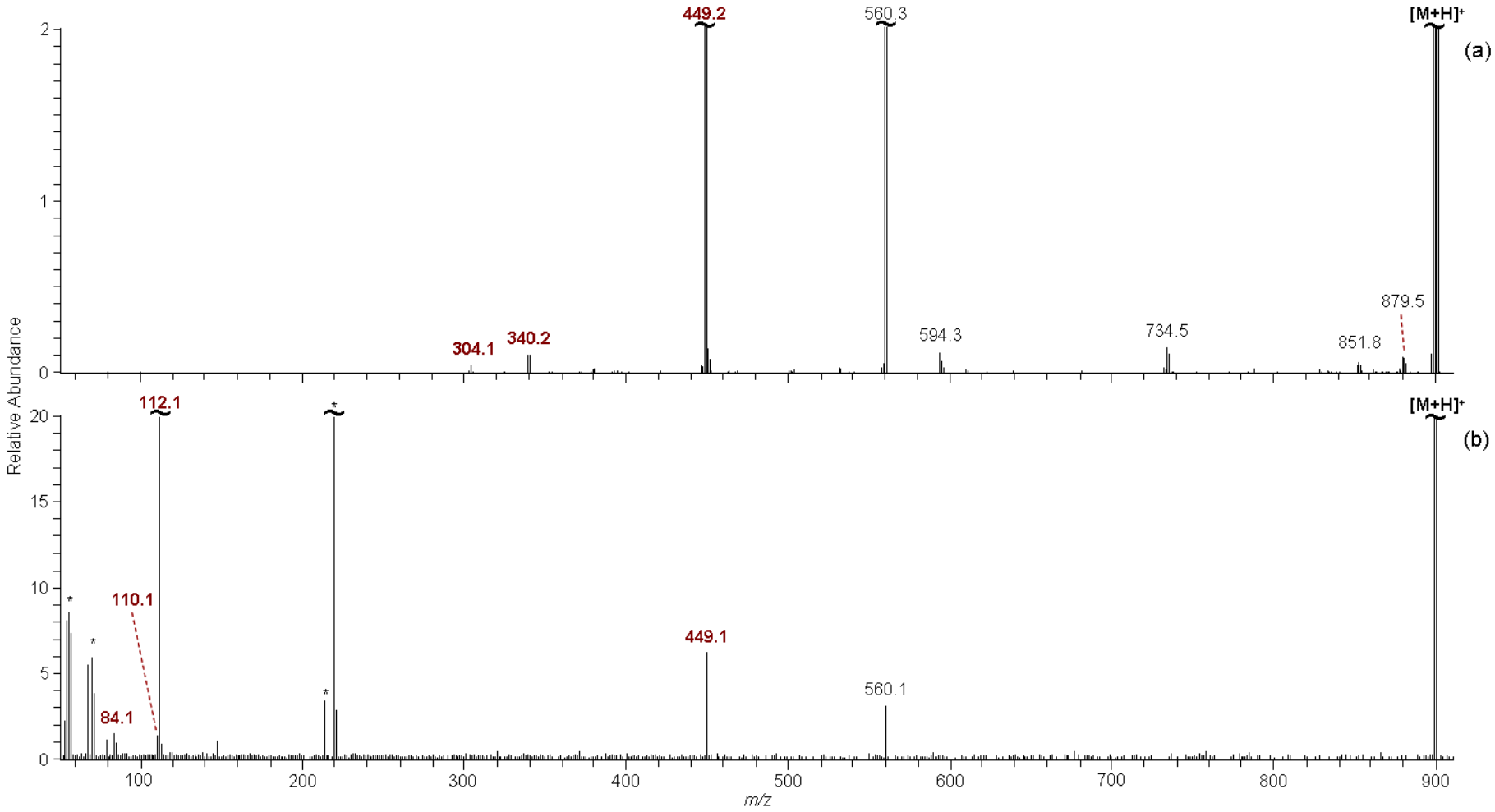

Figure 4.16: (a) LC-CID and (b) LC-EID spectra for LC peak 2 at *m/z* 899.4. Product ions also observed from the MS/MS of cediranib $[M+H]^+$ have been highlighted in red. Peaks labelled * denote artefacts or chemical noise peaks.

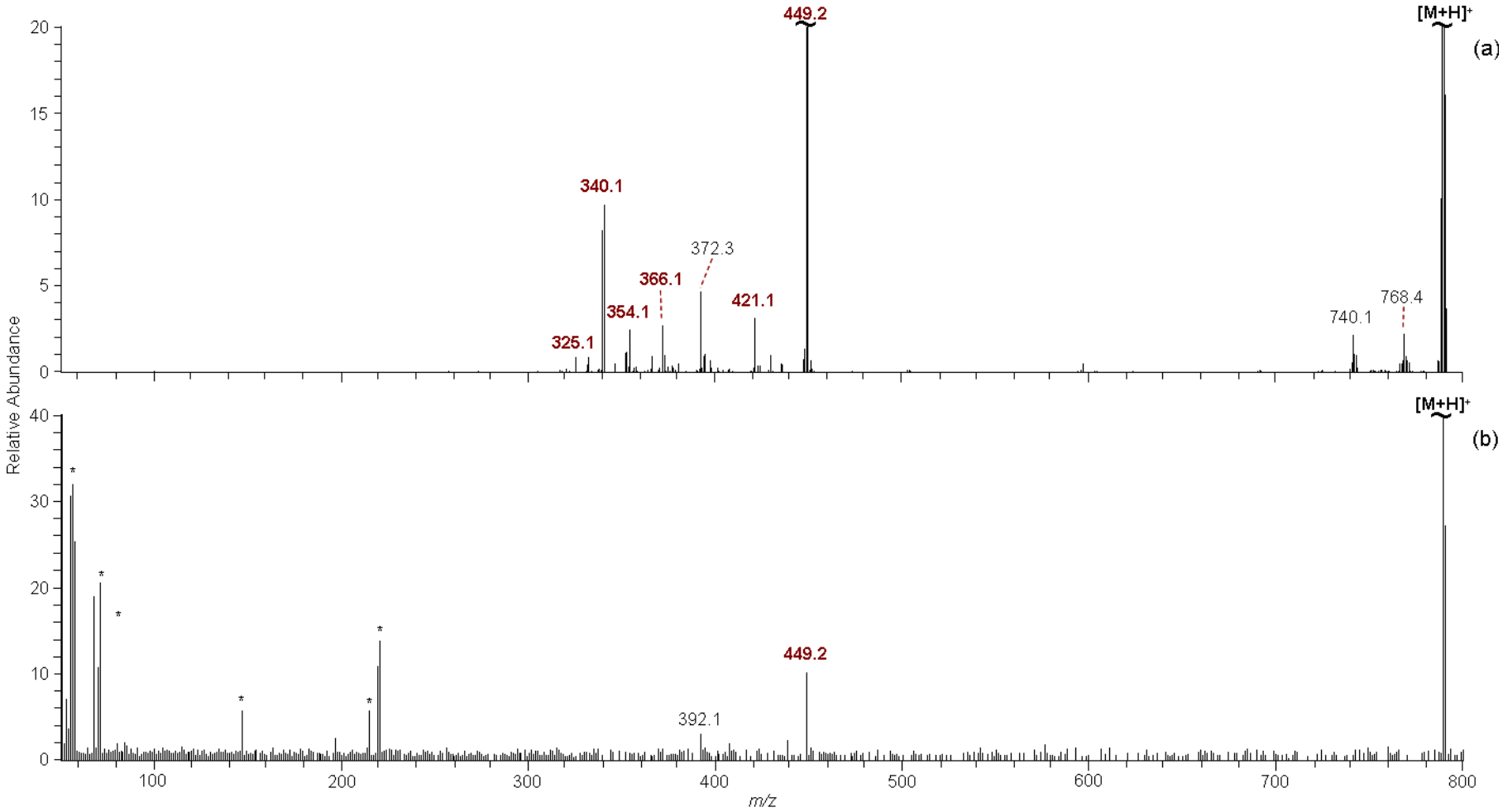

Figure 4.17: (a) LC-CID and (b) LC-EID spectra for the LC peak 4 at *m/z* 788.3. Product ions also observed from the MS/MS of cediranib $[M+H]^+$ have been highlighted in red. Peaks labelled * denote artefacts or chemical noise peaks.

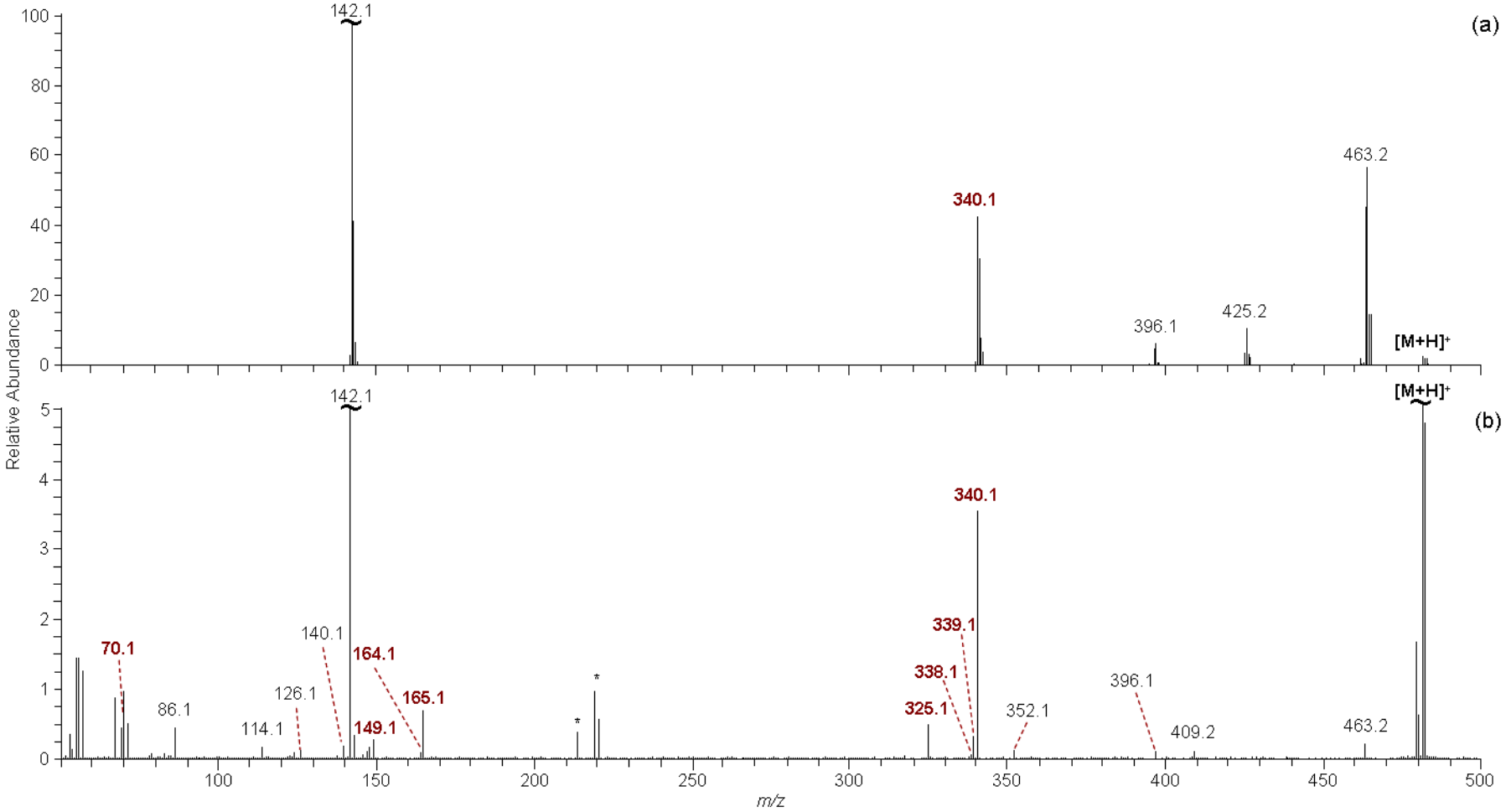

Figure 4.18: (a) LC-CID and (b) LC-EID spectra for the LC peak 5 at *m/z* 481.2. Product ions also observed from the MS/MS of cediranib $[M+H]^+$ have been highlighted in red. Peaks labelled * denote artefacts or chemical noise peaks.

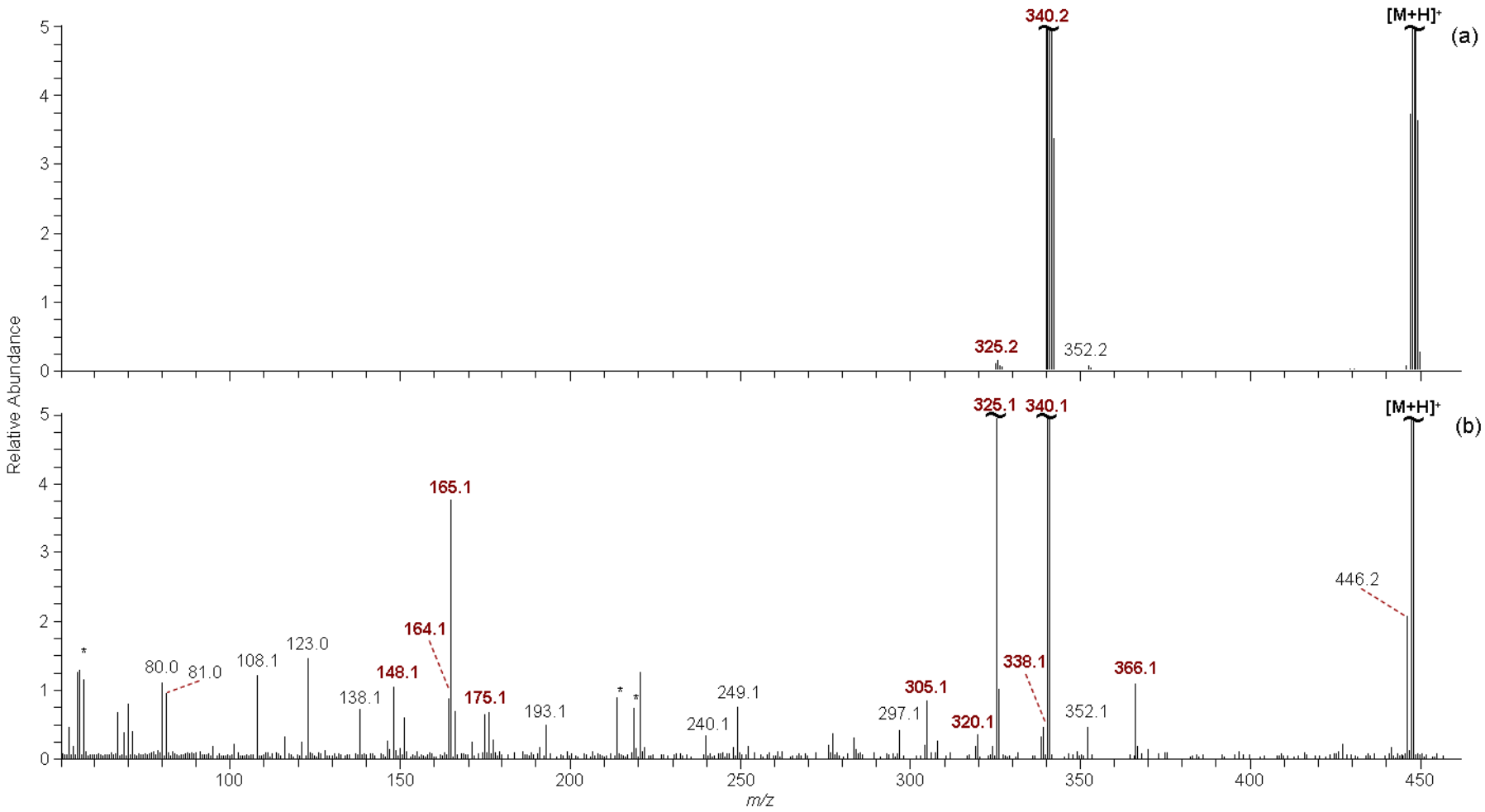

Figure 4.19: (a) LC-CID and (b) LC-EID spectra for LC peak 7 at *m/z* 447.2. Product ions also observed from the MS/MS of cediranib $[M+H]^+$ have been highlighted in red. Peaks labelled * denote artefacts or chemical noise peaks.

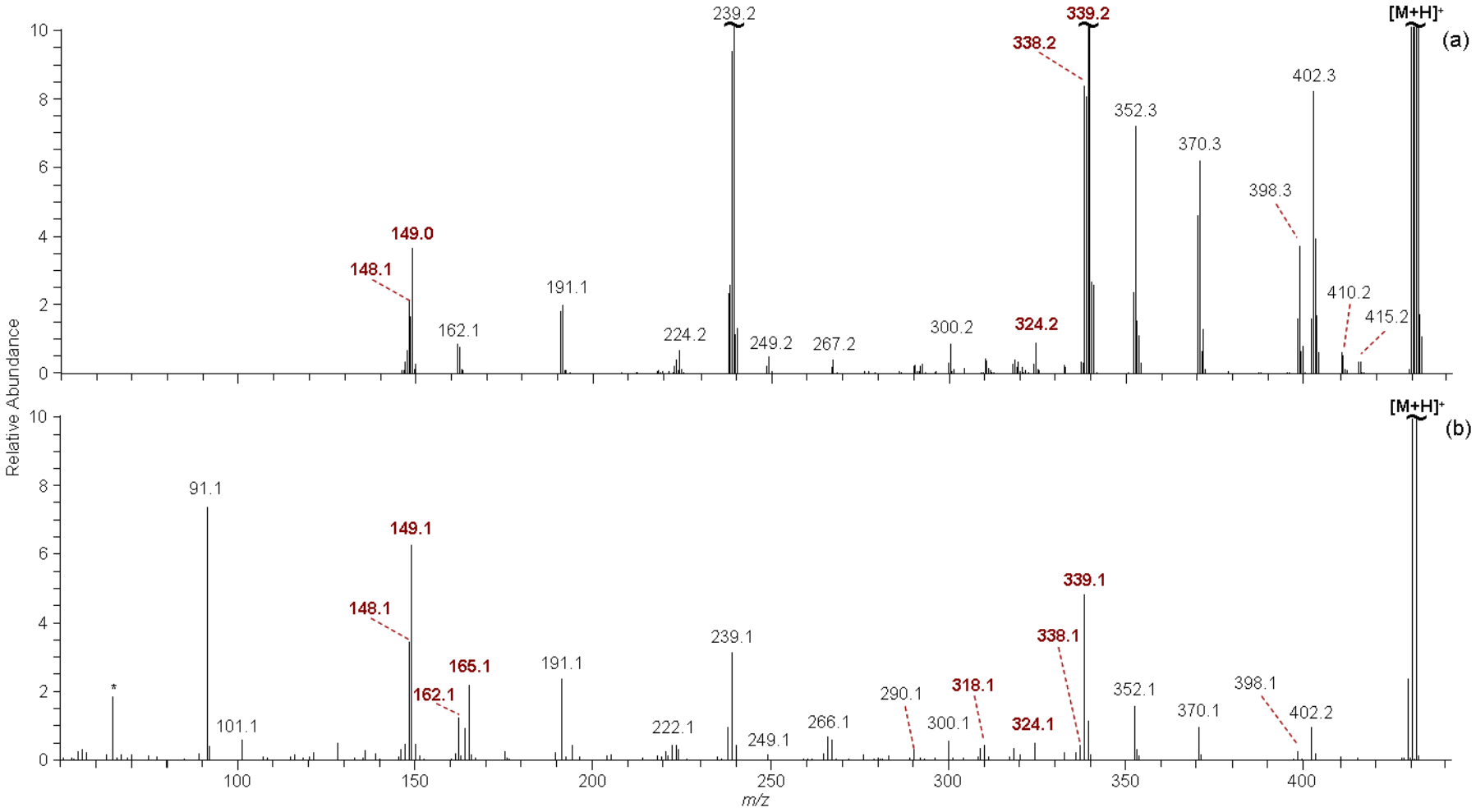

Figure 4.20: (a) LC-CID and (b) LC-EID spectra for LC peak 8 at *m/z* 430.2. Product ions also observed from the MS/MS of cediranib $[M+H]^+$ have been highlighted in red. Peaks labelled * denote artefacts or chemical noise peaks.

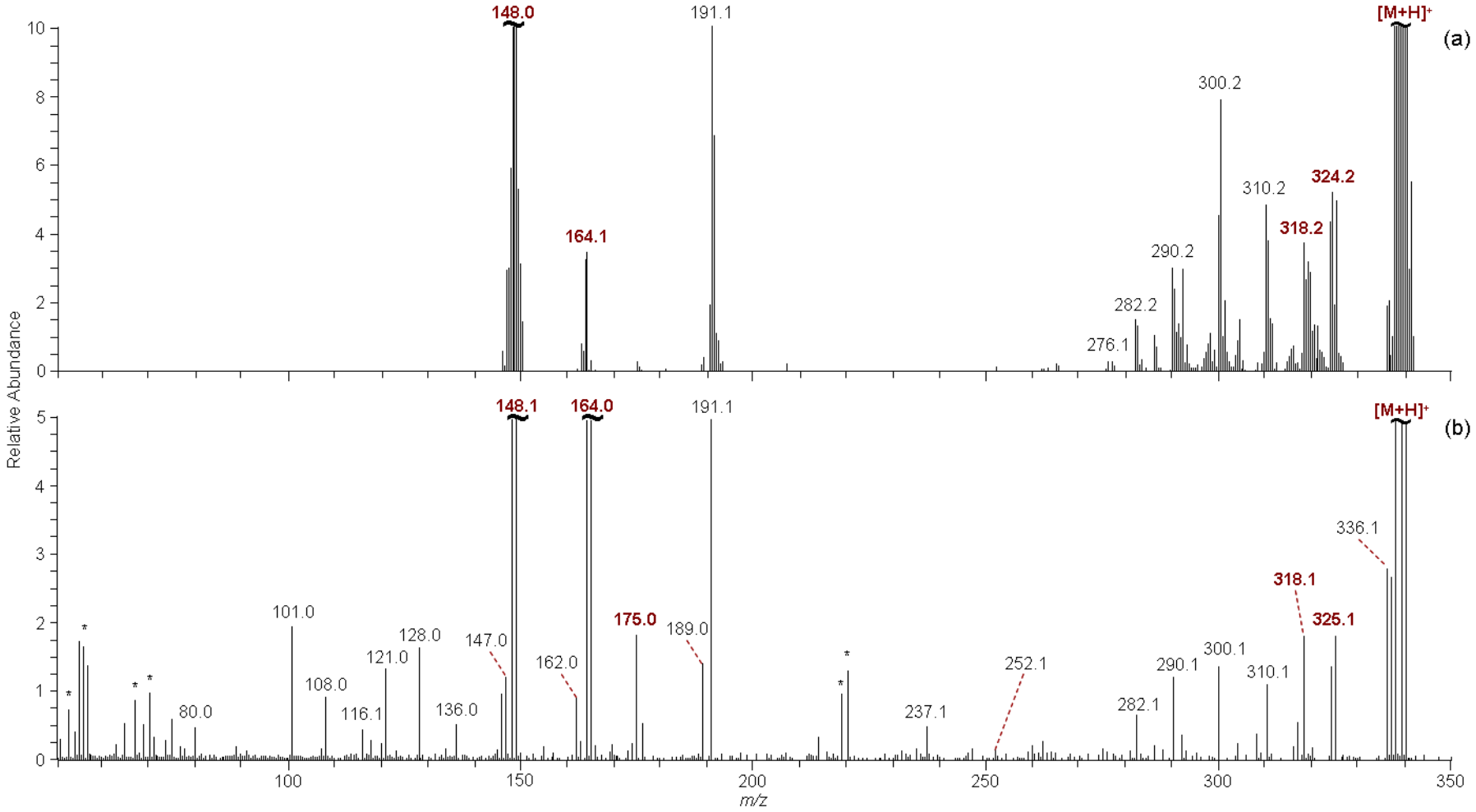

Figure 4.21: (a) LC-CID and (b) LC-EID spectra for LC peak 9 at *m/z* 339.1. Product ions also observed from the MS/MS of cediranib $[M+H]^+$ have been highlighted in red. Peaks labelled * denote artefacts or chemical noise peaks.

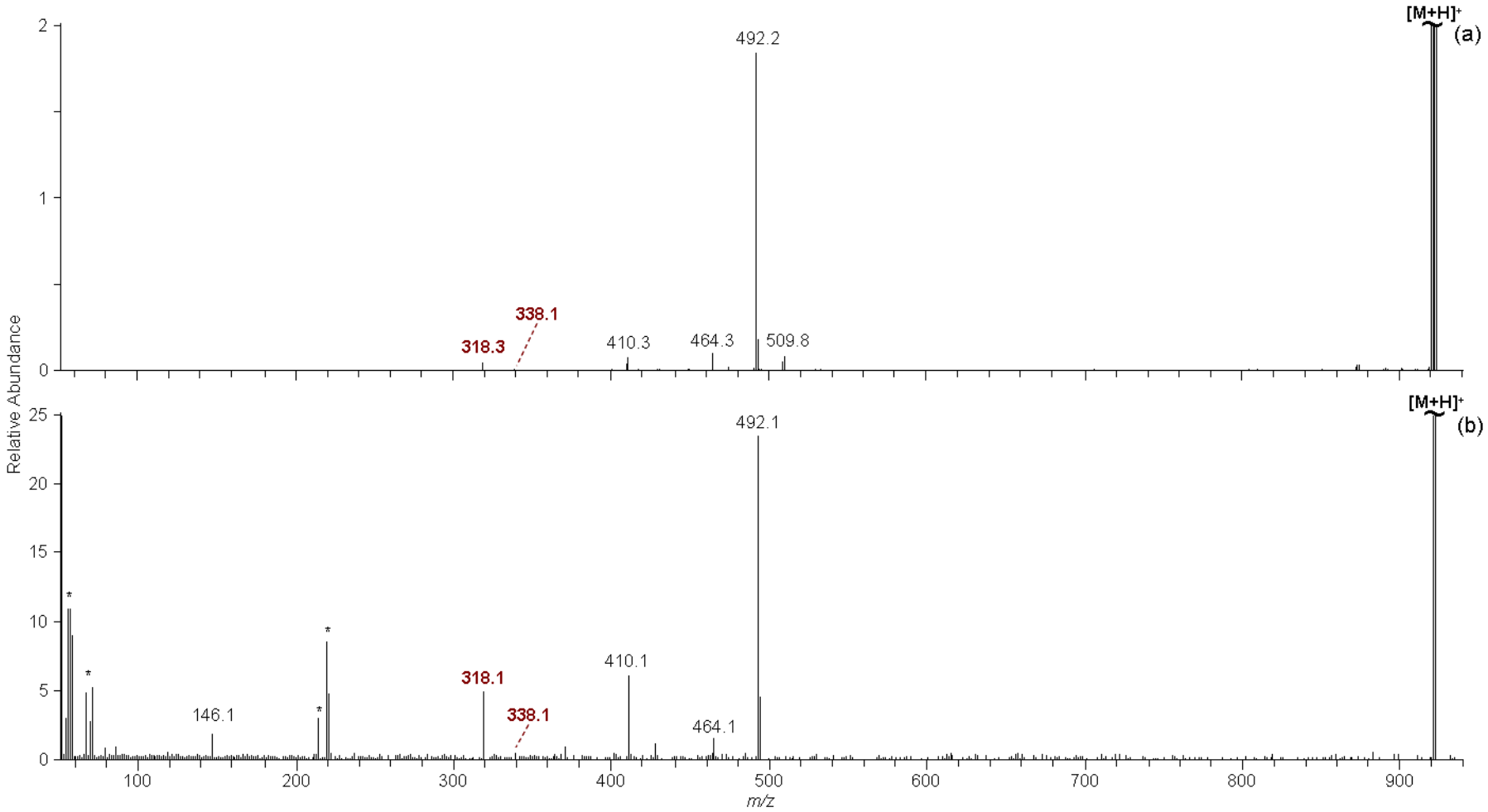

Figure 4.22: (a) LC-CID and (b) LC-EID spectra for LC peak 10 at *m/z* 921.2. Product ions also observed from the MS/MS of cediranib $[M+H]^+$ have been highlighted in red. Peaks labelled * denote artefacts or chemical noise peaks.
peaks.

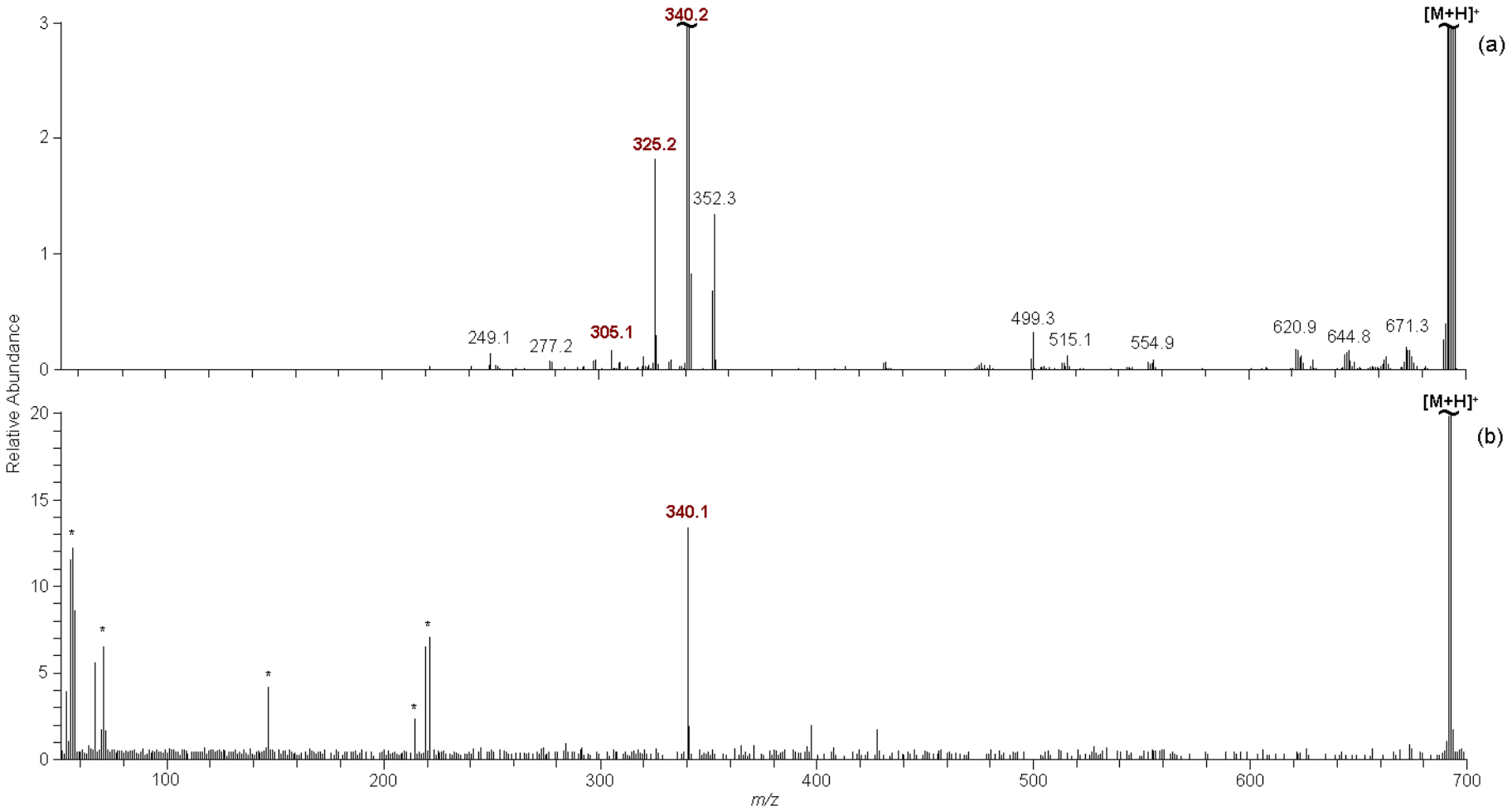

Figure 4.23: (a) LC-CID and (b) LC-EID spectra for LC peak 11 at *m/z* 691.2. Product ions also observed from the MS/MS of cediranib $[M+H]^+$ have been highlighted in red. Peaks labelled * denote artefacts or chemical noise peaks.

4.2.5. LC-EID of sodium adducted species

A recent paper by Mosely *et al.*[5] investigated the use of different charge carrying species and the effect altering the charge carrier has on EID analysis. To further this work, the infusion of sodium iodide post-column was carried out in an attempt to produce the sodium-adducted species for each of the unknown compounds for EID analysis. The probability of observing sodium-adducted species is dependent on the sodium affinity of the species of interest. Despite using a 1 mg mL^{-1} solution of salt, only two sodium-adducted compounds were observed, the cediranib $[M+Na]^+$ species, at *m/z* 473.2, and the sodium-adducted species of LC peak **5** at *m/z* 503.2. Both sodium-adducted species are observed at much lower ion abundances than the $[M+H]^+$ species, indicating that both compounds have a higher proton affinity than sodium affinity.

A comparison between the LC-EID of cediranib $[M+Na]^+$ and $[M+H]^+$ is shown in **Figure 4.24**. There were 17 product ions generated from the EID of cediranib $[M+Na]^+$, of which only 4 were seen to lose the sodium cation to form product ions that were all observed from the MS/MS of the protonated cediranib. The four common product ions correspond to portions of the propylpyrrolidine arm, at *m/z* 112.1, *m/z* 110.1 and *m/z* 84.1, and the indole-quinazoline group at *m/z* 340.1, together encompassing the entire cediranib molecule. The sodium cation was retained by 13 of the remaining product ions, all of which contained the indole portion of the molecule, suggesting that the sodium cation resides in this area of the molecule. Eight of the sodium-adducted product ions were also observed in their protonated form in the MS/MS spectra of the $[M+H]^+$ precursor, while 5 product ions are formed by bond cleavages that were unique to the MS/MS of the $[M+Na]^+$ precursor, indicating that the amount of structural information generated by EID can be maximised by altering the charge-carrying species.

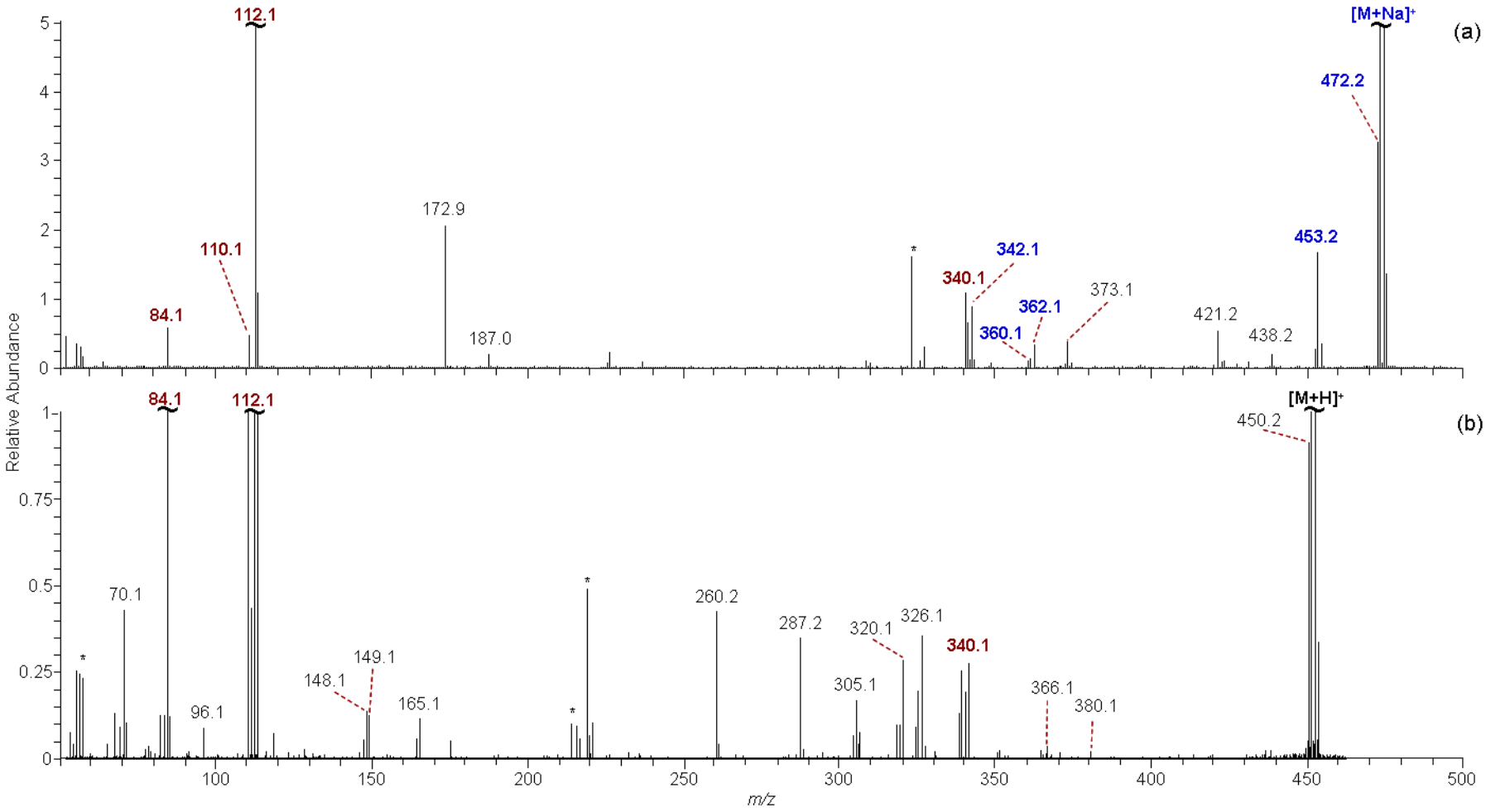

Figure 4.24: LC-EID of cediranib (a) $[M+Na]^+$ and (b) $[M+H]^+$. Product ions highlighted in red are observed in both spectra. Product ions highlighted in blue indicate sodium-adducted product ions that are observed in their protonated form from the MS/MS of cediranib $[M+H]^+$. Peaks labelled * denote artefacts or chemical noise peaks.

A summary of the observations made from the analysis of the cediranib $[M+Na]^+$ and the sodium-adducted LC peak **5** is shown in **Table 4.5**, indicating how many product ions are also observed from the MS/MS of the protonated species, either as the protonated species or as sodium-adducted equivalents.

Precursor Ion	EID Product Ions	Product Ions common to $[M+H]^+$	Na^+ adducts of $[M+H]^+$ product ions	Unique Product Ions
[cediranib + Na]$^+$	17	4	8	5
[LC peak **5** + Na]$^+$	7	1	2	4

Table 4.5: Summary of the EID product ions generated from the $[M+Na]^+$.

EID of the sodium-adducted species generated far fewer product ions than the protonated equivalents, with a 45% and 63% reduction from the cediranib $[M+H]^+$ and [LC peak **5** + H]$^+$ respectively, however both sodium-adducted species provided unique information. The LC-EID analysis of the sodium-adducted species in addition to the protonated precursor ion demonstrates the benefits of analysing multiple charge-carrying species in order to maximise the amount of structural data that can be acquired.

4.2.6. Data-dependent LC-EID of cediranib

The LC-MS/MS experiments thus far have been limited to targeted MS/MS, requiring the analysis of each compound to have its own experimental setup. In the case of cediranib, eleven experiments were needed for each MS/MS technique in order to fully analyse the sample. The number of experiments can be reduced by using data-dependent LC-MS/MS, selecting the most intense ion in each MS scan for subsequent MS/MS analysis and therefore generating MS/MS data for multiple species during one experiment. Preliminary data-dependent experiments have

been carried out on cediranib in an attempt to analyse each species observed in the sample. Due to the non-selective nature of the initial data-dependent analyses, only 7 of the 11 compounds were ever observed as the most intense ion and subsequently analysed by EID. The intentionally high concentration of the target molecule, LC Peak **3** in **Figure 4.5**, overpowered the chromatogram and prevented the analysis of neighbouring LC peaks **2** and **4**. While data-dependent LC-MS/MS reduces the need for several experiments, the analysis of co-eluting species is severely hampered, as evidenced by the MS/MS of species LC peaks **9** and **10** not carried out by the data-dependent analysis due to the more abundant co-eluting species LC peak **8**. The data-dependent LC-EID analysis of cediranib generated a comparable product ion spectrum to the targeted LC-EID analysis (data not shown) due to the high abundance of cediranib $[M+H]^+$, however the data-dependent analyses of the low abundance compounds suffered slightly due to the non-selectivity resulting in the loss of some low abundance product ions, as shown in the LC-EID of LC peak **6** in **Figure 4.25.**

Optimisation of the data-dependent MS/MS parameters could significantly improve the analysis, such as creating an inclusion or exclusion list to focus the analysis on the compounds of interest. Additionally, limiting the number of MS/MS scans carried out for each compound would prevent high abundance ions from suppressing the analysis of lower abundance compounds. Due to the success of targeted LC-EID, further study focused on validating the current approach, and therefore the development and optimisation of data-dependent LC-EID was not carried out.

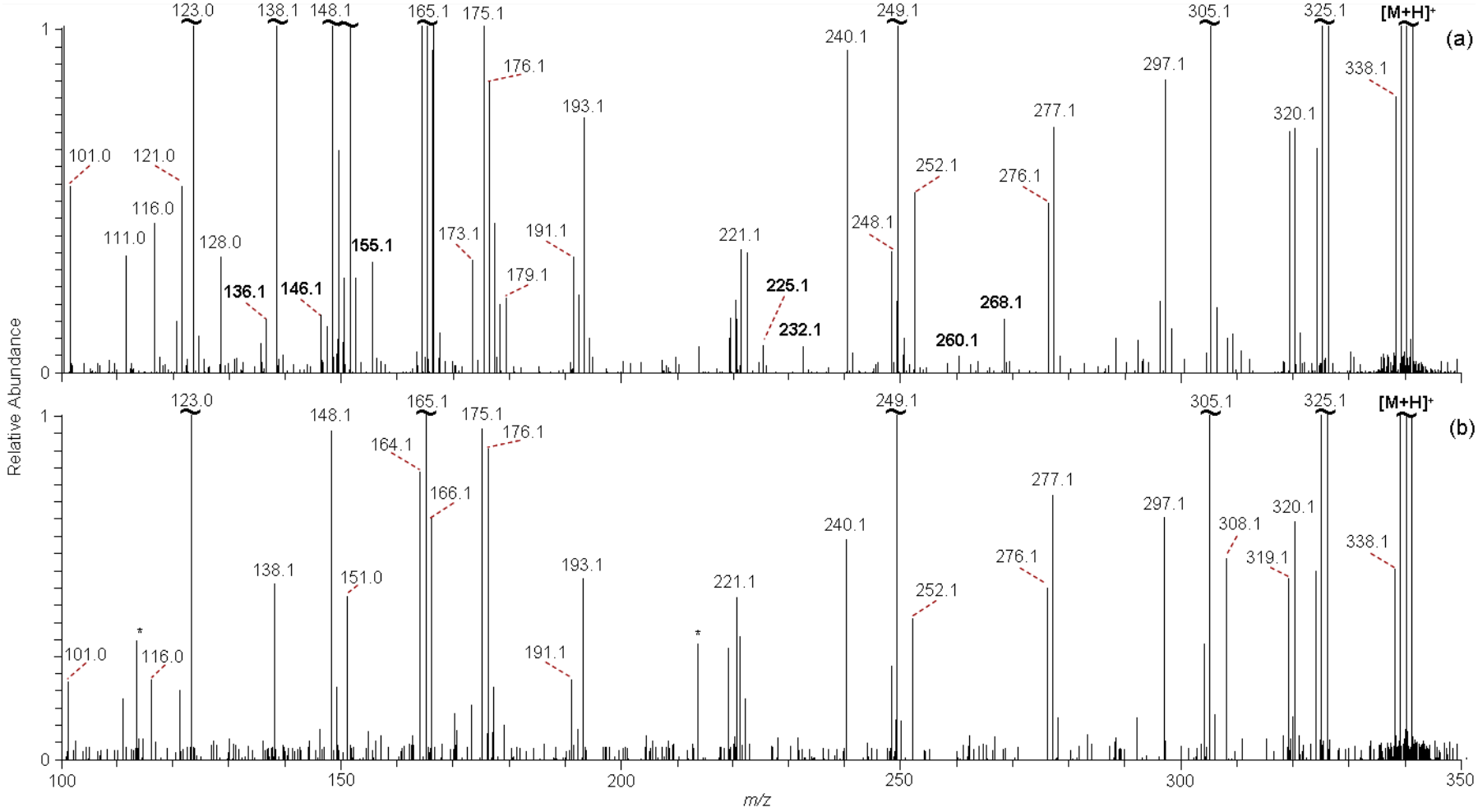

Figure 4.25: (a) Targeted LC-EID compared with (b) data-dependent LC-EID of LC peak 6. Product ions not observed in by data-dependent analysis have been highlighted in bold in (a). Peaks labelled * denote electronic or chemical noise.

4.2.7. Development and validation of LC-EID

Due to the success of LC-EID for analysing the cediranib sample, studies have been carried out to validate the technique using Haloperidol, a pharmaceutical compound with no detectable impurities, which was studied in-depth *via* direct infusion EID in **Chapter 3**. MS/MS has a longer duty-cycle than MS analysis due to the additional steps involved in activating and fragmenting precursor ions. A delay of 0.03 ms and an electron irradiation time of 70 ms contribute towards an increase in scan time when performing EID, as shown in **Figure 4.26**. For the purpose of these experiments, the maximum injection time and the AGC target settings were fixed for all sample concentrations, as detailed in **Chapter 8: Materials and Methods**.

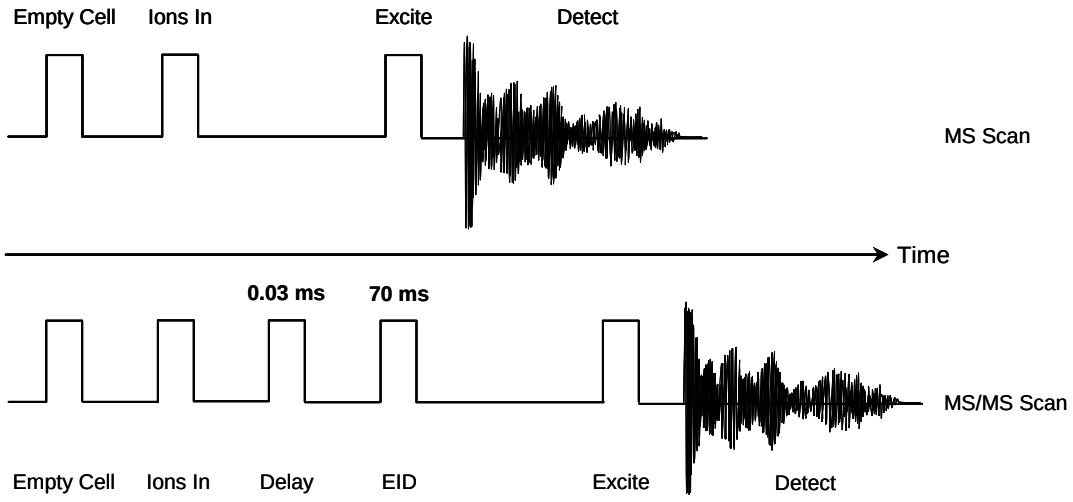

Figure 4.26: Comparison between MS and EID MS/MS scan times.

The number of MS/MS scans achievable is limited to the LC peak width, therefore further work has been carried out in order to reduce the time taken for each EID scan whilst maintaining a high quality and informative product ion spectrum so as to make EID compatible with an LC duty-cycle. The excitation and detection steps make up the majority of scan time, therefore minimising the detection time would have a significant effect on the overall scan time. Acquiring MS/MS data at resolving power 50,000 FWHM, instead of 100,000 FWHM, will halve the detection

time and significantly reduce the overall scan time whilst preserving sufficiently high mass resolution from the FT-ICR. LC-MS/MS analyses are carried out by alternating MS and MS/MS scans, therefore acquiring MS data at 25,000 FWHM would subsequently increase the number of MS/MS scans attainable over a fixed LC peak width. Reduction of the maximum ion accumulation time would have little effect on the resulting MS/MS scan time, unless sample concentration is reduced considerably. The direct infusion LOD experiments, carried out in **Chapter 3**, show that the maximum ion accumulation time was not required at sample concentrations greater than 10 ng mL^{-1}. In order to demonstrate the effect of altering the resolving power, targeted LC-MS/MS analyses were carried out on a sample of Haloperidol. The spectrum shown in **Figure 4.27(a)** was acquired at a resolving power of 100,000 FWHM for alternating MS and MS/MS scans. By comparison, **Figure 4.27(b)** was acquired at 25,000 FWHM for MS and MS/MS scans. The lower resolving power has no discernible effect on the number of product ions generated by LC-EID, however the signal-to-noise is significantly improved owing to more the double the number of MS/MS scans acquired compared to **Figure 4.27(a)**.

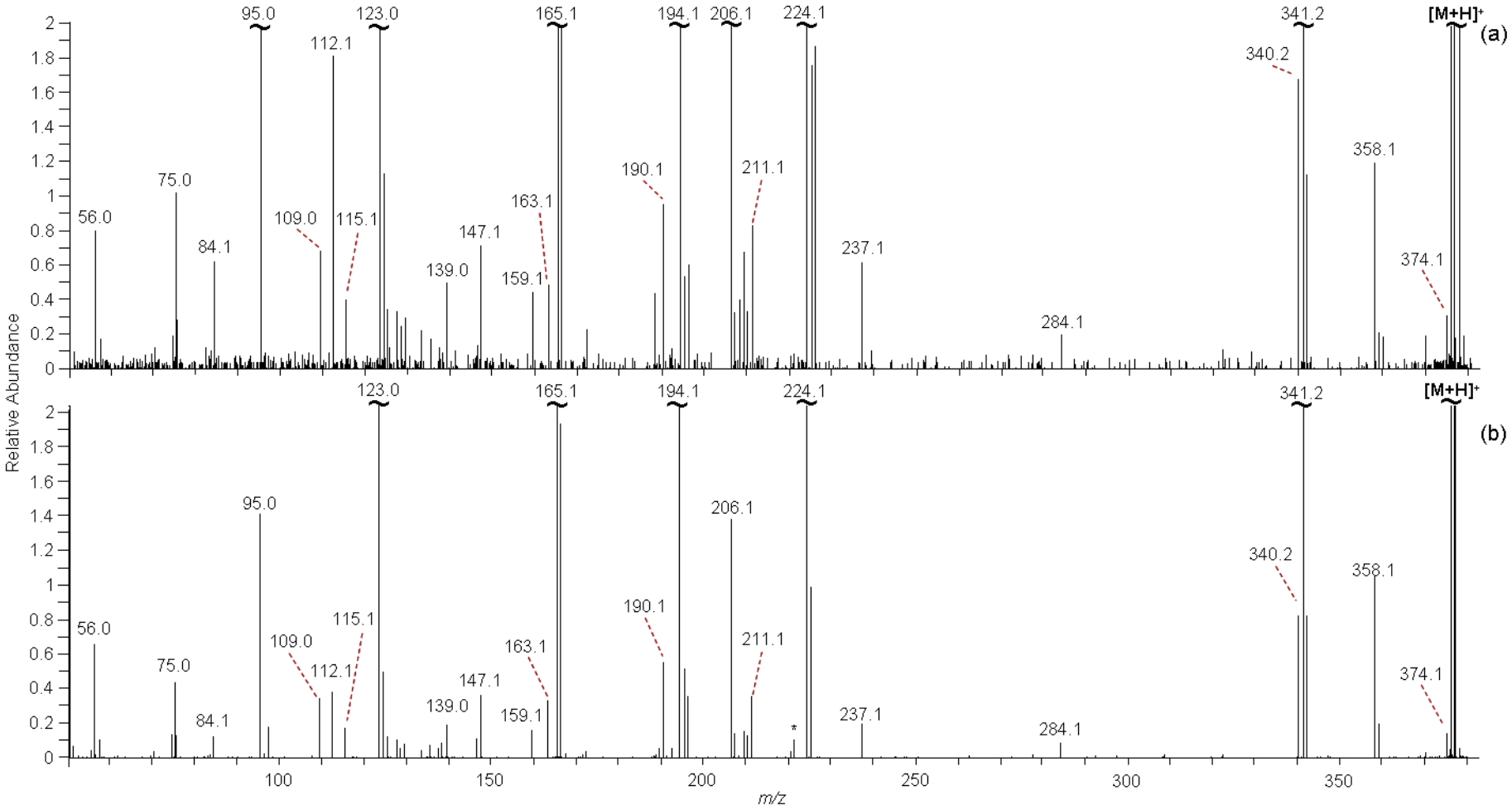

Figure 4.27: LC-EID of Haloperidol carried out at (a) 100,000 FWHM and (b) 25,000 FWHM. Peaks labelled * denote electronic or chemical noise.

Limit of Detection for LC-EID

In order for LC-EID to be a practical analytical technique in the pharmaceutical industry, it must not only be able to analyse complex mixtures, it must be also able to analyse compounds at low concentrations, so as to successfully analyse trace level impurities and degradation products. The work carried out using cediranib has confirmed the feasibility of using LC-EID to analyse and identify trace compounds in genuine pharmaceutical samples, however the concentrations of the low abundance analogues remain unknown. Typical identification thresholds for impurities in drug samples are reported to be < 1% of the target compound, therefore viable analytical techniques must be capable of analysing sample concentration over at least one order of magnitude.[6-7]

In order to test the sensitivity of LC-EID, analyses have been carried out to determine the lower limit of detection, the LC-MS/MS analysis of Haloperidol was carried out over a range of concentrations. Direct infusion LOD studies carried out in **Chapter 3**, performed on sample concentrations between 50 pg mL^{-1} and 5 µg mL^{-1}. Whereas sample concentrations remain constant throughout each direct infusion experiment, LC peaks create a varied concentration range as the sample elutes, therefore it is expected that LC-MS/MS requires higher sample concentrations. The LCMS sensitivity of the LTQ-FT is stated to be in the femtomole range which, when injecting a 10 µL injection of Haloperidol, equates to a sample concentration of approximately 40 pg mL^{-1}. As a result, samples were made up to concentrations ranging from 10 pg mL^{-1} to 1 mg mL^{-1}, and analysed in an increasing order of concentration by LC-EID, LC-CID-FT and LC-CID-IT.

Experiments were carried out in triplicate and the average numbers of product ions for each sample have been charted in **Figure 4.28**. LC-CID-IT analysis generated product ions from the lowest concentration sample, gradually increasing until 0.5 µg

mL^{-1} where the number of product ions plateaus. Due to the loss of low energy ions during transmission between the ion trap and the FT, fewer product ions are observed at each concentration and the lower LOD is increased to 5 ng mL^{-1}, while the maximum number of product ions is observed at 1 µg mL^{-1} for CID-FT. At a concentration of 50 ng mL^{-1} product ions start to appear by EID, gradually increasing in number until 50 µg mL^{-1}, indicating that EID is less sensitive than CID.

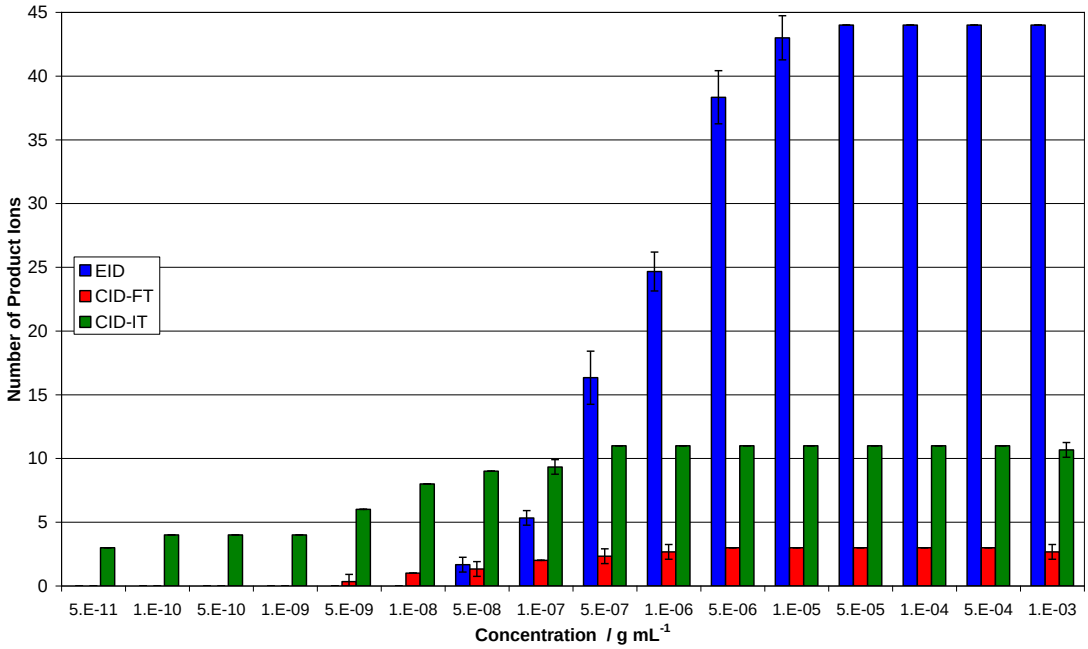

Figure 4.28: Graph indicating the number of product ions generated at each sample concentration from the LC-MS/MS of Haloperidol.

The data generated by LC-MS/MS follows a similar trend to the results from direct infusion, shown in **Figure 3.9**, with CID-IT proving to be the most sensitive technique whereas EID generates the most product ions. As expected, the emergence of product ions from EID and CID-FT occurs at higher sample concentrations for LC-MS/MS than direct infusion data, shown in **Chapter 3**, due to the reduced sample volumes and variable precursor ion abundance across the chromatographic peak. LC-EID is less sensitive than LC-CID, however the number of LC-EID product ions generated surpasses LC-CID at concentrations higher than

0.5 µg mL^{-1}. EID has been shown to generate extensive structural information, complementary to CID, and the development of LC-EID has demonstrated the potential for analysing complex mixtures with components over a wide dynamic concentration range. Variation of parameters, such as the LC column dimensions and packing, gradient conditions, precursor ion and instrument, would be expected to have an effect on the sensitivity of the technique, therefore the detection limits detailed above are specific to the LC-MS/MS of Haloperidol using the specified instrumental parameters, however they give an understanding of the scope of LC-EID.

4.3. Conclusion

Direct infusion EID has already shown great promise in the analysis of a wide range of compounds, demonstrated in **Chapter 3** with the in-depth EID analysis of a range of pharmaceutical molecules. The results discussed herein further confirm the suitability of EID for the analysis of small singly charged cations, and prove that EID can be effectively coupled to chromatography to provide the same in-depth structural information on an LC time-scale to analyse complex mixtures of pharmaceutical compounds with varying precursor ion abundances. Studies carried out to determine the sensitivity of LC-EID using Haloperidol indicate a lower limit of detection in the region of 50 ng mL^{-1}. LC-EID has been able to generate vital information about the low abundance compounds, which would previously require time consuming preparative separation and independent analysis, giving rise to proposed structures or structural fragments. In the case of cediranib, the ten unknown compounds that were present in the reaction mixture are believed to be structurally analogous to the target compound due to the relatively high percentage (≥ 18%) of commonalities between each species and cediranib. The combination of LC-EID and LC-CID data has lead to speculation about the elemental composition of

2 low abundance compounds and confirmed structural similarities to cediranib. LC-EID has been proven to generate useful structural information for the low abundance precursor ions, and is therefore expected to provide fast and efficient information during synthesis when sample quantities may be limited, reducing the need for time-consuming and expensive large-scale experiments prior to preparative chromatography and NMR. The effect of EID was seen to vary depending on the compound, appearing to be more successful for analysing the lower *m/z* (<*m/z* 700) compounds, whereas the analysis of the 3 compounds greater than *m/z* 700 generated fewer than 10 product ions. Only one protonated compound analysed by direct infusion EID in **Chapter 3** had a molecular weight greater than *m/z* 700, Ritonavir, which generated 16 product ions by EID, therefore further work is required to determine whether the precursor ion molecular weight is a key factor in the success of EID MS/MS. The data generated from LC-EID supports the previously discussed dissociation mechanisms, including electronic excitation, vibrational excitation and secondary ionisation followed by electron capture and/or bond dissociation. LC-EID of the $[M+Na]^+$ species reaffirmed the results from the previous study[5] which stated that changing the charge-carrying species has an effect on the product ions generated by EID, creating an additional source of information.

4.4. References

1. Niessen, W.M.A.: Fragmentation of Toxicologically Relevant Drugs in Positive-Ion Liquid Chromatography-Tandem Mass Spectrometry *Mass Spectrom. Rev.* **2011,** *30*, 626-663

2. Williams, K.J., Telfer, B.A., Shannon, A.M., Babur, M., Stratford, I.J., Wedge, S.R.: Inhibition of Vascular Endothelial Growth Factor Signalling using Cediranib (RECENTIN; AZD2171) Enhances Radiation Response and Causes Substantial Physiological Changes in Lung Tumour Xenografts *Br. J. Radiol.* **2008,** *81 Spec No 1*, S21-7

3. Curwen, J.O., Musgrove, H.L., Kendrew, J., Richmond, G.H.P., Ogilvie, D.J., Wedge, S.R.: Inhibition of Vascular Endothelial Growth Factor-A Signaling Induces Hypertension: Examining the Effect of Cediranib (Recentin; AZD2171) Treatment on

Blood Pressure in Rat and the Use of Concomitant Anti Hypertensive Therapy *Clin. Cancer Res.* **2008,** *14*, 3124-3131

4. Nikolinakos, P., Heymach, J.V.: The Tyrosine Kinase Inhibitor Cediranib for Non-Small Cell Lung Cancer and Other Thoracic Malignancies *J. Thorac. Oncol.* **2008,** *3*, S131-S134

5. Mosely, J.A., Smith, M.J.P., Prakash, A.S., Sims, M., Bristow, A.W.T.: Electron-Induced Dissociation of Singly Charged Organic Cations as a Tool for Structural Characterization of Pharmaceutical Type Molecules *Anal. Chem.* **2011,** *83*, 4068-4075

6. Ermer, J., Vogel, M.: Applications of Hyphenated LC-MS Techniques in Pharmaceutical Analysis *Biomed. Chromatogr.* **2000,** *14*, 373-383

7. Kerns, E.H.: Utility of Mass Spectrometry for Pharmaceutical Profiling Applications *Curr. Drug Metab.* **2006,** *7*, 457-466

5. MS and MS/MS Analysis of Proteins Modified by Small Organic Molecules

5.1. Introduction

Proteins have a deep-rooted involvement in key biological processes in living organisms, therefore any modifications or mutations of a protein can have a dramatic effect on the physical, chemical or biological properties of the protein. Such alterations to proteins include biochemical post-translational modifications (PTM), such as phosphorylation[1] or glycosylation[1], and chemical protein modifications such as oxidation, carboxylation, small molecule interactions[2-3] or the interaction with other biological molecules such as lipids.[4-6] Protein modifications are vitally important in controlling or regulating the function and/or structure of the protein, the knowledge of which could further the understanding into the effect of diseases on living cells or the effect of seemingly minor mutations on complex multi-component interactions.[7-9] The identification of protein modifications may also shed light on biologically active sites and exposed regions of the protein structure, the manipulation or mutation of which can have a drastic effect on the ability of the protein to function normally. The interactions between proteins and small pharmaceutical molecules can cause inhibition or enhancement of the protein function, and is therefore a key area of study in the pharmaceutical industry in relation to the treatment of diseases and the effect of drug molecules on naturally occurring or disease-affected proteins. To this end, investigations have been carried out on two proteins, the multiple transferrable resistance regulator protein of *Neisseria gonorrhoeae* and the matrix protein of the human respiratory syncytial virus. Both proteins have been analysed by LC-MS as intact proteins and digested peptides of the unmodified sample and after modification with small molecules.

Intact protein MS, with sufficient resolving power and mass accuracy, can be used to detect any changes in protein molecular weight from the unmodified protein to the modified protein, providing clues as to the nature of any modifications. Enzymatic digestion of the protein sample, the bottom-up approach, cleaves the protein into smaller peptides that can be used to confirm portions of the protein sequence and minimises the effect of protein size on the MS analysis, allowing the possibility for in-depth analysis of proteins of virtually unlimited size.[10] LC-MS provides the high sensitivity needed for the analysis of complex mixtures at varying concentrations, enabling the identification of modified peptides that are often observed at much lower concentrations than their corresponding unmodified peptide. MS/MS analysis of the digested peptides can confirm the amino acid composition of the peptides and narrow down the location of a suspected PTM.[11]

5.1.1. The multiple transferrable resistance regulator (MtrR) protein

The presence of β-lactamase enzymes has been shown to confer antibiotic resistance in bacterial and viral infections due to the enzymatic hydrolysis and subsequently inactivation of β-lactam antibiotics, such as penicillin or cephalosporin. In order to improve the effect of antibiotic treatment, β-lactamase inhibitors have been used to irreversibly inhibit the enzymatic activity of the β-lactamases and allow the antibiotics to combat the underlying infection. The β-lactamase inhibitors tazobactam and clavulanic acid, **Figure 5.1**, are frequently used inhibitors for the treatment of infections containing β-lactamases in conjunction with β-lactam antibiotics. Investigations into the inhibition of the SHV-1 β-lactamase found in *Escherichia coli* and *Klebsiella pneumoniae* and the S130G SHV-1 variant have yielded significant information regarding the interactions between the proteins and inhibitors. MS analysis of intact and enzymatic digests of the modified proteins, in comparison with the unmodified protein, showed a mass increase of less than the

molecular weight of the starting inhibitor molecules, suggesting that the inhibitor is altered upon reaction with the protein.[2-3, 12]

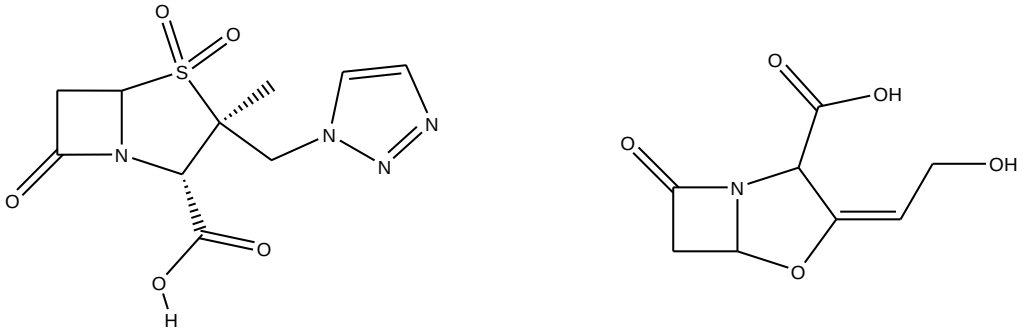

Figure 5.1: Structures of (left) tazobactam, molecular formula $C_{10}H_{12}N_4O_5S$ and (right) clavulanic acid, molecular formula $C_8H_9NO_5$.

The suggested mechanisms for the reaction between the protein residues and tazobactam or clavulanic acid have been detailed in **Figure 5.2** and **Figure 5.3** respectively. The interaction between the protein and inhibitor molecules is purported to take place at the hydroxyl groups of the serine or threonine residues, resulting in the opening of the β-lactam ring of the inhibitor.[2-3] The protein-inhibitor reaction was found to differ between the SHV-1 and the S130G SHV-1 β-lactamases. The SHV-1 enzyme was found to preferentially form the aldehyde hydrate modification of $C_3H_4O_3$, resulting in the mass increase of 88.0 Da, whereas the aldehyde moiety of $C_3H_2O_2$, a modification of 70.0 Da, was determined to be the predominant modification for the S130G SHV-1 variant.

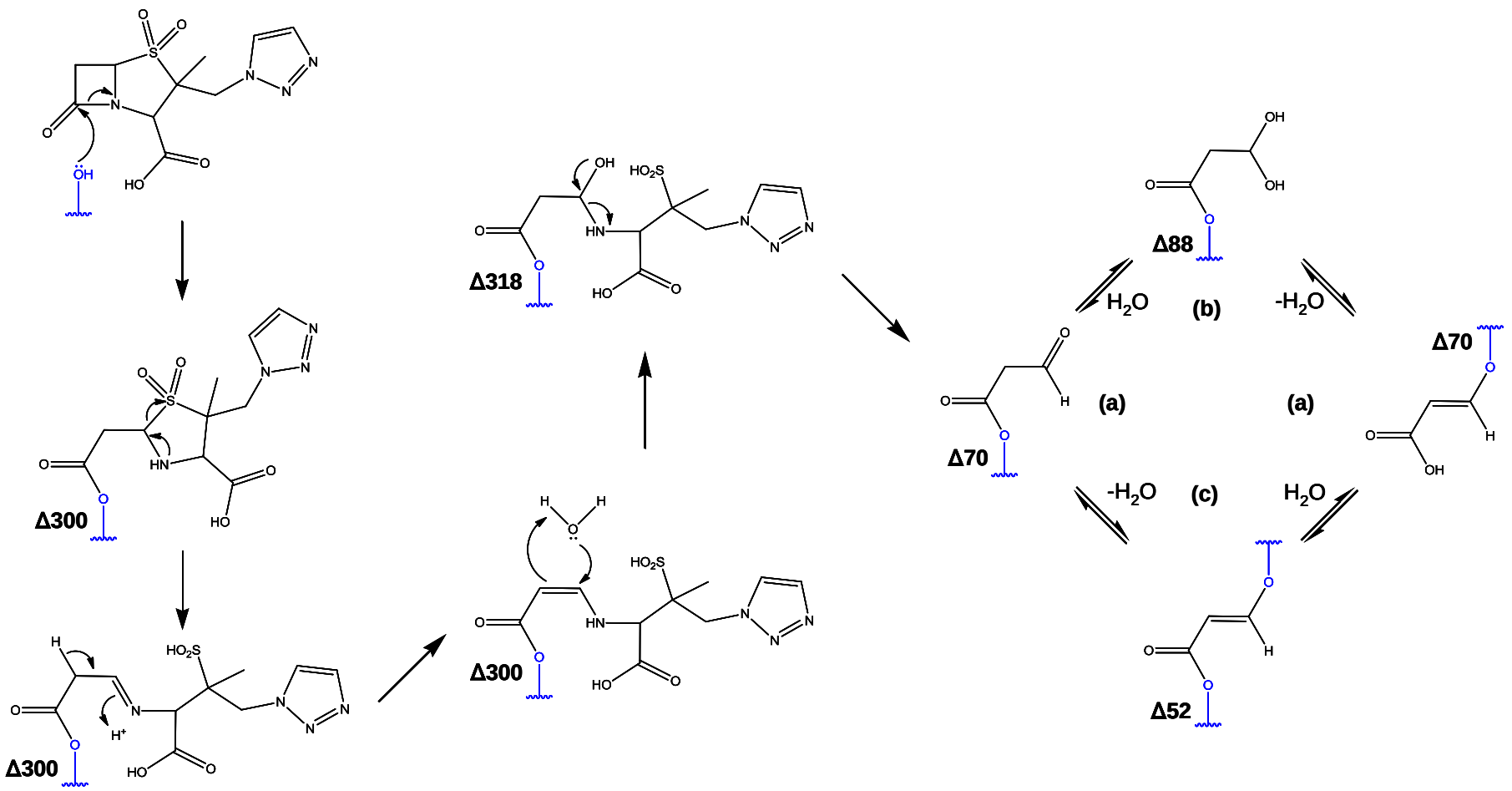

Figure 5.2: Proposed mechanism for the reaction between tazobactam and serine/threonine residues. Atoms labelled in blue belong to the protein.[3]

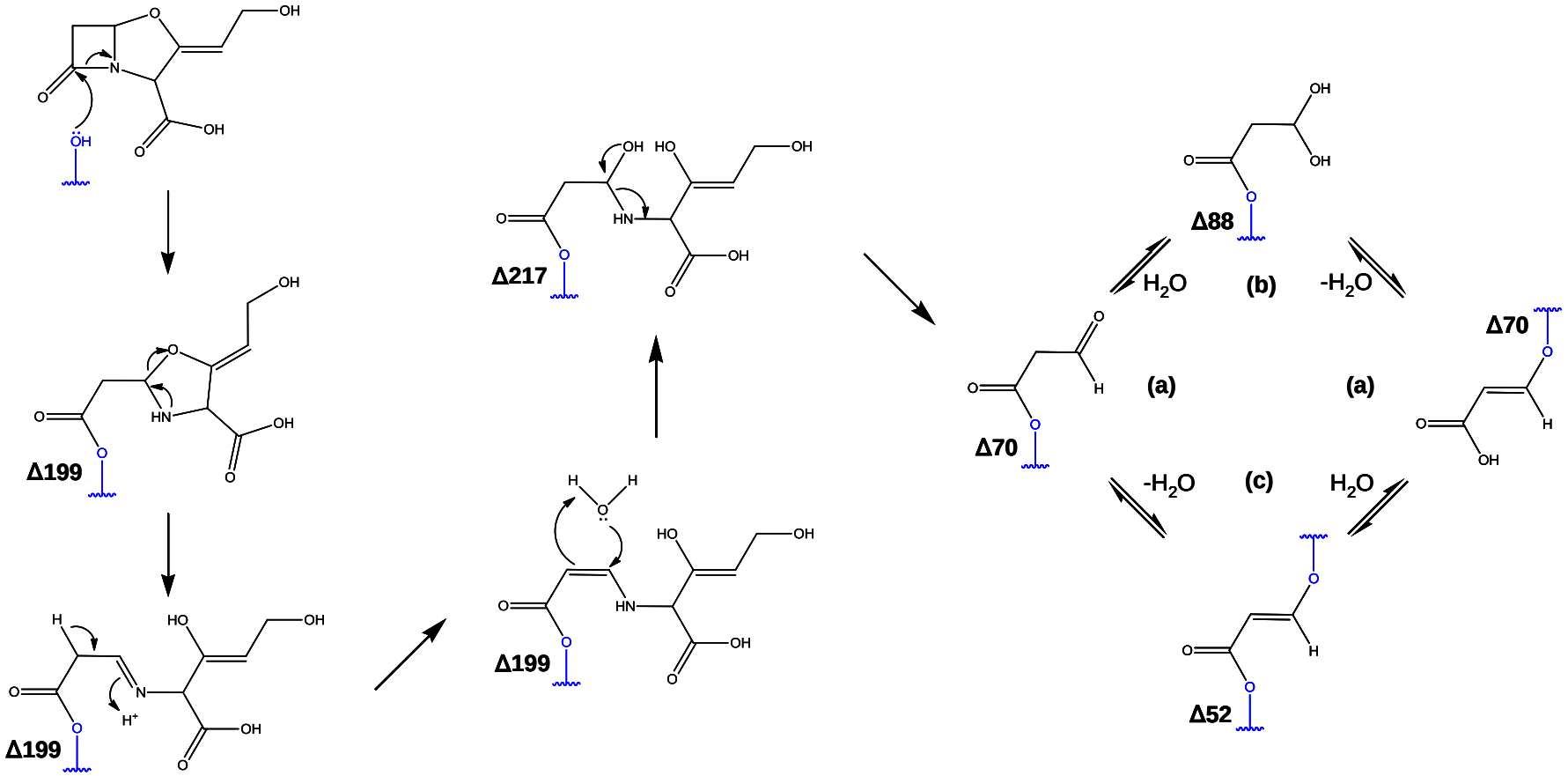

Figure 5.3: Proposed mechanism for the reaction between clavulanic acid and serine/threonine residues. Atoms labelled in blue belong to the protein.[2]

The MtrR protein of *Neisseria gonorrhoeae* has been shown to have a significant effect on antibiotic resistance due to its function in regulating the membrane bound MtrCDE efflux pump involved in ejecting antibiotics from infected cells.[13] Investigations using isothermal titration calorimetry have uncovered the β-lactamase activity of the MtrR protein, as evidenced by the binding and subsequent hydrolysis of β-lactam antibiotics, an additional source of the antibiotic resistance of the virus. The inhibition of the β-lactamase function of the MtrR protein *via* the interaction with β-lactamase inhibitors has been studied with the hope of de-activating the enzymatic activity and reducing antibiotic resistance. In the following study, the β-lactamase inhibitors tazobactam and clavulanic acid were incubated with the MtrR protein (carried out by Matthew F. Burton) and acquired for MS and MS/MS analysis.[14]

5.2. Results and Discussion

5.2.1. MS Analysis of the intact MtrR protein

The unmodified MtrR protein sequence, shown in **Figure 5.4**, corresponds to a protein with a neutral monoisotopic weight of 25241.8 Da and the most abundant isotope at 25256.9 Da.

1	**6**	**11**	**16**	**21**	**26**	**31**	**36**	**41**
HHHHH	HELMR	KTKTE	ALKTK	EHLML	AALET	FYRKG	IARTS	LNEIA
46	**51**	**56**	**61**	**66**	**71**	**76**	**81**	**86**
QAAGV	TRGAL	YWHFK	NKEDL	FDALF	QRICD	DIENC	IAQDA	ADAEG
91	**96**	**101**	**106**	**111**	**116**	**121**	**126**	**131**
GSWTV	FRHTL	LHFFE	RLQSN	DIHYK	FHNIL	FLKCE	HTEQN	AAVIA
136	**141**	**146**	**151**	**156**	**161**	**166**	**171**	**176**
IARKH	QAIWR	EKITA	VLTEA	VENQD	LADDL	DKETA	VIFIK	STLDG
181	**186**	**191**	**196**	**201**	**206**	**211**	**216**	
LIWRW	FSSGE	SFDLG	KTAPR	IIGIM	MDNLE	NHPCL	RRK	

Figure 5.4: Amino acid sequence for the histidine-tagged MtrR protein with an average molecular weight of 25257.9 Da.

The Total Ion Chromatogram (TIC) in **Figure 5.5** was generated from the LC-MS analysis of the unmodified protein. The major peak maximum, from 17.3 to 20 minutes, allowed 150 MS scans to be averaged to generate the MS spectrum shown in **Figure 5.6**, which confirms the presence of a high molecular weight species that has formed a charge state distribution that can be deconvoluted to determine the molecular weight.

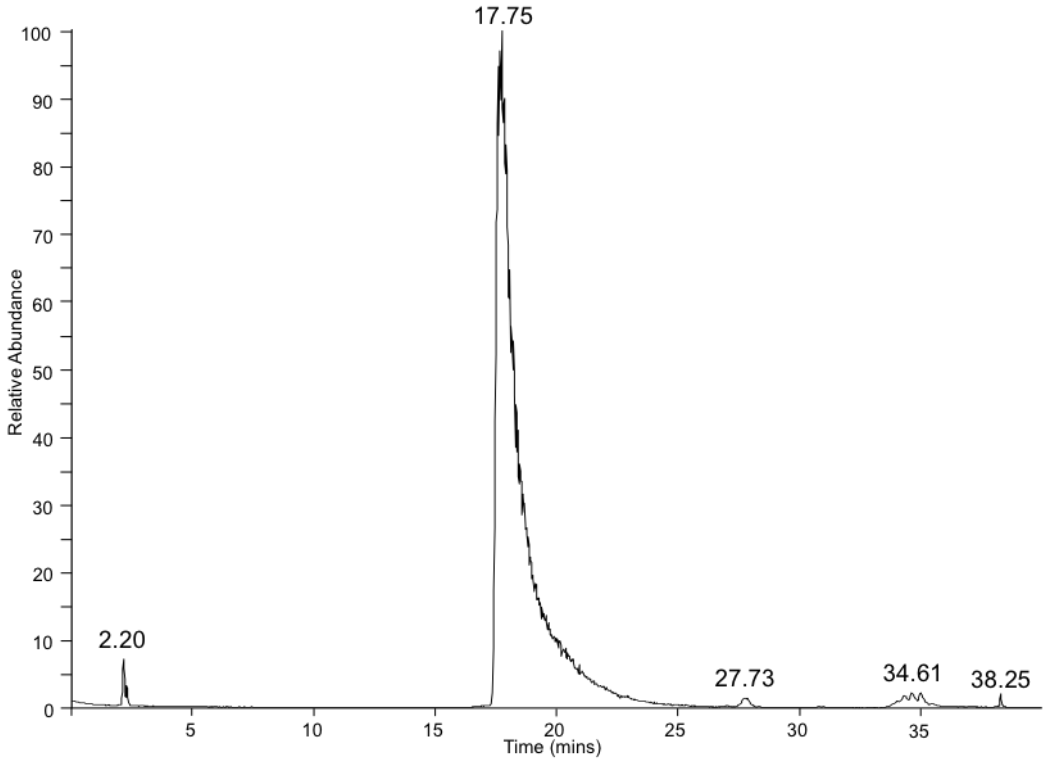

Figure 5.5: Total ion chromatogram generated from the LC-MS analysis of the unmodified MtrR protein.

The mass resolution is sufficient to resolve the isotopic profile of each charge state, as shown in the expansion of the peak at *m/z* 815.7 in **Figure 5.6(inset)** that corresponds to the $[M+31H]^{31+}$ charge state. Deconvolution of the MS spectrum was carried out in order to calculate the singly protonated molecular weight for each multiply charged species, resulting in the spectrum shown in **Figure 5.7**.

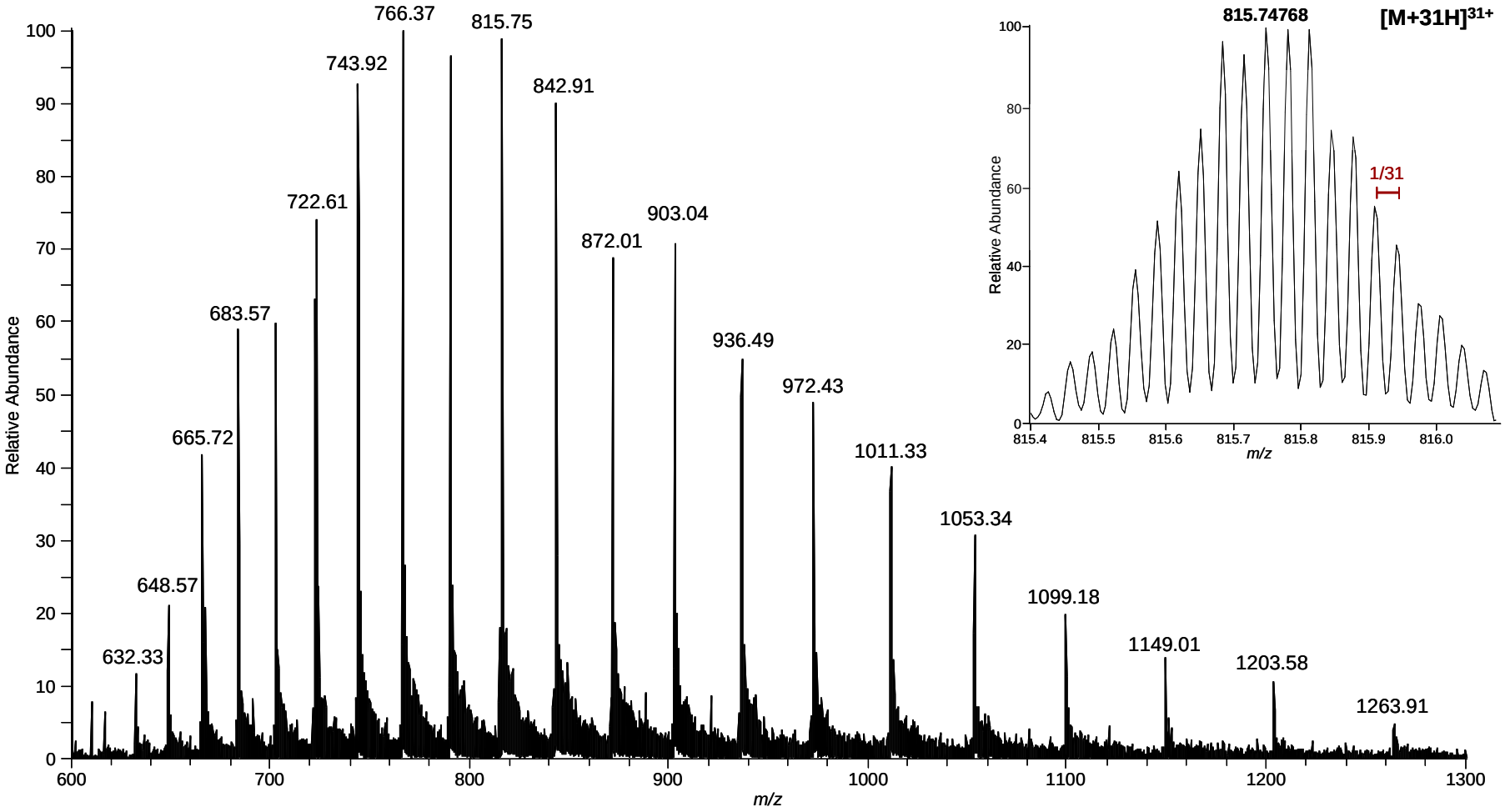

Figure 5.6: MS spectrum generated from the unmodified MtrR protein sample with (inset) expansion over the peak at *m/z* 815.7.

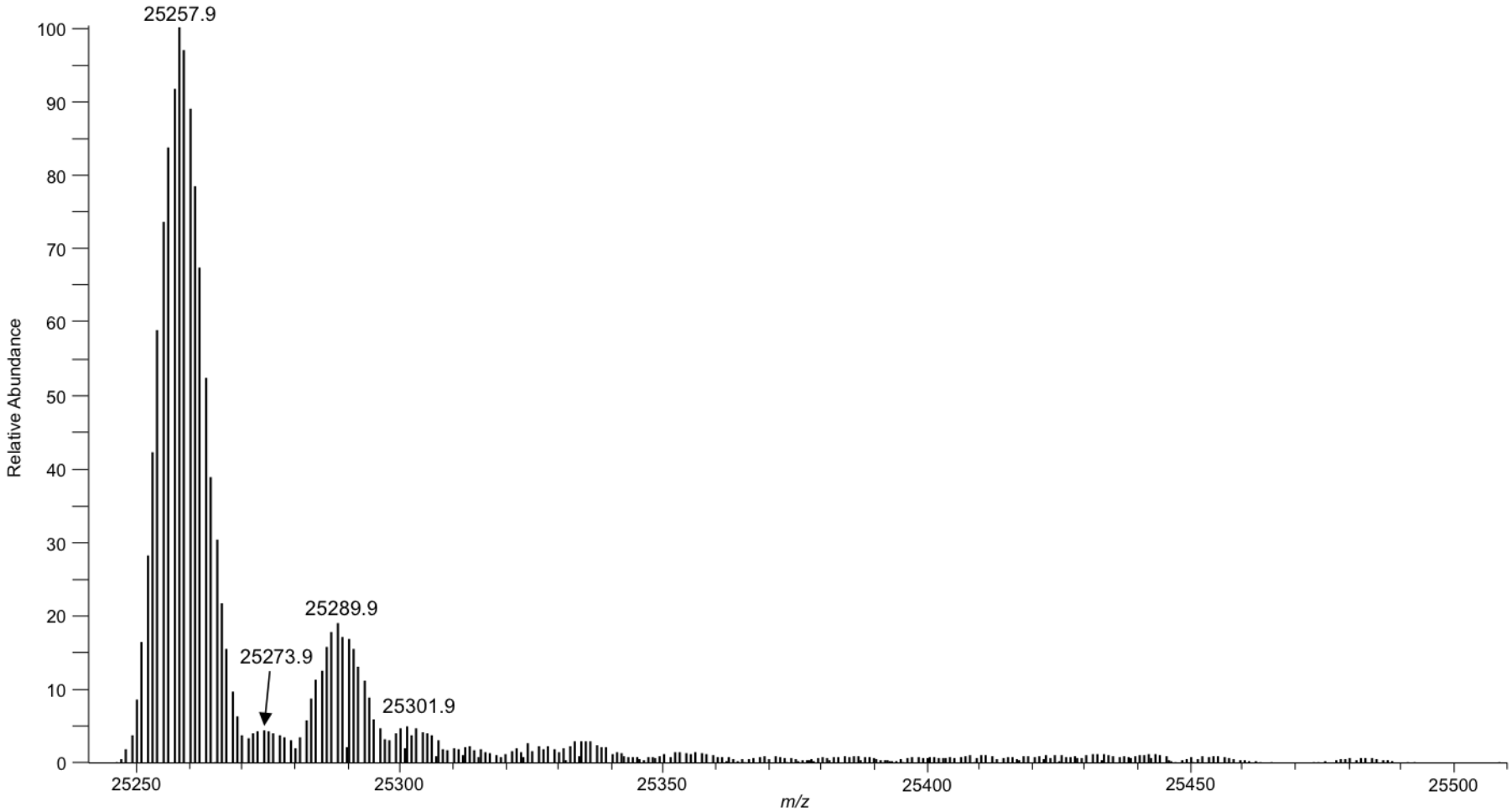

Figure 5.7: MS spectrum of the unmodified MtrR protein, deconvoluted to the $[M+H]^+$ species from the spectrum in Figure 5.6. The species at 25257.9 Da corresponds to the protonated MtrR protein.

The most intense deconvoluted peak at 25257.9 Da is consistent with the protonated form of the unmodified MtrR protein, accurate to within 2 ppm from the most abundant ion of the known amino acid sequence. The deconvoluted peaks observed in the *m/z* region higher than the unmodified protein at 25273.9 Da, 25289.9 Da and 25301.9 Da correspond to modified protein species, consistent with the single oxidation, double oxidation and carboxylation of the MtrR protein respectively. These modifications are proposed to originate from sample preparation.

5.2.2. Incubation of MtrR protein with tazobactam

The MtrR protein was treated with tazobactam to study the interaction between the protein and the inhibitors. The product was analysed by LC-MS, and the resulting MS spectrum was deconvoluted to generate the protonated spectrum shown in **Figure 5.8**. The most intense deconvoluted peak at 25257.9 Da corresponds to the most abundant ion of the protonated MtrR isotopic profile, suggesting that the reaction between the inhibitor and protein did not reach completion or that the reaction forms an equilibrium between the unmodified and modified protein. There is no evidence of the protein having been modified by an intact tazobactam molecule, which would be observed 300.0 Da higher than the unmodified protein at 25558.0 Da. The peak at 25328.0 Da, corresponding to a modification of 70.0 Da to the protein, is consistent with the aldehyde modification of $C_3H_2O_2$ shown in **Figure 5.2(a)**. The expected peak corresponding to the aldehyde hydrate modification (88 Da) shown in **Figure 5.2(b)** is not observed, however the peak at 25342.9 Da is consistent with the addition of $C_3H_3NO_2$ (85 Da) to the MtrR protein. The peak at 25356.0 Da, 98 Da higher than the protein, is believed to correspond to the addition of $C_4H_4NO_2$, whereas the peak at 25401.0 Da is thought to correspond to a modification of $C_5H_5NO_4$, resulting in a species 143.0 Da higher than the unmodified protein. The formation of the three modifications at 85 Da, 98 Da and 143 Da higher

than the unmodified protein are proposed to follow the reaction mechanisms shown in **Figure 5.9.** The reaction of the β-lactamase inhibitors with the hydroxyl group is purported to occur *via* nucleophilic attack at the carboxyl group of the β-lactam ring, as shown in **Figure 5.9**, resulting in ring opening and further reaction. The low abundance peaks that were observed in the unmodified protein sample corresponding to oxidated and carboxylated protein are also observed in the tazobactam treated sample at 25273.9 Da, 25289.9 Da and 25301.9 Da.

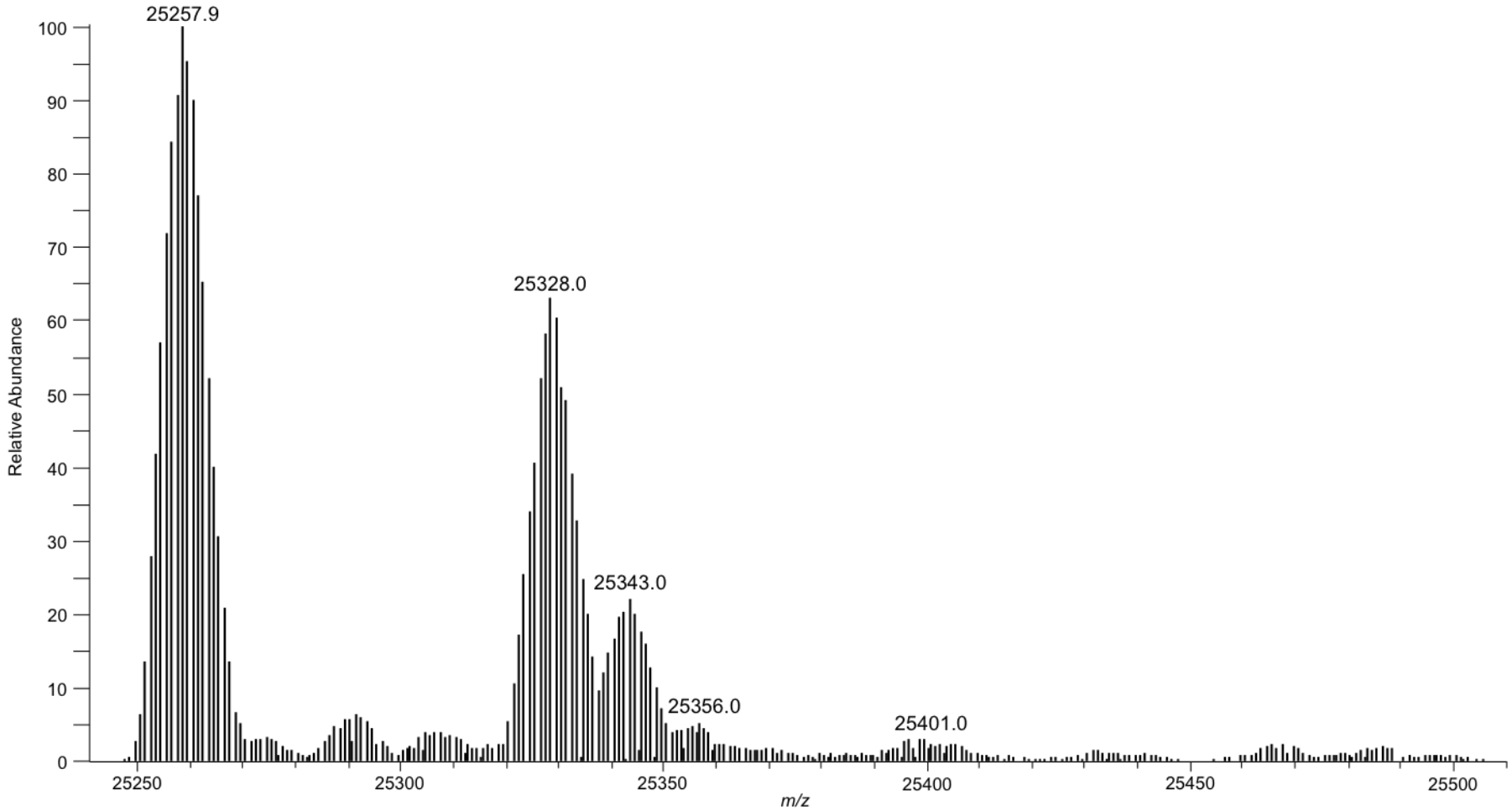

Figure 5.8: MS spectrum, deconvoluted to the [M+H]+ species, of the MtrR protein sample treated with tazobactam. The species at 25257.9 Da corresponds to the protonated MtrR protein. Additional peaks have been discussed further.

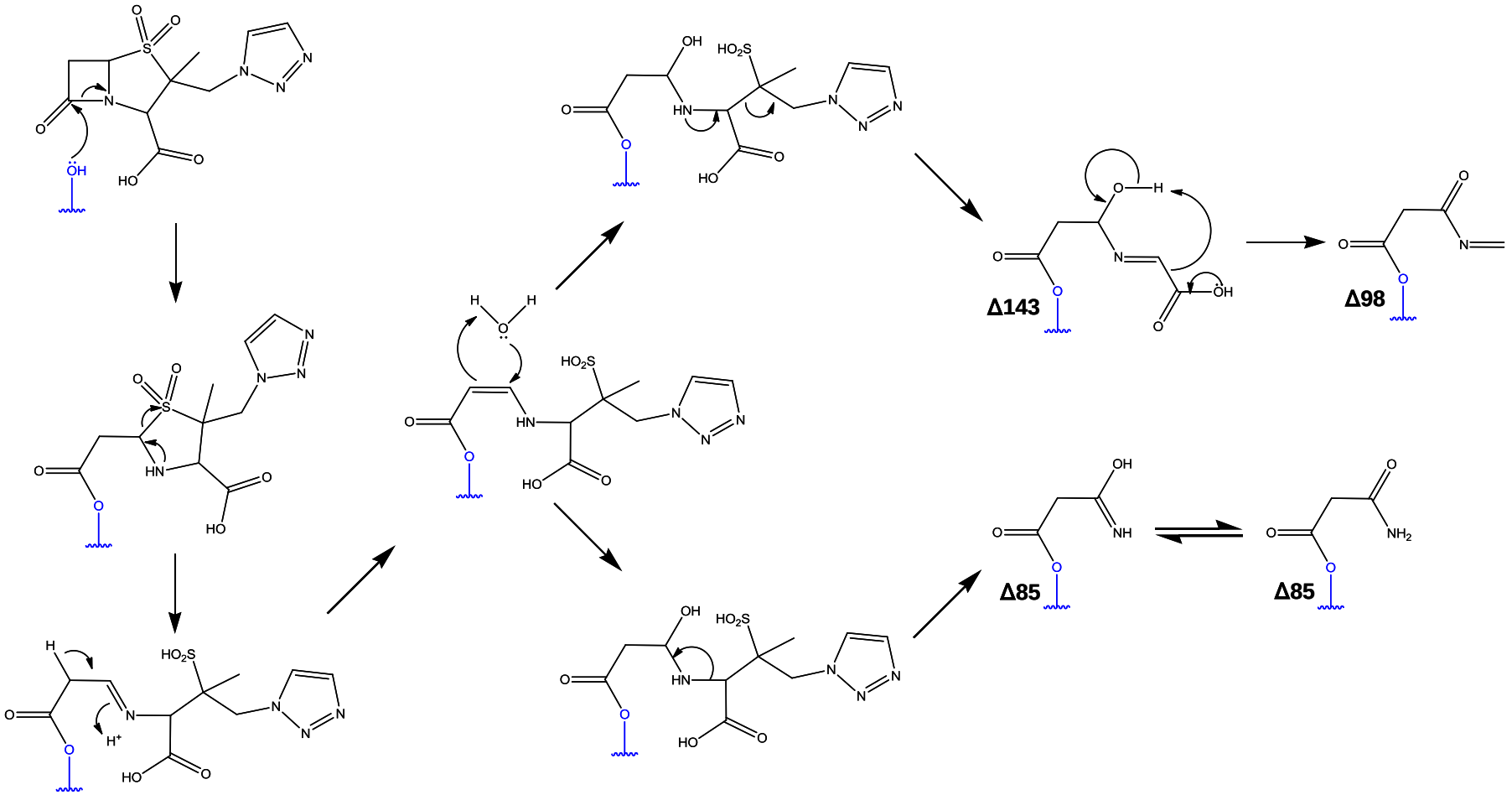

Figure 5.9: Proposed mechanisms for the formation of the tazobactam modifications observed in Figure 5.8.

5.2.3. Incubation of MtrR protein with clavulanic acid

Figure 5.10 shows the MS spectrum of the MtrR protein treated with clavulanic acid and deconvoluted to give the singly protonated ion. The dominant peak in the spectrum corresponds to the unmodified MtrR protein at 25258.0 Da, accurate to within 4 ppm. The low intensity peaks that were observed in the unmodified protein sample in **Figure 5.7** were also observed in the clavulanic acid sample, at 25274.0 Da, 25289.0 Da and 25302.0 Da, corresponding to the oxidated and carboxylated MtrR protein. The deconvoluted peaks at 25328.0 Da, 25343.0 Da and 25401.0 Da that were present in the tazobactam treated sample in **Figure 5.8** are also present in the sample incubated with clavulanic acid, and are proposed to correspond to a modification of $C_3H_2O_2$ (70 Da), $C_3H_3NO_2$ (85 Da) and $C_5H_5NO_4$ (143 Da) respectively, indicating that the clavulanic acid molecule has been altered upon interaction with the protein. The peak at 25455.1 Da is consistent with an addition of 197.0 Da, which is proposed to result from the loss of H_2 following the addition of an intact clavulanic acid molecule. The peaks at 25356.0 Da, 25413.1 Da and 25427.0 Da are also proposed to correspond to modifications resulting from the reaction with the clavulanic acid molecule, consistent with the addition of $C_4H_4NO_2$ (98 Da), $C_6H_6NO_4$ (155 Da) and $C_7H_7NO_4$ (169 Da). The reaction mechanisms shown in **Figure 5.11** have been suggested to explain the observed modifications in **Figure 5.10**. Similarly to the reaction between the MtrR protein and tazobactam, the reaction with clavulanic acid is purported to occur *via* nucleophilic attack at the carboxyl group of the β-lactam ring, as shown in **Figure 5.11**.

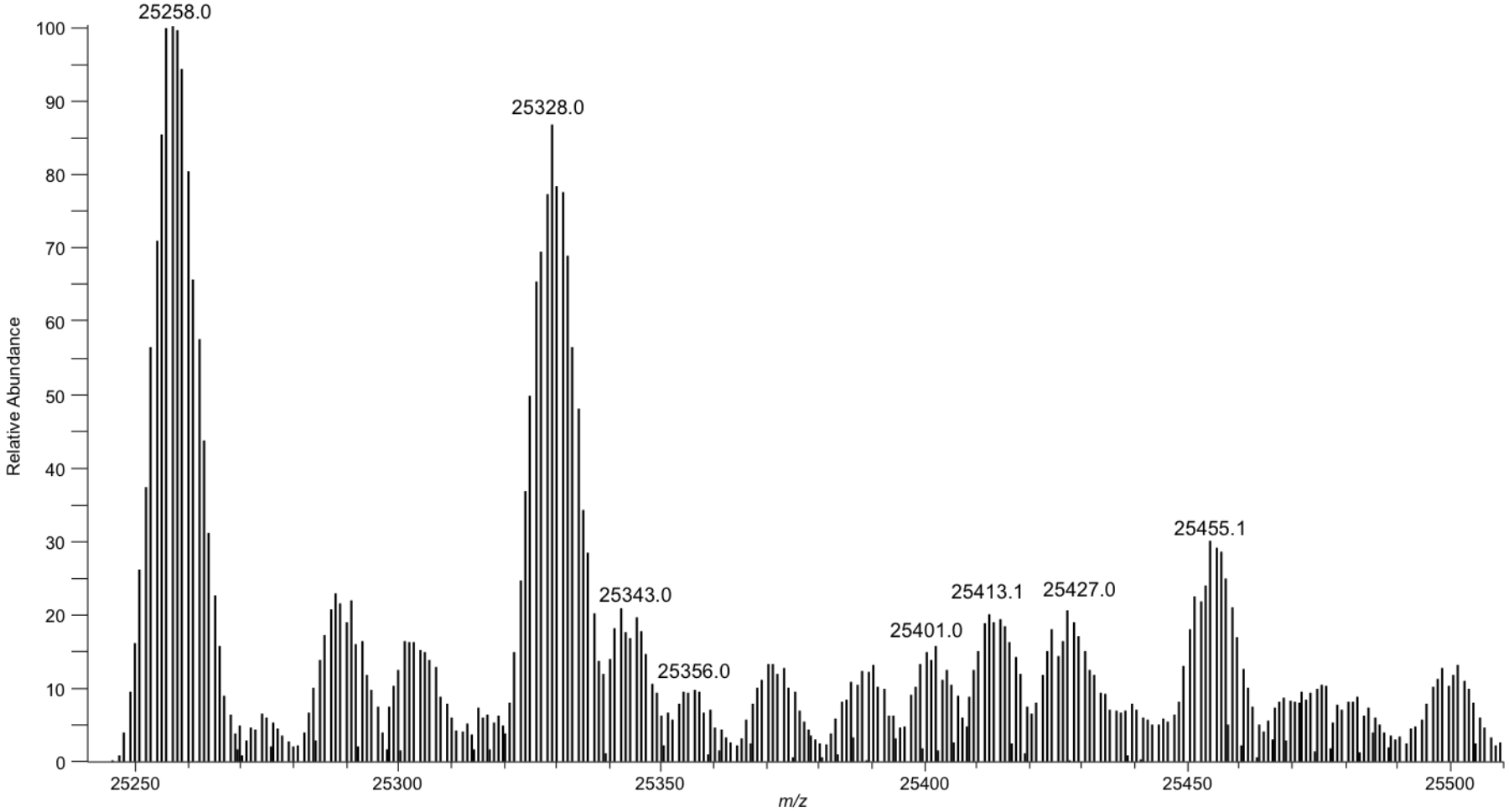

Figure 5.10: MS spectrum of clavulanic acid treated sample, deconvoluted to the $[M+H]^+$. Peaks suspected of corresponding to protein adducts have been labelled according to the mass difference from the unmodified protein at 25258.0 Da.

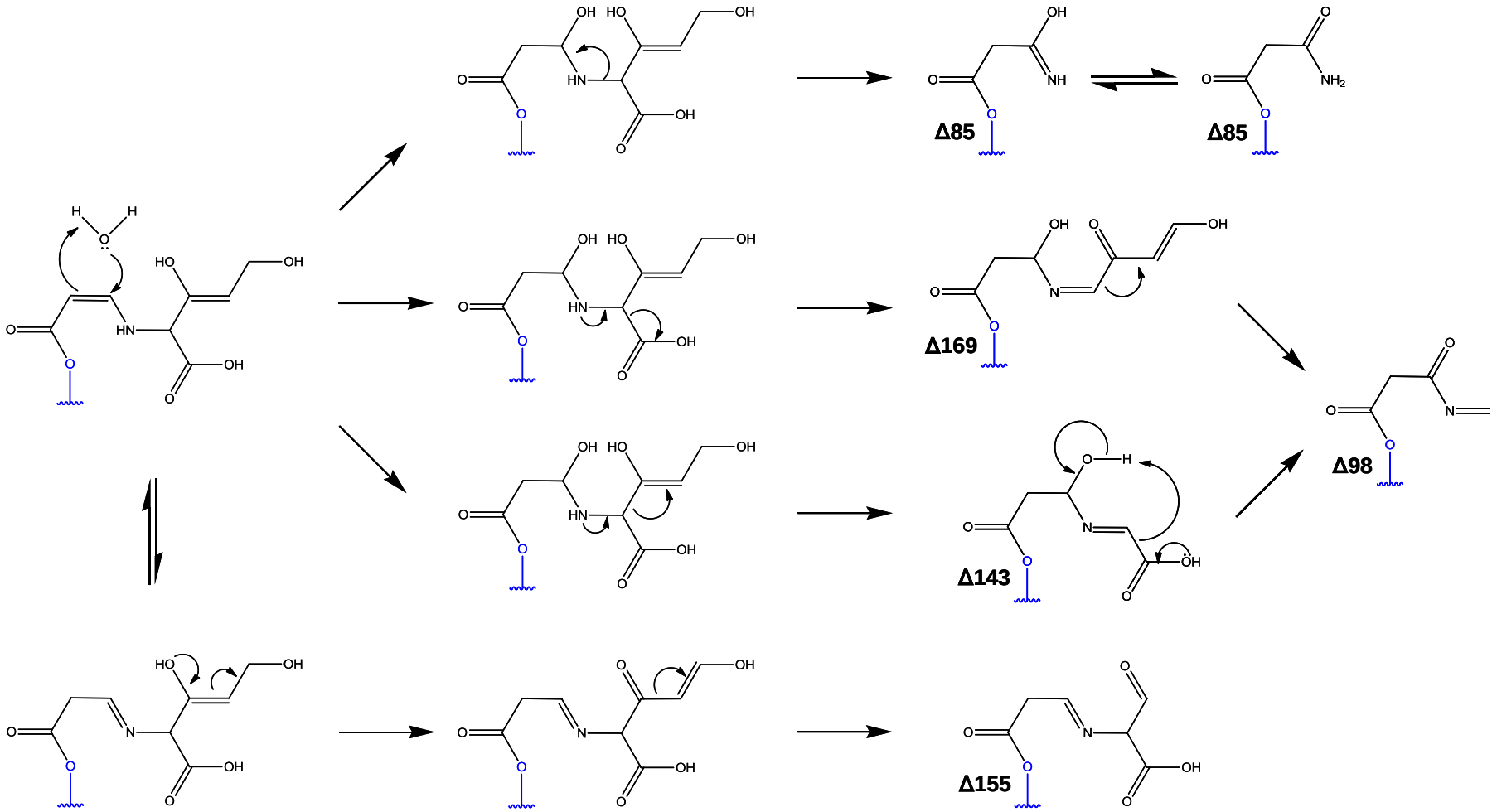

Figure 5.11: Proposed reaction mechanisms of clavulanic acid to generate the observed adducts shown in Figure 5.10.

5.2.4. Tryptic digest of the MtrR protein

The unmodified MtrR protein and the protein samples treated with the β-lactamase inhibitors were digested using trypsin and analysed by LC-MS. The MS spectra, produced by averaging MS scans across each LC chromatogram, were deconvoluted to generate singly protonated ions, as shown in **Figure 5.12**. The enzyme, trypsin, cleaves at the C-terminus of lysine and arginine residues, therefore an *in silico* tryptic digest could be performed on the MtrR amino acid sequence shown in **Figure 5.4**. The *in silico* digest provided a list of all possible tryptic peptides over an unlimited mass range, allowing for up to 10 missed cleavages. A direct comparison between the tryptic digest of the unmodified MtrR protein and the *in silico* digest identified 19 common peptides, accurate to within 3 ppm, that confirmed approximately 70% of the known protein sequence (153 of 218 amino acid residues), as shown in **Figure 5.13**. The data collected from the MS spectrum of the intact unmodified protein sample and the high degree of sequence coverage from the tryptic digest supports the identification of the sample as the expected MtrR protein.

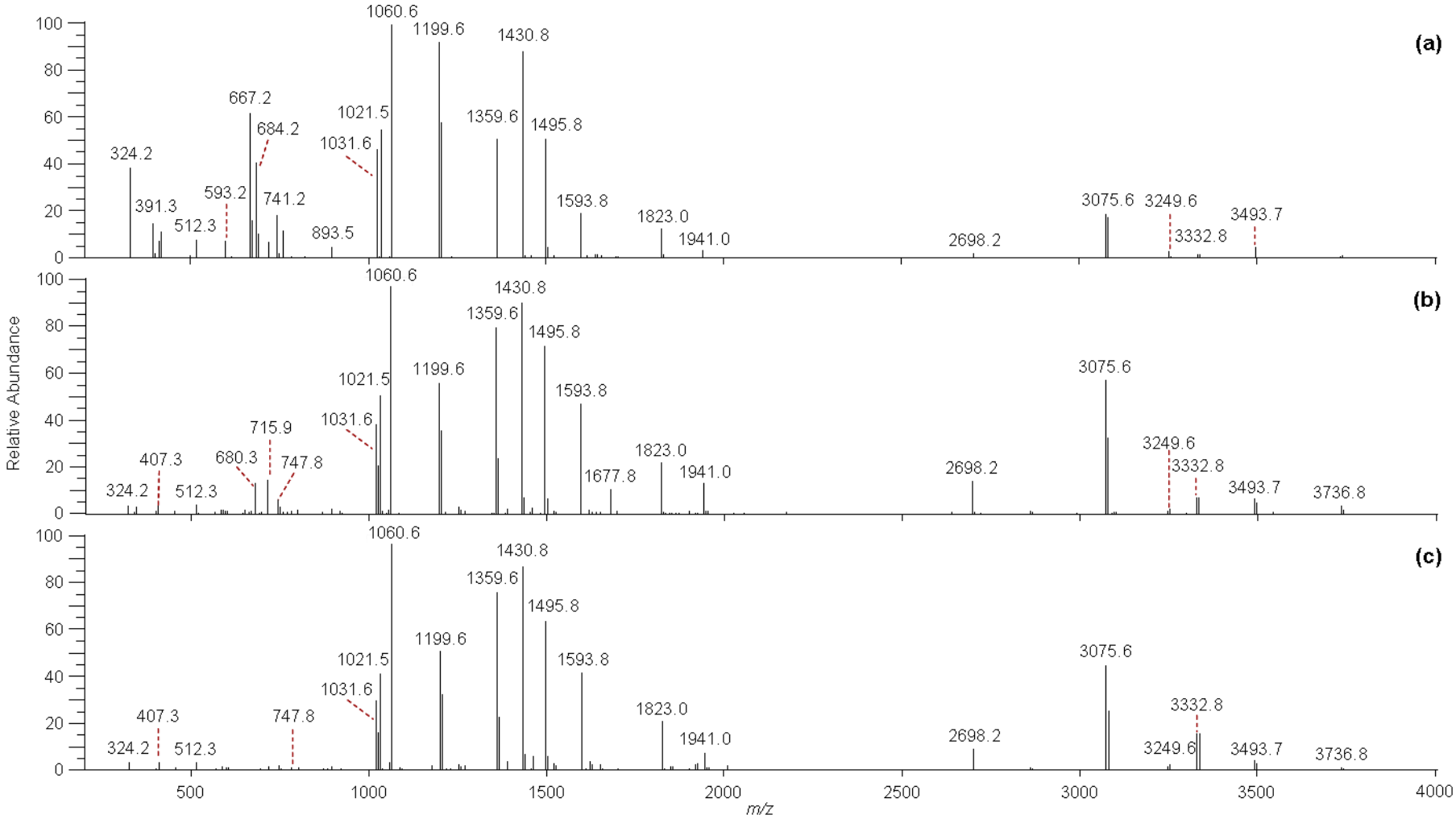

Figure 5.12: Deconvoluted MS spectra for tryptic digests of (a) the unmodified MtrR protein, (b) the tazobactam treated sample and (c) the clavulanic acid treated sample.

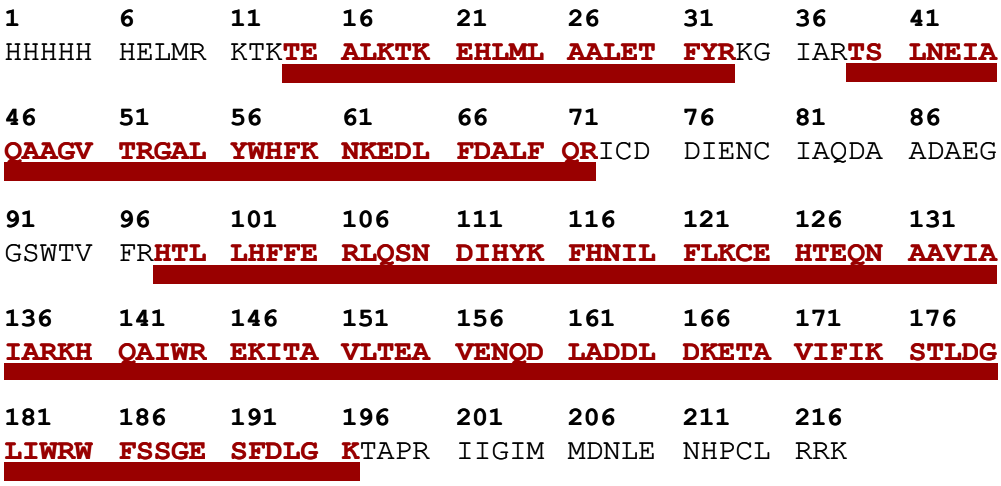

Figure 5.13: MtrR protein sequence highlighting (red) amino acid residues that have been confirmed from the tryptic digest of the unmodified MtrR protein.

The deconvoluted MS spectra generated from the tryptic digests of the modified MtrR protein, see **Figure 5.12**, have been directly compared to the *in silico* digest of the MtrR amino acid sequence. The tazobactam and clavulanic acid treated samples both contained peptides that could be attributed to the MtrR sequence including, but not limited to, the peptides observed in the unmodified protein samples, thereby allowing the percentage sequence coverage to be increased to 93% (203 of 218 residues) as shown in **Figure 5.14**. The parameters of the *in silico* digest were adjusted to include the modifications previously observed in **Figure 5.8** and **Figure 5.10,** corresponding to the empirical formulae of the proposed molecular modifications $C_3H_2O_2$ (70 Da), $C_3H_3NO_2$ (85 Da), $C_4H_4NO_2$ (98 Da), $C_5H_5NO_4$ (143 Da), $C_6H_5NO_4$ (155 Da), $C_7H_7NO_4$ (169 Da) and $C_8H_7NO_5$ (197 Da).

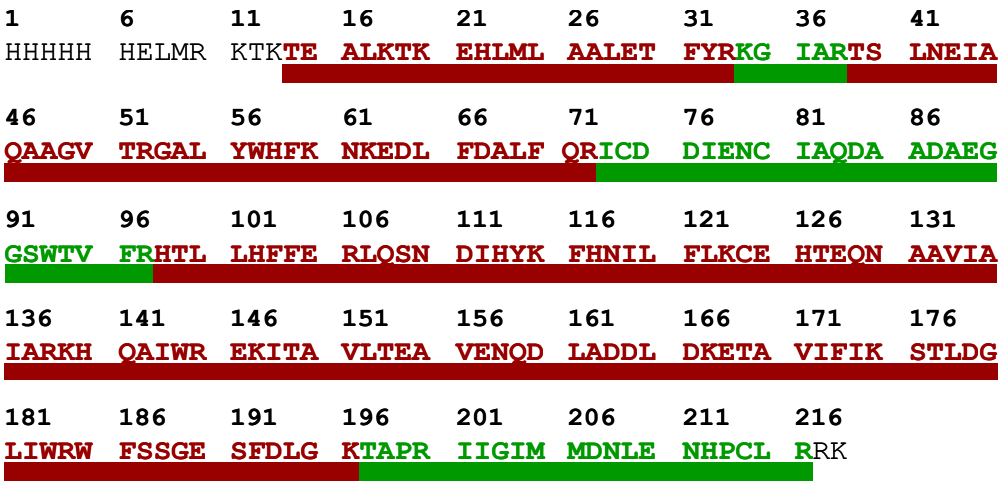

Figure 5.14: MtrR protein sequence highlighting (red) amino acid residues that have been confirmed from the tryptic digest of the unmodified MtrR protein, and (green) the additional residues confirmed from the treated MtrR samples.

There were 4 peptides observed with the proposed modification of $C_3H_2O_2$ (70 Da), all of which were observed in both treated samples. All four peptides were identified as triply charged species, as shown in **Figure 5.15**, which deconvoluted to singly protonated ions at 1269.6 Da, 1663.8 Da, 1695.8 Da and 1893.0 Da. **Figure 5.16** highlights the observed peptides that were modified by $C_3H_2O_2$, with the three proposed modification sites labelled in red. The peak at 1269.6 Da corresponds to the amino acid sequence HTLLHFFER with the $C_3H_2O_2$ modification residing on the Thr-99 residue. The peak at 1695.8 Da corresponds to the peptide CEHTEQNAAVIAIAR, residues 124 – 138, with the proposed modification on the Thr-127 residue. The peaks at 1663.8 Da and 1893.0 Da are both believed to contain amino acid residues 21 – 33, the sequence EHLMLAALETFYR, with the larger peptide containing 2 additional amino acid residues on the C-terminus (TK). There are 2 potential modification sites on the peptide at 1893 Da, at Thr-19 and Thr-30, however the common residues between the two peptide sequences suggests that the modification site is the Thr-30 residue. This indicates that there are 3 modification sites contained within the 4 modified peptides, all of which are proposed to be threonine residues.

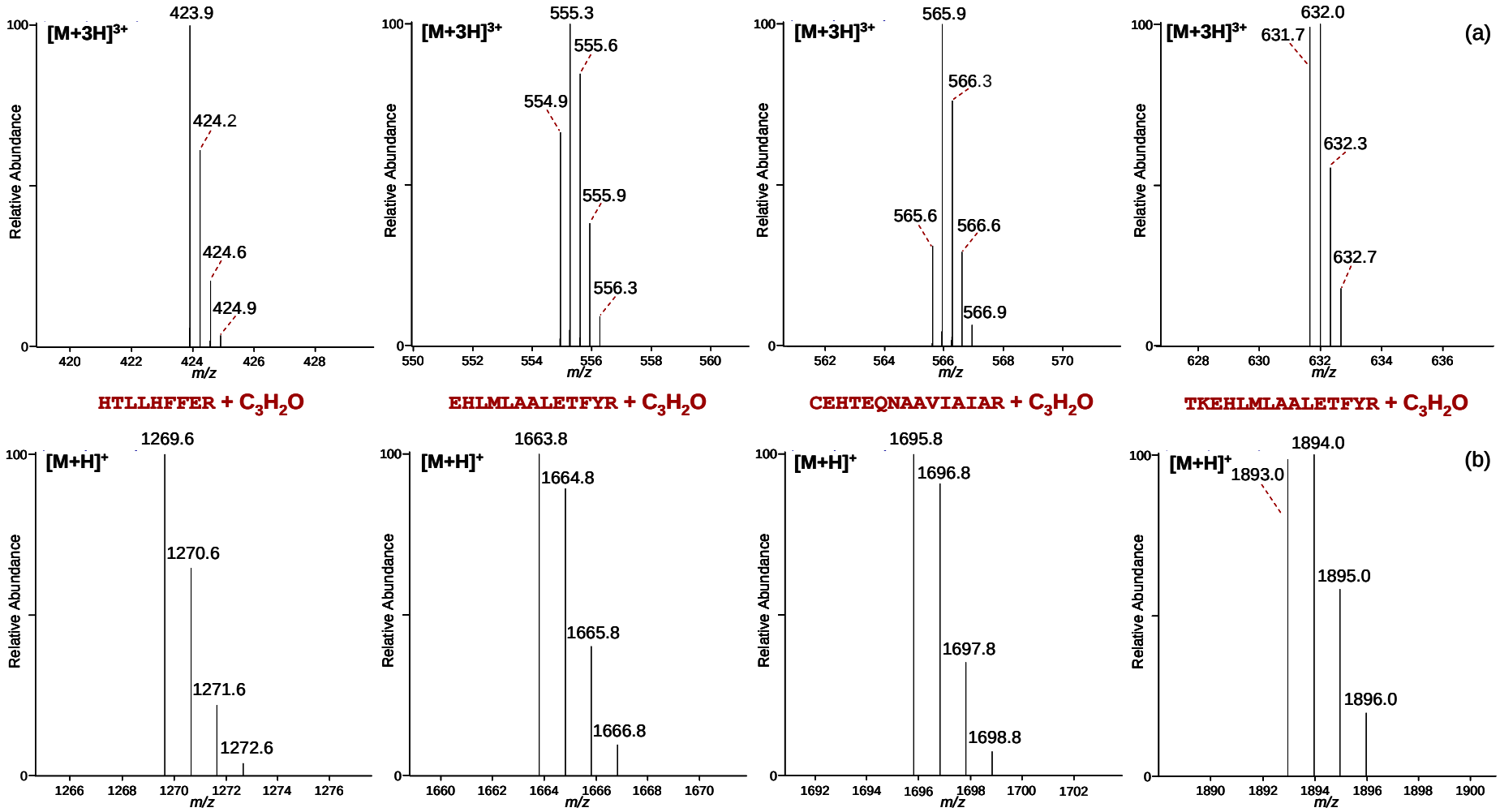

Figure 5.15: MS spectra of (a) the $[M+3H]^{3+}$ species of the 4 peptides modified by $C_3H_2O_2$ and (b) the corresponding protonated species generated by deconvolution.

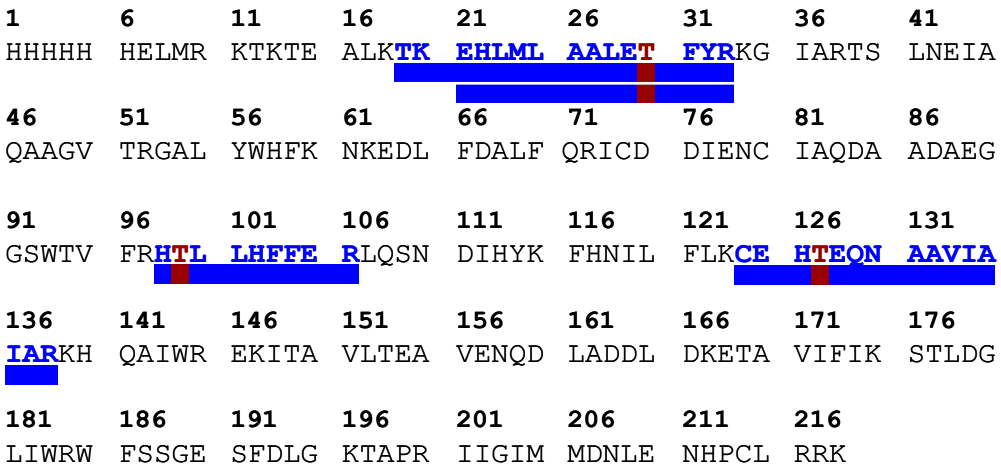

Figure 5.16: Peptides labelled in blue were observed in the modified MtrR protein samples with the proposed modification of $C_3H_2O_2$ (70 Da) on residues labelled in red.

A quadruply charged peak at *m/z* 934.0 was only observed in the tazobactam treated sample and is consistent with the deconvoluted $[M+H]^+$ species 3732.7 Da. This peak is the 32-residue peptide WFSSGESFDLGKTAPRIIGIMMDNLENHPCLR, containing 4 potential modification sites, and one proposed modification $C_4H_4NO_2$ (98 Da). Evidence for the modification $C_5H_5NO_4$ (143 Da) can be seen in both treated samples at the deconvoluted peak 1965.9 Da, and in the clavulanic acid treated sample only at 4918.6 Da. The peak at 1965.9 Da corresponds to the peptide TKEHLMLAALETFYR, residues 19 – 33 of the MtrR protein sequence with two threonine residues as possible modification sites. The peak at 4918.6 Da is consistent with residues 21 – 62, corresponding to the sequence EHLMLAALETFYRKGIARTSLNEIAQAAGVTRGALYWHFKNK, a 42-residue peptide containing 4 possible modification sites. Both peptides contain residues 21 – 33, a sequence also contained within two of the peptides identified in **Figure 5.16** with the $C_3H_2O_2$ (70 Da) modification, suggesting that the modification site of all 4 peptides may be the same, however this cannot be confirmed without further analysis of the peptides by MS/MS.

A summary of all the suspected modified tryptic peptides observed in the protein digests of the tazobactam-modified protein and the clavulanic acid-modified protein are shown in **Table 5.1**. Accurate mass measurements for each peak confirm the identity of each peptide to within 4 ppm, all of which were determined to contain only one modification. The $C_3H_2O_2$ modification is the most abundant modification in the LCMS spectra of the intact treated protein samples and the tryptic digests, suggesting that it is the most stable protein modification.

Residues	Theoretical Monoisotopic $[M+H]^+$ Da	Accuracy /ppm		Modification
		Tazobactam	Clavulanic Acid	
[19 - 33]	1892.95750	0.6	0.6	70 Da
[19 – 33]	1965.97387	0.6	0.6	143 Da
[21 - 33]	1663.81485	1.7	3.0	70 Da
[21 - 62]	4918.55735	-	0.0	143 Da
[98 - 106]	1269.63748	-0.4	-0.3	70 Da
[124 - 138]	1695.81189	0.2	0.7	70 Da
[185 - 216]	3732.78454	3.6	-	98 Da

Table 5.1: Summary of the identified peptides from the trypsin digests of the unmodified MtrR protein, the tazobactam modified sample and the clavulanic acid modified sample.

The absence of tryptic peptides containing the modifications $C_3H_3NO_2$ (85 Da), $C_6H_5NO_4$ (155 Da), $C_7H_7NO_4$ (169 Da) and $C_8H_7NO_5$ (197 Da) that were observed in the intact protein MS spectrum (see **Figure 5.8** and **Figure 5.10**) is thought to be partly due to the significantly higher intensity of the species resulting from the modification $C_3H_2O_2$ (70 Da). The unobserved modifications may also correspond to short-lived intermediates that react further to create a more stable modification species, a theory supported by studies carried out by Brown *et al.* involving the incubation of TEM-2 β-lactamase from *E. coli* with clavulanic acid.[15]

5.2.5. ECD of a proposed modified peptide

The deconvoluted peak at 1269.6 Da, which was proposed to correspond to the amino acid sequence HTLLHFFER, was analysed by LC-MS/MS to confirm the peptide sequence and the location of the $C_3H_2O_2$ modification. Due to the known inhibitor-protein interactions between the serine or threonine residues of the protein and the β-lactam ring of the inhibitor molecule, the modification was expected to reside on the threonine residue of the targeted peptide. The lability of the modification is unknown, therefore ECD was used to analyse the selected peptide due to its ability to preserve chemical modifications while generating a high degree of sequence coverage. The $[M+3H]^{3+}$ species at *m/z* 423.8 was targeted with electrons of 2.31 eV, resulting in the MS/MS spectrum shown in **Figure 5.17**. A total of 10 MS/MS scans were generated from the LC-ECD of the *m/z* 423.8 species, which when considering the low abundance of the precursor ion resulted in the low signal-to-noise (S/N) of the observed product ions. The major product ion from the ECD of the $[M+3H]^{3+}$ precursor ion, is the charge reduced species $[M+2H]^{2+}$ at *m/z* 635.3. As shown in **Figure 5.17**, LC-ECD generated 88% sequence coverage (7 out of 8 bonds broken) from *a, c, y* and *z+1* product ions. The *a* and *c* product ions observed are consistent with ions including the proposed modification, whereas the *y* and *z+1* ions correspond to unmodified residues, thereby narrowing down the location of the C_3H_2O modification to the histidine or threonine residue at the N-terminus of the peptide.

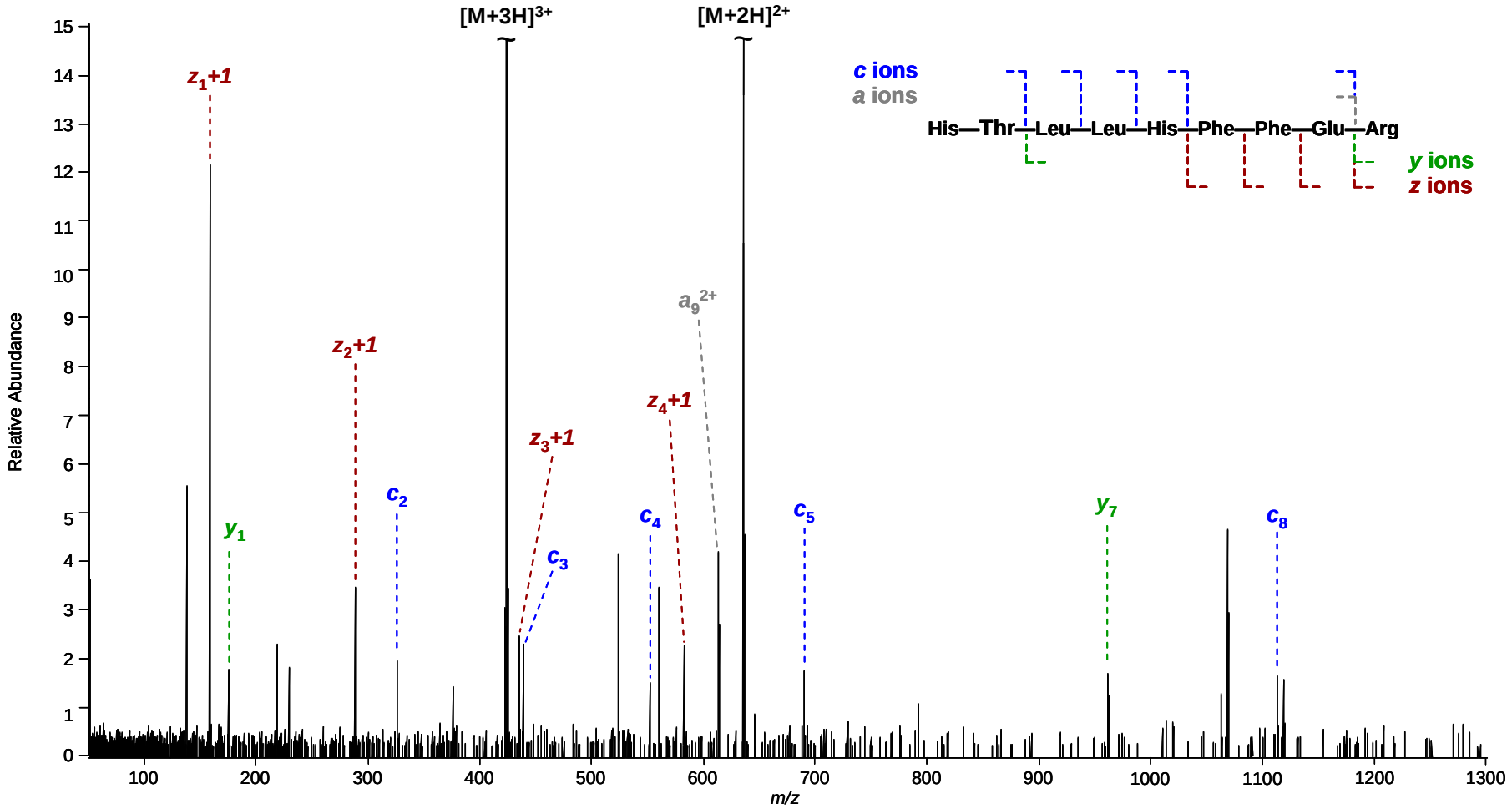

Figure 5.17: LC-ECD spectrum generated from the $[M+3H]^{3+}$ species of the modified peptide HTLLHFFER, narrowing down the location of the $C_3H_2O_2$ modification on the histidine or threonine residues.

Table 5.2 summarises the product ion assignments and their corresponding mass accuracies, allowing the peptide sequence to be characterised. All product ions have been found to be accurate to within 2 ppm to the expected molecular formula, confirming the peptide sequence assignment. The c_2 ion, highlighted in red in **Table 5.2**, confirms the location of the modification to the two N-terminal residues, the His-98 or the Thr-99 residue in the MtrR amino acid sequence shown in **Figure 5.4**.

Observed *m/z*	Ion	Molecular Formula	Accuracy / ppm
159.10022	z_1+1	$C_6H_{13}N_3O_2$	-0.0
175.11891	y_1	$C_6H_{15}N_4O_2$	-0.2
288.14281	z_2+1	$C_{11}H_{20}N_4O_5$	-0.0
326.14578	c_2	$C_{13}H_{20}N_5O_5$	-0.4
423.88400	**$[M+3H]^{3+}$**	**$C_{60}H_{87}N_{16}O_{15}$**	**-0.0**
435.21168	z_3+1	$C_{20}H_{29}N_5O_6$	1.0
439.23072	c_3	$C_{19}H_{31}N_6O_6$	1.7
552.31442	c_4	$C_{25}H_{42}N_7O_7$	0.7
582.28042	z_4+1	$C_{29}H_{38}N_6O_7$	1.3
613.32758	a_9^{2+}	$C_{59}H_{86}N_{16}O_{13}$	0.2
635.32251	$[M+2H]^{2+}$	$C_{60}H_{86}N_{16}O_{15}$	0.2
689.37171	c_5	$C_{31}H_{49}N_{10}O_8$	-1.8
961.52719	y_7	$C_{47}H_{69}N_{12}O_{10}$	1.8
1112.55242	c_8	$C_{54}H_{74}N_{13}O_{13}$	0.1

Table 5.2: Summary of the product ions generated by LC-ECD of the modified peptide shown in Figure 5.17. The precursor ion is highlighted in bold.

5.2.6. The matrix (M) Protein

The M protein is a membrane protein from the human respiratory syncytial virus (hRSV), a virus that infects the respiratory tract and causes breathing difficulties. The analysis of membrane proteins is often hampered by the abundance of hydrophobic regions on the protein. The hydrophobicity of membrane proteins also affects their ability to remain soluble under aqueous conditions and promotes protein oligomerisation or aggregation, which further impedes analysis.[16] The M protein

sequence, shown in **Figure 5.18**, corresponds to a monoisotopic molecular weight of 29231.3 Da and the most abundant peak at 29249.3 Da.

1	**6**	**11**	**16**	**21**	**26**	**31**	**36**	**41**
HMLEM	ETYVN	KLHEG	STYTA	AVQYN	VLEKD	DDPAS	LTIWV	PMFQS
46	**51**	**56**	**61**	**66**	**71**	**76**	**81**	**86**
SMPAD	LLIKE	LANVN	ILVKQ	ISTPK	GPSLR	VMINS	RSAVL	AQMPS
91	**96**	**101**	**106**	**111**	**116**	**121**	**126**	**131**
KFTIC	ANVSL	DERSK	LAYDV	TTPCE	IKACS	LTCLK	SKNML	TTVKD
136	**141**	**146**	**151**	**156**	**161**	**166**	**171**	**176**
LTMKT	LNPTH	DIIAL	CEFEN	IVTSK	KVIIP	TYLRS	ISVRN	KDLNT
181	**186**	**191**	**196**	**201**	**206**	**211**	**216**	**221**
LENIT	TTEFK	NAITN	AKIIP	YSGLL	LVITV	TDNKG	AFKYI	KPQSQ
226	**231**	**236**	**241**	**246**	**251**	**256**		
FIVDL	GAYLE	KESIY	YVTTN	WKHTA	TRFAI	KPRED		

Figure 5.18: Amino acid sequence of M protein.

The LC-MS of the M protein generated a broad peak in the TIC, as shown in **Figure 5.19**. The MS spectrum averaged from 79 scans under the peak maximum, shown in **Figure 5.19**, revealed at least two overlapping protein charge state envelopes, as indicated in **Figure 5.20**. The MS spectrum was deconvoluted to the $[M+H]^+$ species, resulting in the spectrum shown in **Figure 5.21**, which indicated some discrepancies between the expected most abundant ion calculated from the known amino acid sequence, 29250.3 Da, and the experimental average molecular weight. The MS spectrum of the M protein observed two protein distributions at 29351.4 Da and 29431.4 Da, corresponding to 101.1 Da and 181.1 Da higher than expected. The unknown proteins were subjected to further investigation in order to determine whether they are consistent with unexpected modifications to the M protein or whether they correspond to entirely different proteins.

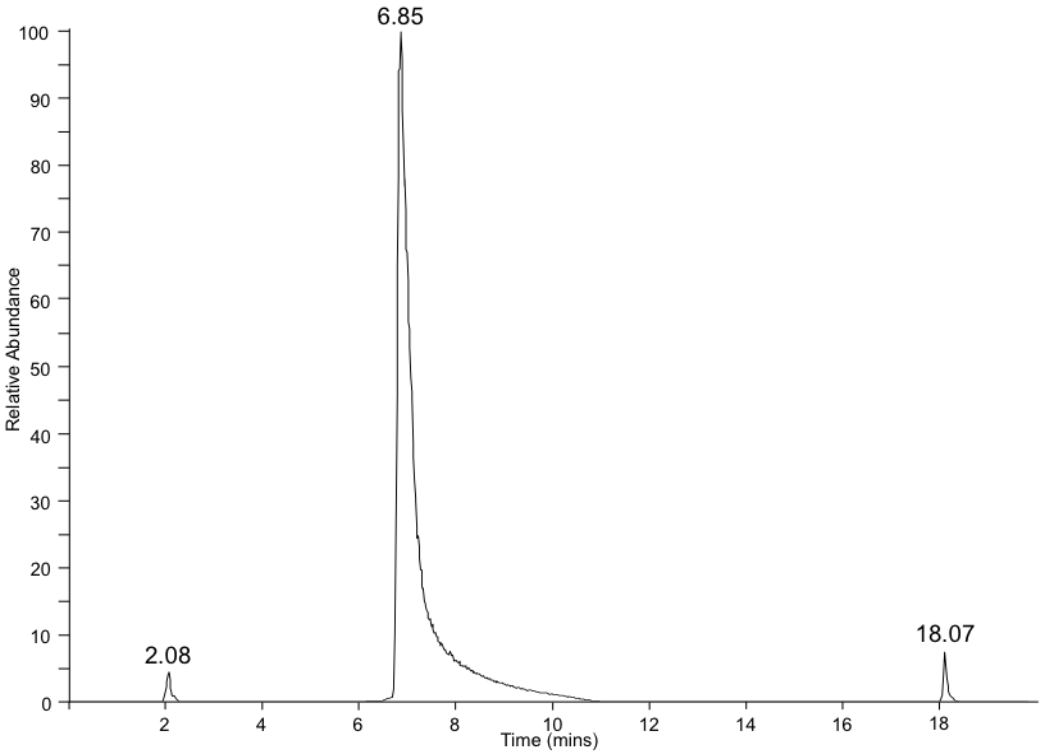

Figure 5.19: TIC generated from the LC-MS analysis of the M protein.

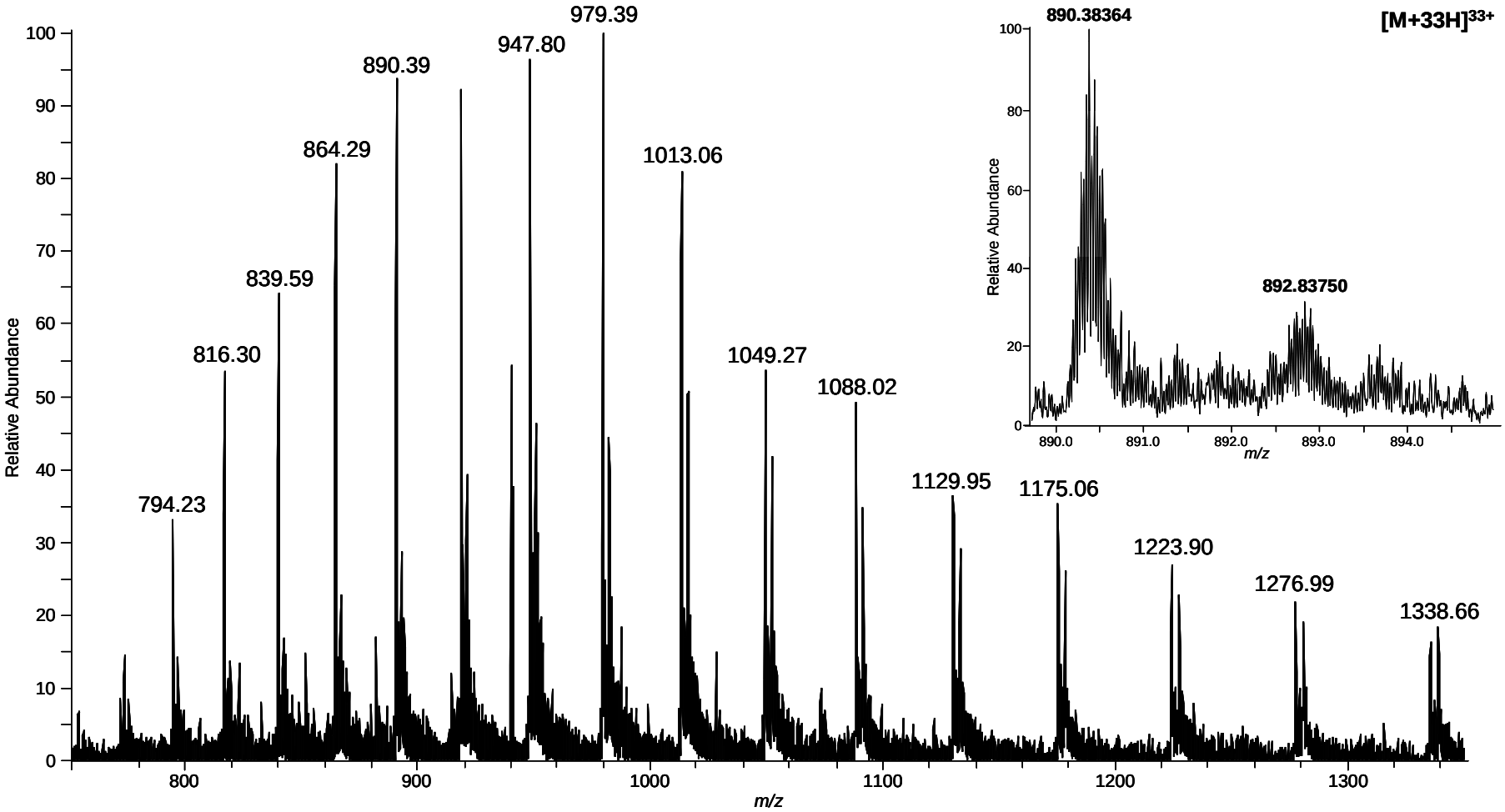

Figure 5.20: MS spectrum of the M protein indicating the presence of at least two species, and (inset) an expansion of the 33+ charge state.

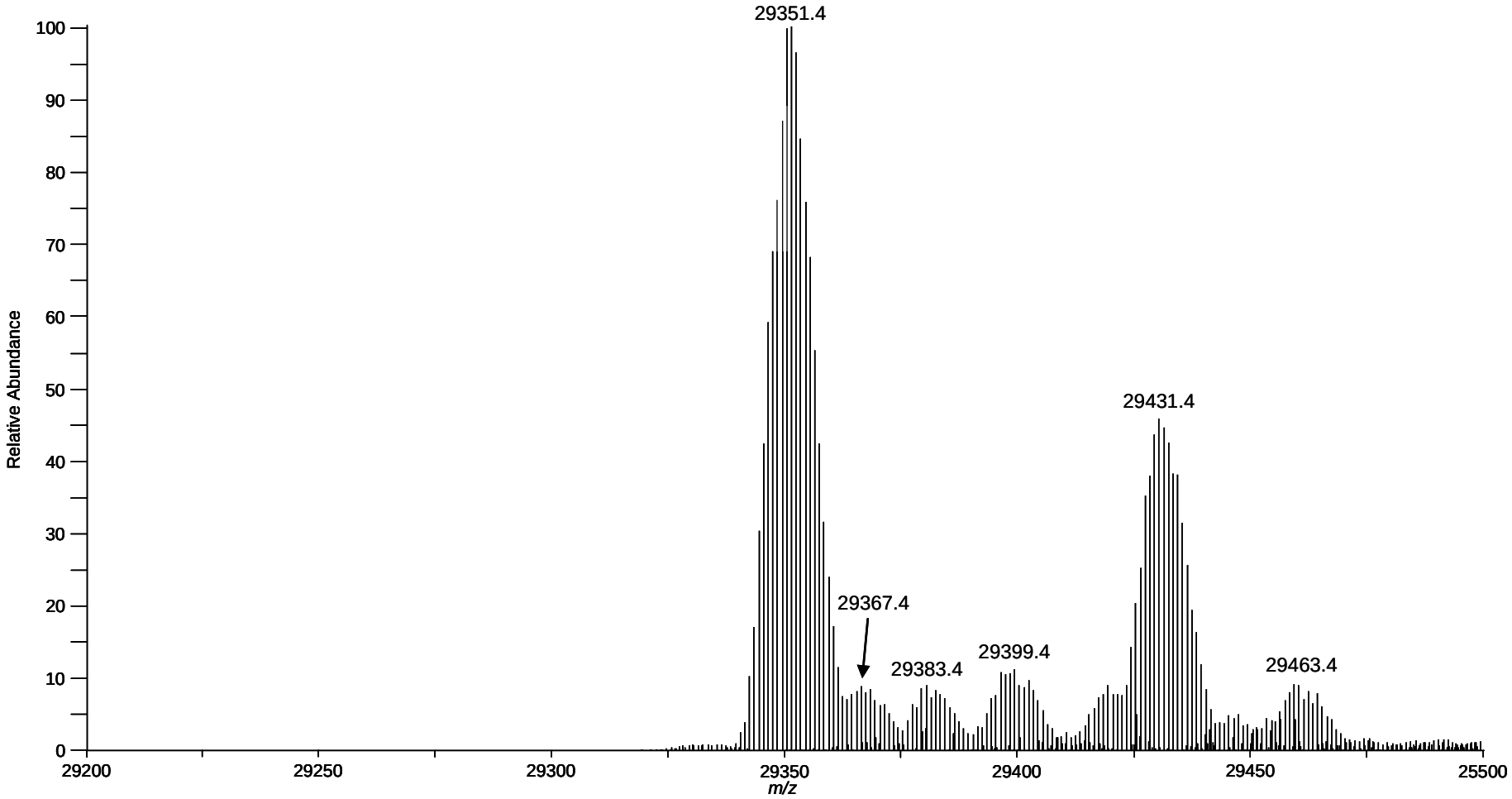

Figure 5.21: MS spectrum for the M protein, deconvoluted to the $[M+H]^+$ species, indicating protein species at higher m/z than expected.

5.2.7. Tryptic Digest of M Protein

In order to investigate the discrepancy in mass, a sample of the unmodified M protein was digested using trypsin and analysed by LC-MS. The resulting MS spectrum was deconvoluted to generate the protonated species for each observed species, as shown in **Figure 5.22**. An *in silico* tryptic digest of the M protein was carried out using the known amino acid sequence, shown in **Figure 5.18**, calculating theoretical tryptic peptides to the $[M+H]^+$ species and allowing for peptides containing up to 10 missed cleavages over an unlimited mass range in order to ensure a thorough interpretation of the experimental data. A direct comparison between the enzymatic digest and the *in silico* digest identified 28 peptides common to both that allowed the confirmation of 222 out of 260 amino acid residues from the known sequence, resulting in 85% sequence coverage. The remaining unidentified peaks were studied in order to identify the root of the unknown molecular weight discrepancy. Two deconvoluted peaks were discovered, at 1495.7 Da and 6271.0 Da, which were found to correspond to 101.0 Da higher than an expected M protein tryptic peptide. The suggested amino acid sequences from the *in silico* digest for both peaks corresponded to portions of the N-terminus of the M protein, as shown in **Figure 5.22**, implying that the unknown modification or mutation had taken place on one of residues 1 – 11 of the M protein.

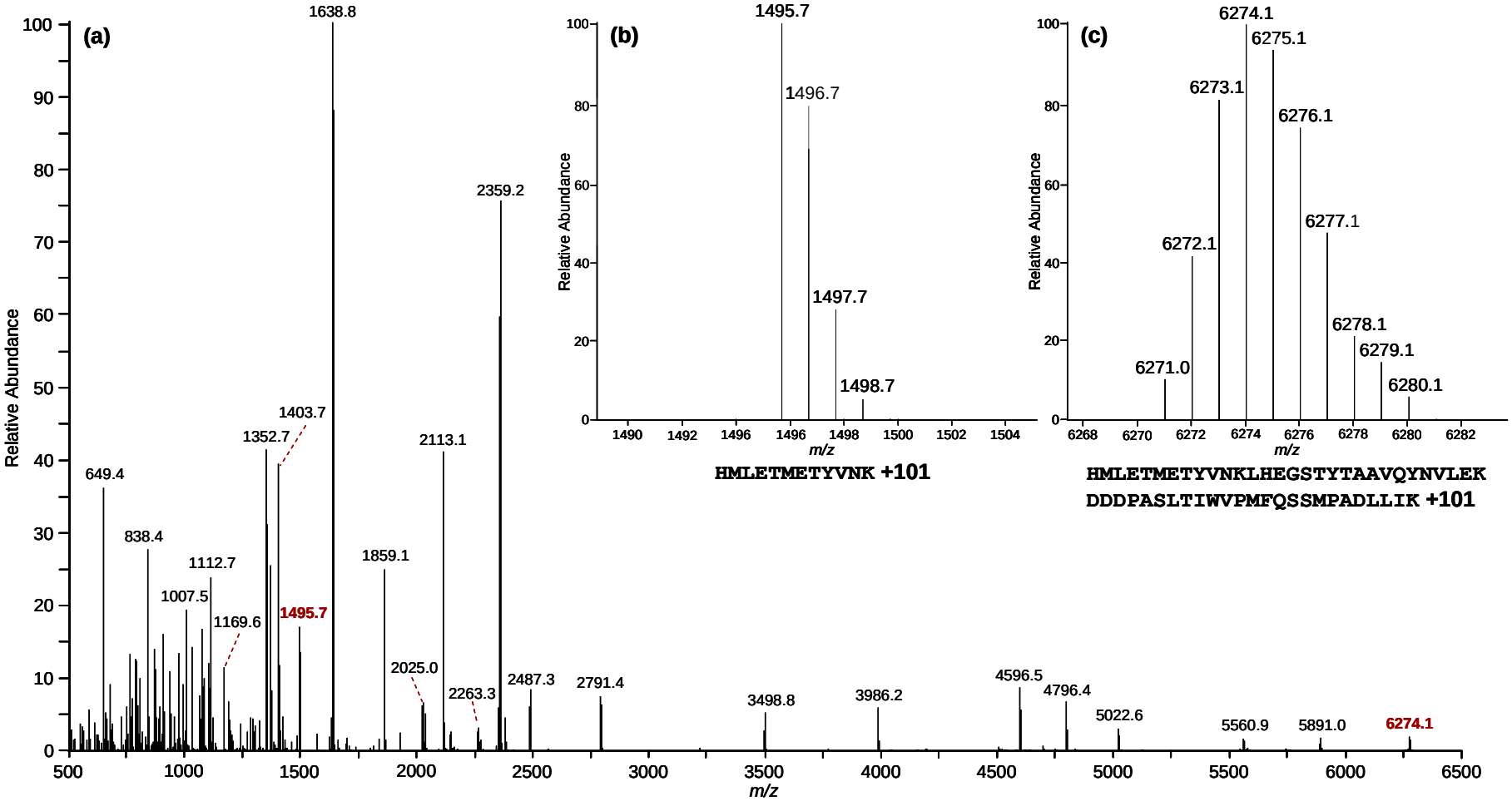

Figure 5.22(a): Deconvoluted MS spectrum of the trypsin-digested M protein. Two peaks at (b) *m/z* 1495.7 and (c) *m/z* 6271.0 are proposed to correspond to N-terminal peptides with the unknown addition of 101 Da.

LC-CID and LC-ECD analysis were performed on the $[M+2H]^{2+}$ species at *m/z* 748.3, which was thought to correspond to the amino acid sequence HMLEMETYVNK plus the unknown modification of 101.1 Da, in order to confirm the nature of the modification. The MS/MS spectra generated by both CID and ECD, shown in **Figure 5.23**, indicated that the increase in molecular weight was not caused by the modification of one of the amino acid residues, but instead corresponded to an additional amino acid in the peptide, an additional threonine residue located after the Glu-4 residue. The ions observed in the MS/MS spectra have been summarised in **Table 5.3**, confirming the product ion assignments accurate to within 4 ppm. ECD generated 9 backbone cleavages out of 11 (81%) whereas CID was shown to cleave all 11 bonds (100%) as shown in **Figure 5.23**. The complementary information generated by ECD and CID allows confidence in the assignment of the extra threonine residue. The complete sequencing of the peptide allowed the confirmation of the N-terminus of the M protein and increased the sequence coverage from 85% to 92% (239 out of 261 residues), as indicated in **Figure 5.24**. A comparison between each observed species and its corresponding theoretical monoisotopic mass for the $[M+H]^{+}$ species has confirmed the proposed molecular composition of each product ion to within 5 ppm, as shown in **Table 5.3**.

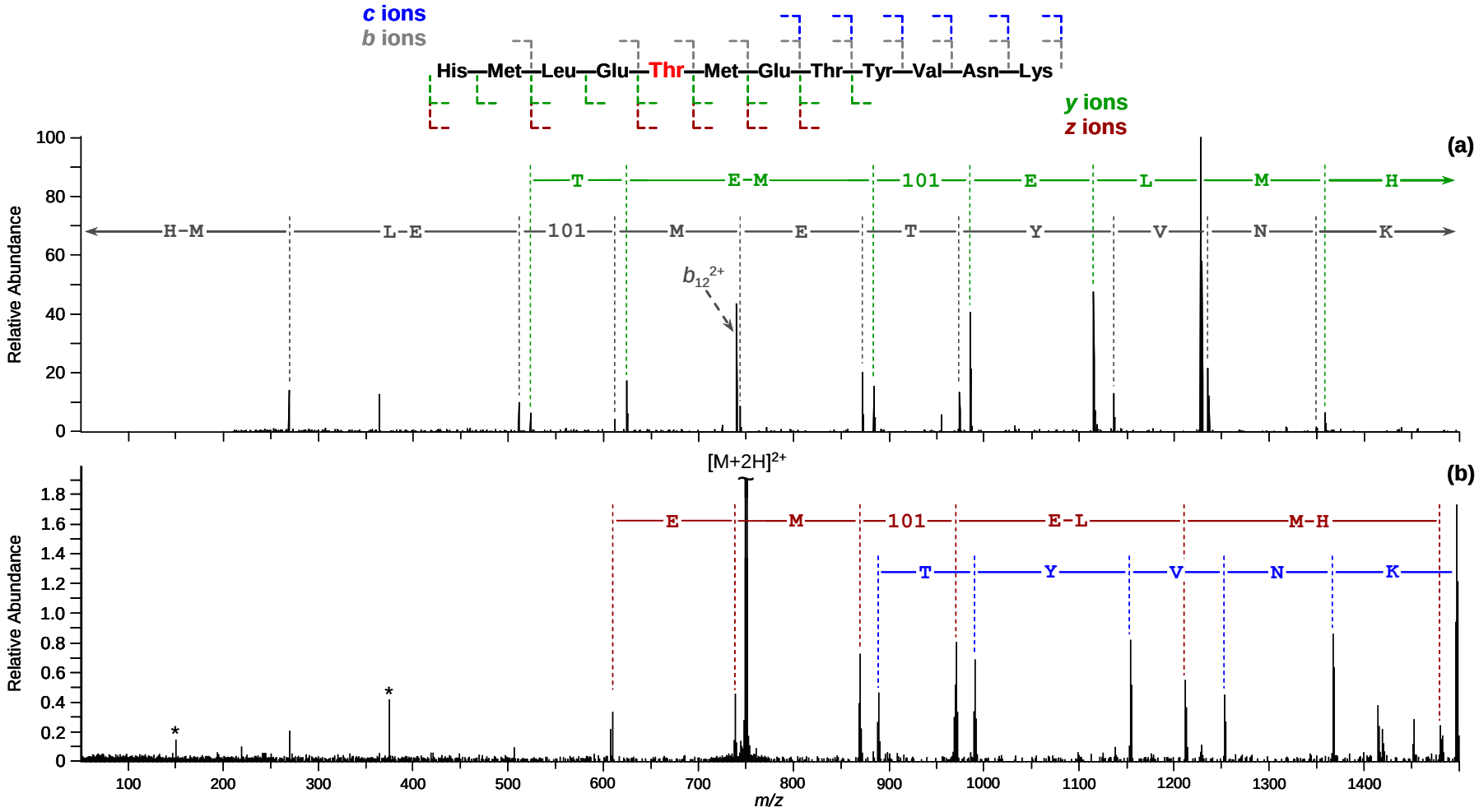

Figure 5.23(a): LC-CID and (b) LC-ECD spectra from the $[M+2H]^{2+}$ *m/z* 748.3. The addition of 101 Da has been identified as an extra threonine residue. Peaks labelled * denote artefact peaks and can be disregarded.

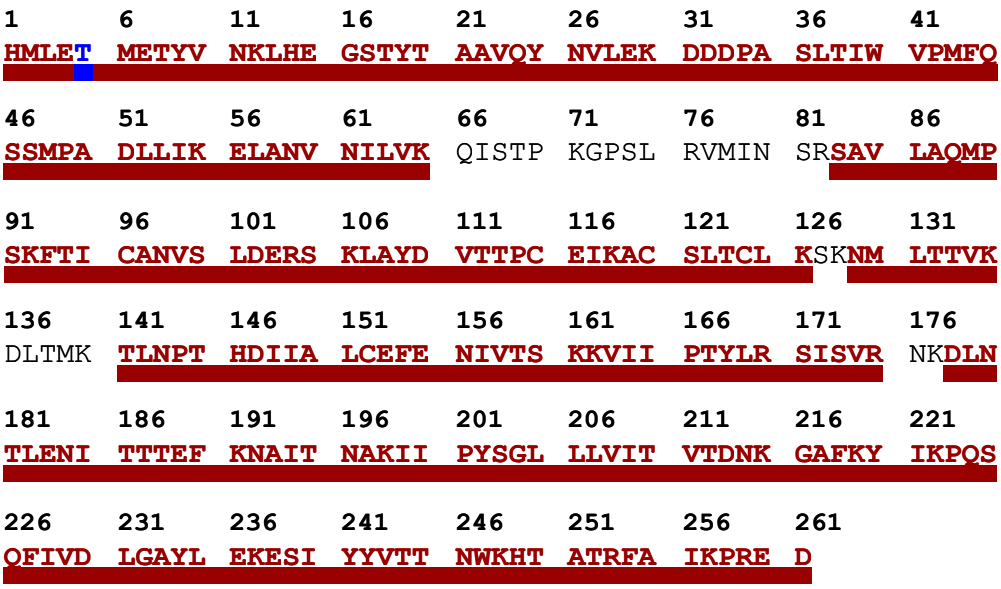

Figure 5.24: Updated M protein sequence indicating the additional threonine residue in blue.

Observed *m/z*	Ion	Molecular Formula	ECD / ppm	CID / ppm
269.10597	b_2	$C_{11}H_{17}N_4O_2S$		-2.6
511.23249	b_4	$C_{22}H_{35}N_6O_6S$		-1.6
523.28607	y_4	$C_{24}H_{39}N_6O_7$		-2.7
608.31548	$z_5 + 1$	$C_{28}H_{44}N_6O_9$	-1.6	
612.27962	b_5	$C_{26}H_{42}N_7O_8S$		-2.2
624.33306	y_5	$C_{28}H_{46}N_7O_9$		-3.2
737.35884	$z_6 + 1$	$C_{64}H_{105}N_{16}O_{21}S_2$	-0.2	
739.34265	b_{12}^{2+}	$C_{64}H_{102}N_{16}O_{20}S_2$		-2.2
743.32032	b_6	$C_{31}H_{51}N_8O_9S_2$		-1.5
748.34906	**$[M+2H]^{2+}$**	**$C_{64}H_{104}N_{16}O_{21}S_2$**	**-0.8**	**-**
868.39925	$z_7 + 1$	$C_{38}H_{60}N_8O_{13}S$	-0.3	
872.36181	b_7	$C_{36}H_{58}N_9O_{12}S_2$		-2.5
884.41521	y_7	$C_{38}H_{62}N_9O_{13}S$		-3.4
889.39096	c_7	$C_{36}H_{61}N_{10}O_{12}S_2$	0.4	
969.44833	$z_8 + 1$	$C_{42}H_{67}N_9O_{15}S$	1.2	
973.40912	b_8	$C_{40}H_{65}N_{10}O_{14}S_2$		-2.6
985.46384	y_8	$C_{42}H_{69}N_{10}O_{15}S$		-1.9
990.43745	c_8	$C_{40}H_{68}N_{11}O_{14}S_2$	-0.9	
1114.50679	y_9	$C_{47}H_{76}N_{11}O_{18}S$		-1.6
1136.47245	b_9	$C_{49}H_{74}N_{11}O_{16}S_2$		-2.0
1153.50314	c_9	$C_{49}H_{77}N_{12}O_{16}S_2$	1.3	
1211.57788	$z_{10} + 1$	$C_{53}H_{85}N_{11}O_{19}S$	3.3	
1227.59091	y_{10}	$C_{53}H_{87}N_{12}O_{19}S$		-1.5
1235.54237	b_{10}	$C_{54}H_{83}N_{12}O_{17}S_2$		-0.5
1252.57280	c_{10}	$C_{54}H_{86}N_{13}O_{17}S_2$	2.2	
1358.63009	y_{11}	$C_{58}H_{96}N_{13}O_{20}S$		-2.4
1366.61759	c_{11}	$C_{58}H_{92}N_{15}O_{19}S_2$	3.4	
1479.67909	$z_{12} + 1$	$C_{64}H_{101}N_{15}O_{21}S_2$	4.0	
1495.69706	$[M+H]^+$	$C_{64}H_{103}N_{16}O_{21}S_2$	3.4	

Table 5.3: Summary of the product ion assignments for the peaks generated by LC-MS/MS in Figure 5.23. The precursor ion is highlighted in bold.

The assignment of the deconvoluted peak at 29351.4 Da in **Figure 5.21** as the unmodified M protein allows the other observed protein species to be re-assigned accordingly, as shown in **Figure 5.25**. The protein at 29431.4 Da corresponds to the phosphorylated M protein resulting from the net addition of HPO_3 to the protein, proposed to originate from the phosphate buffer used for protein storage. The peaks at 29367.4 Da, 29383.4 and 29399.4 Da are thought to correspond to oxidated M protein species, resulting from the addition of 1, 2 and 3 oxygen atoms respectively, also likely to occur from sample preparation. The peak at 29463.4 Da is thought to correspond to the double oxidation of the phosphorylated species.

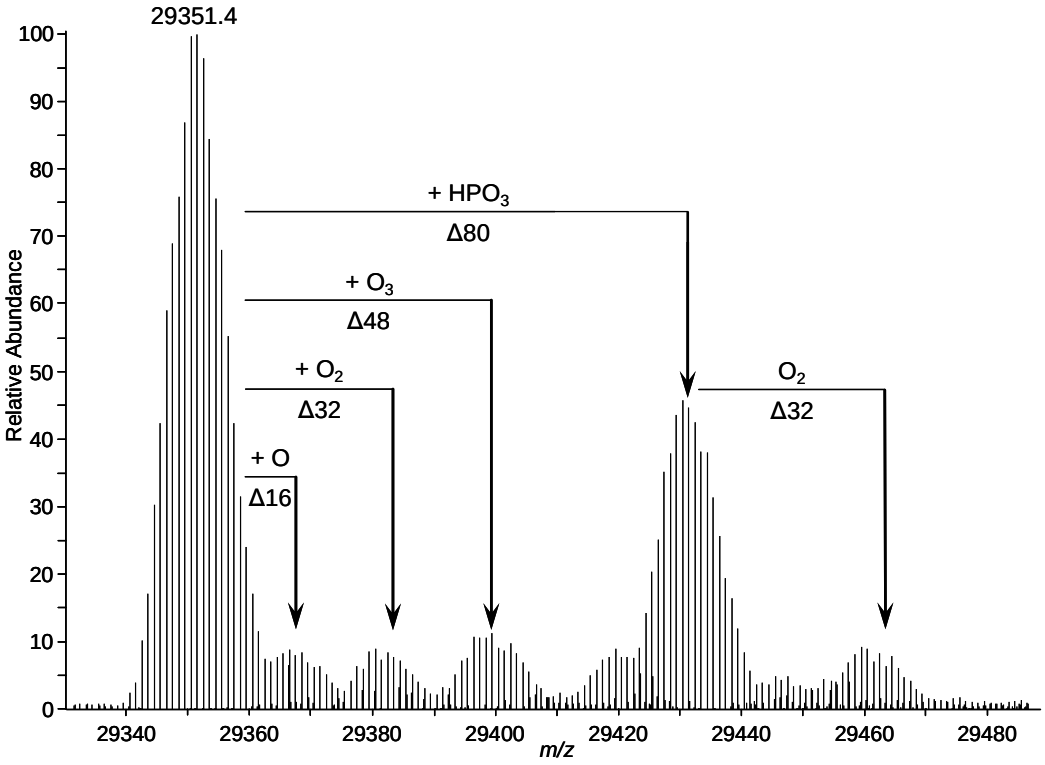

Figure 5.25: Deconvoluted M protein spectrum (from Figure 5.21) indicating suspected protein modifications.

The mass accuracies have been calculated with respect to the theoretical most abundant ion for each protein species, all of which have been found to be accurate to within 4 ppm. Tryptic peptides containing modifications consistent with the

oxidated or phosphorylated protein species were not observed in the tryptic digest spectrum shown in **Figure 5.22**, preventing the identification of the oxidation or phosphorylation sites.

5.2.8. Fluorescent labelling of M Protein

Fluorescent Resonance Energy Transfer (FRET) microscopy is a frequently used technique for studying cell membranes and their interaction with proteins and lipids by observing the transfer of fluorescent energy between the donor and acceptor.[17] In order to study the membrane-binding properties of the M protein by FRET, the protein must first be reacted with a fluorescent label to produce the fluorescent donor.[18] The reaction between the M protein and the fluorescent label, 4-chloro-7-nitrobenzofurazan (NBD-Cl), shown in **Figure 5.26**, is purported to proceed *via* the reaction between the label and the amine groups of lysine residues or the thiol groups of cysteine residues, resulting in the loss of HCl and the production of a green fluorescent complex (~ 400-500 nm).[19-20] Analysis has been carried out on the labelled protein with the intention of confirming the interaction between the label and the protein, and determining the number and location of any NBD modifications to the protein.

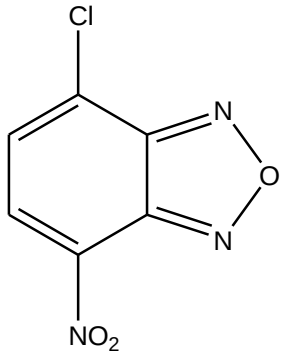

Figure 5.26: Structure of the NBD-Cl fluorescent label that reacts with cysteine or lysine residues to give the added molecular formula $C_6HN_3O_3$.

The sample of M protein treated with NBD-Cl was analysed by LCMS and deconvoluted to the singly protonated species, see **Figure 5.27**, which resulted in 3 major species at 29351.4 Da, 29431.4 Da and 29514.4 Da. The unmodified protein at 29351.4 Da remained the most abundant species, indicating that the reaction was not carried to completion or that the reaction forms an equilibrium between the modified and unmodified protein. The loss of HCl upon reaction is confirmed by the deconvoluted peak at 29514.4 Da, which was found to correspond to the addition of the empirical formula of $C_6HN_3O_3$ consistent with the addition of one NBD molecule to the intact M protein, with a mass accuracy of 0.9 ppm. The phosphorylated protein species at 29431.4 Da does not appear to have a corresponding NBD-modified species, suggesting that the phosphorylation may inhibit the NBD modification.

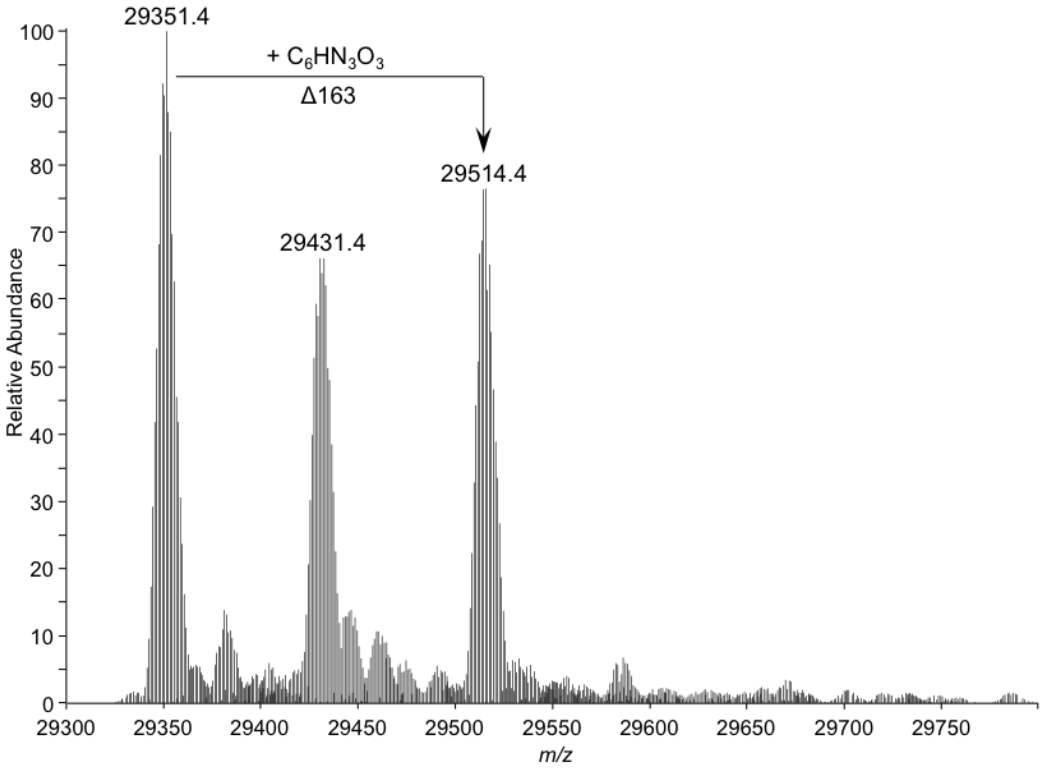

Figure 5.27: MS spectrum of the modified M protein sample deconvoluted to the $[M+H]^+$ species.

5.2.9. Tryptic digest of NBD-modified M Protein

A sample of the NBD-treated M protein was digested using trypsin and analysed by LC-MS. The spectrum generated from the MS analysis of the digest was deconvoluted to generate the $[M+H]^+$ for each species. The parameters of the *in silico* tryptic digest of the M protein sequences were adjusted to include the optional modification of $C_6HN_3O_3$ (NBD) on all lysine or cysteine residues. When the enzymatic digest of the treated protein was directly compared to the *in silico* digest, 29 tryptic peptides were identified, of which 28 were determined to correspond to portions of the sequence without the NBD modification, including peptides not previously observed in the unmodified protein digests and therefore resulting in increased sequence coverage to 96% (250 out of 261 residues confirmed), as shown in **Figure 5.28**. The deconvoluted peak at 1346.7 Da matches the theoretically modified peptide `QISTPKGPSLR` with the NBD modification proposed to reside on the lysine residue, an assignment that has been confirmed with an accuracy of 1.4 ppm. A direct comparison between the tryptic peptides observed in the unmodified M protein sample and the NBD-treated sample highlighted peptides unique to each sample, which may indicate a change in the secondary and/or tertiary structure of the protein as a result of the NBD modification subsequently altering which parts of the protein are accessible to the enzyme.

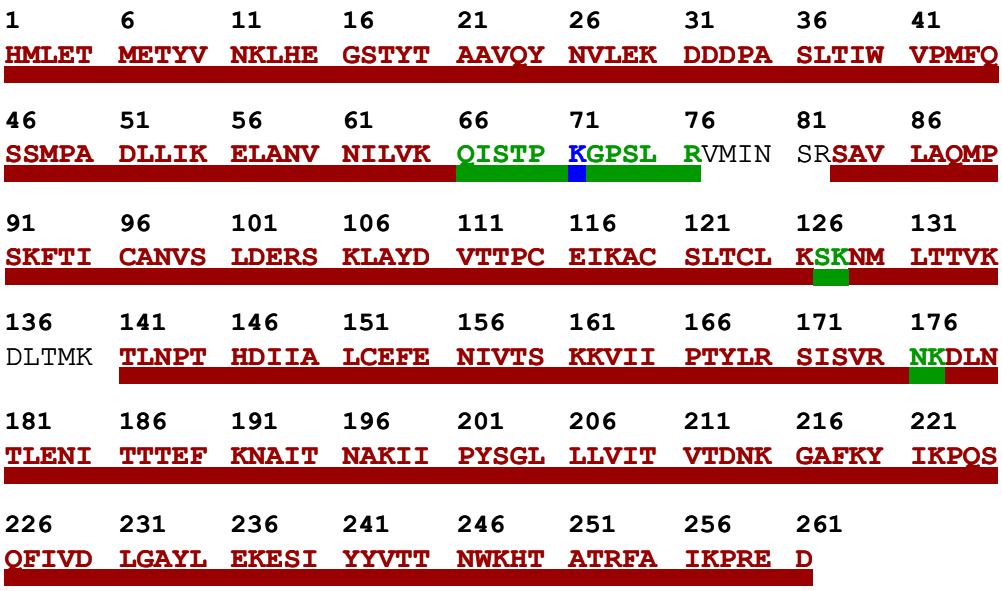

Figure 5.28: Confirmed sequence coverage of the M protein. The residues labelled in green were only observed in the digest of the modified protein sample. The proposed modification site, Lys-71, has been labelled in blue.

Figure 5.29 shows the crystal structure modelled from the experimental X-ray diffraction data of the M protein using the sequence in **Figure 5.18** (modelled using residues 3 – 259).[21] The part of the structure in red corresponds to portions of the sequence confirmed by the tryptic digest of the unmodified protein, whereas the regions in green correspond to the peptides confirmed from the NBD-protein digest only. The location of the proposed modification site on the Lys-71 residue (named as per the amino acid sequence in **Figure 5.28**) has been shown in blue on the crystal structure in **Figure 5.29**. The Lys-71 residue is observed on a flexible loop portion of the protein structure, free from any noticeable steric hindrance from the other residues that may obstruct the site from modification.

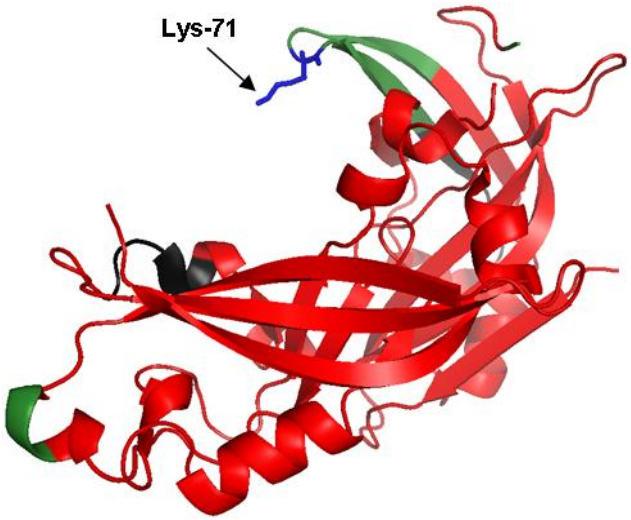

Figure 5.29: Crystal structure[§] of the M protein modelled using the amino acid sequence in Figure 5.18. The proposed modification site has been labelled in blue.[21]

The phosphorylated M protein species was not seen to have been labelled upon incubation with NBD-Cl, as shown in **Figure 5.27**, suggesting that the phosphorylation inhibits the NBD modification. Protein phosphorylation is known to occur on serine, threonine or tyrosine residues[1], and therefore would not be expected on the proposed NBD modification site at Lys-71, however the Ser-68 , Thr-69 and Ser-74 residues are all in close proximity to the proposed modification site and may be involved in phosphorylation. The tertiary protein structure also brings residues Thr-94 and Tyr-109 into close proximity to the Lys-71.

The crystal structure shown in **Figure 5.29**, modelled using the original M protein sequence shown in **Figure 5.18**, did not identify the presence of the extra amino acid at the N-terminus, instead mistaking the threonine residue for the neighbouring glutamic acid residue. The misinterpretation of the X-ray crystal structure of the M Protein is due to the flexibility of the protein termini, which resulted in more

[§] X-ray diffraction data recorded at a resolution of 1.60 Å.

disordered X-ray diffraction data at the termini and prevented the sequence error from being discovered.

5.3. Conclusion

5.3.1. MtrR Protein

The observed interaction of the MtrR protein by tazobactam and clavulanic acid supports the proposed β-lactamase function of the protein. The MS analysis of the trypsin-digested MtrR protein samples were compared to an *in silico* digest and resulted in a high percentage of the sequence being confirmed. Full MS analysis of the intact modified protein samples has proposed several modifications arising from incubation with the β-lactamase inhibitors. The search for modifications in the tryptic digest of the modified samples noted 4 peaks consistent with the modification of $C_3H_2O_2$ (70 Da), proposed to correspond to three modified amino acid residues, Thr-30 and Thr-99 and Thr-127. Two peptides were observed with the modification of $C_5H_5NO_4$ (143 Da), one that corresponds to the same peptide sequence (residues 19 – 33) that was determined to contain the modification of $C_3H_2O_2$ (70 Da) at the Thr-30 residue. The second peptide containing the 143 Da modification corresponds to a 42-residue peptide with 4 possible modification sites. One peptide was identified with the proposed modification $C_4H_4NO_2$ (98 Da) however the peptide sequence contains 4 possible modification sites that would require further analysis by MS/MS to determine. The results detailed herein suggest that the modification(s) of the MtrR protein occurs at different sites on the protein, indicating a lack of specificity between the inhibitor and the protein.

LC-MS/MS analysis of the modified peptide observed at *m/z* 423.8, deconvoluted to *m/z* 1269.6, has confirmed the peptide sequence and narrowed down the location of the suspected modification to the two amino acid residues at the N-terminus of the

peptide, supporting the suspected modification site at the Thr-99 residue. The homology model shown in **Figure 5.30** has been modelled from the MtrR amino acid sequence in **Figure 5.4**, using a similar protein with a known crystal structure. The portion of the amino acid sequence that was identified from the unmodified MtrR protein digest has been coloured red, while the residues observed in the modified MtrR digest samples only have been coloured green. The 3 proposed modification sites for the $C_3H_2O_2$ (70 Da) modification have been highlighted in blue, all of which appear to be situated at the outer surface of the protein tertiary structure, free from the steric hindrance of other residues in the protein.

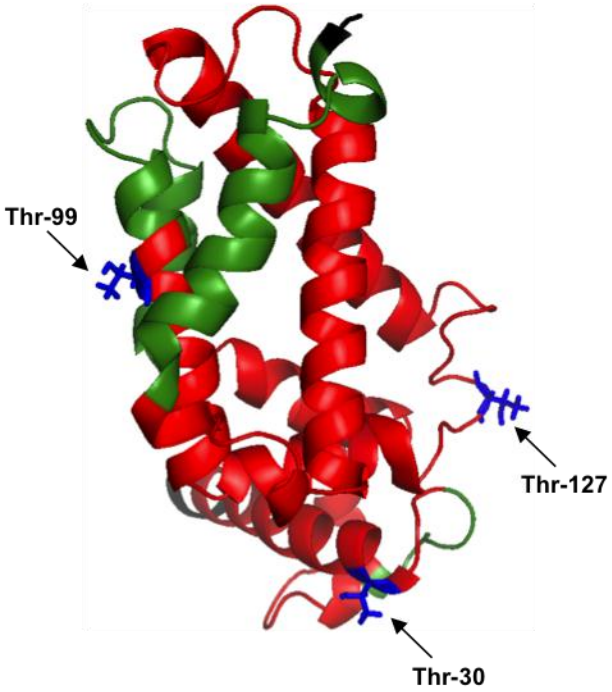

Figure 5.30: Homology model of the MtrR protein.[14] The 3 residues proposed to contain modifications have been highlighted in blue.

The peptides observed with modifications $C_4H_4NO_2$ (98 Da) and $C_5H_5NO_4$ (143 Da) were found to contain multiple potential modification sites and therefore have not been highlighted on the homology model. Further LC-MS/MS analysis is required to

confirm the modified amino acid residues for 3 peptides proposed to contain the modifications $C_4H_4NO_2$ (98 Da) and $C_5H_5NO_4$ (143 Da).

5.3.2. M Protein

The intact M protein has shown inconsistencies between the expected molecular weight and the measured molecular weight, implying that the amino acid sequence had been modified or mutated. MS and MS/MS analysis has been used to successfully identify the major protein species, discovering a discrepancy in the molecular weight and successfully identifying the mass discrepancy as an unexpected extra threonine residue located near the N-terminus of the protein. The updated protein sequence has subsequently been confirmed with 96% sequence coverage from MS analysis of the tryptic digests. The incubation of the M protein with the fluorescent label NBD-Cl was found to result in an M-NBD complex containing one NBD molecule. A study of the trypsin digested sample of the modified protein revealed the location of the label to a 10-residue portion of the sequence with only one potential modification site.

The use of LC-MS/MS techniques such as CID and ECD has been shown to provide vital information regarding peptide sequencing and the identification of protein modifications, cementing its importance in biological and chemical analysis.

5.4. References

1. Blom, N., Sicheritz-Pontén, T., Gupta, R., Gammeltoft, S., Brunak, S.: Prediction of Post-Translational Glycosylation and Phosphorylation of Proteins from the Amino Acid Sequence *Proteomics* **2004,** *4*, 1633-1649

2. Sulton, D., Pagan-Rodriguez, D., Zhou, X., Liu, Y.D., Hujer, A.M., Bethel, C.R., Helfand, M.S., Thomson, J.M., Anderson, V.E., Buynak, J.D., Ng, L.M., Bonomo, R.A.: Clavulanic Acid Inactivation of SHV-1 and the Inhibitor-Resistant S130G SHV-1 Beta-Lactamase - Insights Into the Mechanism of Inhibition *J. Biol. Chem.* **2005,** *280*, 35528-35536

3. Pagan-Rodriguez, D., Zhou, X., Simmons, R., Bethel, C.R., Hujer, A.M., Helfand, M.S., Jin, Z., Guo, B., Anderson, V.E., Ng, L.M., Bonomo, R.A.: Tazobactam Inactivation of SHV-1 and the Inhibitor-resistant Ser130 → Gly SHV-1 β-Lactamase *J. Biol. Chem.* **2004,** *279*, 19494-19501

4. Sanderson, J.M.: Peptide-Lipid Interactions: Insights and Perspectives *Org. Biomol. Chem.* **2005,** *3*, 201-212

5. McPhee, H.K., Carlisle, J.L., Beeby, A., Money, V.A., Watson, S.M.D., Yeo, R.P., Sanderson, J.M.: Influence of Lipids on the Interfacial Disposition of Respiratory Syncytical Virus Matrix Protein *Langmuir* **2011,** *27*, 304-311

6. Dods, R.H., Mosely, J.A., Sanderson, J.M.: The Innate Reactivity of a Membrane Associated Peptide Towards Lipids: Acyl Transfer to Melittin Without Enzyme Catalysis *Org. Biomol. Chem.* **2012**,

7. Jensen, O.N.: Modification-Specific Proteomics: Systematic Strategies for Analysing Post-Translationally Modified Proteins *Trends Biotechnol.* **2000,** *18*, 36-42

8. Jensen, O.N.: Modification-Specific Proteomics: Characterization of Post-Translational Modifications by Mass Spectrometry *Curr. Opin. Chem. Biol.* **2004,** *8*, 33-41

9. Stensballe, A., Jensen, O.N., Olsen, J.V., Haselmann, K.F., Zubarev, R.A.: Electron Capture Dissociation of Singly and Multiply Phosphorylated Peptides *Rapid Commun. Mass Spectrom.* **2000,** *14*, 1793-1800

10. Sinz, A.: Chemical Cross-Linking and Mass Spectrometry to Map Three-Dimensional Protein Structures and Protein–Protein Interactions *Mass Spectrom. Rev.* **2006,** *25*, 663-682

11. Bakhtiar, R., Guan, Z.Q.: Electron Capture Dissociation Mass Spectrometry in Characterization of Post-Translational Modifications *Biochem. Biophys. Res. Commun.* **2005,** *334*, 1-8

12. Thomson, J.M., Distler, A.M., Prati, F., Bonomo, R.A.: Probing Active Site Chemistry in SHV beta-Lactamase Variants at Ambler Position 244 - Understanding Unique Properties of Inhibitor Resistance *J. Biol. Chem.* **2006,** *281*, 26734-26744

13. Warner, D.M., Shafer, W.M., Jerse, A.E.: Clinically Relevant Mutations that Cause Derepression of the Neisseria Gonorrhoeae MtrC-MtrD-MtrE Efflux Pump System Confer Different Levels of Antimicrobial Resistance and In Vivo Fitness *Mol. Microbiol.* **2008,** *70*, 462-478

14. Burton, M.F. Investigating Antimicrobial Resistance Mechanisms in *Neisseria gonorrhoeae* using Peptide Probes. Doctoral Thesis, Durham University, 2009.

15. Henderson, G., Murray, J., Yeo, R.P.: Sorting of the Respiratory Syncytial Virus Matrix Protein into Detergent-Resistant Structures is Dependent on Cell-Surface Expression of the Glycoproteins *Virology* **2002,** *300*, 244-254

16. McPhee, H.K. A Study of the Membrane Binding Properties of the Matrix Protein from Human Respiratory Syncytical Virus. Doctoral Thesis, Durham University, 2009.

17. Sekar, R.B., Periasamy, A.: Fluorescence resonance energy transfer (FRET) microscopy imaging of live cell protein localizations *J. Cell Biol.* **2003,** *160*, 629-633

18. Liu, R., Sharom, F.J.: Proximity of the Nucleotide Binding Domains of the P-glycoprotein Multidrug Transporter to the Membrane Surface: A Resonance Energy Transfer Study† *Biochemistry* **1998,** *37*, 6503-6512

19. Houk, T.W., Ovnic, M., Karipides, S.: pH and Polymerization Dependence of the Site of Labeling of Actin by 7-chloro-4-nitrobenzo-2-oxa-1,3-diazole *J. Biol. Chem.* **1983,** *258*, 5419-5423

20. Baines, B.S., Allen, G., Brocklehurst, K.: Highly Electrophilic Character of 4-chloro-7-nitrobenzofurazan and Possible Consequences for its Applications as a Protein-labeling Reagent *Biochem. J.* **1977,** *163*, 189-192

21. Money, V.A., McPhee, H.K., Mosely, J.A., Sanderson, J.M., Yeo, R.P.: Surface Features of a Mononegavirales Matrix Protein Indicate Sites of Membrane Interaction *P. Natl. Acad. Sci. USA* **2009,** *106*, 4441-4446

6. Conclusions

Electron Induced Dissociation has been shown to provide complementary data to existing MS and MS/MS techniques, generating a high degree of fragmentation from a variety of compounds and molecular ions. The results obtained thus far indicate a particular affinity for analysing positively charged precursor ions by EID, while altering various instrumental parameters such as electron irradiation time has been shown to affect the production and intensity of the product ions formed *via* negative ion EID, indicating a potential for improvement. The combination of liquid chromatography with EID has shown huge promise for analysing complex mixtures of small organic molecules, providing a vast amount of structural information from previously unknown compounds of varying ion abundances. The product ion data generated by EID of a range of small organic molecules have suggested competing fragmentation mechanisms, forming a combination of odd-electron and even-electron fragments as well as unique bond cleavages and product ions.

The use of Electron Capture Dissociation in the field of proteomics has been known to provide valuable data regarding the identification of post-translational modifications, and has been used to locate and identify modifications resulting from interactions between proteins and small organic molecules. Using proteolytic digestion, LC-MS and LC-MS/MS, investigations into the sequence and small molecule modifications of the MtrR protein and the M protein have identified protein sequence anomalies and suggested locations and structural characteristics of modifications to the protein backbone.

7. Future Work

7.1. Electron Induced Dissociation

EID analysis thus far has been performed predominantly on, but not exclusively focussed on protonated, deprotonated and sodium adducted species. Further study into the effect of electron energy on the resulting product ion spectra should determine whether the optimal electron energy level for EID MS/MS is affected by altering the charge-carrying species or the charge polarity. The data carried out thus far has focussed on compounds containing aromatic rings and heteroatoms. A more expansive range of compounds, involving systematic changes to analogous molecules, would hope to determine whether the trends observed are affected by the specific functional groups or elemental components of the precursor ion. Further investigations would hope to indicate whether different charge-carrying species preferentially reside at different locations, and whether precursor ion fragmentation can be manipulated to focus on specific portions of the molecule by altering the charge carrier.

Results described herein have shown that EID is better suited for analysing positive precursor ions than negative ions, generating limited unique information from the anionic compounds analysed thus far. Preliminary steps to improve the data generated by negative ion EID have involved the alteration of the electron irradiation time, which has been shown to have a positive effect on ion abundances and product ion formation as the duration time is increased. Further work should involve the extension of the current data, increasing the electron irradiation duration to the maximum limit of the LTQ-FT, 2000 ms, in order to explore any underlying trends. Additionally, experiments should be carried out on molecular ions with different

charge-carrying species in order to determine whether the effect of electron irradiation time is universal or precursor ion dependant.

MS and MS/MS spectral libraries, such as the National Institute of Standards and Technology (NIST) databases, typically include EI and CID spectra that allow users to search the databases using observed product ions and their corresponding relative intensities. Work thus far has determined that the product ions generated by EID are complementary to EI and CID, with the observed product ion spectra often containing ions common to one or both techniques, however the major factor preventing the search of current databases using EID product ions is the significant variation in product ion relative intensities compared to EI and CID data. Further study into the reproducibility of EID spectra would hope to demonstrate the benefits for incorporating EID data into existing spectral libraries to further develop the identification of unknown compounds.

The development of LC-EID has primarily focused on targeted LC-MS/MS, analysing one compound of interest per experiment. Preliminary investigations into data-dependent analyses, carrying out analysis of multiple compounds during one chromatographic experiment, experienced difficulties due to co-eluting ions of varying abundances. Data-dependent EID analyses requires further development to become an adaptable analytical technique for analysing complex mixtures. An alternative approach would involve setting up a segmented a LC-MS/MS method, targeting specific precursor ions during defined time segments, thereby allowing multiple ions to be analysed during one experiment. This method would ensure that only ions of interest are analysed, however co-eluting species would still pose an issue.

7.2. Protein MS Analysis

Due to rapid sample depletion of the MtrR protein, a limited number of LC-MS and LC-MS/MS experiments have been carried out thus far. Future work will include the repeated incubation of the MtrR protein with the β-lactamase inhibitors in order to determine whether the inhibitor-protein reactions are repeatable and to allow LC-MS/MS analysis to be carried out on the other suspected modified peptides. Incubating the MtrR protein and inhibitor for more time may increase the ratio of modified protein to unmodified protein, which would also improve the chances of observing modified peptides at an intensity suitable for LC-MS/MS and identifying other modification sites. The repetition of the incubation studies will also allow reaction monitoring to be carried out for each inhibitor in order to confirm whether some of the observed modifications are short-lived intermediates that will disappear over time as other species are formed. The *in silico* digests have thus far been carried out under the assumption that the inhibitor molecules only react with serine or threonine residues on the protein. Allowing for the possibility of modifications on other amino acid residues may lead to the identification of other modification sites that are not currently expected.

Fluorescence experiments carried out on the intact NBD-modified M protein indicate that the label primarily binds to a cysteine residue before transferring to a lysine residue upon incubation at 37 °C, as evidenced from a slight shift in the fluorescence and UV spectra.[**] The fluorescent labelling studies will be repeated in order to determine whether the modification site is always found on the Lys-71 residue, or whether NBD modification can be found a different amino acid, such as a cysteine residue. LC-MS/MS will be performed on the suspected modified peptide so as to confirm the location of the modification to within one amino acid residue.

[**] Carried out by James A. Freeth

The intact M protein has been found to degrade over time into smaller proteins of approximately 13-14 kDa in size. These degradation products appear to correspond to C-terminal containing proteins, cleaving along the amino acid chain linking the N-terminal domain to the C-terminal domain. Money *et al.* generated a model of the electrostatic surface of the M protein, noting that the C-terminal domain contained a large positively charged area that is proposed to interact with the negatively charged cell membrane. The N-terminal domain was found to contain a sizeable negatively charged region and is thought to be involved in protein-protein interactions. The absence of the reciprocal N-terminal domain in the MS spectrum is believed to be due to the overall negative charge on the domain, therefore further work will include analysing the degraded M protein by negative electrospray ionisation to confirm the presence of the N-terminal domain and to determine whether this domain is seen to oligomerise.

Future work will also include the development of MS procedures for analysing more hydrophobic and more difficult membrane proteins.

8. Materials and Methods

8.1. Default Instrumental Conditions and Parameters

8.1.1. LTQ-FT

An LTQ-FT mass spectrometer (Thermo-Finnigan Corporation, Germany) equipped with a 7.0 Tesla superconducting magnet and an ESI source was used for all FT-ICR-MS and FT-ICR-MS/MS analyses. Direct infusion analysis was administered *via* a syringe pump at a flow rate of 5 µL min^{-1}. Ion source conditions such as N_2 sheath gas flow, auxiliary gas flow, sweep gas flow, capillary voltage and tube lens were optimised to achieve the most stable and optimal signal for the ion of interest. The capillary needle was heated to 250 °C. The source cone voltage was held between 4 – 4.5 kV in positive ionisation mode and at -3.5 kV in negative ionisation mode. The LTQ linear ion trap contains a helium damping gas at a pressure of 10^{-3} Torr, used for collisional cooling of trapped ions as well as CID experiments. Isolation of the precursor ion for MS/MS analysis takes place in the ion trap using an isolation window of *m/z* 4 (unless otherwise stated) in order to encompass the entire isotopic profile of the ion of interest while eliminating any other ions. AGC for the ion trap was set at $3x10^4$ ions for MS scans and $1x10^4$ ions for MS/MS scans. FT experiments were carried out using a default maximum injection time of 1 s for MS analyses and 1.5 s for MS/MS analyses. Two microscans were recorded and averaged for each MS/MS scan in order to improve the sensitivity of the data produced. LC-MS/MS analyses were carried out by targeting a specific ion of interest and alternating MS and MS/MS scans throughout the experiment. A resolving power of 50,000 FWHM was used for LC-MS/MS analyses in the FT-ICR cell in order to minimise scan time while maintaining good mass resolution. All other experiments were carried out at 100,000 FWHM. AGC for the FT-ICR was set at $5x10^5$ ions for MS scans and $2x10^5$ ions for MS/MS scans. Spectra were analysed

using XCalibur QualBrowser version 2.0.7 (Thermo Fisher Scientific Inc.). When required, post-acquisition calibration was carried out using the embedded program Recalibrate Offline (Thermo Fisher Scientific Inc.) and performed using the empirical formulae of the precursor ion and, where possible, a known product ion.

Detection of CID product ions was carried out in either the LTQ ion trap (CID IT) or the FT-ICR cell (CID), and has been stated where appropriate. The normalised collision energies applied for CID analysis on the LTQ-FT have been stated in arbitrary units, as per manufacturer's software. ECD and EID analyses were carried out using low energy electrons generated by an indirectly heated dispenser cathode situated behind the FT-ICR cell. The calibration of the cathode was carried out using Substance P (purchased from Sigma-Aldrich, Dorset, UK), adjusting the voltage offset applied to the cathode so that the most efficient energy level for ECD analysis was 5 (arbitrary units). The corresponding electron energy has been calculated using **Equation 8.1**.

Electron Energy = Energy Level – Voltage Offset. **Equation 8.1**

The electron energies quotes have been adjusted according to the voltage offset applied to the cathode at the time of analysis. A default electron irradiation time of 70 ms and a delay of 0.03 ms were maintained, unless otherwise stated. IRMPD analyses were carried out on a similarly equipped LTQ-FT mass spectrometer, courtesy of AstraZeneca (Alderley Edge, UK), fitted with a 20 W CO_2 IR laser situated behind the FT-ICR cell and entering the cell through a ZnSe coated lens. The power and duration of the laser pulse was varied according to the resulting product ion spectra, between 10 – 100% and 50 – 300 ms respectively.

8.1.2. Xevo QToF / QToF Premier XE

QToF-MS and QToF-MS/MS analyses were carried out on one of two instruments; a Xevo QToF (Waters Ltd, UK) or a QToF Premier XE (Waters Ltd, UK) both equipped with an ESI source. The Xevo QToF included an interchangeable ASAP source with an auxiliary ESI probe incorporated into the ASAP source housing for simultaneous calibrant infusion during analysis. Spectra were analysed using MassLynx version 4.1 (Waters Ltd, UK). Accurate mass measurements were carried out using the embedded program Elemental Composition version 4.0.

ESI analysis was carried out *via* direct infusion using an in-built infusion system at a flow rate of up to 15 µL min^{-1}. The source temperature was set between 120 °C – 150 °C and the voltage applied to the capillary needle was ±3 kV depending on the polarity of ionisation. The nitrogen desolvation gas was heated to a temperature of 450 °C and infused at a flow rate of 600 L hr^{-1}. ASAP analysis was carried out on both solid and solution state samples, as stated where appropriate, by applying the sample to the exterior of a sealed glass melting point tube. The N_2 desolvation gas, used to volatilise the sample, was infused at a flow rate of 600 L hr^{-1} and the temperature in the range 100 °C – 600 °C according to the sample being analysed and the resulting MS spectrum. A current of 2.5 µA was applied to the corona needle. The auxiliary ESI probe was used, where stated, to infuse a 50:50 (v/v) mixture of methanol and water in order to create a proton-rich environment within the source enclosure.

The voltage offset applied to the MS source cone was 25 V. The argon buffer gas in the collision cell was maintained at a pressure of 7 psi with a gas flow rate of 0.3 mL min^{-1} and applied a voltage of 4 V (MS analyses only). The length of time taken per scan was 1 s. The detected mass range was varied according to the ion(s) of interest. Spectra were recorded in centroid mode. QToF-CID analyses were carried

out by increasing the collision energy applied to the ions in order to promote collisions with the argon buffer gas. The collision energy was varied according to the sample being analysed and the subsequent MS/MS spectrum, usually between 20 V – 40 V, and has been stated where necessary.

8.1.3. GC Trace

All GC-MS analyses were carried out on a GC Trace (Thermo-Finnigan Corporation, Germany) fitted with an EI source. 1 µL aliquots of each sample were injected through a GC inlet heated to 220 °C to evaporate the solvent and subsequently infused into a helium carrier gas flow of 25 mL min^{-1} prior to a 20:1 split. The resulting gas flow of approximately 1 mL min^{-1} was directed onto a 30 m VF—5MS GC column with a 0.25 mm inner diameter and a 0.25 µm film thickness. A 26 minute temperature gradient was used, ramping from an initial temperature of 40 °C to a maximum at 300 °C at a rate of 10 °C min^{-1}. The emission current applied to the heated wire filament (electron source) was 150 µA, the electron energy was 70eV, and the MS source temperature was set at 200 °C. Ions were detected over the mass range *m/z* 20 - *m/z* 680 using a single quadrupole mass spectrometer. Spectra were analysed using XCalibur QualBrowser version 2.0.7 (Thermo Fisher Scientific Inc.).

8.2. Instrumental Parameters for Chapter 3

8.2.1. Sample Preparation

All solvents were HPLC grade, purchased from Sigma-Aldrich, Dorset, UK. Cediranib, Ritonavir, Gefitinib, Omeprazole and samples labelled with the prefix AZ- were supplied by AstraZeneca, Avlon, UK. All other samples were purchased from Sigma-Aldrich, Dorset, UK. The haloperidol dilution series was carried out using samples of haloperidol made up in methanol to a range of concentrations; from 10

pg mL^{-1} and 50 pg mL^{-1} increasing ten-fold until 0.5 mg mL^{-1} and 1 mg mL^{-1}. All other samples analysed by direct infusion were made up to 5 µg mL^{-1} and 10 µg mL^{-1} in methanol and selected according to the intensity of the ion(s) of interest.

8.2.2. Mass Spectrometry

The offset applied to the cold cathode electron gun was set to 1.21 V, resulting in approximate electron energies of 18.79 eV for EID and hECD experiments and 3.79 eV for low energy EID and ECD experiments. Electron energy studies involved increasing the energy level stepwise from 0 to 25 arbitrary units which corresponds to approximately -0.21 eV to 23.79 eV (in increments of 1 eV), allowing 90 seconds acquisition time per energy level. An electron irradiation time of 70 ms, a delay of 0.03 ms and a maximum injection time of 1.5 s were maintained. One microscan per MS/MS scan was recorded for the haloperidol dilution series. The laser power for IRMPD analysis was optimised for each compound to produce the greatest degree of fragmentation. The IRMPD pulse duration was varied according to the resultant spectra.

8.3. Instrumental Parameters for Chapter 4

8.3.1. Sample Preparation

A sample of cediranib was obtained courtesy of AstraZeneca, Avlon, UK. All solvents were HPLC grade, purchased from Sigma-Aldrich, Dorset, UK. Cediranib was made up to three different concentrations in methanol depending on the method of analysis; 2 mg mL^{-1} sample for LC-MS and LC-MS/MS, 5 µg mL^{-1} sample for direct infusion MS and MS/MS and a 1 mg mL^{-1} sample for GC-MS.

8.3.2. Chromatography

For the purposes of chromatography, 10 µL aliquots of the cediranib sample were injected onto a Luna C18 (2) 3 µm, 100 Å, 2x150 mm column (Phenomenex) which required a 200 µL min^{-1} mobile phase flow rate. Gradient conditions started at 95% (H_2O + 0.1% formic acid) / 5% (CH_3CN + 0.1% formic acid) and finished at 5% (H_2O + 0.1% formic acid) / 95% (CH_3CN + 0.1% formic acid. A 12 minute gradient was used, resulting in an overall analysis time of 20 minutes to include a wash step at 100% acetonitrile and equilibration of starting solvent conditions. In order to induce sodium-adducted species, a 1 mg mL^{-1} solution of sodium iodide solution was infused post-column using a T-piece, *via* syringe pump at a flow-rate of 2 µL min^{-1}.

8.3.3. Mass Spectrometry

Direct infusion QTof-CID was performed at a normalised collision energy of 25 V. For the LC-MS/MS analysis of the compound observed at *m/z* 921 (LC peak **10**) the isolation width was increased to *m/z* 8 in order to incorporate the chlorine isotope. The normalised collision energy for LC-CID detected in the LTQ ion trap was generated at CID energy 18 (as per manufacturer's software) and LC-CID data detected in the FT were produced at CID energy 30. The voltage offset applied to the cathode was 2.5 V for LC-EID experiments resulting in the approximate electron energy of 17.5 eV for EID analysis. The offset during direct infusion EID analysis and ECD analysis was 2.1 V resulting in the corresponding electron energy of 17.9 eV and 2.9 eV respectively.

8.4. Instrumental Parameters for Chapter 5

8.4.1. Sample Preparation

All solvents and reagents were purchased from Sigma-Aldrich, Dorset, UK. HPLC grade solvents were used. Samples of recombinant MtrR protein were obtained from Matthew F. Burton (Durham University). Samples of recombinant M protein were obtained from James A. Freeth (Durham University).

8.4.2. Chromatography

Two columns were used for liquid chromatography depending on the nature of the compounds being analysed. Protein LC-MS was carried out on a X-Bridge BEH300 C_4 3.5 µm, 2.1x150 mm column (Waters, Ltd.) capable of a solvent flow rate of 200 µL min^{-1}. Peptide LC-MS analysis was carried out on an Atlantis dC_{18} 5 µm, 1.0 x 50 mm column (Waters, Ltd) with a maximum solvent flow rate of 100 µL min^{-1}. Samples were injected onto the relevant column with an injection volume of between 1 – 10 µL, depending on the sample concentration. Gradient conditions started at 95% (H_2O + 0.1% formic acid) / 5% (CH_3CN + 0.1% formic acid) and finished at 5% (H_2O + 0.1% formic acid) / 95% (CH_3CN + 0.1% formic acid). The length of the LC gradient was optimised to 12 minutes, allowing for an overall experiment time of 20 minutes to incorporate a wash step at 100% acetonitrile and equilibration of starting solvent conditions. LC-MS and LC-MS/MS of the tryptic digests were performed using the peptide column, using a 13 minute LC gradient, but at a reduced flow rate of 100 µL min^{-1} resulting in a total analysis time of 20 minutes.

8.4.3. MtrR Protein

Modification of the protein was carried out by incubating equal parts of MtrR protein (39 µM) with tazobactam or clavulanic acid (8 mg mL^{-1}) at 37 °C for up to 4 hours. The protein was precipitated using an excess of ice cold acetone and the mixture was stored at -20 °C for 1 hour. The trypsin digest was performed using a starting

solution containing 0.2 mg mL^{-1} trypsin in hydrochloric acid (1 mM), of which 1 µL was added to 20 µL of ammonium hydrogen carbonate buffer (25 mM). The protein-trypsin mixture was incubated at 37 °C overnight, before freeze-drying to remove the solvent. The resulting peptide mixture was re-dissolved in 50:50 water:acetonitrile (v/v) for MS analysis.

LC-MS/MS Analysis of Tryptic Peptide of MtrR Protein

LC-MS/MS of one MtrR tryptic peptide was carried out by targeting the $[M+3H]^{3+}$ ion at *m/z* 423.8 for analysis. A total of 10 MS/MS scans were found to contain useable data to produce the MS/MS spectrum shown in **Figure 5.17.** The offset applied to the cathode was 3.69 V, resulting in an electron energy of 2.31 eV being applied to the precursor ion. A maximum injection time of 1000 ms was used in order to reduce the length of time taken for each scan.

8.4.4. M Protein

Samples of M protein were obtained in phosphate buffered saline containing 137 mM sodium chloride (NaCl), 2.7 mM potassium chloride (KCl), 8 mM disodium hydrogen phosphate (Na_2HPO_4) and 1.46 mM potassium dihydrogen phosphate (KH_2PO_4). The protein concentration varied according to the results from protein expression. Modification of M protein, performed by J. A. Freeth, was achieved by mixing M protein (~ 20 µM) and 4-chloro-7-nitrobenzofurazan (1 mM in DMSO) in a 1:1 molar ratio. The resultant mixture was incubated at room temperature for 1 hour at pH 7.4. The protein sample was dialysed into water in order to remove salts and buffers from the sample.

Tryptic Digests

In order to perform the tryptic digest of the M protein, a buffer solution of Tris(hydroxymethyl)aminomethane (50 mM) and calcium chloride (10 mM), pH 7.6

(hereafter referred to as Tris buffer), which was used as a key component in the solutions involved in digestion. Protein samples were made up to an approximate concentration of 0.5 mg mL^{-1} in Tris buffer. Trypsin was dissolved in 1% acetic acid to a concentration of 10 µg $µL^{-1}$, of which 2 µL was added to 80 µL of Tris buffer to a final concentration of 0.25 mg mL^{-1} trypsin. Dithiothreitol (DTT) was dissolved in Tris buffer to a final concentration of 100 mg mL^{-1}. A 1 µL aliquot of the trypsin solution and 3 µL of DTT solution were added to each 100 µL volume of protein. The resultant mixture was shaken at 37 °C for 1-2 hours prior to MS analysis.

LC-MS/MS Analysis of Tryptic Peptide of M Protein

LC-MS/MS was carried out on one M protein tryptic peptide, proposed to correspond to an N-terminal peptide, by targeting the $[M+2H]^{2+}$ ion at *m/z* 748.3 for analysis. A total of 7 CID MS/MS scans and 6 ECD MS/MS scans were found to contain useable data to produce the MS/MS spectra shown in **Figure 5.23.** The ECD offset applied to the cathode was 2.11 V, resulting in an electron energy of 4.89 eV being applied to the precursor ion. CID analysis was carried out at a normalised collision energy of 20. A maximum injection time of 1000 ms was used for both LC-MS/MS analyses in order to reduce the length of time taken for each scan.

9. Appendix A: Supplementary Information for Chapter 3 – Electron Induced Dissociation of Small Singly Charged Molecules.

9.1. Effect of electron energy on mass accuracy

As the electron energy was increased, the mass accuracy of the precursor ion was seen to deteriorate, as illustrated in **Figure 9.1**, noting a sharp increase in the mass deviation of the precursor ion as the energy is increased beyond 7.79 eV. A similar decline in the mass accuracy of the product ions is also observed as the electron energy increases.

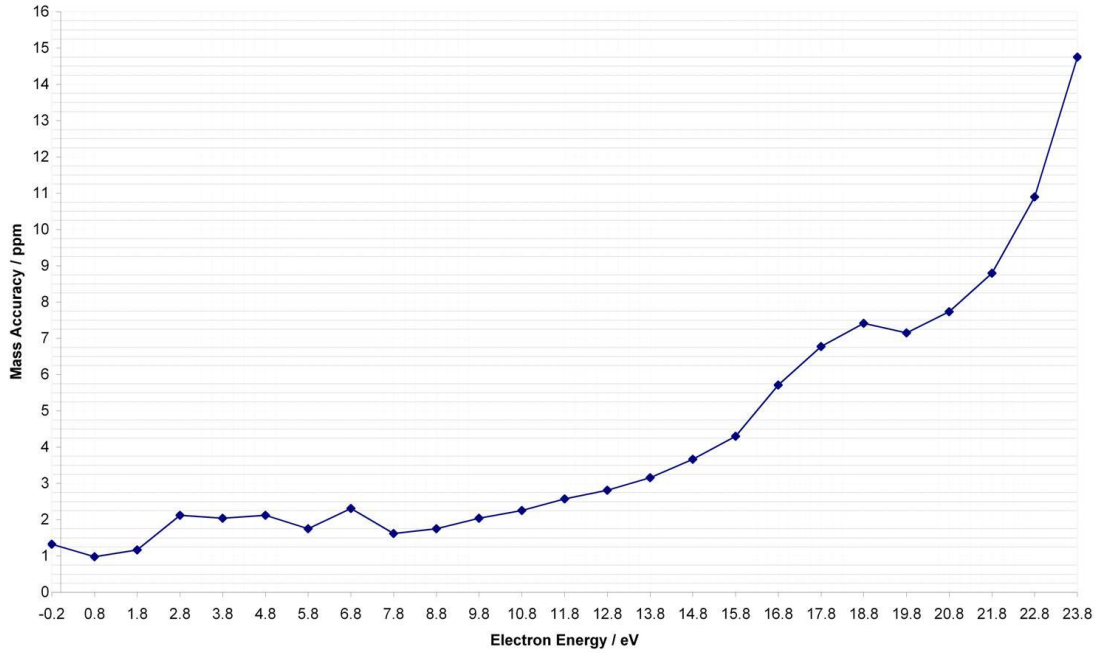

Figure 9.1: The effect of increasing the electron energy on the mass accuracy of the Haloperidol [M+H]+ precursor.

9.2. Validation of artefact peaks

As the electron energy was increased, a number of peaks are seen to appear in the low *m/z* region (< *m/z* 120) that could not be assigned as fragments of the precursor ion, and were therefore purported to correspond to contaminants being emitted from

the cathode or the FT-ICR cell at high electron energies. The accurate mass measurements suggest that these peaks correspond to hydrocarbons emanating from the ECD cathode or the inner surface of the FT-ICR cell under the high energy conditions.

In order to establish which peaks could be removed from further consideration, two control spectra were recorded during an infusion of methanol with the ESI spray voltage turned off in order to disable electrospray ionisation. The distribution of peaks observed in **Figure 9.2(a)** is considered to be electronic or chemical noise originating from the FT-ICR cell. When the ECD cathode was turned on and emitting high energy electrons (~ 28 eV), peaks in the low *m/z* region emerge, as shown in **Figure 9.2(b)** and expanded in **Figure 9.3**.

The peaks observed in the control spectra have been disregarded in all MS and MS/MS spectra.

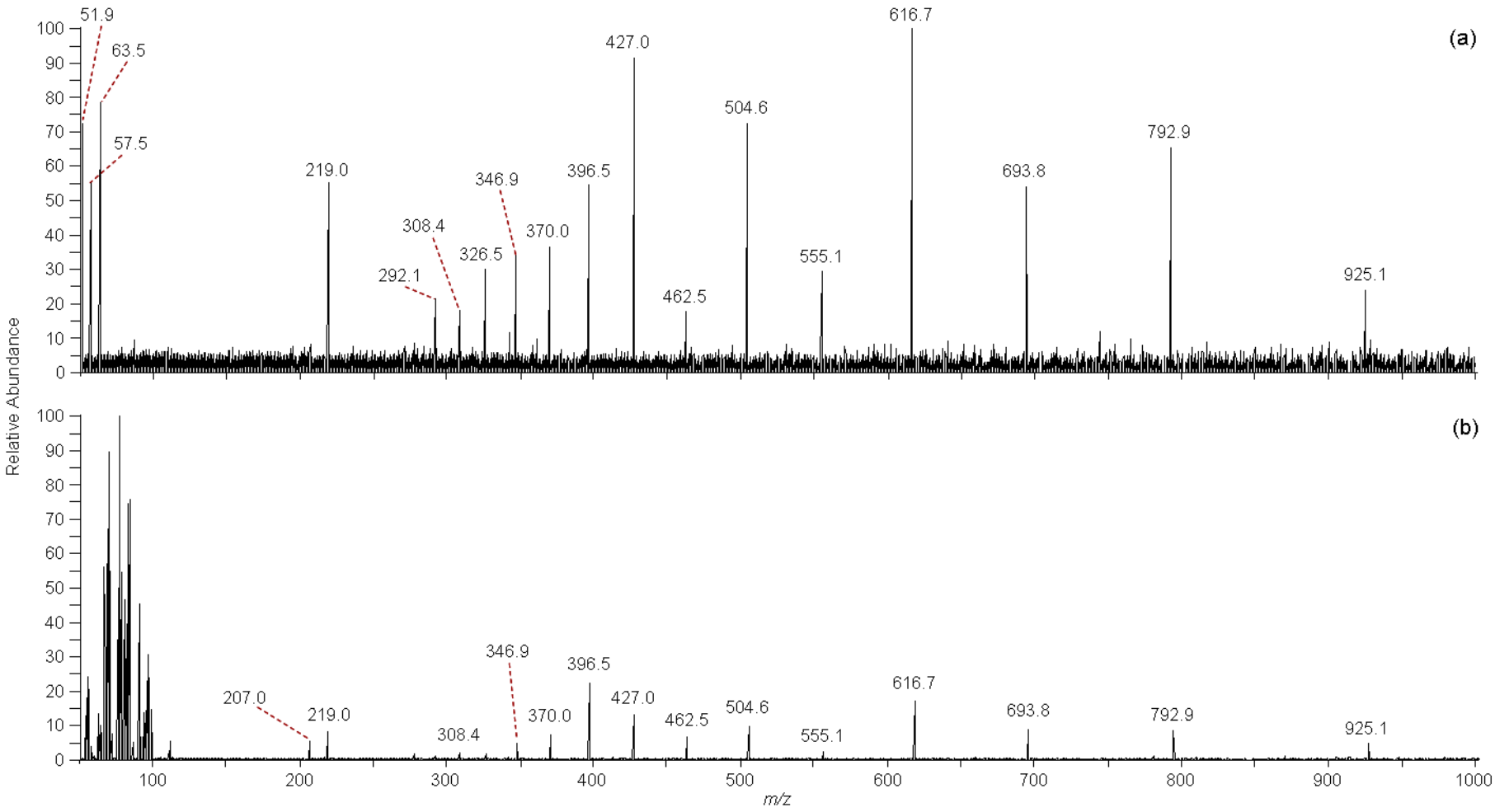

Figure 9.2: MS control spectra indicating artefact peaks (a) with the ECD cathode switched off (b) with the ECD cathode on.

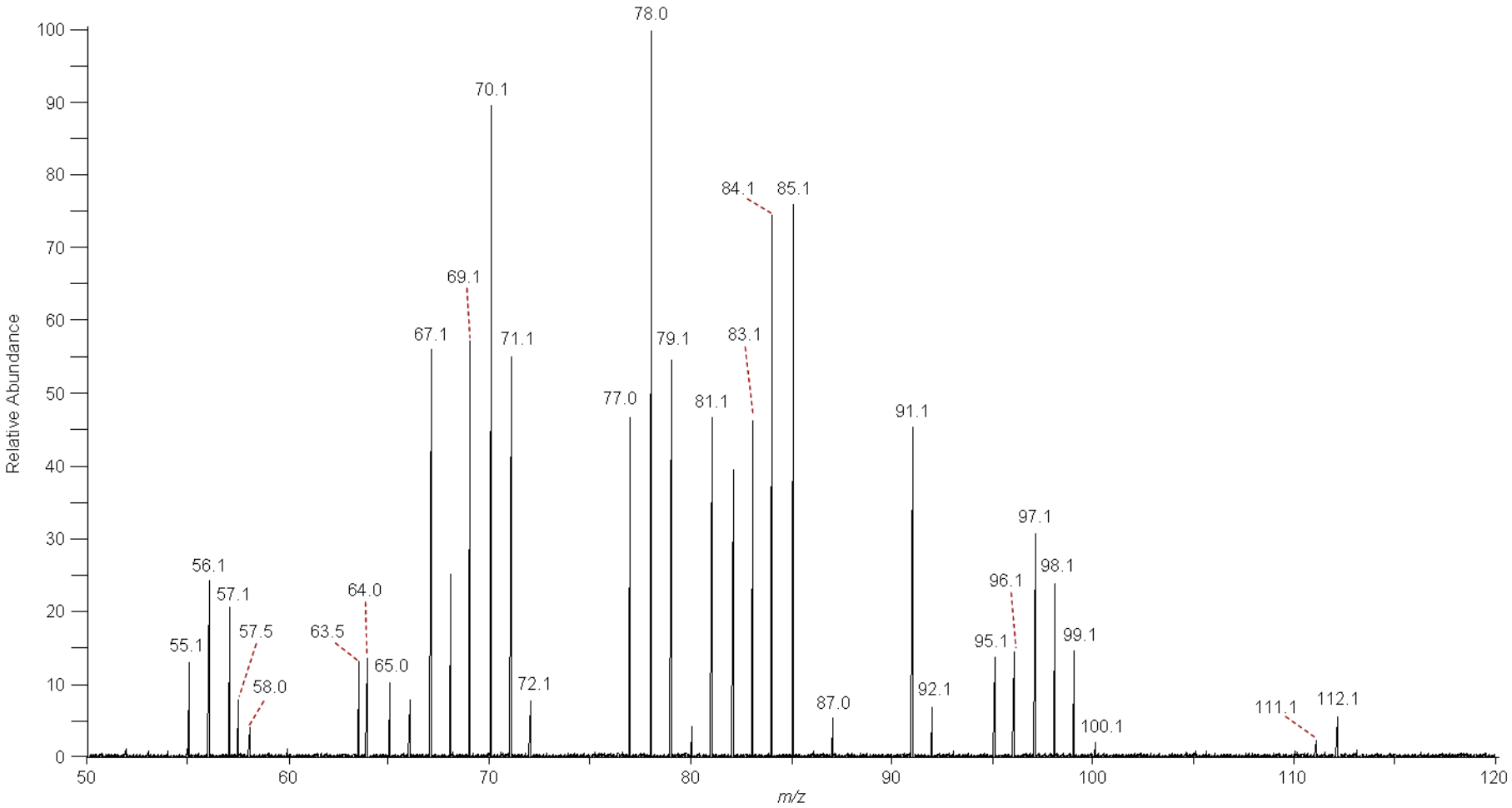

Figure 9.3:Expansion of Figure 9.2(b) showing the low m/z peaks that emerge at high electron energies.

10. Appendix B: Supplementary Information for Chapter 4 – The Development of Electron Induced Dissociation for use in conjunction with LC-MS to analyse complex mixtures.

The following tables detail the product ions generated for cediranib and the two unknown compounds that have been examined in **Chapter 4**, including the assigned molecular formulae, the corresponding RDB values and the mass deviation between the measured *m/z* and the theoretical *m/z* for the proposed formulae for each observed ion. The precursor ion for each experiment has been highlighted in bold. Spectra have been calibrated post-acquisition using the theoretical *m/z* values of the precursor ion and in some cases a known product ions, marked * in the tables; Ions observed in the ion trap have been quoted to the nearest integer unless there is corresponding FT data to accurately assign molecular formulae and accurate mass measurements. Ions labelled 'Y' indicate the presence of an ion at the specified *m/z*.

10.1. LC-MS/MS of cediranib

Table 10.1 details the product ions generated from MS/MS analysis of the protonated cediranib species observed at *m/z* 451.2. The resulting FT data was calibrated using the theoretical *m/z* of the precursor ion with the molecular formula $C_{25}H_{28}N_4O_3F$ and, for EID only, the propylpyrrolidine group with the proposed molecular formula $C_7H_{14}N$.

Theoretical *m/z*	Molecular Formula	RDB	EID / ppm	CID FT / ppm	CID IT
451.21400	**$C_{25}H_{28}N_4O_3F$**	**13.5**	***0.0**	***0.0**	**Y**
450.20617	$C_{25}H_{27}N_4O_3F$	14	2.6	-	-
449.19835	$C_{25}H_{26}N_4O_3F$	14.5	-0.2	-	Y
431.20777	$C_{25}H_{27}N_4O_3$	14.5	-	0.3	Y
421.3	*unknown*	-	-	-	Y
405.1	*unknown*	-	-	-	Y
392.3	*unknown*	-	-	-	Y
380.14050	$C_{21}H_{19}N_3O_3F$	13.5	0.3	-	Y
366.12485	$C_{20}H_{17}N_3O_3F$	13.5	1.6	-	Y
354.12485	$C_{19}H_{17}N_3O_3F$	12.5	-	-0.5	Y
340.10920	$C_{18}H_{15}N_3O_3F$	12.5	2.1	-0.6	Y
339.10137	$C_{18}H_{14}N_3O_3F$	13	1.6	-	-
338.09355	$C_{18}H_{13}N_3O_3F$	13.5	0.9	-	-
326.09355	$C_{17}H_{13}N_3O_3F$	12.5	1.0	-	-
325.08572	$C_{17}H_{12}N_3O_3F$	13	1.5	-	-
324.11428	$C_{18}H_{15}N_3O_2F$	12.5	1.2	-	Y
320.10297	$C_{18}H_{14}N_3O_3$	13.5	1.3	-	-
319.09514	$C_{18}H_{13}N_3O_3$	14	1.4	-	-
318.08732	$C_{18}H_{12}N_3O_3$	14.5	1.5	-	-
306.08732	$C_{17}H_{12}N_3O_3$	13.5	1.3	-	-
305.07949	$C_{17}H_{11}N_3O_3$	14	1.4	-	-
304.10805	$C_{18}H_{14}N_3O_2$	13.5	1.3	-	-
287.16283	$C_{16}H_{21}N_3O_2$	8	0.9	-	-
280.7	*unknown*	-	-	-	Y
260.15193	$C_{15}H_{20}N_2O_2$	7	1.0	-	-
232.2	*unknown*	-	-	-	Y
175.06660	$C_{10}H_8N_2F$	7.5	0.4	-	-
165.05844	C_9H_8NOF	6	0.2	-	-
164.05062	C_9H_7NOF	6.5	0.4	-	-
149.06353	C_9H_8NF	6	0.1	-	-
148.05570	C_9H_7NF	6.5	0.2	-	-
143.8	*unknown*	-	-	-	Y
128.10699	$C_7H_{14}NO$	1.5	0.2	-	Y
118.06513	C_8H_8N	5.5	0.4	-	-
112.11208	$C_7H_{14}N$	1.5	*0.0	-	-
111.10425	$C_7H_{13}N$	2	0.1	-	-
110.09643	$C_7H_{12}N$	2.5	0.1	-	-
96.08078	$C_6H_{10}N$	2.5	0.1	-	-
84.08078	$C_5H_{10}N$	1.5	0.3	-	-
83.07295	C_5H_9N	2	0.4	-	-
82.06516	C_5H_8N	2.5	0.4	-	-
70.06517	C_4H_8N	1.5	0.6	-	-

Table 10.1: Summary of product ions observed from the MS/MS of cediranib $[M+H]^+$.

10.2. LC-MS/MS of unknown species in cediranib sample

Table 10.2 details the product ions generated from MS/MS analysis of the species detected in LC peak **1**, observed at *m/z* 562.3. The resulting FT data was calibrated

using the theoretical *m/z* of the precursor ion with the proposed molecular formula $C_{32}H_{41}N_5O_3F$, determined from the previously run MS spectrum.

Theoretical *m/z*	Molecular Formula	RDB	EID / ppm	CID FT / ppm	CID IT	Present in cediranib
562.31879	**$C_{32}H_{41}N_5O_3F$**	**14.5**	***-0.0**	**-**	**Y**	**-**
560.30314	$C_{32}H_{39}N_5O_3F$	15.5	0.7	-	Y	-
542.31257	$C_{32}H_{40}N_5O_3$	15.5	3.4	-	Y	-
532.3	*unknown*	-	-	-	Y	-
503.3	*unknown*	-	-	-	Y	-
491.3	*unknown*	-	-	-	Y	-
465.3	*unknown*	-	-	-	Y	-
451.21400	$C_{25}H_{28}N_4O_3F$	13.5	2.3	-	-	Y
449.19835	$C_{25}H_{26}N_4O_3F$	14.5		-	Y	Y
436.19052	$C_{24}H_{25}N_4O_3F$	14	2.3	-	-	-
433.3	*unknown*	-	-	-	Y	-
380.14050	$C_{21}H_{19}N_3O_3F$	13.5	-	-	Y	Y
360.13427	$C_{21}H_{18}N_3O_3$	14.5	1.4	-	-	-
340.10920	$C_{18}H_{15}N_3O_3F$	12.5	2.3	-	-	Y
336.2	*unknown*	-	-	-	Y	-
326.09355	$C_{17}H_{13}N_3O_3F$	12.5	1.0	-	-	Y
319.09514	$C_{18}H_{13}N_3O_3$	14	-0.2	-	-	Y
318.08732	$C_{18}H_{12}N_3O_3$	14.5	1.5	-	-	Y
308.08298	$C_{17}H_{11}N_3O_2F$	13.5	4.4	-	-	-
304.10805	$C_{18}H_{14}N_3O_2$	13.5	-	-	Y	Y
290.09240	$C_{17}H_{12}N_3O_2$	13.5	2.4	-	-	-
259.3	*unknown*	-	-	-	Y	-
223.21688	$C_{14}H_{27}N_2$	2.5	0.6	-	Y	-
183.3	*unknown*	-	-	-	Y	-
146.06004	C_9H_8NO	6.5	0.2	-	-	-
140.14338	$C_9H_{18}N$	1.5	0.0	-	-	-
126.12773	$C_8H_{16}N$	1.5	0.3	-	-	-
118.06513	C_8H_8N	5.5	0.4	-	-	Y
112.11208	$C_7H_{14}N$	1.5	*0.0	-	-	Y
111.10425	$C_7H_{13}N$	2	0.1	-	-	Y
110.09643	$C_7H_{12}N$	2.5	0.1	-	-	Y
96.08078	$C_6H_{10}N$	2.5	0.3	-	-	Y
84.08078	$C_5H_{10}N$	1.5	0.4	-	-	Y
70.06513	C_4H_8N	1.5	0.8	-	-	Y

Table 10.2: Summary of product ions generated from the MS/MS of LC Peak 1, observed at *m/z* 562.2.

Table 10.3 details the product ions generated from MS/MS analysis of the species detected in LC peak **6**, observed at *m/z* 340.1. The resulting FT data was calibrated

using the theoretical *m/z* of the precursor ion with the proposed molecular formula $C_{18}H_{15}N_3O_3F$, determined from the previously run MS spectrum.

Theoretical *m/z*	Molecular Formula	RDB	EID / ppm	CID FT / ppm	CID IT	Present in cediranib
340.10920	**$C_{18}H_{15}N_3O_3F$**	**12.5**	***0.0**	***0.0**	**Y**	**Y**
339.10137	$C_{18}H_{14}N_3O_3F$	13	1.4	-0.3	-	Y
338.09355	$C_{18}H_{13}N_3O_3F$	13.5	0.6	0.3	Y	Y
336.07790	$C_{18}H_{11}N_3O_3F$	14.5	-0.8	0.9	-	-
325.08572	$C_{17}H_{12}N_3O_3F$	13	1.1	0.6	Y	Y
324.07790	$C_{17}H_{11}N_3O_3F$	13.5	0.5	1.7	Y	Y
320.10297	$C_{18}H_{14}N_3O_3$	13.5	0.4	1.2	Y	Y
319.09514	$C_{18}H_{13}N_3O_3$	14	0.2	0.5	Y	Y
318.08732	$C_{18}H_{12}N_3O_3$	14.5	1.4	1.1	Y	Y
312.11428	$C_{17}H_{15}N_3O_2F$	11.5	0.3	1.2	Y	-
310.09863	$C_{17}H_{13}N_3O_2F$	12.5	0.5	1.3	Y	-
308.08298	$C_{17}H_{11}N_3O_2F$	13.5	0.1	1.2	Y	-
305.07949	$C_{17}H_{11}N_3O_3$	14	0.5	1.0	Y	Y
304.07167	$C_{17}H_{10}N_3O_3$	14.5	0.5	-	Y	Y
300.07675	$C_{18}H_{10}N_3O_2$	15.5	-	1.1	Y	-
297.09081	$C_{16}H_{12}N_3O_2F$	12	-0.0	1.1	Y	-
296.08298	$C_{16}H_{11}N_3O_2F$	12.5	-0.4	-	-	-
292.10805	$C_{17}H_{14}N_3O_2$	12.5	-0.1	0.8	Y	-
290.09240	$C_{17}H_{12}N_3O_2$	13.5	0.2	1.3	Y	-
288.07675	$C_{17}H_{10}N_3O_2$	14.5	-0.5	-	-	-
282.2	*unknown*	-	-	-	Y	-
277.08458	$C_{16}H_{11}N_3O_2$	13	-0.5	1.0	Y	-
276.07675	$C_{16}H_{10}N_3O_2$	13.5	-0.5	-	-	-
275.06893	$C_{16}H_9N_3O_2$	14	-0.3	-	-	-
269.07208	$C_{15}H_{10}N_2O_2F$	11.5	-0.3	-	Y	-
268.08807	$C_{15}H_{11}N_3OF$	11.5	-0.5	-	-	-
267.08024	$C_{15}H_{10}N_3OF$	12	-	-	Y	-
265.07717	$C_{16}H_{10}N_2OF$	12.5	-	-	Y	-
262.09749	$C_{16}H_{12}N_3O$	12.5	-0.7	-	Y	-
260.08184	$C_{16}H_{10}N_3O$	13.5	-0.6	-	-	Y
254.08499	$C_{15}H_{11}N_2OF$	11	-0.6	-	-	-
253.07717	$C_{15}H_{10}N_2OF$	11.5	-0.5	-	-	-
252.09315	$C_{15}H_{11}N_3F$	11.5	-1.0	1.0	Y	-
249.08966	$C_{15}H_{11}N_3O$	12	-0.9	0.9	Y	-
248.08184	$C_{15}H_{10}N_3O$	12.5	-0.9	-	-	-
240.09315	$C_{14}H_{11}N_3F$	10.5	-1.3	-	-	-
237.2	*unknown*	-	-	-	Y	-
232.08692	$C_{15}H_{10}N_3$	12.5	-0.9	-	-	Y
225.08225	$C_{14}H_{10}N_2F$	10.5	-1.6	-	-	-
222.07876	$C_{14}H_{10}N_2O$	11	-1.2	-	-	-
221.07094	$C_{14}H_9N_2O$	11.5	-1.4	-	-	-
210.05878	$C_{13}H_7N_2F$	11	-1.5	-	-	-
207.2	*unknown*	-	-	-	Y	-
203.06037	$C_{14}H_7N_2$	12.5	-2.2	-	-	-
193.06077	$C_9H_9N_2O_3$	6.5	-2.1	-	-	-
191.04512	$C_9H_7N_2O_3$	7.5	-2.1	-	Y	-
189.02947	$C_9H_5N_2O_3$	8.5	-2.1	-	Y	-
178.03729	$C_8H_6N_2O_3$	7	-3.0	-	-	-

177.06585	$C_9H_9N_2O_2$	6.5	-2.6	-	-	-
176.05803	$C_9H_8N_2O_2$	7	-2.4	-	-	-
175.06660	$C_{10}H_8N_2F$	7.5	-2.5	-	Y	Y
173.05095	$C_{10}H_6N_2F$	8.5	-2.6	-	-	-
170.05602	$C_6H_8N_3O_3$	4.5	-	-2.5	-	-
165.05844	C_9H_8NOF	6	-2.7	-	-	Y
164.05062	C_9H_7NOF	6.5	-2.8	-	-	Y
164.03422	$C_8H_6NO_3$	6.5	-2.6	0.9	Y	-
155.06037	$C_{10}H_7N_2$	8.5	-2.9	-	-	-
152.03422	$C_7H_6NO_3$	5.5	-3.0	-	-	-
151.02639	$C_7H_5NO_3$	6	-3.0	-	-	-
149.06353	C_9H_8NF	6	-3.1	-	Y	Y
148.05570	C_9H_7NF	6.5	-3.1	-	Y	Y
147.04788	C_9H_6NF	7	-3.0	-	Y	-
146.06004	C_9H_8NO	6.5	-3.0	-	-	-
144.04439	C_9H_6NO	7.5	-3.0	-	-	-
138.05496	$C_7H_8NO_2$	4.5	-3.2	-	Y	-
136.05570	C_8H_7NF	5.5	-3.2			
136.03930	$C_7H_6NO_2$	5.5	-3.3	-	Y	-
135.04788	C_8H_6NF	6	-3.3	-	-	-
134.02365	$C_7H_4NO_2$	6.5	-3.2	-	-	-
128.04948	C_9H_6N	7.5	-3.3	-	-	-
123.03148	$C_6H_5NO_2$	5	-3.6	-	-	-
121.04480	C_8H_6F	5.5	-3.5	-	-	-
120.03698	C_8H_5F	6	-3.6	-	-	-
116.04948	C_8H_6N	6.5	-3.6	-	-	-
108.04439	C_6H_6NO	4.5	-3.7	-	Y	-
101.03858	C_8H_5	6.5	-3.7	-	-	-
95.03657	C_5H_5NO	4	-3.8	-	-	-
80.04948	C_5H_6N	3.5	-3.8	-	-	-

Table 10.3: Summary of product ions generated from the MS/MS of LC Peak 6, observed at *m/z* 340.1.

10.3. LC-EID of cediranib $[M+Na]^+$

Table 10.4 details the product ions generated from MS/MS analysis of the sodium-adducted cediranib species observed at *m/z* 473.2. The resulting FT data was calibrated using the theoretical *m/z* of the precursor ion with the molecular formula $C_{25}H_{27}N_4O_3FNa$ and the propylpyrrolidine group with the proposed molecular formula $C_7H_{14}N$. Peaks labelled (-Na/+H) indicate product ions that are present as a sodium-adducted species in the EID spectrum of the $[M+Na]^+$, and as a protonated species in the EID of the $[M+H]^+$.

Theoretical *m/z*	Molecular Formula	RDB	EID / ppm	Present in $[M+H]^+$
473.19594	**$C_{25}H_{27}N_4O_3FNa$**	**13.5**	***0.0**	**N/A**
472.18812	$C_{25}H_{26}N_4O_3FNa$	14	2.4	Y (-Na/+H)
453.18971	$C_{25}H_{26}N_4O_3Na$	14.5	2.0	Y (-Na/+H)
452.18189	$C_{25}H_{25}N_4O_3Na$	15	2.7	-
438.16624	$C_{24}H_{23}N_4O_3Na$	15	0.5	-
421.16350	$C_{24}H_{22}N_4O_2Na$	15.5	2.3	-
373.11970	$C_{20}H_{17}N_3O_2FNa$	13	2.1	-
362.09114	$C_{18}H_{14}N_3O_3FNa$	12.5	1.6	Y (-Na/+H)
361.08332	$C_{18}H_{13}N_3O_3FNa$	13	1.1	Y (-Na/+H)
360.07549	$C_{18}H_{12}N_3O_3FNa$	13.5	1.7	Y (-Na/+H)
342.08491	$C_{18}H_{13}N_3O_3Na$	13.5	1.7	Y (-Na/+H)
341.07709	$C_{18}H_{12}N_3O_3Na$	14	1.6	Y (-Na/+H)
340.10920	$C_{18}H_{15}N_3O_3F$	12.5	1.7	Y
327.06144	$C_{17}H_{10}N_3O_3Na$	14	1.5	Y (-Na/+H)
187.04039	C_9H_7ONFNa	6	0.8	-
112.11208	$C_7H_{14}N$	1.5	*0.0	Y
110.09643	$C_7H_{12}N$	2.5	-0.1	Y
84.08078	$C_5H_{10}N$	1.5	-0.3	Y

Table 10.4: Summary of product ions generated from the MS/MS of sodium-adducted cediranib, observed at *m/z* 473.2.

11. Appendix C: Supplementary Information for Chapter 5 – MS and MS/MS Analysis of Proteins Modified by Small Organic Molecules.

The following tables detail the MS analysis of the tryptic digests of the protein samples that have been discussed in **Chapter 5**, including sequence information, molecular formulae, theoretical *m/z* values and the corresponding mass deviation associated with the experimentally obtained data.

Table 11.1 details the tryptic peptides generated by enzymatic digestion of the native MtrR protein, the tazobactam treated protein and the clavulanic acid treated protein. The peptides highlighted in red are proposed to contain modifications to the native amino acid sequence.

Table **11**.**2** details the tryptic peptides generated by enzymatic digestion of the native M protein and the NBD-labelled M protein. The peptide highlighted in red is proposed to contain the NBD modification.

Residues	Theoretical Monoisotopic $[M+H]^+$ *m/z*	Native MtrR /ppm	Tazobactam /ppm	Clavulanic Acid /ppm	Sequence	Protonated Molecular Formula
[12- 18] [14- 20]	790.46689	0.310	-0.651	-0.664	TKTEALK TEALKTK	$C_{34}H_{63}N_9O_{12}$
[14- 18]	561.32425	0.422	-0.825	-0.772	TEALK	$C_{24}H_{44}N_6O_9$
[19- 33]	1822.95202	0.929	0.260	0.403	TKEHLMLAALETFYR	$C_{83}H_{132}N_{21}O_{23}S$
[19- 33]	**1892.95750**	**-**	**0.573**	**0.621**	**TKEHLMLAALETFYR + $C_3H_2O_2$**	**$C_{86}H_{134}N_{21}O_{25}S$**
[19- 33]	**1965.97387**	**-**	**0.616**	**0.634**	**TKEHLMLAALETFYR + $C_5H_5NO_4$**	**$C_{88}H_{137}N_{22}O_{27}S$**
[21- 33]	1593.80937	1.34	0.273	0.405	EHLMLAALETFYR	$C_{73}H_{113}N_{18}O_{20}S$
[21- 34]	1721.90434	-	-	0.042	EHLMLAALETFYRK	$C_{79}H_{125}N_{20}O_{21}S$
[21- 33]	**1663.81485**	**-**	**1.723**	**2.973**	**EHLMLAALETFYR + $C_3H_2O_2$**	**$C_{76}H_{115}N_{18}O_{22}S$**
[21- 62]	**4918.55735**	**-**	**-**	**0.024**	**EHLMLAALETFYRKGIARTSLNEIAQAAGVTRGALYWH FKNK + $C_5H_5NO_4$**	**$C_{222}H_{346}N_{63}O_{62}S$**
[34- 38]	544.3565	-	-0.967	-1.004	KGIAR	$C_{23}H_{45}N_9O_6$
[35- 38]	416.26159	-	-0.994	-0.946	GIAR	$C_{17}H_{33}N_7O_5$
[39- 52]	1430.75978	1.767	0.788	0.795	TSLNEIAQAAGVTR	$C_{59}H_{104}N_{19}O_{22}$
[39- 72]	3910.00348	-	-	1.215	TSLNEIAQAAGVTRGALYWHFKNKEDLFDALFQR	$C_{178}H_{270}N_{49}O_{51}$
[53- 60]	1021.52541	0.066	-0.502	-0.492	GALYWHFK	$C_{52}H_{69}N_{12}O_{10}$
[53- 72]	2498.26154	-	-	0.733	GALYWHFKNKEDLFDALFQR	$C_{119}H_{169}N_{30}O_{30}$
[61- 72]	1495.75397	1.037	0.128	0.329	NKEDLFDALFQR	$C_{67}H_{103}N_{18}O_{21}$
[63- 72]	1253.61608	1.374	0.400	0.608	EDLFDALFQR	$C_{57}H_{85}N_{14}O_{18}$
[73-138]	7597.70557	-	-	1.485	ICDDIENCIAQDAADAEGGSWTVFRHTLLHFFERLQSN DIHYKFHNILFLKCEHTEQNAAVIAIAR	$C_{338}H_{511}N_{95}O_{100}S_3$
[98-106]	1199.63200	0.014	-0.653	-0.636	HTLLHFFER	$C_{57}H_{83}N_{16}O_{13}$
[98-106]	**1269.63748**	**-**	**-0.411**	**-0.293**	**HTLLHFFER + $C_3H_2O_2$**	**$C_{60}H_{85}N_{16}O_{15}$**
[107-115]	1117.56365	-0.052	-0.715	-0.706	LQSNDIHYK	$C_{49}H_{76}N_{14}O_{16}$
[107-138]	3736.93804	1.476	0.141	0.133	LQSNDIHYKFHNILFLKCEHTEQNAAVIAIAR	$C_{168}H_{263}N_{48}O_{47}S$
[116-123]	1031.60366	0.210	-0.177	-0.090	FHNILFLK	$C_{52}H_{79}N_{12}O_{10}$
[116-138]	2638.39224	1.385	0.142	0.199	FHNILFLKCEHTEQNAAVIAIAR	$C_{119}H_{189}N_{34}O_{32}S$
[124-138]	1625.80641	-	-0.513	-0.261	CEHTEQNAAVIAIAR	$C_{67}H_{113}N_{22}O_{23}S$
[124-138]	**1695.81189**	**-**	**0.169**	**0.652**	**CEHTEQNAAVIAIAR + $C_3H_2O_2$**	**$C_{70}H_{115}N_{22}O_{25}S$**
[139-145]	938.53190	-0.517	-1.018	-0.964	KHQAIWR	$C_{43}H_{67}N_{15}O_9$
[140-145]	810.43693	-0.151	-0.681	-1.076	HQAIWR	$C_{37}H_{55}N_{13}O_8$

[146-175]	3331.75191	3.26	1.948	2.153	EKITAVLTEAVENQDLADDLDKETAVIFIK	$C_{147}H_{244}N_{35}O_{52}$
[148-167]	2173.08705	-	2.025	2.145	ITAVLTEAVENQDLADDLDK	$C_{92}H_{154}N_{23}O_{37}$
[148-175]	3074.61435	3.788	-	2.224	ITAVLTEAVENQDLADDLDKETAVIFIK	$C_{136}H_{225}N_{32}O_{48}$
[176-184]	1060.57857	0.980	0.358	0.509	STLDGLIWR	$C_{48}H_{77}N_{13}O_{14}$
[185-196]	1359.62156	1.730	0.995	1.083	WFSSGESFDLGK	$C_{63}H_{87}N_{14}O_{20}$
[185-200]	1784.86022	-	-	0.401	WFSSGESFDLGKTAPR	$C_{81}H_{118}N_{21}O_{25}$
[185-216]	**3732.78454**	**-**	**3.608**	**-**	**WFSSGESFDLGKTAPRIIGIMMDNLENHPCLR + $C_4H_4NO_2$**	**$C_{164}H_{253}N_{45}O_{49}S_3$**
[197-200]	444.25651	-	-0.941	-0.946	TAPR	$C_{18}H_{33}N_7O_6$
[201-216]	1868.91796	-	-	-1.721	IIGIMMDNLENHPCLR	$C_{79}H_{134}N_{23}O_{23}S_3$

Table 11.1: Summary of all observed peptides from the native and modified MtrR protein digests. Peptides confirmed to have modifications have been highlighted in red.

Residues	Theoretical Monoisotopic $[M+H]^+$ *m/z*	Native M /ppm	M-NBD /ppm	Sequence	Protonated Molecular Formula
[1- 12]	1495.69196	0.554	-0.322	HMLETMETYVNK	$C_{64}H_{102}N_{16}O_{21}S_2$
[1- 55]	6271.04224	-0.006	-	HMLETMETYVNKLHEGSTYTAAVQYNVLEKDDDPASLTIWVPMFQSSMPADLLIK	$C_{280}H_{433}N_{67}O_{88}S_4$
[13- 30]	2023.01310	0.987	2.691	LHEGSTYTAAVQYNVLEK	$C_{90}H_{139}N_{23}O_{30}$
[13- 55]	4794.36812	1.045	2.322	LHEGSTYTAAVQYNVLEKDDDPASLTIWVPMFQSSMPADLLIK	$C_{216}H_{333}N_{51}O_{68}S_2$
[13- 65]	5888.01766	1.064	-	LHEGSTYTAAVQYNVLEKDDDPASLTIWVPMFQSSMPADLLIKELANVNILVK	$C_{266}H_{420}N_{64}O_{82}S_2$
[31- 55]	2790.37287	1.704	3.431	DDDPASLTIWVPMFQSSMPADLLIK	$C_{126}H_{196}N_{28}O_{39}S_2$
[56- 65]	1112.66739	-0.095	0.822	ELANVNILVK	$C_{50}H_{89}N_{13}O_{15}$
[66- 76]	**1346.68114**	**-**	**1.420**	**QISTPKGPSLR + NBD**	**$C_{57}H_{91}N_{19}O_{19}$**
[83- 92]	1031.55539	0.143	0.890	SAVLAQMPSK	$C_{44}H_{78}N_{12}O_{14}S$
[83-104]	2380.19993	-2.998	-2.175	SAVLAQMPSKFTICANVSLDER	$C_{102}H_{170}N_{28}O_{33}S_2$
[93-104]	1367.66238	0.624	1.597	FTICANVSLDER	$C_{58}H_{94}N_{16}O_{20}S$
[105-118]	1567.80362	3.642	4.433	SKLAYDVTTPCEIK	$C_{69}H_{114}N_{16}O_{23}S$
[107-118]	1352.67663	-0.192	0.688	LAYDVTTPCEIK	$C_{60}H_{97}N_{13}O_{20}S$

[119-126]	838.41612	0.308	1.274	ACSLTCLK	$C_{34}H_{63}N_9O_{11}S_2$
[119-128]	1053.54311	-	-3.050	ACSLTCLKSK	$C_{43}H_{80}N_{12}O_{14}S_2$
[129-135]	806.44405	0.470	2.355	NMLTTVK	$C_{34}H_{63}N_9O_{11}S$
[141-161]	2358.20097	0.508	1.614	TLNPTHDIIALCEFENIVTSK	$C_{104}H_{168}N_{26}O_{34}S$
[141-162]	2486.29594	0.561	1.631	TLNPTHDIIALCEFENIVTSKK	$C_{110}H_{180}N_{28}O_{35}S$
[141-175]	3984.19907	1.203	2.161	TLNPTHDIIALCEFENIVTSKKVIIPTYLRSISVR	$C_{180}H_{299}N_{47}O_{52}S$
[162-170]	1102.69829	0.443	1.069	KVIIPTYLR	$C_{53}H_{91}N_{13}O_{12}$
[163-170]	974.60333	0.884	1.910	VIIPTYLR	$C_{47}H_{79}N_{11}O_{11}$
[176-191]	1880.96000	-	2.590	NKDLNTLENITTTEFK	$C_{81}H_{133}N_{21}O_{30}$
[178-191]	1638.82211	0.179	1.307	DLNTLENITTTEFK	$C_{71}H_{115}N_{17}O_{27}$
[178-198]	2351.20889	0.347	1.589	DLNTLENITTTEFKNAITNAK	$C_{101}H_{167}N_{27}O_{37}$
[178-215]	4191.27988	-0.136	-	DLNTLENITTTEFKNAITNAKIIPYSGLLLVITVTDNK	$C_{188}H_{312}N_{46}O_{61}$
[178-219]	4594.50183	1.916	2.942	DLNTLENITTTEFKNAITNAKIIPYSGLLLVITVTDNKGAFK	$C_{208}H_{341}N_{51}O_{65}$
[199-215]	1859.08883	1.013	1.723	IIPYSGLLLVITVTDNK	$C_{87}H_{147}N_{19}O_{25}$
[199-219]	2262.31078	1.489	2.431	IIPYSGLLLVITVTDNKGAFK	$C_{107}H_{176}N_{24}O_{29}$
[220-237]	2112.13757	0.479	1.507	YIKPQSQFIVDLGAYLEK	$C_{100}H_{154}N_{22}O_{28}$
[220-248]	3496.80388	1.163	2.207	YIKPQSQFIVDLGAYLEKESIYYVTTNWK	$C_{166}H_{246}N_{36}O_{47}$
[220-261]	5019.60434	1.677	-	YIKPQSQFIVDLGAYLEKESIYYVTTNWKHTATRFAIKPRED	$C_{233}H_{352}N_{58}O_{66}$
[238-248]	1403.68416	0.315	1.170	ESIYYVTTNWK	$C_{66}H_{94}N_{14}O_{20}$

Table 11.2: Summary of all observed tryptic peptides in the native and modified M protein samples. The NBD-modified peptide has been highlighted in red.

analytical chemistry

ARTICLE

pubs.acs.org/ac

Electron-Induced Dissociation of Singly Charged Organic Cations as a Tool for Structural Characterization of Pharmaceutical Type Molecules

Jackie A. Mosely,[†,*] Michael J. P. Smith,[†] Aruna S. Prakash,[†] Martin Sims,[‡] and Anthony W. T. Bristow[‡]

[†]Department of Chemistry, Durham University, South Road, Durham, DH1 3LE, United Kingdom

[‡]Analytical Sciences, Pharmaceutical Development, AstraZeneca, Macclesfield, Cheshire, SK10 2NA, United Kingdom

ABSTRACT: Collision-induced dissociation (CID) and electron-induced dissociation (EID) have been investigated for a selection of small, singly charged organic molecules of pharmaceutical interest. Comparison of these techniques has shown that EID carried out on an FTICR MS and CID performed on a linear ion trap MS produce complementary data. In a study of 33 molecule-cations, EID generated over 300 product ions compared to 190 product ions by CID with an average of only 3 product ions per precursor ion common to both tandem MS techniques. Even multiple stages of CID failed to generate many of the product ions observed following EID. The charge carrying species is also shown to have a very significant effect on the degree of fragmentation and types of product ion resulting from EID. Protonated species behave much like the ammonium adduct with suggestion of a hydrogen atom from the charge carrying species strongly affecting the fragmentation mechanism. Sodium and potassium are retained by nearly every product ion formed from $[M + Na]^+$ or $[M + K]^+$ and provide information to complement the EID of $[M + H]^+$ or $[M + NH_4]^+$. In summary, EID is proven to be a fitting partner to CID in the structural elucidation of small singly charged ions and by studying EID of a molecule-ion holding different charge carrying species, an even greater depth of detail can be obtained for functional groups commonly used in synthetic chemistry.

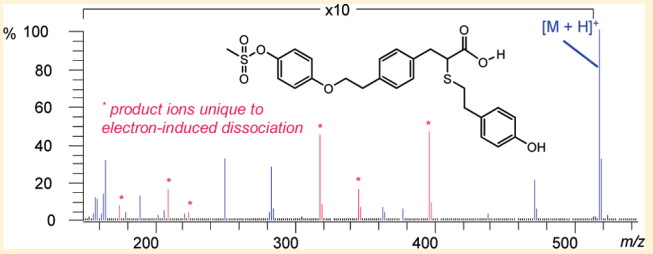

Mass spectrometry is one of the most valuable analytical techniques employed by the pharmaceutical industry in the quest of compound characterization, to the extent that virtually every analytical or synthetic laboratory has access to this kind of technology. This is due, in part, to online compatibility with separation techniques such as gas or liquid chromatography, which allows even highly complex mixtures to be simplified ahead of the mass spectrometer. Sheer sensitivity toward compounds in very low abundance, particularly in the presence of more concentrated samples, as is typical of impurities arising from synthesis, makes up-front separation a necessity in many cases. Tandem mass spectrometry, the ability to further isolate desired precursor ions in the gas phase and subject them to conditions that induce fragmentation, undoubtedly adds that extra dimension of molecular information. For the pharmaceutical industry, the resulting fragmentation patterns from the tandem mass spectrometry of small organic molecules can provide a means to structural characterization, identification of impurities or degradation products and metabolites. Historically, characteristic fragmentation patterns from electron impact (EI) ionization have been established to the point that spectral libraries from EI ionized chemicals are routinely used to identify compounds "on-the-fly".[1] True tandem MS can be achieved in numerous ways including collision-induced dissociation (CID)[2,3] and surface-induced dissociation (SID),[4] infrared multiphoton dissociation (IRMPD),[5,6] electron capture dissociation (ECD)[7] and electron transfer dissociation (ETD).[8] Most common by far is CID, and recent studies into the reproducibility of CID product ion spectra have demonstrated that CID MS data is sufficiently reproducible across a range of different instrument types to allow instrument-independent CID libraries to be considered a viable approach to structural identification.[9] ECD, a relatively new technique, has found its niche in the proteomics arena and routinely provides data, complementary to CID data, for the tandem MS studies of peptides[10] and intact proteins.[11] Whereas CID induces bond cleavage via the lowest energy pathways,[12] crucially ECD has been shown to fragment some bonds leaving labile functional groups attached, thus able to locate and identify such modifications as phosphorylation,[13] glycosylation,[14] acetylation[15] or sulphation.[16] Subsequently, a great deal of research has been carried out into the fragmentation mechanisms occurring during ECD.[7,17] The concept of ECD has been mainly considered for multiply charged species, whether for multiply protonated species[18] or species containing a metal atom with a valence of n (where $n > 1$).[19−22] These studies have led to the proposal of two different mechanisms. The first mechanism, the hot hydrogen atom mechanism, was described by Zubarev and co-workers and suggests an incoming electron neutralizing

Received: January 7, 2011
Accepted: April 7, 2011
Published: April 07, 2011

Table 1. Number of Product Ions Observed Following CID in the LTQ and EID in the LTQFT and a Comparison of Product Ions Common to Both Techniques

	number of product ions observed > m/z 80		
compound name	EID	CID (MS^2)	product ions common to EID and CID (number common product ions; m/z of the common product ions)
$[haloperidol + H]^+$	5	4	3; (m/z 123, 165, 194)
$[sulfamethazine + H]^+$	9	8	6; (m/z 92, 108, 124, 156, 186, 213)
$[diphenhydramine + H]^+$	6	2	2; (m/z 88, 167)
$[diphenhydramine\ fragment]^+$	>7	1	1; (m/z 152)
$[caffeine + H]^+$	7	4	2; (m/z 110, 138)
$[reserpine + H]^+$	13	15	6; (m/z 195, 236, 365, 397, 436, 448)
$[raffinose + Na]^+$	>21	5	4; (m/z 203, 275, 305, 365)
$[terfenadine + H]^+$	10	2	2; (m/z 436, 454)
$[tazobactam + H]^+$	13	6	3; (m/z 168, 257, 283)
$[AZ\_A + H]^+$	>14	14	1; (m/z 340)
$[AZ\_A + 2H]^2+$	15	15	5; (m/z 216, 310, 325, 338, 366)
$[AZ\_B(i) + H]^+$	4	4	1; (m/z 399)
$[AZ\_B(ii) + H]^+$	2	2	2; (m/z 325, 280)
$[AZ\_B(ii) + Na]^+$	7	11	4; (m/z 331, 400, 464, 515)
$[AZ\_B(iii) + H]^+$	18	12	7; (m/z 165, 179, 224, 238, 272, 316, 167*)
$[AZ\_B(iii) + Na]^+$	7	5	2; (m/z 125, 163)
$[AZ\_B(iv) + H]^+$	6	5	0
$[AZ\_C(i) + H]^+$	>16	2	1; (m/z 471)
$[AZ\_C(i) + NH_4]^+$	>18	3	2; (m/z 471, 516)
$[AZ\_C(i) + Na]^+$	>19	12	6; (m/z 250, 263*, 278, 295, 357, 460)
$[AZ\_C(ii) + H]^+$	12	4	2; (m/z 91, 93, 103, 120)
$[AZ\_C(iii) + H]^+$	0	3	
$[AZ\_C(iii) + NH_4]^+$	>9	4	4; (m/z 211, 354*, 381, 398)
$[AZ\_C(iii) + Na]^+$	17	8	6; (m/z 234, 262, 278, 306, 342, 384*)
$[AZ\_C(iii) + K]^+$	10	7	3; (m/z 147, 154*, 358)
$[AZ\_C(iv) + H]^+$	10	10	2; (m/z 120, 164)
$[AZ\_C(iv) + NH_4]^+$	12	2	2; (m/z 408, 352)
$[AZ\_C(iv) + Na]^+$	15	4	2; (m/z 330,374)
$[AZ\_C(iv) + K]^+$	6	3	1; (m/z 390)
$[AZ\_C(v) + H]^+$	3	>7	3; (m/z 146, 164, 336)
$[AZ\_C(v) + NH_4]^+$	6	4	3; (m/z 164, 336, 392)
$[AZ\_C(v) + Na]^+$	13	1	3; (m/z 120, 164, 358)
$[AZ\_C(v) + K]^+$	6	5	2; (m/z 164, 374)
Total Number of precursor ions studied			
33	**> 330**	**> 190**	**Average 3 peaks in common**
			**** suspected corresponding EID fragment 1 m/z higher than CID***

the positive charge on a solvated carbonyl group of a peptide and inducing hydrogen atom transfer which results in cleavage of the $N-C_\alpha$ bond.[23,24] More recently, the second mechanism, proposed by Tureček et al., describes electron capture that does not result in a mobile hydrogen atom.[25−27] Here, electron attachment to a peptide amide π^* orbital, which is viable as such orbitals can be stabilized by Coulomb interaction with a positive charge, results in a strong base that undergoes proton transfer leading to bond cleavage within the amide ($N-C_\alpha$). Both of these mechanisms only concern initial electron capture and primary fragmentation. Secondary fragmentation has been reported whereby nonergodic electron capture generates a radical species that, following radical migration, can lead to multiple radical rearrangements resulting in numerous cleavage sites.[28−30] It is, however, important to note that most mechanistic studies have involved peptides.

Investigation into the electron interactions with single positively charged molecules in an FTICR MS has not been thoroughly examined as it has been assumed that charge neutralization will occur when a single positively charged ion captures an electron, resulting in a neutral species,[31] although studies as long ago as 1979 clearly show this not to be the case if electron energy is sufficiently high.[32] In this research, and subsequent studies, Cody and Freiser showed that interaction between radical cations and electrons can be used to provide valuable structural information.[32,33] Budnik and Zubarev later showed that a singly protonated peptide could be further ionized by "fast" electrons and that subsequent capture of "slow"

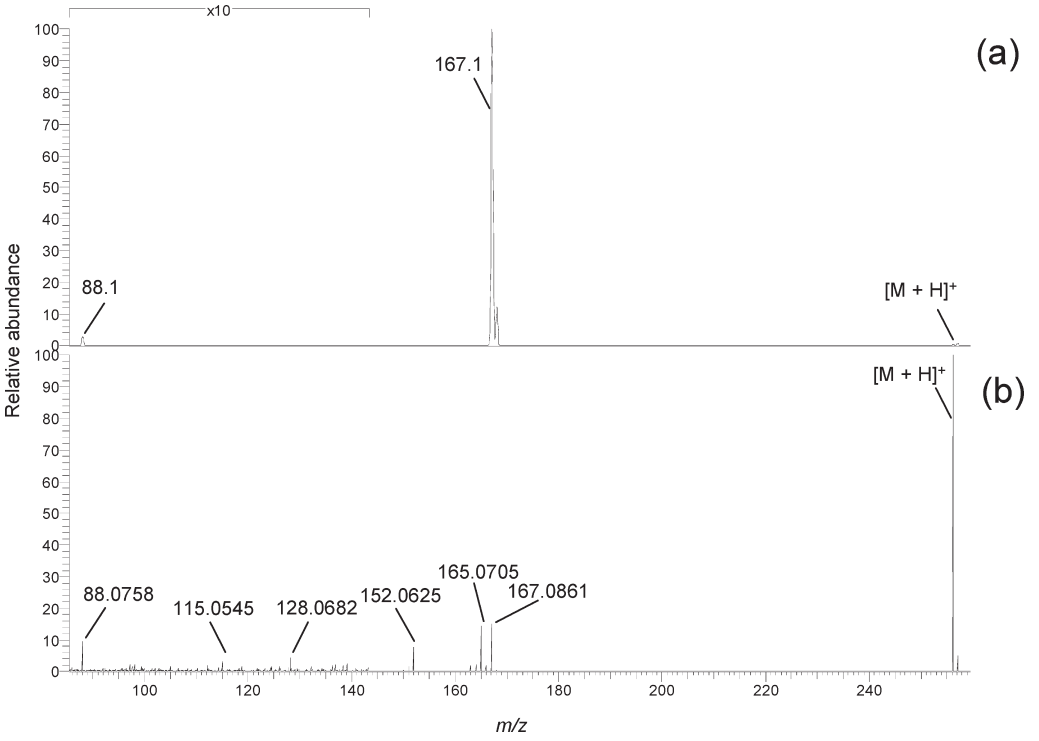

Figure 1. MS^2 spectra for protonated diphenhydramine. (a) LTQ CID spectrum obtained with normalized collision energy of 20 and (b) LTQFT EID spectrum obtained with electron energy set to 20%. Collision energy and electron energy values were set as per manufacturers' software.

Scheme 1. Dissociation of Diphenhydramine[a]

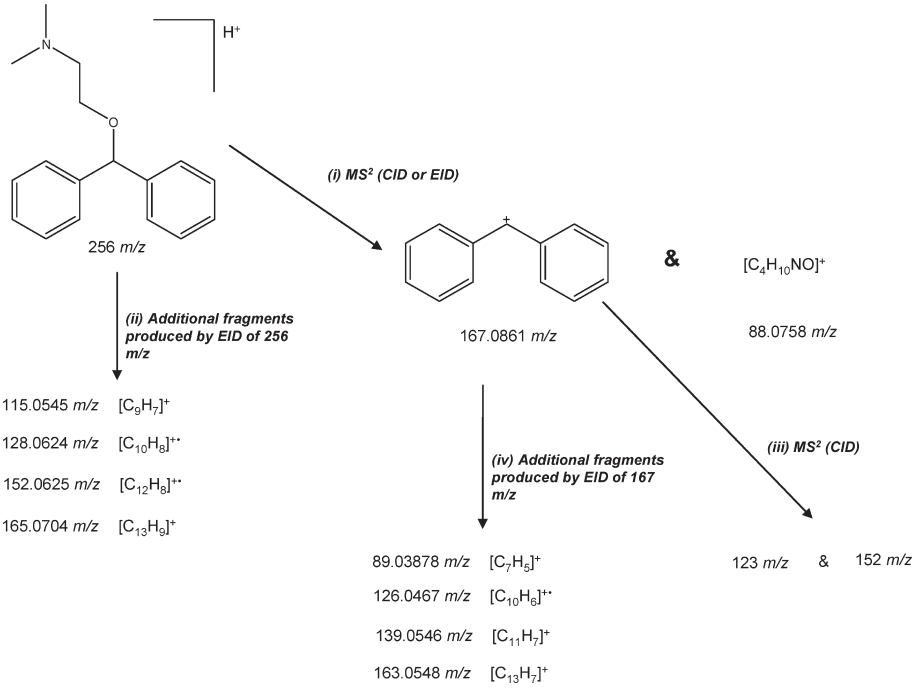

[a] (i) Product ions common to CID and EID of 256 *m/z*. (ii) Additional fragments produced from EID of 256 *m/z*. (iii) CID of 167 *m/z*. (iv) EID of 167 *m/z*. All EID mass measurements were performed in the FTICR MS and are accurate to <1 ppm. The CID experiments resulting in 123 m/z and 152 m/z were performed in the LTQ ion trap and were measured to nominal mass.

electrons could result in fragmentation.[34] Yet, only a few studies have been done since to investigate the interaction between electrons and ions (protonated or deprotonated) holding a single charge and the fragmentation that results from this electron-induced dissociative (EID) technique. Lioe and O'Hair reported EID fragmentation efficiency of singly protonated aromatic

dx.doi.org/10.1021/ac200045n |*Anal. Chem.* 2011, 83, 4068–4075

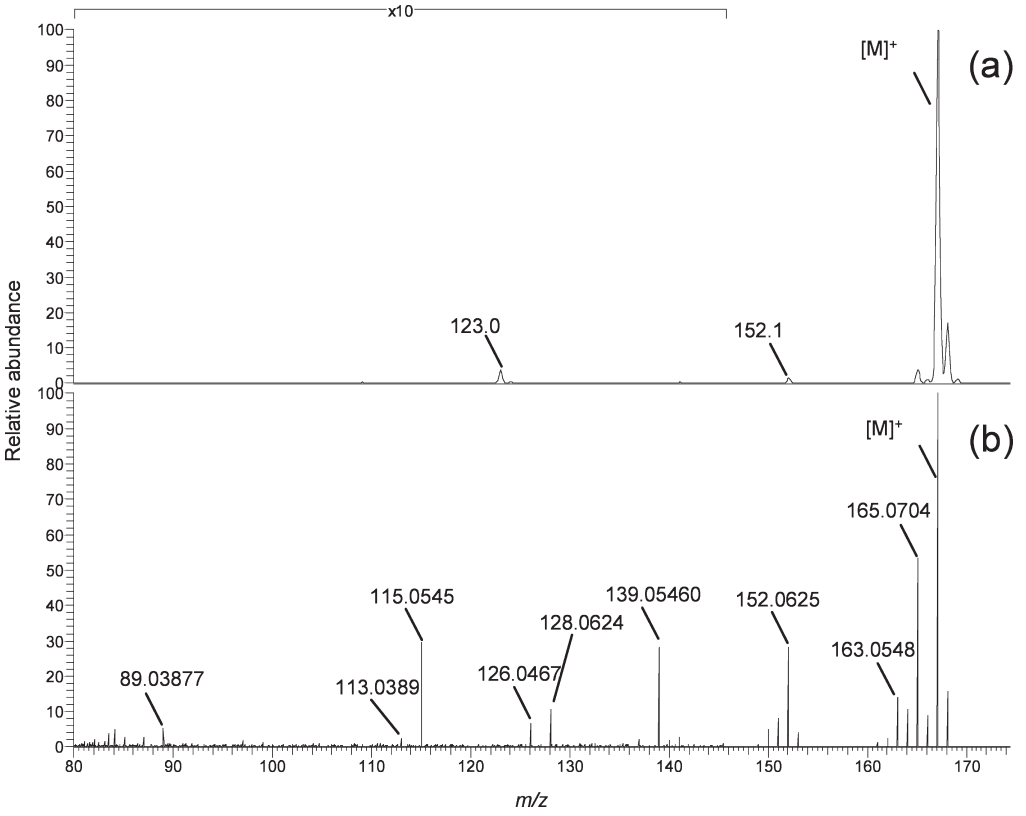

Figure 2. MS^2 spectra for the precursor ion 167.1 *m/z*, formed from in-source dissociation of protonated diphenhydramine. (a) LTQ CID spectrum obtained with normalized collision energy of 25 and (b) LTQFT EID spectrum obtained with electron energy set to 20%. Collision energy and electron energy values were set as per manufacturers' software.

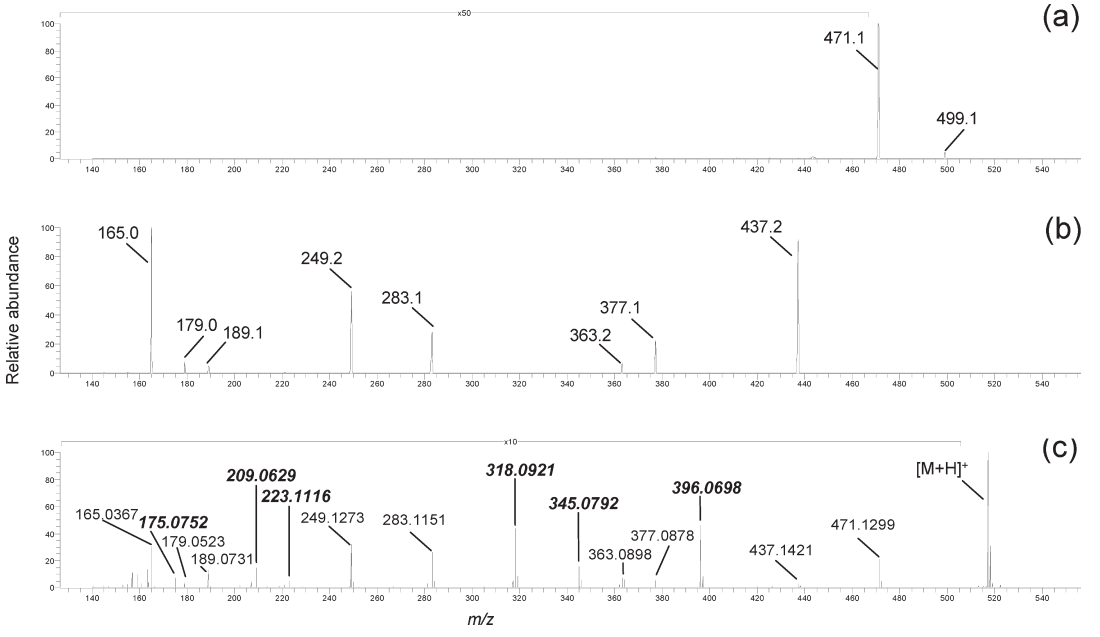

Figure 3. Comparison of CID and EID for compound AZ_C(i). (a) LTQ MS^2 spectrum for the protonated precursor ion at 517.1 *m/z* leading to (b) MS^3 of 471.1 *m/z*. These CID spectra were obtained with normalized collision energy of 20. (c) LTQFT EID spectrum for the precursor ion 517.1 *m/z* obtained with electron energy set to 20%. Collision energy and electron energy values were set as per manufacturers' software. Peak assignments are given in Table 2.

amino acids at high electron energies.[35] The experiment, akin in approach to hot ECD (hECD) for multiply charged molecules, demonstrated that electron energies of approximately 15−25 eV induced fragmentation that resulted in different product ions to CID.

dx.doi.org/10.1021/ac200045n |*Anal. Chem.* 2011, 83, 4068–4075

Sargaeva et al. used electron energies of this order to show that EID, as well as ECD, could be used to differentiate between aspartic and isoaspartic acid residues in a peptide.[36] Wolff et al. have investigated EID for singly deprotonated glycosaminoglycans and show EID produces far greater fragmentation for these molecules than IRMPD.[37] By comparison, Håkansson et al.'s study of singly deprotonated phosphate-containing metabolites concluded with EID providing complementary data to IRMPD and CID, yet EID was not as efficient as the other techniques.[38]

This study has not only successfully dissociated small positive singly charged ions through collisions with electrons but shown that high quality data that is produced is shown to be complementary to both CID and EI.

EXPERIMENTAL SECTION

Sample Preparation. A wide variety of small organic molecules of varying chemical structures were dissolved to produce a concentration of 1 μg mL^{-1} in methanol or acetonitrile depending on solubility. Named compounds were commercially available and were purchased from Sigma-Aldrich, Dorset, U.K. All solvents and reagents were also purchased from Sigma-Aldrich, Dorset, U.K. Compounds identified with the prefix AZ were supplied courtesy of AstraZeneca, Avlon, U.K.

Mass Spectrometry. Mass spectrometry measurements were made using a ThermoFinnigan LTQFT mass spectrometer equipped with a 7.0 T magnet (Bremen, Germany). Samples were introduced into an electrospray ion source using a syringe pump delivering a flow at 5 μL min^{-1}. The nitrogen sheath gas was set to 3 arbitrary units on the manufacturers' software; the auxiliary gas and the sweep gas were negligible, thus providing a stable signal. The heated capillary was set to 250 °C. The electrospray ion source was operated with a spray voltage of 4.0 kV, and the tube lens was optimized to deliver the maximum intensity for the desired positive ion. For all MS/MS experiments, the isolation window was set to comfortably encompass the full isotopic envelope. CID experiments were carried out in the LTQ using helium as the collision gas. The collision energy was optimized between settings of 15 and 25 for the normalized collision energy as per the manufacturers' software, to produce the desired degree of fragmentation. Product ions were measured by the LTQ-MS and the FTICR MS. EID was performed by an indirectly heated dispenser cathode within the FTICR MS. Cathode offset was 2.9 V and the energy, as set in the software, was between 15 and 25%, thus giving an electron energy of between 12.1 and 22.1 eV. Operating at these elevated electron energies is often termed hot ECD. The electron irradiation duration was 70 ms. Data was recorded and processed using Xcalibur software (version 2.0) (ThermoFinnigan, San Jose, CA).

RESULTS AND DISCUSSION

EID and CID results were compared for a selection of small molecules. Table 1 lists the compounds investigated and summarizes the tandem mass spectrometry results. Diphenhydramine provides a good example of a particular problem that can arise from a limitation of CID. The CID spectrum of protonated diphenhydramine (Figure 1a) shows only two peaks, one corresponding to a highly abundant product ion at 167.1 m/z and one relatively low abundant product ion at 88.1 m/z. Scheme 1(i) demonstrates the fragmentation pathway, that is, cleavage at a single location, the middle of the molecule-ion, resulting in two possible charged fragments that reveal limited structural information. In comparison, EID, which also results in the same two product ions as CID, generates additional product ions as shown in Figure 1b, providing information regarding the structure of the aromatic portion of diphenhydramine. These extra fragments are detailed in Scheme 1(ii). In fact, by increasing the tube lens voltage to optimize the intensity of the in-source dissociation product 167.1 m/z, this even electron fragment of diphenhydramine could be selected as the precursor ion for further tandem mass spectrometric studies. EID of 167.1 m/z produced four times the number of product ions when compared to CID (Table 1 and Figure 2). Some of the EID product ions were observed previously from the fragmentation of 256.2 m/z; however, four new peaks arose from the fragmentation of 167.1 m/z (Scheme 1(iv)), and when all EID product ions are considered together, the overall information attained matches that from traditional EI data.[39,40]

As with diphenhydramine, CID in the ion trap was only able to provide limited structural information regarding the compound AZ_C(i) ($[M + H]^+$ = 517 m/z). Here, the two product ions corresponding to the loss of water and formic acid from protonated AZ_C(i) give no insight as to molecular structure. These results are shown in Figure 3a. An additional stage of CID, MS^3 of 517.1 m/z and 471.1 m/z, led to a further eight product ions as given in Figure 3b. In comparison, a single EID spectrum of the protonated precursor 517.1 m/z resulted in an identical set of

Table 2. Summary of EID Product Ions for the Compound AZ_C(i)

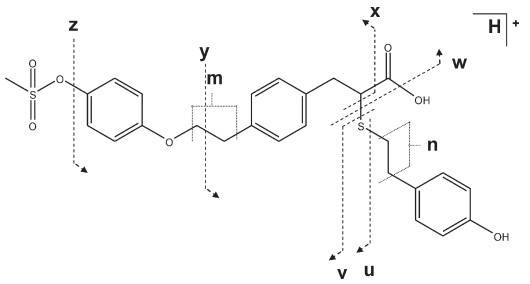

EID product ion (m/z)	proposed formula	mass deviation from theoretical m/z value/ppm	structure of product ions unique to EID
165.0367	C_9H_9OS	−1.04	
175.0752	$C_{11}H_{11}O_2$	−0.95	**yv**
179.0523	$C_{10}H_{11}OS$	−0.96	
189.0731	$C_{12}H_{13}S$	−0.83	
209.0629	$C_{11}H_{13}O_2S$	−0.66	**mn**
223.1116	$C_{16}H_{15}O$	−0.64	**zx**
249.1273	$C_{18}H_{17}O$	−0.49	
283.1151	$C_{18}H_{19}OS$	−0.15	
318.0921	$C_{17}H_{18}O_4S$	0.09	**x**
345.0792	$C_{18}H_{17}O_5S$	0.32	**w**
363.0898	$C_{18}H_{19}O_4S_2$	0.40	
377.0878	$C_{19}H_{21}O_4S_2$	0.49	
396.0698	$C_{18}H_{20}O_6S_2$	0.65	**u**
437.1421	$C_{25}H_{25}O_5S$	0.87	
471.1299	$C_{25}H_{27}O_5S_2$	1.06	

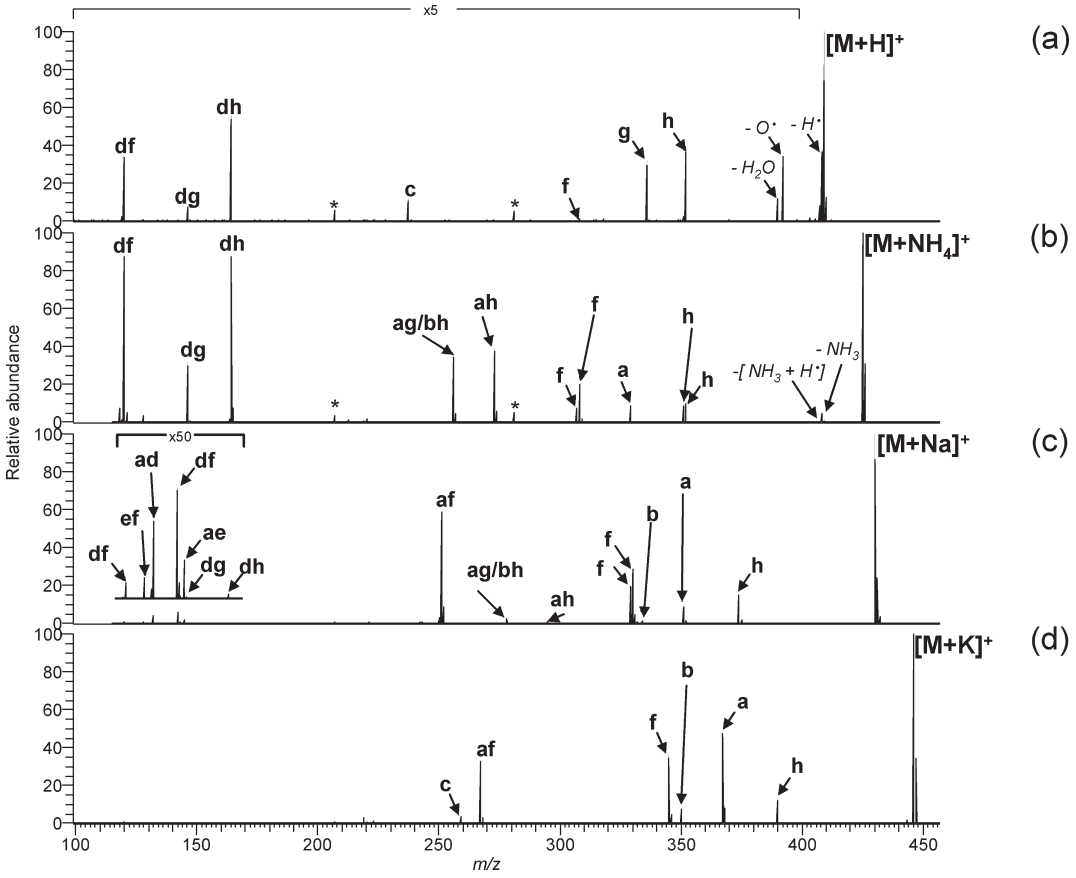

Figure 4. Comparison of the LTQFT EID data for the compound AZ_C(iv) with different charge carrying species. (a) $[M + H]^+$, (b) $[M + NH_4]^+$, (c) $[M + Na]^+$, and (d) $[M + K]^+$. LTQFT EID spectrum obtained with electron energy set to 20%. Collision energy and electron energy values were set as per manufacturers' software. Note, * indicate the presence of silicones. Peak assignments are given in Table 3.

product ions as the combined effort of MS^2 and MS^3 by CID, plus several additional peaks unique to EID (Figure 3c). This complementary information now allows empirical formulas to be proposed for six extra fragments, highlighted in Table 2. These fragments encompass the majority of the structure of the molecule including a peak at 396 *m/z* which represents cleavage at **u**, the thioether, resulting in the loss of ethyl phenol. Cleavage at or close to the thioether is common to the six unique EID fragments. The peaks at 345 *m/z* and 318 *m/z* (cleavage at **w** and **x** respectively) both retain the mesylate end group whereas 223 *m/z*, 209 *m/z* and 175 *m/z* all result from multiple bond cleavages releasing the central part of the molecule. These internal fragments are given in Table 2 as **zx**, **mn** and **yv** respectively. In the case of **mn**, two bonds have been suggested for each of **m** and **n** as cleavage at either location would result in product ions of the same empirical formula. Although in this case the full molecule can also be pieced together from MS^3 CID data, the complementary fragments observed by EID demonstrate the full extent of information that can be attained from a single EID MS/MS experiment using an instrument with very high resolving power and precise accurate mass measurement.

Numerous molecule-ions carrying only a single positive charge have been studied, and for the 33 species listed in Table 1, EID generated over 330 product ions, 1.5 times more than generated by CID, indicating that for many compounds EID can provide a greater depth of information. Perhaps the most interesting fact, however, is the small overlap in the data obtained by the two techniques. On average, there were only three product ions common to both EID and CID, highlighting the complementary nature of these experimental approaches.

Effect of the Charge Carrying Species on EID. Many of the compounds used in this investigation were observed as proton, sodium, ammonium, and potassium adducts. The nature of the charge-carrying species can be seen to affect the product ions generated. EID spectra for compound AZ_C(iv) are given in Figure 4, and interestingly, but perhaps not surprisingly, the vast majority of the positively charged fragments retain the nitrogen atom. The protonated molecule (Figure 4a) fragments heavily within the BOC-aniline portion of the molecule. Loss of $H^\bullet$, $O^\bullet$, and H_2O are not structurally helpful; however, there are three fragments corresponding to the break up of *t*-butyl. Loss of C_4H_8, C_4H_8O, and $C_5H_8O_2$ clearly characterize this portion of the molecule with the ninth *t*-butyl hydrogen relocated to the amine for stabilization resulting in NH_3^+ as the terminal group of this fragment ion. Fragmentation is depicted in Table 3 where the bonds labeled **h**, **g** and **f** are cleaved respectively. Information regarding the aniline BOC can still be obtained from the ammonium adduct via cleavage at **h** and **f** as shown in Figure 4b; however, these neutral losses of C_4H_8 and $C_5H_8O_2$ from the ammonium adduct are both accompanied by neutral losses of NH_3 and $[NH_3 + H^\bullet]$[41] and are visually recognizable as pairs of peaks separated by 1 *m/z*. Exact mass measurement with the FTICR confirms assignment. The pairing of peaks separated by 1 *m/z* associated with all *t*-butyl fragments from the

dx.doi.org/10.1021/ac200045n |*Anal. Chem.* 2011, 83, 4068–4075

Table 3. Summary of EID Product Ions for the Compound AZ_C(iv)

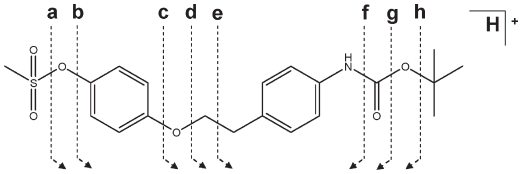

	terminal product ions		internal product ions	
precursor ion	empirical formula	bond cleavage site	empirical formula	bond cleavage site
$[M + H]^+$	$C_{13}H_{19}NO_3$	**c**	$C_8H_{10}N$	**df**
	$C_{16}H_{18}NO_6S$	**h**	C_9H_8NO	**dg**
	$C_{16}H_{18}NO_5S$	**g**	$C_9H_{10}NO_2$	**dh**
	$C_{15}H_{18}NO_4S$	**f**		
$[M + NH_4]^+$	$C_{16}H_{17}NO_6S$	**h**	$C_8H_{10}N$	**df**
	$C_{16}H_{18}NO_6S$	**h**	C_9H_8NO	**dg**
	$C_{15}H_{17}NO_4S$	**f**	$C_9H_{10}NO_2$	**dh**
	$C_{15}H_{18}NO_4S$	**f**	$C_{15}H_{14}NO_3$	**ag/bh**
	$C_{19}H_{23}NO_4$	**a**	$C_{15}H_{15}NO_4$	**ah**
$[M + Na]^+$	$C_{16}H_{17}NO_6SNa$	**h**	C_7H_7NNa	**ef**
	$C_{15}H_{17}NO_4SNa$	**f**	C_8H_9NNa	**df**
	$C_{15}H_{16}NO_4SNa$	**f**	$C_6H_5O_2Na$	**ad**
	$C_{19}H_{22}NO_4Na$	**a**	$C_7H_6O_2Na$	**ae**
	$C_{19}H_{21}NO_3Na$	**b**	$C_{15}H_{15}NO_4Na$	**ah**
			$C_{15}H_{13}NO_3Na$	**ag/bh**
			$C_{14}H_{14}NO_2Na$	**af**
			$C_8H_{10}N$	**df**
			$C_9H_{10}NO_2$	**dh**
$[M + K]^+$	$C_{16}H_{17}NO_6SK$	**h**	$C_{14}H_{14}NO_2K$	**af**
	$C_{15}H_{17}NO_4SK$	**f**		
	$C_{19}H_{22}NO_4K$	**a**		
	$C_{19}H_{21}NO_3K$	**b**		
	$C_{13}H_{18}NO_2K$	**d**		

ammonium adduct suggests that two processes may be occurring during EID: electron interaction causing charge transfer from NH_4^+ to the compound and proton transfer to the compound, each resulting in fragmentation. Bond cleavage at **h** and **f**, involving relocation of the ninth *t*-butyl hydrogen, was also observed when the charge carrying species was an alkali metal cation. Overall, the protonated molecule-ion provides more significant information regarding the aniline BOC end of the molecule.

Similarity between the dissociation of the ammonium adduct and the alkali metal cation adducts can been seen at the mesylate end of the molecule. For the ammonium adduct, in contrast to the *t*-butyl fragmentation peak pairing, a single peak was observed corresponding to cleavage at position **a**, resulting in the simultaneous neutral loss of $CH_3SO_2^{\bullet}$ and NH_3, suggesting proton transfer may have occurred. Evidence for small neutral losses from the mesylate end of the molecule becomes far more prevalent when the molecule carries an alkali metal cation such as Na^+ or K^+. In fact, the most intense peaks from $[M + Na]^+$ and $[M + K]^+$ relate to cleavage at bonds labeled **a** (neutral loss of $CH_3SO_2^{\bullet}$) and **b** (neutral loss of methane sulfonic acid, CH_3SO_3H) in Table 3. It is theorized that the larger cationic species reside on or in close proximity to the aromatic ring[42] adjacent to the mesylate, thus directing interaction with an electron to this locale, resulting in preferential bond cleavage in this area and may explain the ability of a hydrogen to relocate to during bond cleavage at **b** to result in the neutral loss of CH_3SO_3H. The protonated species now stands alone as there is a complete absence of any cleavage at **a** and **b**, but instead a unique cleavage at **c** on the central side of the aromatic ring.

As observed for the EID of compound AZ_C(i), multiple bonds were also broken for AZ_C(iv). Small neutral loses from both ends of the molecule leave the central portion of the molecule carrying the charge. This evidence is given by the three product ions at the lower *m/z* region of the spectrum for $[M + H]^+$ (Figure 4a) corresponding to $[C_8H_{10}N]^+$ (**df**), $[C_9H_8NO]^+$ (**dg**) and $[C_9H_{10}NO_2]^+$ (**dh**). In comparison, fragmenting the ammonium adduct led to the same three product ions at the low *m/z* range as shown in Figure 4b. There is only very weak evidence for the three product ions $[C_8H_{10}N]^+$, $[C_9H_8NO]^+$ and $[C_9H_{10}NO_2]^+$ resulting from the EID of $[M + Na]^+$ (Figure 4c) and a complete absence of these peaks from the EID of $[M + K]^+$ (Figure 4d). This would suggest a hydrogen atom from the original charge carrying species is heavily involved in the formation of these product ions that correspond to the central portion of the molecule. Weak evidence for $[C_8H_{10}N]^+$ (**df**) from $[M + Na]^+$ does suggest the possibility that, in the absence of any protons on the charge carrying species, a hydrogen can be abstracted from another part of the molecule, but that this is not as favorable as retaining the original charge carrying atom as shown by the relative intensity of the product ion $[C_8H_9Na]^+$. There is further evidence for multiple bond cleavage for $[M + NH_4]^+$, $[M + Na]^+$, and $[M + K]^+$. The beginnings of a trend can be seen with $[M + NH_4]^+$ and $[M + Na]^+$ both fragmenting at **ag/bh** and **ah**. In addition, $[M + Na]^+$ also fragments at **af**, this being the only fragmentation site for $[M + K]^+$.

Overall, a degree of similarity can be seen between the EID of the proton adduct and ammonium adduct and then between the ammonium adduct and the alkali metal cation adducts. Ammonium was not retained in its entirety by any of the product ions but was seen to donate either the charge or a proton to product ions. This is in contrast to the alkali metal adducted species where the sodium is retained by all but two product ions from $[M + Na]^+$ and potassium is retained by every product ion from $[M + K]^+$ as shown in Table 3. Irrespective of dissociation mechanisms involved, changing the charge carrying species can be used to extract increasing amounts of molecular information, with ammonium and sodium providing the optimum for this particular molecule.

CONCLUSION

For the molecules employed in this study, EID was shown to provide a much greater depth of information. In many cases, EID resulted in a much greater number of product ions than CID, with very little overlap between the two techniques. The complementary nature of these techniques can be significantly enhanced by changing the charge-carrying species. This can be explained by different charge-carrying species residing at different locations of these small molecules and as such heavily influence the product ions generated. In practice, EID appears

to allow very specific parts of a molecule to be probed. For example, the *t*-butyl functional group of the molecule studied can be easily classified from the ammonium adduct as pairs of peaks corresponding to small neutral losses from this functional group allow this portion of the molecule to be assigned at a glance. Conversely, location of a sodium or potassium cation at an aromatic portion of the molecule closest to the mesylate group would go some way to explaining why the mesylate portion of the molecule is better characterized from these adducts. Overall, EID results from proton and ammonium adducts were reasonably comparable, with ammonium providing a slight advantage. The presence of a sodium cation gave similar but slight improvement over potassium. What is clear is the involvement of more than one dissociation mechanism coming into play, particularly evident from the ammonium adduct where proton transfer and charge transfer can both be observed.

AUTHOR INFORMATION

Corresponding Author

*Dr. Jackie A. Mosely, Department of Chemistry, Durham University, South Road, Durham, DH1 3LE, U.K. E-mail: jackie.mosely@durham.ac.uk. Fax: 44 (0) 191 334 2051.

ACKNOWLEDGMENT

We thank EPSRC and AstraZeneca for financial support.

REFERENCES

(1) Halket, J. M.; Waterman, D.; Przyborowska, A. M.; Patel, R. K.; Fraser, P. D.; Bramley, P. M. *J. Exp. Bot.* **2005**, *56*, 219–243.
(2) Cooks, R. G. *J. Mass Spectrom.* **1995**, *30*, 1215–1221.
(3) Glish, G. L.; Burinsky, D. J. *J. Am. Soc. Mass Spectrom.* **2008**, *19*, 161–172.
(4) Laskin, J.; Denisov, E. V.; Shuklu, A. K.; Barlow, S. E.; Futrell, J. H. *Anal. Chem.* **2002**, *74*, 3255–3261.
(5) Little, P. D.; Speir, J. P.; Senlo, M. W.; O'Connor, P. B.; McLafferty, F. W. *Anal. Chem.* **1994**, *66*, 2809–2815.
(6) Tonner, D. S.; McMahon, T. B. *Anal. Chem.* **1997**, *69*, 4735–4740.
(7) Zubarev, R. A.; Kellerher, N. L.; McLafferty, F. W. *J. Am. Chem. Soc.* **1998**, *120*, 3265–3266.
(8) Syka, J. E. P.; Coon, J. J.; Schroeder, M. J.; Shabanowitz, J.; Hunt, D. F. *Proc. Natl. Acad. Sci. U.S.A.* **2004**, *101*, 9528–9533.
(9) Bristow, A. W. T.; Webb, K. S.; Lubben, A. T.; Halket, J. *Rapid Commun. Mass Spectrom.* **2004**, *18*, 1447–1454.
(10) Nielsen, M. L.; Savitski, M. M.; Zubarev, R. A. *Mol. Cell. Proteomics* **2005**, 4835–4845.
(11) Zubarev, R. A.; Horn, D. M.; Fridriksson, E. K.; Kellerher, N. L.; Kruger, N. A.; Lewis, M. A.; Carpenter, B. K.; McLafferty, F. W. *Anal. Chem.* **2000**, *72*, 563–573.
(12) Mayer, P. M.; Poon, C. *Mass Spectrom. Rev.* **2009**, *28*, 608–639.
(13) Crease, A. J.; Cooper, H. J. *J. Am. Soc. Mass Spectrom.* **2008**, *19*, 1263–1274.
(14) Håkansson, K.; Cooper., H. J.; Emmett, M. R.; Costello, C. E.; Marshall, A. G. *Anal. Chem.* **2001**, *73*, 4530–4536.
(15) Guan, Z. Q. *J. Am. Soc. Mass Spectrom.* **2002**, *12*, 1443–1447.
(16) Kellerher, N. L.; Zubarev, R. A.; Bush, K.; Furle, B. C.; McLafferty, F. W.; Walsh, C. T. *Anal. Chem.* **1999**, *71*, 4250–4253.
(17) Jones, W. J.; Sasski, T.; Goodlett, D. R.; Tureček, F. *J. Am. Soc. Mass Spectrom.* **2007**, *18*, 432–444.
(18) Cooper, H. J.; Hakansson, K.; Marshall, A. G. *Mass Spectrom. Rev.* **2005**, *24*, 210–222.
(19) Mosely, J. A.; Murray, B. S.; Parker, D. *Eur. J. Mass Spectrom.* **2009**, *15*, 154–155.
(20) Laskin, J.; Yang, Z.; Chu, I. K. *J. Am. Chem. Soc.* **2008**, *130*, 3218–3230.
(21) Kleinnijenhuis, A. J.; Mihalca, R.; Heeren, R. M. A.; Heck, A. J. R. *Int. J. Mass Spectrom.* **2006**, *253*, 217–224.
(22) Liu, H.; Håkansson, K. *J. Am. Soc. Mass Spectrom.* **2006**, *17*, 1731–1741.
(23) Zubarev, R. A.; Kruger, N. A.; Fridriksson, E. K.; Lewis, M. A.; Horn, D. M.; Carpenter, B. K.; McLafferty, F. W. *J. Am. Chem. Soc.* **1999**, *121*, 2857–2862.
(24) Zubarev, R. A.; Haselmann, K. F.; Budnik, B.; Kjeldsen, F.; Jensen, F. *Eur. J. Mass. Spectrom.* **2002**, *8*, 337–349.
(25) Turecek, F.; Syrstad, E. A. *J. Am. Chem. Soc.* **2003**, *125*, 3353–3369.
(26) Syrstad, E. A.; Turecek, F. *J. Am. Soc. Mass Spectrom.* **2005**, *16*, 208–224.
(27) Turecek, F. *J. Am. Chem. Soc.* **2003**, *125*, 5954–5963.
(28) Leymarie, N.; Costello, C. E.; O'Connor, P. B. *J. Am. Chem. Soc.* **2003**, *125*, 8949–8958.
(29) Cooper, H. J.; Hudgins, R. R.; Håkansson, K.; Marshall, A. G. *Int. J. Mass Spectrom. Ion Processes* **2003**, *228*, 723–728.
(30) O'Connor, P. B.; Cheng, L.; Cournoyer, J. J.; Pittman, J. L.; Belyayev, M.; Budnik, B. A. *J. Am. Soc. Mass Spectrom.* **2006**, *17*, 576–585.
(31) Sleno, L.; Volmer, D. A. *J. Mass Spectrom.* **2004**, *39*, 1091–1112.
(32) Cody, R. B.; Freiser, B. S. *Anal. Chem.* **1979**, *51*, 547–551.
(33) Cody, R. B.; Freiser, B. S. *Anal. Chem.* **1987**, *59*, 1056–1059.
(34) Budnik, B. A.; Zubarev, R. A *Chem. Phys. Lett.* **2000**, *316*, 19.
(35) Lioe, H.; O'Hair, R. A. J. *Anal. Bioanal. Chem.* **2007**, *389*, 1429–1437.
(36) Sargaeva, N. P.; Cheng, L.; O'Connor, P. B. *Anal. Chem.* **2009**, *81*, 9778–9786.
(37) Wolff, J. J.; Laremore, T. N.; Aslam, H.; Linhardt, R. J.; Amster, I. J. *J. Am. Soc. Mass Spectrom.* **2008**, *19*, 1449–1458.
(38) Yoo, H.; Haichaun, L.; Håkansson, K. *Anal. Chem.* **2007**, *79*, 7858–7886.
(39) *NIST Chemistry WebBook*, http://webbook.nist.gov/chemistry.
(40) Seno, H.; Hattori, H.; Kumazawa, T.; Suzuki, O. *Forensic Sci. Int.* **1993**, *62*, 187–208.
(41) Gellene, G. I.; Porter, R. F. *J. Phys. Chem.* **1984**, *88*, 6680–6684.
(42) Dougherty, D. A. *Science* **1996**, *271*, 163–168.

J. Am. Soc. Mass Spectrom. (2012) 23:850–857
DOI: 10.1007/s13361-012-0338-6

RESEARCH ARTICLE

Using Electron Induced Dissociation (EID) on an LC Time-Scale to Characterize a Mixture of Analogous Small Organic Molecules

Aruna S. Prakash,[1] Michael J. P. Smith,[1] Zied Kaabia,[1] Glenn Hurst,[1] Ci Yan,[1] Martin Sims,[2] Anthony W. T. Bristow,[2] Peter Stokes,[1] David Parker,[1] Jackie A. Mosely[1]

[1]Department of Chemistry, Durham University, South Road, Durham, DH1 3LE, UK
[2]Analytical Science, Pharmaceutical Development, AstraZeneca, Macclesfield, Cheshire, SK10 2NA, UK

Abstract

LC ESI FTICR MS of a sample of cediranib identified this pharmaceutical target molecule plus an additional 10 compounds of interest, all of which were less than 10% total ion current (TIC) peak intensity relative to cediranib. LC FTICR tandem mass spectrometry using electron induced dissociation (EID) has been achieved and has proven to be the best way to generate useful product ion information for all of these singly protonated molecules. Cediranib $[M+H]^+$ fragmented by EID to give 29 product ions whereas QTOF-CID generated only one very intense product ion, and linear ion trap-CID, which generated 10 product ions, but all with poor S/N. Twenty-six of the EID product ions were unique to this fragmentation technique alone. By considering the complementary LC-EID and LC-CID data together, all 10 unknown compounds were structurally characterized and proven to be analogous to cediranib. Of particular importance, EID produced unique product ion information for one of the low level cediranib analogues that enabled full characterization of the molecule such that the presence of an extra propylpyrrolidine group was discovered and proven to be located on the pyrrolidine ring of cediranib, solving an analytical problem that could not be solved by collision induced dissociation (CID). Thus, it has been demonstrated that EID is in harmony with the chromatography duty-cycle and the dynamic concentration range of synthetic compounds containing trace impurities, providing crucial analytical information that cannot be obtained by more traditional methodologies.

Key words: Tandem mass spectrometry by electron induced dissociation, Structural characterization of pharmaceuticals, LC MS/MS for low abundant compounds

Introduction

Liquid chromatography-mass spectrometry (LC-MS) is an integral part of drug discovery and development in the pharmaceutical industry, routinely used to reveal and characterize trace-level impurities, by-products, and degradation products, which are common occurrences in synthetic chemistry reactions [1]. The need to identify all components present alongside a synthetically produced target compound is often hampered by the fact that these undesirable molecules can be structurally similar to the target compound, yet present at much lower concentrations. LC ESI MS/MS has the sensitivity with which to detect molecules at low concentrations and the experimental flexibility to extract

Electronic supplementary material The online version of this article (doi:10.1007/s13361-012-0338-6) contains supplementary material, which is available to authorized users.

Correspondence to: Jackie Mosely; *e-mail:* jackie.mosely@durham.ac.uk

Received: 24 May 2011
Revised: 4 January 2012
Accepted: 5 January 2012
Published online: 31 January 2012

information that can lead to proposed empirical formulae and molecular structure [2–6]. There are many MS/MS techniques available, the most common one used in the pharmaceutical industry being collision induced dissociation (CID). CID involves collisions between precursor ions and neutral gaseous atoms or molecules, which results in the conversion of a precursor ion's kinetic energy into internal energy. This increase in internal energy causes bond dissociation within the precursor ion, typically favoring the lowest energy fragmentation pathways [7–9]. Problems often arise upon the CID analyses of analogous compounds as product ions observed from the cleavage of the weakest bonds may not allude to the location of, or nature of, such small structural molecular changes, demanding that other analytical approaches be explored. A more recent addition to the tandem MS toolbox is electron capture dissociation (ECD), an electron-based fragmentation technique primarily used to fragment and characterize multiply charged peptide and protein cations [10–12]. It involves the interaction of low energy electrons (1–5 eV) with multiply protonated species, resulting in charge reduction and bond cleavage [13, 14]. ECD of peptides/proteins has been shown to produce a simple but regular distribution of product ions that complement the CID distribution, but the ability of ECD to preserve labile covalently bound modifications gives this technique a distinct advantage over CID [15–18]. In an attempt to gain yet further information regarding peptide structure, Zubarev et al. increased the ECD electron energy beyond what is common for multiply charged peptides (>10 eV), generating hotter electrons [13, 19]. Applying these higher energy electrons to multiply charged peptides is known as hot electron capture dissociation (hECD) and has been shown to produce a significant increase in side chain fragmentation producing an even greater depth of information [20, 21]. More recently, the interaction between hotter electrons and singly charged cations has been shown to induce fragmentation and is referred to as electron induced dissociation (EID) [19, 22–29]. In a very recent study with pharmaceutical type molecules, EID produced extensive product ion data that largely complemented CID, was comparable to electron ionization (EI), and was more tolerant to a wider range of charge carrying species than CID [29].

ECD is somewhat notorious for its lack of efficiency compared with other techniques such as CID [10, 15]. Historically, in order to achieve usable spectra, samples of high concentration were preferred and S/N allowed to build-up by accumulating many spectra. Significant inroads have been made in optimizing methodologies to facilitate ECD of peptides on the LC time-scale [3, 4, 30]. For EID to be widely pertinent to real-world applications, it too must be coupled to chromatographic techniques, producing spectra of sufficient quality that information can be gained for compounds of a wide dynamic concentration range from the limited number of spectra achievable across a chromatographic peak. This development will show that LC-EID is achievable, plus it provides unique information not afforded by LC-CID. The power to generate multiple datasets of complementary information on one instrument in the very short LC time-scale facilitates greater in-depth analysis of complex mixtures of small molecules, which are typical of the pharmaceutical industry.

Experimental

Sample Preparation and Sample Introduction

The sample of cediranib was supplied by AstraZeneca, Macclesfield, UK. All solvents were purchased from Sigma-

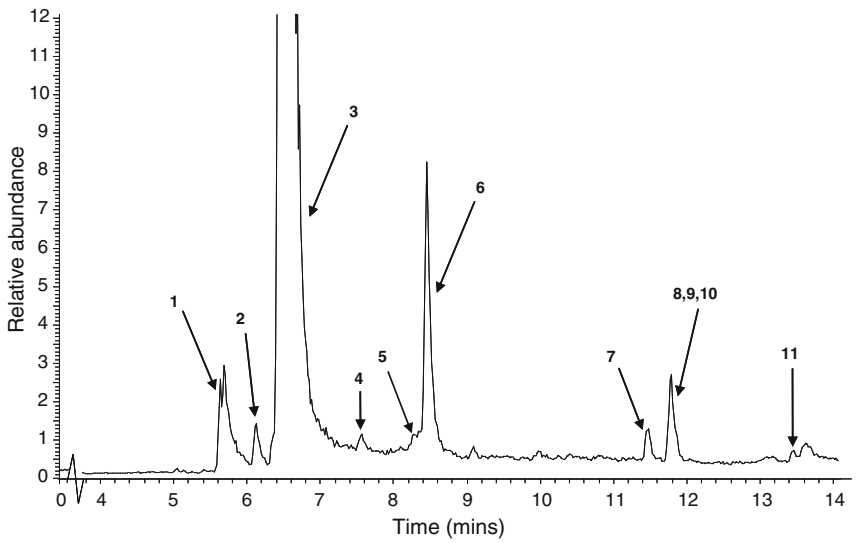

Figure 1. Total Ion Chromatogram (TIC) from LC FTICR MS analysis of cediranib. Peaks labeled **1** to **11** indicate the presence of components proven to be from the cediranib sample. A comparison of sample and control is given in supplementary information Figure S1

Table 1. Summary of product ions following LC-CID and LC-EID of cediranib labeled LC peak number **3** and analogues labeled LC peak number **1**, **2**, and **4**–**11**

LC peak number	Observed MS peak *m/z*	Proposed molecular formula for $[M+H]^+$	Number of product ions observed		Number of product ions common between EID and CID	Number of product ions common between Cediranib (peak **3**) and an analogue
			EID	CID		
1	562	$C_{32}H_{41}O_3N_5F$	17	15	2	11
2	899	$C_{50}H_{53}O_6N_8F_2$	5	7	2	5
3	451	$C_{25}H_{28}O_3N_4F$	29	10	3	N/A
4	788	$C_{43}H_{40}O_6N_7F_2$	2	11	1	4
5	481	$C_{25}H_{26}O_5N_4F$	12	5	4	4
6	340	$C_{18}H_{15}O_3N_3F$	21	15	5	9
7	447	$C_{25}H_{24}O_3N_4F$	19	3	3	6
8	430	$C_{25}H_{21}O_3N_3F$	17	21	9	8
9	339	$C_{18}H_{14}O_3N_3F$	17	9	9	6
10	921	Unknown	4	8	3	2
11	691	$C_{37}H_{29}O_6N_6F_2$	2	16	1	4

Aldrich, Dorset, UK. For the chromatography, a solution of cediranib was made to 2 mg mL^{-1} in methanol; 10 µL aliquots were injected on to either a Luna 3 µm C18 (2), 100 Å, 150×2 mm column (Phenomenex) with a mobile phase flow rate of 200 µL min^{-1} for a 12 min separation or a 4.5 min separation using a Zorbax SB-C18 1.8 µm 4.6× 50 mm column (Agilent Technologies) with a mobile phase flow rate of 1 mL min^{-1} and a 1:4 split prior to the mass spectrometer. Gradient conditions started at 95% (H_2O+ 0.1% formic acid)/5% (CH_3CN+0.1 % formic acid) and finished at 5 % (H_2O+0.1% formic acid)/95% (CH_3CN+0.1 % formic acid). A 5 µg mL^{-1} solution of cediranib in methanol was used for occasional experiments requiring direct infusion. In such instances a syringe pump delivered the sample solution at a flow rate of 5 µL min^{-1}.

Mass Spectrometry

Unless stated otherwise, measurements were made using a ThermoFinnigan LTQFT mass spectrometer fitted with a 7 Tesla magnet and equipped with an electrospray ion source (Bremen, Germany). The following ion source parameters were optimized for the most stable ion signal: the nitrogen sheath gas was kept between 8 and 10 arbitrary units, the auxiliary gas and sweep gas were set between 2 and 4 arbitrary units, as per the manufacturer's software, the capillary was heated to 250 °C, and the spray voltage was held at 4–4.5 kV. The tube lens voltage was varied to deliver the optimal ion intensity.

Isolation of the precursor ions was carried out in the LTQ ion trap with a fixed isolation window of 4 *m/z* in order to include the full isotopic profile of the compound of interest. All LC-MS/MS experiments were performed by alternating MS and MS/MS scans throughout the chromatographic run. CID experiments were performed entirely within the LTQ ion trap using helium as a collision gas and optimized at a normalised collision energy level of 25 as per the manufacturer's software, unless otherwise stated. EID was performed entirely within the FTICR cell using an indirectly heated dispenser cathode. To generate 'hot' electrons required for EID and hECD, the electron energy was set at 20 arbitrary units, as per the manufacturer's software. The cathode offset was 2.5 V for LC-MS/MS experiments and 2.1 V for the direct infusion experiments, resulting in approximate electron energies of 17.5 and 17.9 eV, respectively. For ECD, the electron energy was set at 5 arbitrary units, as per the manufacturer's software, and the cathode offset was 2.1 V resulting in an approximate electron energy of 2.9 eV. The electron irradiation time was fixed at 70 ms. Data was recorded using the acquisition software Xcalibur ver. 2.0.7 (Thermo Fisher Scientific Inc.) and processed using the embedded program Qual Browser. Comparative direct infusion ESI QTOF MS measurements were made on a Waters QTOF Premier (Manchester, UK). QTOF-CID experiments were performed using ion source parameters that optimized the precursor ion peak intensity, argon as a collision gas and a collision energy of 25 eV.

Results ad Discussion

LC-MS/MS of Cediranib

The process for manufacturing cediranib, as with all pharmaceuticals, is rigorously developed and controlled to ensure that any impurities present are well below internationally recognized safety limits. The inherent sensitivity of mass spectrometric methods allows detection of trace level impurities that are below these permitted safe levels. A process development sample of cediranib containing higher

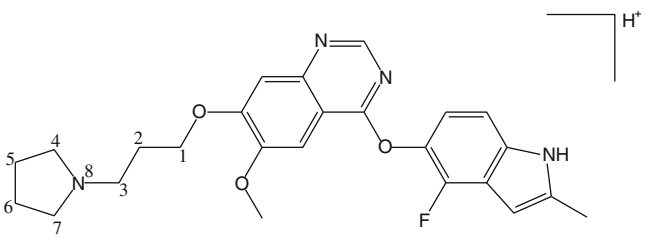

Figure 2. Structure of cediranib with the propylpyrrolidine subunit atoms labeled C(1) to C(7) and N(8)

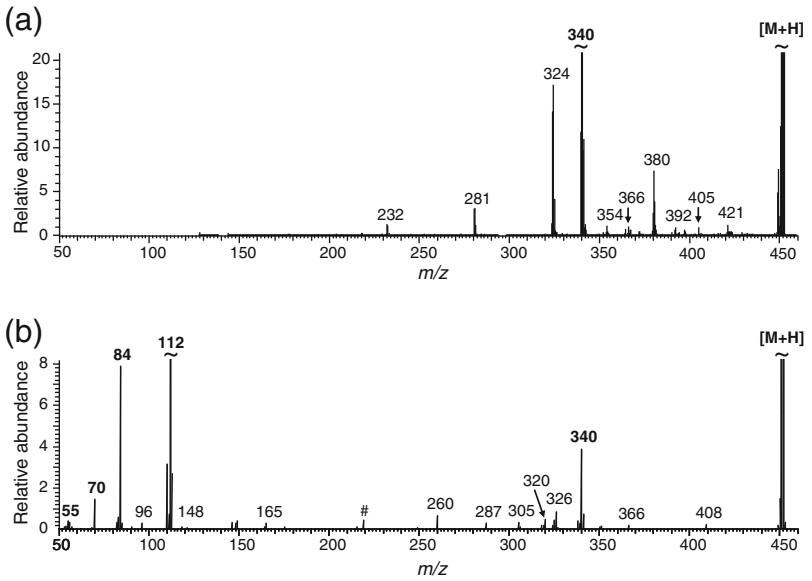

Figure 3. Comparison of tandem MS for protonated cediranib, eluting at 6.55 min (peak **3** in Figure 1), by **(a)** LC-CID performed on an LTQ ion trap MS (average of 274 scans) and **(b)** LC-EID performed on an FTICR MS (average of 21 scans). # Indicates external interference in the FTICR MS and should be discounted. Product ions in bold represent fragmentation relating to the propylpyrrolidine arm

levels of impurities than the marketed compound was analyzed by LC FTICR MS, which separated and detected eleven different compounds of varying ion abundance. Those compounds are labeled **1** to **11** on the total ion chromatogram shown in Figure 1. The most intense peak, **3**, relates to a precursor ion at 451.21370 *m/z*, which corresponds to the empirical formula $C_{25}H_{28}N_4O_3F$ with an accuracy of 0.7 ppm and is taken to be protonated cediranib, as expected. Accurate mass measurements for **1**, **2**, and **4** to **11** suggested molecular formulae in each case, as given in Table 1, however molecular structures remained unknown.

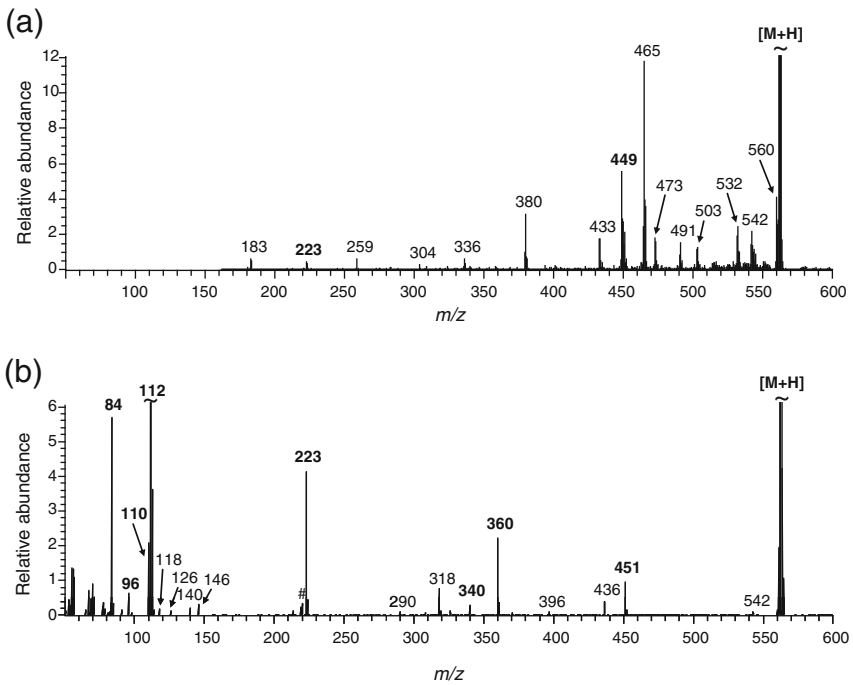

Figure 4. **(a)** LC-CID (average of 157 scans) and **(b)** LC-EID (average of 12 scans) of 562 *m/z* eluting at 5.69 min, labeled peak **1** in Figure 1. Product ions labeled in bold represent fragmentation relating to the propylpyrrolidine arms, including 223 and 360 *m/z*, which confirm the location of the modification. # Indicates external interference in the FTICR MS and should be discounted

Initial CID experiments to probe the structure of cediranib (Figure 2) were carried out by direct infusion of sample into a QTOF MS. The protonated cediranib molecule fragmented to give only one product ion peak at 112 *m/z* (S/N>30,000/1, data not shown), corresponding to the cleavage of the C(1)–O bond of the propylpyrrolidine arm. This provides very little useful information about the molecular structure, highlighting the need for additional analytical techniques. Identification of the unknown species by tandem mass spectrometry was hampered by their low ion abundances, particularly in the presence of such a hugely abundant target compound. Coupling MS with chromatography minimized in-source ion suppression, improving precursor ion S/N in preparation for MS/MS. In this instance, both CID and EID have been employed to target and identify the unknown species present in the cediranib sample. Figure 3a shows the spectrum obtained from the LC-CID of cediranib performed and detected in the LTQ of the LTQFT. The single product ion at 112 *m/z* that was observed from the QTOF CID is not observed due to the one-third cut-off, which affects MS/MS carried out in quadrupole ion traps [31]. This results in the majority of CID product ions being present in the higher *m/z* region, including 340 *m/z*, which corresponds to the neutral loss of the propylpyrrolidine moiety. By comparison, the results from LC-EID shown in Figure 3b display the opposite trend for product ion distribution, providing unique information at the lower *m/z* range. The peak at 112.11208 *m/z* corresponds to the empirical formula $C_7H_{14}N$ with an accuracy of 0.04 ppm, confirming the identity of the propylpyrrolidine arm of the molecule. Comparison of LC-CID and LC-EID product ion spectra really highlights the complementary nature of these two techniques, supporting previous studies [29], but also demonstrates that both are achievable in the LC timescale.

LC-MS/MS of Unknown Species

The first of the unknown species to be studied was the first to elute from the column, peak **1** with a retention time of 5.69 min (see Figure 1). This relates to a mass peak 562.31897 *m/z*, which corresponds to the empirical formula $C_{32}H_{41}N_5O_3F$ with an accuracy of 0.3 ppm. The LC FTICR MS/MS of this precursor ion is given in Figure 4 for (a) LC-CID and (b) LC-EID. Comparison shows the LC-EID data to be the most immediately useful data, despite being a summation of 13 times less spectra than for LC-CID. Accurate mass measurement on the product ion at 451 *m/z* proposed a molecular formula $C_{25}H_{28}N_4O_3F$ with an accuracy of 0.1 ppm. This is the same empirical formula as protonated cediranib, so at a glance the likely relationship between these two molecules is established. The neutral loss from 562 to 451 *m/z* during EID is consistent with a fragment having the empirical formula $C_7H_{13}N$ and is considered to be most likely due to the addition of a second propylpyrrolidine arm onto the parent molecule during synthesis. Further indication into the structural similarities can be gained by comparing the LC-EID for cediranib shown in Figure 3b directly with the LC-EID of 562 *m/z* in Figure 4b. LC-EID of cediranib and the unknown species at 562 *m/z* resulted in the product ions 70, 84, and 112 *m/z* and accurate mass measurements allowed the empirical formulae C_4H_8N, $C_5H_{10}N$ and $C_7H_{14}N$ to be assigned, respectively. These three fragments are all from the propylpyrrolidine arm, a conclusion supported by visually comparing Figure 4b against EI mass spectral library records for a number of molecules with alkylpyrrolidine functional groups. Also in common is a product ion at 340 *m/z*, confirmed by accurate mass measurement despite lower S/N in Figure 4b, which corresponds to the protonated indolphenol structure given in Figure 5a and represents cediranib minus the propylpyrrolidine arm that is such an intense product ion in itself. In total, nine product ions observed in the LC-EID of the unknown compound at 562 *m/z* can be explained by comparison with the LC-EID of protonated cediranib, lending credence to the proposal that both molecules are closely structurally related. Now that the unknown molecule with $[M+H]^+$=562 *m/z* is considered to be related to cediranib, the difference being an additional propylpyrrolidine moiety, the question remains as to the location of the second propylpyrrolidine. There are eight

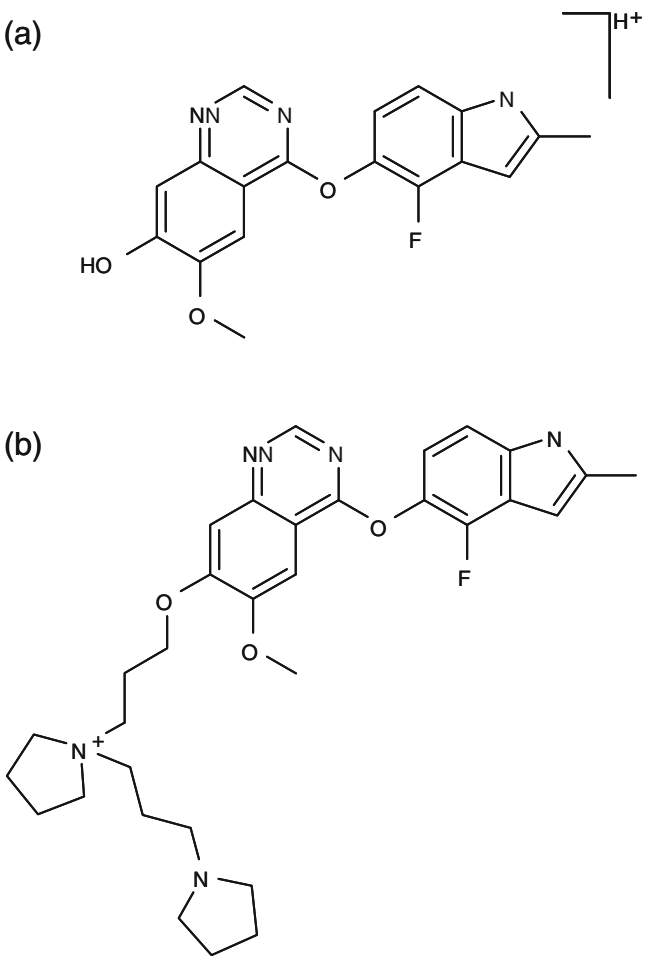

Figure 5. Structures of **(a)** indolphenol and **(b)** quaternary ion

peaks observed in Figure 4b for the LC-EID spectrum of 562 *m/z*, which are not observed from the LC-EID of protonated cediranib, two of which provide insight to the location of the extra functional group. First, the peak at 223 *m/z* has been determined to have a molecular formula of $C_{14}H_{27}N_2$ (0.7 ppm error), consistent with two propylpyrrolidine arms. As the C(1)–O is the main cleavage site within this molecule, this suggests that the addition of the second propylpyrrolidine is situated on one of seven carbon atoms labeled C(1) to C(7) or the nitrogen atom N(8) as described in Figure 2. In fact, evidence for this at very low abundance is also present in the LC-CID spectrum in Figure 4a. Second, the peak at 360 *m/z* has been identified as a fragment with the molecular formula $C_{21}H_{18}N_3O_3$ (1.4 ppm error), which is proposed to correspond to the loss of one intact propylpyrrolidine moiety plus the pyrrolidine ring of the second arm and hydrogen fluoride ($C_7H_{14}N_1+C_4H_8N_1+$ HF). This further implies that the addition is located on the pyrrolidine ring C(4)–C(7) or N(8). NMR analysis of the extracted impurity corroborates the MS findings and further identifies the location of the second propylpyrrolidine as the N(8) atom, giving a quaternary ion as shown in Figure 5b.

The remaining unknown compounds labeled **2**, **4**–**11** in Figure 1 have been investigated using the same LC-CID and LC-EID methodology and results are summarized in Table 1. Here, the total number of product ions has been counted for each technique (LC-CID and LC-EID). It can clearly be seen that EID provides a usable number of product ions for all the precursor ions studied, and that the number of EID product ions is comparable or often greater than to CID. The most interesting fact here, though, comes from comparing the observed product ion *m/z* values for each technique. There is very little overlap between the observed product ions, highlighting the complementary nature of these two techniques. Delving further shows that when this complementary data is considered as a whole, the number of peaks that each unknown compound has in common with cediranib is sufficiently high to suggest a strong likelihood that each unknown species is chemically related to the cediranib. As with the compound at LC peak **1** (Figure 1), further analytical techniques may be ultimately required to confirm the full molecular structure, however in this case the unknown species labeled **2**, **4**–**11** remain proprietary information of the pharmaceutical company and cannot be discussed further.

Tandem MS of $[M+2H]^{2+}$ for Cediranib

Cediranib was observed in two charge states: singly and doubly protonated. Doubly charged ions were not observed

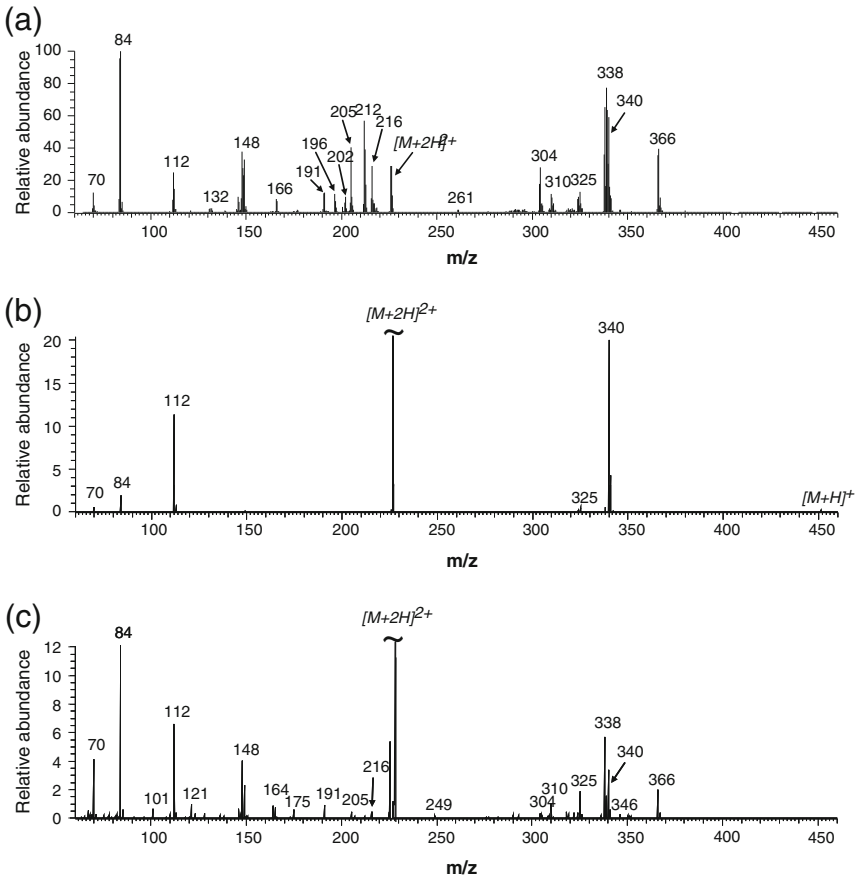

Figure 6. Tandem mass spectrometry of doubly protonated cediranib by direct infusion. Comparison of **(a)** CID (normalized collision energy of 18) with **(b)** ECD (electron energy = 2.9 eV) and **(c)** hECD (electron energy = 17.9 eV)

for any of the weakly abundant, co-sprayed cediranib analogues. The doubly protonated adduct of cediranib, despite being considerably less abundant, would tend to be the precursor ion of choice as multiply charged species are generally accepted to provide the superior product ion spectrum [32, 33]. Figure 6a shows CID for 226 *m/z*, $[M+2H]^{2+}$ for cediranib performed with a normalized collision energy of 18. As could be expected, this spectrum represents a huge improvement over the CID of the singly protonated precursor (Figure 3a) in terms of number of product ions observed and provides comparable data to EID of the singly protonated species (Figure 3b).

As mentioned previously, the interaction between low energy electrons and multiply charged cations is considered to result in the capture of an electron and subsequent bond dissociation, a technique known as electron capture dissociation (ECD). When the ECD approach was employed to study the $[M+2H]^{2+}$ for cediranib (Figure 6b), irradiation with low energy electrons (electron energy=2.9 eV) gave very limited information. There is weak evidence of deprotonation from $[M+2H]^{2+}$ to give $[M+H]^{+}$ but the main dissociation point is cleavage of the C(1)–O bond (Figure 2) to create product ions corresponding to protonated indolphenol and the propyl-pyrrolidine arm. In an experiment akin to hECD, using identical instrumental conditions to the EID experiments, the impact of hotter electrons (electron energy=17.9 eV) was able to induce a much greater degree of dissociation as shown in Figure 6c. This spectrum closely resembles EID of $[M+H]^{+}$ (Figure 3b) and CID of $[M+2H]^{2+}$ (Figure 6a) in terms of relating product ions to structure. Overall, ECD was of no benefit when characterising this small molecule but hECD of the doubly charged species and EID of the singly charged species are both informative suggesting that the charge state of the precursor ion is not as crucial for the electron based fragmentation techniques.

Conclusion

The electron energy required to generate the optimum mass spectrum in terms of number of product ions and the S/N ratio of the peaks is of the order of 18 eV, regardless of whether the molecule is singly or doubly protonated, although if this choice is presented, the doubly protonated precursor ion would be more desirable. Using this value for electron energy, rapid EID has been achieved on the LC timescale and for compounds of a wide dynamic abundance. Perhaps most importantly, LC-EID has proven to be a very powerful tool in that it provided crucial information about the identity and location of a molecular modification to an impurity that would otherwise require preparative isolation and NMR, a time-consuming and expensive alternative. This solution facilitates identification and characterization at a much earlier stage of drug development where sample may be limited.

Acknowledgments

The authors thank the Durham Mass Spectrometry Group for help and support, AstraZeneca for the donation of the compounds, and the EPSRC for funding.

References

1. Pan, C., Liu, F., Ji, Q., Wang, W., Drinkwater, D., Vivilecchia, R.: The use of LC/MS, GC/MS, and LC/NMR hyphenated techniques to identify a drug degradation product in pharmaceutical development *J. Pharmaceut. Biomed.* **40**, 581–590 (2006)
2. Lee, M.S., Kerns, E.H.: LC/MS applications in drug development *Mass Spectrom. Rev.* **18**, 187–279 (1999)
3. Palmblad, M., Tsybin, Y.O., Ramström, M., Bergquist, J., Håkansson, P.: Liquid chromatography and electron-capture dissociation in Fourier transform ion cyclotron resonance mass spectrometry. *Rapid Commun. Mass Spectrom.* **16**, 988–992 (2002)
4. Creese, A.J., Cooper, H.J.: Liquid chromatography electron capture dissociation tandem mass spectrometry (LC-ECD-MS/MS) versus liquid chromatography collision-induced dissociation tandem mass spectrometry (LC-CID-MS/MS) for the identification of proteins. *J. Am. Soc. Mass Spectrom.* **18**, 891–897 (2007)
5. Holcapek, M., Kolarova, L., Nobilis, M.: High-performance liquid chromatography-tandem mass spectrometry in the identification and determination of phase I and phase II drug metabolites. *Anal. Bioanal. Chem.* **391**, 59–78 (2008)
6. Ma, S., Subramanian, R.: Detecting and characterizing reactive metabolites by liquid chromatography/tandem mass spectrometry. *J. Mass Spectrom.* **41**, 1121–1139 (2006)
7. Sleno, L., Volmer, D.A.: Ion activation methods for tandem mass spectrometry. *J. Mass Spectrom.* **39**, 1091–1112 (2004)
8. Shukla, A.K., Futrell, J.H.: Tandem mass spectrometry: dissociation of ions by collisional activation. *J. Mass Spectrom.* **35**, 1069–1090 (2000)
9. McLafferty, F.W.: Tandem Mass Spectrometry. *Science* **214**, 280–287 (1981)
10. Zubarev, R.A., Kelleher, N.L., McLafferty, F.W.: Electron capture dissociation of multiply charged protein cations: A nonergodic process. *J. Am. Chem. Soc.* **120**, 3265–3266 (1998)
11. Bakhtiar, R., Guan, Z.Q.: Electron capture dissociation mass spectrometry in characterization of peptides and proteins *Biotechnol. Lett.* **28**, 1047–1059 (2006)
12. Zubarev, R.A.: Reactions of polypeptide ions with electrons in the gas phase. *Mass Spectrom. Rev.* **22**, 57–77 (2003)
13. Zubarev, R.A., Haselmann, K.F., Budnik, B., Kjeldsen, F., Jensen, F.: Towards an understanding of the mechanism of electron-capture dissociation: a historical perspective and modern ideas. *Eur. J. Mass Spectrom.* **8**, 337–349 (2002)
14. Syrstad, E.A., Turecek, F.: Toward a general mechanism of electron capture dissociation. *J. Am. Soc. Mass Spectrom.* **16**, 208–224 (2005)
15. Cooper, H.J., Håkansson, K., Marshall, A.G.: The role of electron capture dissociation in biomolecular analysis. *Mass Spectrom. Rev.* **24**, 201–222 (2005)
16. Zubarev, R.A., Horn, D.M., Fridriksson, E.K., Kelleher, N.L., Kruger, N.A., Lewis, M.A., Carpenter, B.K., McLafferty, F.W.: Electron capture dissociation for structural characterization of multiply charged protein cations. *Anal. Chem.* **72**, 563–573 (2000)
17. Polfer, N.C., Haselmann, K.F., Zubarev, R.A., Langridge-Smith, P.R. R.: Electron capture dissociation of polypeptides using a 3 Tesla Fourier transform ion cyclotron resonance mass spectrometer. *Rapid Commun. Mass Spectrom.* **16**, 936–943 (2002)
18. Mosely, J.A., Murray, B.S., Parker, D.: Electron-capture dissociation and collision-induced dissociation of lanthanide metal–ligand complexes and lanthanide metal–ligand complexes bound to phosphopeptides. *Eur. J. Mass Spectrom.* **15**, 145–155 (2009)
19. Lioe, H., O'Hair, R.A.J.: Comparison of collision-induced dissociation and electron-induced dissociation of singly protonated aromatic amino acids, cysteine and related simple peptides using a hybrid linear ion trap-FT-ICR mass spectrometer. *Anal. Bioanal. Chem.* **389**, 1429–1437 (2007)
20. Kjeldsen, F., Haselmann, K.F., Budnik, B.A., Jensen, F., Zubarev, R. A.: Dissociative capture of hot (3–13 eV) electrons by polypeptide

polycations: an efficient process accompanied by secondary fragmentation. *Chem. Phys. Lett.* **356**, 201–206 (2002)
21. Cooper, H.J., Hudgins, R.R., Håkansson, K., Marshall, A.G.: Secondary fragmentation of linear peptides in electron capture dissociation. *Int. J. Mass Spectrom.* **228**, 723–728 (2003)
22. Ly, T., Yin, S., Loo, J.A., Julian, R.R.: Electron-induced dissociation of protonated peptides yields backbone fragmentation consistent with a hydrogen-deficient radical. *Rapid Commun. Mass Spectrom.* **23**, 2099–2101 (2009)
23. Kaczorowska, M.A., Cooper, H.J.: Electron induced dissociation: a mass spectrometry technique for the structural analysis of trinuclear oxo-centred carboxylate-bridged iron complexes. *J. Am. Soc. Mass Spectrom.* **21**, 1398–1403 (2010)
24. Budnik, B.A., Haselmann, K.F., Elkin, Y.N., Gorbach, V.I., Zubarev, R.A.: Applications of electron-ion dissociation reactions for analysis of polycationic chitooligosaccharides in Fourier transform mass spectrometry. *Anal. Chem.* **75**, 5994–6001 (2003)
25. Feketeová, L., Wong, M.W., O'Hair, R.A.J.: The role of metal cation in electron-induced dissociation of tryptophan. *Eur. Phys. J. D* **60**, 11–20 (2010)
26. Yoo, H.J., Håkansson, K.: Determination of double bond location in fatty acids by manganese adduction and electron induced dissociation. *Anal. Chem.* **82**, 6940–6946 (2010)
27. Budnik, B.A., Zubarev, R.A.: $MH^{2+\bullet}$ ion production from protonated polypeptides by electron impact: observation and determination of ionization energies and a cross-section. *Chem. Phys. Lett.* **316**, 19–23 (2000)
28. Sargaeva, N.P., Lin, C., O'Connor, P.B.: Identification of aspartic and isoaspartic acid residues in amyloid β peptides, including Aβ1−42, using electron−ion reactions. *Anal. Chem.* **81**, 9778–9786 (2009)
29. Mosely, J.A., Smith, M.J.P., Prakash, A.S., Sims, M., Bristow, A.W.T.: Electron-induced dissociation of singly charged organic cations as a tool for structural characterization of pharmaceutical type molecules. *Anal. Chem.* (2011). doi:10.1021/ac200045n
30. Creese, A.J., Cooper, H.J.: The effect of phosphorylation on the electron capture dissociation of peptide ions. *J. Am. Soc. Mass Spectrom.* **19**, 1263–1274 (2008)
31. March, R.E.: An introduction to quadrupole ion trap mass spectrometry. *J. Mass Spectrom.* **32**, 351–369 (1997)
32. Smith, R.D., Loo, J.A., Edmonds, C.G., Barinaga, C.J., Udseth, H.R.: New developments in biochemical mass spectrometry: electrospray ionization. *Anal. Chem.* **62**, 882–899 (1990)
33. Loo, J.A., Edmonds, C.G., Smith, R.D.: Tandem mass spectrometry of very large molecules: serum albumin sequence information from multiply charged ions formed by electrospray ionization. *Anal. Chem.* **63**, 2488–2499 (1991)